

A FLUID DYNAMICS MODEL OF ANGIOGRAPHIC INJECTIONS:  
POSSIBLE IMPROVEMENTS THROUGH THE USE OF  
DRAG REDUCING POLYMERS

A THESIS

Presented to

The Faculty of the Division of Graduate Studies

By

Walter A. Carpenter

In Partial Fulfillment  
of the Requirements for the Degree  
Doctor of Philosophy in the  
School of Aerospace Engineering

Georgia Institute of Technology

September, 1977

A FLUID DYNAMICS MODEL OF ANGIOGRAPHIC INJECTIONS:  
POSSIBLE IMPROVEMENTS THROUGH THE USE OF  
DRAG REDUCING POLYMERS

Approved:

Don P. Giddens, Chairman

Robert F. Mabon

Robert/Gl Roper

Date approved by Chairman 11/17/77

## ACKNOWLEDGMENTS

I am sincerely grateful to my advisor, Dr. Don P. Giddens, for all the help and encouragement he has given me in this endeavor. His concern and active interest in both the research and the student have made this a most rewarding and informative experience.

I wish to thank the members of the reading committee for their comments and suggestions; Dr. Robert Mabon whose enthusiasm served as a support in more difficult times, and Dr. Robert G. Roper whose openness to discussion cost him many hours.

Special thanks also go to Dr. R. A. Cassanova who helped me on some of the more technical aspects of the experimentation and Robert L. Roach whose computer expertise saved me a considerable amount of time. To all the others who have spent time to discuss this research and other affairs, I give my sincere thanks.

I wish also to express my gratitude to the National Institutes of Health for partially funding this endeavor under grants HL 15519 and HL 20835.

Special thanks go to Mrs. Peggy Weldon for her patience and skillful typing.

To my parents and my fiance whose patience I have tried many times, fooled you, I made it!

## TABLE OF CONTENTS

	Page
ACKNOWLEDGMENTS . . . . .	ii
LIST OF TABLES . . . . .	v
LIST OF ILLUSTRATIONS . . . . .	vi
SUMMARY . . . . .	xiii
Chapter	
I. INTRODUCTION . . . . .	1
II. PRELIMINARY INVESTIGATION . . . . .	14
Development of the Flow Model	
Catheter or Injection Reynolds Numbers	
Arterial Reynolds Numbers	
Momentum Ratios	
Polymer Considerations	
Flow Model Summary	
Initial Flow Facility	
Photographic Investigation	
Final Flow Model	
III. INSTRUMENTATION AND DATA REDUCTION . . . . .	40
Data Acquisition Equipment	
Monitoring and Test Equipment	
Data Reduction Equipment	
Reduction of LDA Information	
LDA Settings	
LDA Data Processing	
IV. DISCUSSION OF RESULTS . . . . .	56
LDA Investigations	
Centerline Decay	
Initial Conditions	
Centerline Velocity Decay	
Centerline Fluctuation Measurements	
Centerline Spectra	

## TABLE OF CONTENTS (Continued)

	Page
Radial Variations	
Water with the BLT	
Polymer with the BLT	
Comparisons	
Retrograde Flow Region	
Spectra	
Primary Mixing Region	
V. CONCLUSIONS AND RECOMMENDATIONS . . . . .	130
Summary of Results	
Photographic Investigations	
LDA Investigations	
Conclusions	
Discussion and Recommendations	
APPENDICES	
I. PERIPHERAL ANGIOGRAPHY: HISTORY AND COMPLICATIONS . . .	142
II. ADDITIONAL INFORMATION ON THE DISA 55L LDA SYSTEM . . .	145
III. SAMPLE PROGRAM . . . . .	166
IV. CASSON MODEL . . . . .	169
V. ADDITIONAL RESULTS AND DISCUSSION . . . . .	174
Centerline Spectra	
Radial Variations	
Comparisons Spectra	
BIBLIOGRAPHY . . . . .	206
VITA . . . . .	211

## LIST OF TABLES

Table	Page
1. Possible Injection Reynolds Numbers . . . . .	17
2. Possible Reynolds Numbers Found in Arteries . . . . .	20
A-1. Frequency Ranges for LDA Tracker . . . . .	162
A-2. Frequency Response as Value of Percent Bandwidth . . . . .	162

## LIST OF ILLUSTRATIONS

Figure	Page
1. Flor Model - Recirculating System . . . . .	25
2. Flow Model - Bloo Down System . . . . .	27
3. Photographic Visualization . . . . .	28
4. Injection of Water without BLT $Re_c = 2000$ . . . . .	30
5. Injection of Water without BLT $Re_c = 7000$ . . . . .	32
6. Injection of Polymer Solution without BLT $Re_c = 4700$ . . . . .	34
7. Injection of Polymer Solution with BLT $Re_c = 7000$ . . . . .	37
8. Arrangement of LDA System . . . . .	44
9. Change in Sampling due to Medium Change . . . . .	44
10. Block Diagram of LDA System . . . . .	45
11. Polymer Effectiveness Test Apparatus . . . . .	47
12. Relative Viscosity Test Apparatus . . . . .	47
13. Comparison of LDA to Hot Film Spectra . . . . .	50
14. Flow Chart of LDA Data Reduction . . . . .	54
15. Comparison of Catheter Velocity Profiles to Theory, Re = 7000 . . . . .	58
16. Comparison of Catheter Velocity Profiles to Theory, Re = 7000 . . . . .	59
17. Centerline Decay of Velocity . . . . .	61
18. Centerline Variation of $U'_{rms}/U_{FR}$ . . . . .	63
19. Centerline Variation of $U'_{rms}/U_L$ . . . . .	66
20. Comparison of Centerline Spectra at $X/D = -.54$ . . . . .	68

## LIST OF ILLUSTRATIONS (Continued)

Figure	Page
21. Spectrum Displaying Helical Instability, $X/D = 2.71$ . . . . .	69
22. Comparison of Centerline Spectra at $X/D = 21.71$ . . . . .	71
23. Velocity Profiles, Water with BLT, $X/D$ from -0.54 to 10.85 . . . . .	73
24. Velocity Profiles, Water with BLT, $X/D$ from 10.85 to 54.27 . . . . .	74
25. Velocity Profiles, Polymer Solution with BLT, $X/D$ from -0.54 to 10.85 . . . . .	76
26. Velocity Profile, Polymer Solution with BLT, $X/D$ from 10.85 to 54.27 . . . . .	77
27. Comparison of Polymer Solution to Water Velocity Profile, $X/D = -0.54$ . . . . .	78
28. Comparison of Polymer Solution to Water Fluctuation Profile, $X/D = -0.54$ . . . . .	79
29. Comparison of Polymer Solution to Water Intensity Profile, $X/D = -0.54$ . . . . .	80
30. Comparison of Polymer Solution to Water Velocity Profile, $X/D = 0.54$ . . . . .	81
31. Comparison of Polymer Solution to Water Intensity Profile, $X/D = 0.54$ . . . . .	82
32. Comparison of Polymer Solution to Water Intensity Profile, $X/D = 0.54$ . . . . .	83
33. Comparison of Polymer Solution to Water Velocity Profile, $X/D = 2.71$ . . . . .	85
34. Comparison of Polymer Solution to Water Fluctuation Profile, $X/D = 2.71$ . . . . .	86
35. Comparison of Polymer Solution to Water Intensity Profile, $X/D = 2.71$ . . . . .	87
36. Jet Spreading Using Half Velocities . . . . .	88

## LIST OF ILLUSTRATIONS (Continued)

Figure	Page
37. Comparison of Polymer Solution to Water Velocity Profile, $X/D = 5.42$ . . . . .	90
38. Comparison of Polymer Solution to Water Fluctuation Profile, $X/D = 5.42$ . . . . .	91
39. Comparison of Polymer Solution to Water Intensity Profile, $X/D = 5.42$ . . . . .	92
40. Comparison of Polymer Solution to Water Velocity Profile, $X/D = 10.85$ . . . . .	93
41. Comparison of Polymer Solution to Water Fluctuation Profile, $X/D = 10.85$ . . . . .	94
42. Comparison of Polymer Solution to Water Velocity Profile, $X/D = 16.28$ . . . . .	95
43. Comparison of Polymer Solution to Water Velocity Profile, $X/D = 27.14$ . . . . .	97
44. Comparison of Polymer Solution to Water Velocity Profile, $X/D = 27.14$ . . . . .	98
45. Comparison of Polymer Solution to Water Velocity Profile, $X/D = 54.27$ . . . . .	99
46. Length of Near Wall Retrograde Flow Regions . . . . .	101
47. Radial Variation of Spectra, Water Injection, $X/D = -0.54$ . . . . .	103
48. Radial Variation of Spectra, Water Injection, $X/D = 0.54$ . . . . .	104
49. Radial Variation of Spectra Water Injection, $X/D = 0.54$ . . . . .	106
50. Radial Variation of Spectra, Water Injection, $X/D = 2.71$ . . . . .	107
51. Radial Variation of Spectra, Water Injection, $X/D = 2.71$ . . . . .	109

## LIST OF ILLUSTRATIONS (Continued)

Figure	Page
52. Radial Variation of Spectra, Water Injection, X/D = 5.42 . . . . .	111
53. Radial Variation of Spectra, Water Injection, X/D = 10.85 . . . . .	113
54. Radial Variation of Spectra, Water Injection, X/D = 16.28 . . . . .	114
55. Radial Variation of Spectra, Water Injection, X/D = 54.27 . . . . .	115
56. Radial Variation of Spectra, Polymer Solution, X/D = -0.54 . . . . .	116
57. Radial Variation of Spectra, Polymer Solution, X/D = 0.54 . . . . .	118
58. Radial Variation of Spectra, Polymer Solution, X/D = 0.54 . . . . .	119
59. Radial Variation of Spectra, Polymer Solution, X/D = 2.71 . . . . .	120
60. Radial Variation of Spectra, Polymer Solution, X/D = 2.7 . . . . .	121
61. Radial Variation of Spectra, Polymer Solution, X/D = 5.43 . . . . .	123
62. Radial Variation of Spectra, Polymer Solution, X/D = 10.85 . . . . .	125
63. Radial Variation of Spectra, Polymer Solution, X/D = 16.28 . . . . .	126
64. Radial Variation of Spectra, Polymer Solution, X/D = 54.27. . . . .	128
A-1. Formation of Interference Fringes . . . . .	147
A-2. Pulses from Schmitt Trigger with Various Threshold Values . . . . .	149
A-3. LDA Geometry, Differential Mode . . . . .	151

## LIST OF ILLUSTRATIONS (Continued)

Figure	Page
A-4. Block Diagram of LDA Tracker . . . . .	153
A-5. Operation of Bragg Cell. . . . .	157
A-6. LDA Geometry, Differential Mode, 40 mHz Shift . . . . .	163
A-7. Production of Ambiguity, Reference Beam Mode . . . . .	164
A-8. Sample Program Number I . . . . .	167
A-9. Sample Program Number II . . . . .	168
A-10. Comparison of Casson to Newtonian, $U_{FR} = 40$ cm/sec $R_o = 1.25$ cm . . . . .	171
A-11. Comparison of Casson to Newtonian, $U_{FR} = 25$ cm/sec $R_o = .75$ cm . . . . .	172
A-12. Comparison of Casson to Newtonian, $U_{FR} = 14.5$ cm/sec $R_o = 0.25$ cm . . . . .	173
A-13. Centerline Variation of Energy Spectra, Water Without BLT . . . . .	175
A-14. Centerline Variation of Energy Spectra, Water Without BLT . . . . .	176
A-15. Centerline Variation of Energy Spectra, Water with BLT . . . . .	177
A-16. Centerline Variation of Energy Spectra, Water with BLT . . . . .	178
A-17. Centerline Variation of Energy Spectra, Polymer Solution without BLT . . . . .	179
A-18. Centerline Variation of Energy Spectra, Polymer Solution without BLT . . . . .	180
A-19. Centerline Variation of Energy Spectra, Polymer Solution with BLT . . . . .	181
A-20. Centerline Variation of Energy Spectra, Polymer Solution with BLT . . . . .	182

## LIST OF ILLUSTRATIONS (Continued)

Figure	Page
A-21. Fluctuation Profiles, Water with BLT, X/D from -0.54 to 10.85 . . . . .	184
A-22. Fluctuation Profiles, Water with BLT, X/D from 10.85 to 54.27 . . . . .	185
A-23. Intensity Profiles, Water with BLT, X/D from 0.54 to 10.85 . . . . .	186
A-24. Intensity Profiles, Water with BLT, X/D from 10.85 to 54.27 . . . . .	187
A-25. Fluctuation Profiles, Polymer Solution with BLT, X/D from -0.54 to 10.85 . . . . .	188
A-26. Fluctuation Profiles, Polymer Solution with BLT, X/D from 10.85 to 54.27 . . . . .	189
A-27. Intensity Profiles, Polymer Solution with BLT X/D from -0.54 to 10.85 . . . . .	190
A-28. Intensity Profiles, Polymer Solution with BLT, X/D from 10.75 to 54.27 . . . . .	191
A-29. Comparison of Polymer Solution to Water Intensity Profile, X/D = 10.85 . . . . .	193
A-30. Comparison of Polymer Solution to Water Fluctuation Profile, X/D = 16.28 . . . . .	194
A-31. Comparison of Polymer Solution to Water Intensity Profile, X/D = 16.28 . . . . .	195
A-32. Comparison of Polymer Solution to Water Fluctuation Profile, X/D = 21.71 . . . . .	196
A-33. Comparison of Polymer Solution to Water Intensity Profile, X/D = 21.71 . . . . .	197
A-34. Comparison of Polymer Solution to Water Fluctuation Profile, X/D = 27.14 . . . . .	198
A-35. Comparison of Polymer Solution to Water Intensity Profile, X/D = 27.14 . . . . .	199

## LIST OF ILLUSTRATIONS (Continued)

Figure	Page
A-36. Comparison of Polymer Solution to Water Fluctuation Profile, $X/D = 54.27$ . . . . .	200
A-37. Comparison of Polymer Solution to Water Intensity Profile, $X/D = 54.27$ . . . . .	201
A-38. Radial Variation of Spectra, Water Injection, $X/D = 21.71$ . . . . .	202
A-39. Radial Variation of Spectra, Water Injection, $X/D = 27.14$ . . . . .	203
A-40. Radial Variation of Spectra, Polymer Solution, $X/D = 21.71$ . . . . .	204
A-41. Radial Variation of Spectra, Polymer Solution, $X/D = 27.14$ . . . . .	205

## SUMMARY

An experimental model of an angiographic injection has been studied. The model utilized was a concentrically mounted jet exiting into a confined co-flowing stream. The Reynolds number and moments employed were representative of actual injection parameter. A dilute solution of Separan AP-30 was studied as an alternate injectant and compared to a water injection. The outer flow consisted of water in both cases. The model was studied via photographic techniques and Laser Doppler Anemometry.

The photographic investigation was instrumental in the development of the flow model and provided information which correlated with the LDA investigation. Photographs were produced for various catheter Reynolds numbers, with the outer Reynolds number being held constant at 1000. Injections were made using water and a 50 ppm solution of Separan AP-30. At Reynolds numbers below transition both injectants produced similar jets. However, above transition the polymer maintained a laminar-like behavior while the water produced a turbulent jet. To maintain similarity between the two injectants a boundary layer trip (BLT) was placed into the catheter. The photographic investigation was then repeated. The BLT was found to be effective in eliminating the pseudo-laminar behavior of the polymer solution injection.

Based upon the photographic study and a consideration of actual clinical injections a model with an outer Reynolds of 1000 and an inner Reynolds number of 7000 was selected for study in greater detail via an

an LDA system. The LDA system was utilized because of its many advantages over other types of anemometers. Through the use of the LDA system in conjunction with a Fourier Analyzer, axial components of the mean velocity, turbulence fluctuations, and power spectral densities were obtained for a variety of axial and radial locations. Centerline measurements were made for both water and polymer solution injections with and without the presence of the BLT in the catheter. In depth measurements were later made for the injections in which the BLT was employed.

The centerline studies indicated an enhanced decay at the axial velocity component for both types of polymer solution injection, particularly in the near field. While this would tend to indicate a more rapid jet spreading, the radial velocity studies provided information to the contrary.

The water jet actually spread more rapidly in the near field, based upon the half-width of the velocity profiles. Yet, in the more downstream regions the polymer jet, with its higher turbulence intensity, eventually entrained fluid more rapidly and the reattachment point of the recirculation region was achieved earlier. The near wall effects of the polymer solution jet were found to be less than the comparable water injection. This was manifested as a reduced recirculation region for the polymer injection. Near field energy spectra for the polymer injection were found to have a higher energy content in the lower frequencies and lower overall energy content at locations near the wall.

The polymer solution was found to greatly alter the flow field with large dominant eddy size, increased energy content and increased

centerline decay at velocity being major characteristics. On the basis of the flow studies, the addition of a drag reducing polymer to a contrast agent to improve the angiographic procedure was found to produce more adverse circumstances than benefits. The flow model also indicated a need to exercise extreme care in the placement of the catheter during an angiographic procedure. Further research in the area of catheter design as a means of improving the angiographic injection procedure would seem appropriate.

## CHAPTER I

## INTRODUCTION

Peripheral angiography is a major diagnostic procedure in modern medicine. Since its inception in the early 1900's, angiography has evolved into a sophisticated and complex procedure. The word angiography is derived from the Greek words angos meaning vessel and graphe to write. In an angiographic procedure an X-ray visualization is produced. This is accomplished through the injection of a radiopaque dye into the vascular region under study. In peripheral angiography the catheter may be introduced into the vasculature via either the trachial or femoral arteries. After insertion, the catheter is then "snaked" to the region of interest (1,2). In the resulting "X-ray" or angiogram the vessel lumen appears as a clear photographic or X-ray opaque region. From the angiogram the physician is able to obtain information concerning the health of the vascular region. Angiography is not, however, risk-free and informed consent is a necessary precursor to the procedure.

In the disease state known as atherosclerosis, angiography is a very important diagnostic tool. The physician can obtain certain information from the symptoms described by the patient and by listening to the sounds produced by the turbulent flow past the stenosis. But, determination of the actual size and location of a stenosis is dependent, at present, on angiographic techniques. Complications during an angiographic procedure may occur. The complications are of either a chemical

or mechanical nature. Chemical effects are usually due to the hyperosmolarity of the contrast agent. The result, in many instances, is a burning sensation, nausea, momentary increase followed by a prolonged decrease in blood pressure and a variation in heart rate. These symptoms may vary depending on the contrast medium and the location of the injection site (3-8). Also of concern is the formation of blood clots on the catheter. This is especially prevalent in catheter designs using side holes. Upon removal of the catheter these clots may be scraped off the catheter resulting in potentially harmful emboli. The second cause of complications is the result of the mechanics of the injection. Damage to the arterial endothelial cells has been reported to occur at shear stresses in excess of approximately  $400 \text{ dynes/cm}^2$ , a value not outside the range of shear rates possible in an angiographic injection. A second example of mechanical damage is a result of the high stagnation pressures which can be produced in an angiographic injection. In an investigation dealing with atherosclerosis, potential hazards may develop if the injection is made too close to the plaque. Because of the high pressures which can develop, it is possible that a section of the plaque may be dislodged. In carotid angiography the consequences could be disastrous, possibly resulting in either stroke or death.

Because of the frequent use and inherent dangers of angiography, the fluid dynamics of an injection has become an important consideration. Present day procedures, in an attempt to minimize the puncture wound, are restricted to the use of small diameter catheters (diameters varying from 0.6 to 1.2 mm). This, combined with the need for a large

bolus of radiopaque dye for adequate contrast, has resulted in high pressure, high flow rate injections. Increased mixing of the injectant fluid with the blood would improve contrast in the neighborhood of the catheter tip and then, perhaps, decrease the volume of the contrast agent required. The use of a long-chained, drag reducing polymer would allow delivery of the same amount of dye at a lower dividing pressure. The resulting combination of lower pressure and smaller volume could be important in reducing the incidence of chemical and mechanical complications occurring during an angiographic procedure.

From an engineering standpoing, these injections represent a very complex flow system consisting of asymmetry, bends, branches, wall flexibility, pulsatile flow and perhaps in future injections, polymer effects. To test the effects of long chained drag reducing polymers on injections, comparative studies between injections of dilute polymer solutions and pure solvent should be implemented. Since control of so many parameters is an insurmountable problem making comparisons impossible, a simplified model should be employed. The model used in this research is that of a co-axial jet exiting into a confined co-flowing stream.

Co-axial, co-flowing streams are not a new configuration of study. Several investigations have been conducted using air and pure gases. Forestall and Shapiro (10) using helium as a tracer gas measured the concentration and velocity profiles of a jet with co-flow. Becker et al. (11) discussed a parameter based on momentum iatias as being an important similarity parameter for such a flow. The jet expansion, for an axisymmetric case, was studied experimentally by Curlet and Rico (12).

Razinsky and Brighton (13) made measurements of static wall pressure, mean velocities, turbulent velocities, and Reynolds stresses throughout the flow field for various velocity ratios. In many applications of co-axial flow, a recirculating region may be produced by jet entrainment. Hill (14) included some study of recirculation in his analytical and experimental investigations. Further, Exley and Brighter (15) have experimentally and analytically investigated the separation and reattachment points for a large number of velocity ratios. Becker et al. (16) related the momentum parameter to the statistical location of the "eye" and upstream edge of the recirculation eddy.

Because the very near jet region of a co-flowing system may be compared analytically to that of a free jet (14), a review of some free jet investigation is appropriate. Some of the earliest work in the structure of free jets was contributed by Anderson (16,17). Primary investigations were in vortex shedding frequencies (Pheifen tones) of free jets. By using a CO<sub>2</sub> sharp edge jet and shadow graph technique, Anderson was able to show the downstream movement and coalescing at the vortex rings to different Reynolds numbers. Becker and Massara (18), using an acoustically excited air jet (with nozzle), investigated the vortex evolution over a large range of Reynolds numbers. Crow and Champagne (19) also studied vortex shedding, which they called the orderly structure of turbulent jets. By using acoustic forcing, it was found that maximum resonance occurred at a Strouhal number of 0.3, the Strouhal number being based on the frequency at the vortex, the exit velocity of the jet and the jet diameter. Later, Chan (20) expanded this work by taking axial and radial measurements of pressure variations,

in an acoustically excited jet. Using normalized coordinates, agreement of the pressure variations for different axial and radial positions was obtained. Gibson (21) used hot wire techniques to obtain turbulent spectra for round jets and found the spectra to follow the Kolmogorov theory ( $-5/3$  slope) over two decades.

Up to this point, all information related to the selected flow model has dealt with injection of a pure solvent. In order to make comparisons of an injection of a dilute polymer solution to that of a pure solvent, some review of previous polymer investigations should be instigated. An excellent starting place for understanding polymer studies may be found in a review paper by Hoyt (22). In this review, a short history of the drag reducing phenomenon is given. Toms (23), although the first to attribute the reduction in pipe flow driving pressure to an altered wall effect, was not the first to notice the drag reduction phenomenon. During World War II, the flow characteristics of thickened gasoline were under study. In turbulent flow, the pressure loss per unit length of pipe was found to be less for the thickened gasoline than for the pure gasoline. This effect was explained as a result of shear dependent viscosity (non-Newtonian behavior). In 1959 the thesis works of R. G. Shaver (24) and D. W. Dodge (25) were published. Both works noticed that some non-Newtonian fluids showed lower than expected friction factors. Shaver and Merrill, using flow visualization found that, in solutions of sodium carboxymethyl cellulose, the turbulence appeared to be much lower compared to similar non-polymer flow. Also during this time, oil companies discovered that certain gums used

to suspend sand in sand-water mixtures, caused a decrease in friction. Not long after that, the Navy became active in drag reduction research. The Navy's first major contribution came through the work of A. G. Fabula (26). Fabula identified a very effective friction reducing polymer, polyethylene oxide, only a few parts per million by weight is needed by effective drag reduction. Until about 1963, this information was available to theologians, chemical engineers and oil field technologists. Then in 1963 the phenomenon was introduced to the hydrodynamicists. Since then, there has been a wealth of material published on the subject.

At this point, a brief description of an effective polymer is in order. To be effective in drag reduction, the polymer must be at high molecular weight and long chained in structure. (The flow field must be turbulent.) Several substances fill these requirements. Some of them are Guar Gum, Poly (ethylene oxide), Polyacrylamide, and Sodium carboxymethylcellulose. Each of these polymers is composed of many sub units which are joined to form the necessary long chained high molecular weight molecule.

Lumley (27) presents several criteria concerning effective drag reduction. These criteria are:

1. A high molecular weight is necessary. As molecular weight increases, effectiveness increases.
2. Linearity and flexibility are beneficial. Molecules with few branches are most effective (See also Frommer et al. (28)).
3. Maximum drag reduction occurs at concentrations which in uniform distributions give little chance for the polymer molecules to be contact.

4. The effect occurs when the smallest turbulence length scales are approximately two orders of magnitude larger than the root mean square of the molecule diameter.

5. The effect occurs first when the predicted time scale of the polymer solution (based on dilute solution statistical mechanics) is approximately the same as the smallest turbulent time scale of the flow.

6. The polymer causes a "non-Newtonian effect." Solutions display resistance to surface tension, leading to speculation at intense straining in the shear layer.

After its introduction to the hydrodynamicists, the majority of research in drag reduction dealt with pipe flow. Wells and Spangler (29) showed that drag reduction in turbulent pipe flow is due to polymer effect at the wall. This was accomplished by injecting a polymer solution into a pure solvent turbulent pipe flow. The polymer solution was injected into two regions; 1) along the wall and 2) along the centerline. No noticeable drag reduction was seen in the second case (based on pressure drop) until the polymer solution mixed and reached the wall. The first case showed immediate reduction in drag.

This work was later substantiated by Walters and Wells (30). In their investigation the polymer solution was injected through a porous wall into the turbulent field. Detailed velocity and concentration profiles were made. The results indicated that the increase in the thickness of the viscous sublayer is accompanied by an increase in diffusion sublayer thickness for a uniform injection of polymer. The experiments also included the injection of polymer along the wall. The results

showed that this type of injection was more effective at drag reduction, than the porous wall injection. Both experiments, however showed that the drag reduction phenomenon occurs at the wall and that some form of viscous sublayer increase is indicated.

Lumley (27) used an expansion of Reynolds theory for shear flow (and experimental evidence) to argue that the effect of the polymer occurs only in the viscous sublayer and is possibly due to the "memory" of the fluid (visco elasticity). The law of the wall is shown to apply for non Newtonian as well as Newtonian fluids. In drag reduction, there is an increase in flow rate within the tube at a constant wall shear stress, indicating a necessary change in the viscous sublayer. As flow rate increases in non polymer (Newtonian) cases the viscous sublayer decreases. The energy is dissipated in the most efficient way. This is believed to be counter rotating vortex pairs with their planes and circulation tipped normal to the direction of maximum strain rate. In the non Newtonian (polymer) case the same mechanism is believed to apply. The polymer solution, however, resists simple shearing motions causing the vortices to be larger and extract energy more efficiently. This increase in vortex size leads to an increase in viscous sublayer thickness.

On the molecular level Lumley postulates a flow field change due to the distortion of the equilibrium configuration of the long chained polymer. At equilibrium the molecule is essentially spherical. When in the shear field of the vortices of the viscous sublayer, the molecule is stretched and entangles with other molecules. The resulting entanglements resist the streamwise vortices causing an increase in size of the

viscous sublayer vortices.

Fortuna and Hanratty (31) obtained measurements of the average velocity gradient and the root mean square values of the gradient fluctuations at the wall. Intensities and energy spectra of the fluctuations were also obtained. Based on this information, Fortuna and Hanratty suggest an increase in the size of the counter rotating vortices of the viscous sublayer upon the addition of a drag reducing polymer to the fluid. This is consistent with the results reported by Lumley. Both studies represent the idea of alignment of molecular coils in the vortex field.

Virk (32) presents a variation in the description of this effect. Based on velocity profiles, a three zone model of the polymer solution profile is developed. Moving outward from the wall is the usual viscous sublayer. From the axis inward is the Newtonian plug region where the velocity profile is shifted upward but parallel to the Newtonian law of the wall. Virk hypothesizes a third, elastic sublayer located between the viscous sublayer and the Newtonian plug region. The elastic sublayer is believed to follow the ultimate profile which is obtained at maximum drag reduction. That is, the elastic sublayer grows as drag reduction increases, until at maximum drag reduction, the elastic sublayer provides the entire cross section. Virk also states that the polymer retards the radial turbulent transport by decoupling the axial flow field rather than by reducing the turbulent effects. No mechanism is given on the molecular level but the model seems to agree with experimental results.

Turbulent pipe flow is not the only flow field to be influenced by

the advent of drag reducing polymers. Several investigations have been concerned with variations in free jet spreading due to polymer interaction. Gadd (33) injected a polymer solution into a like medium. In his study, he presented polymer degradation, viscoelastic relationships and eddy decay. Through flow visualization he showed the jet as having a smaller spreading angle than a pure solvent case of same Reynolds number. D. A. White (34) investigated the free jet problem using a recirculating system. Guar Gum, Hydroxyethyl cellulose (HEC) and Polyox P301 were used. The Guar Gum and HEC solutions show no change in jet expansion. Polyox, however, exhibited an increase in jet expansion. The increase was believed to be the result of increased entrainment due to increased turbulence.

Increased jet expansion was also described by Vlasar et al. (35). Using a Laser Doppler Anemometer (LDA), centerline velocities and turbulent intensities were acquired. The centerline decay of velocity was greater for the polymer solution than for the pure solvent. This suggests an increase in jet spreading. Also using LDA techniques, Barker (36) studied free jet (polymer) expansion. Using a jet nozzle no effect of the polymer was seen. When a fully developed pipe flow was used instead of the nozzle, an increase in jet spreading was observed. Barker attributes the difference between the effect of the jet nozzle and turbulent pipe flow to a change in exit conditions. All these works support the idea that no effect of the polymer is seen until there is a high shear-rate region.

A. A. Bore et al. (37) first suggested the use of drag reducing

polymers in radiopaque dyes as a possible means of reducing the high driving pressures needed in some angiographic injections. Menon (38) presented a study of a jet exiting into a co-axial, co-flowing stream. The work was motivated by angiographic injection possibilities. The injections were made with a co-axial jet exiting into a non recirculating co-flowing turbulent stream of like fluid. Three cases were considered. They are: 1) water injections, 2) polymer solution injections at same driving pressures and 3) water injections to match flow rates found in case (2) (increased flow rate due to drag reduction). The following results were reported:

1) Since the flow was non recirculating, the momentum of the jet did not greatly alter the flow near the wall.

2) Due to the finite thickness of the catheter, a wake is produced. This is seen as a sharp spike in the energy spectra immediately downstream of the jet.

3) Drag reduction is seen in the system.

4) The polymer solution exhibits a more rapid decay of centerline velocities than the pure water case.

5) The polymer influence is exhibited primarily in the region from the centerline to the mixing layer of the developing region.

6) Polymer effects are negligible at distances greater than 10 diameters downstream.

7) Polymer shows higher energy content in the large scale eddies of the developing region.

Menon's research is perhaps the first study to present evidence of polymer effects in the mixing region of a jet. Up to this time, major

emphasis has been on the effects of the polymer in the region near the wall. Barker (36) relates the change in jet expansion to changed exit plane conditions. No mention is made about the mixing region. Menon's work is, therefore, important in that it opens research in the effects of drag reducing polymers on the jet mixing region.

There are, however, several limitations which have been placed on the medical applications at Menon's research. Because it was the initial study of its type, high Reynolds numbers were used. The model took the form of a turbulent jet exiting into a turbulent outer flow region. Because a hot film probe was used, other restrictions were placed on the model. Since the probe calibration is dependent on the fluid properties, injections had to be made into like fluids. The probe is also subject to flow direction errors. For this reason recirculation regions could not be considered. As a result, the flow model was restricted to the injection of like fluids at high Reynolds numbers with no recirculation.

In angiographic injection of the flow rates are seldom turbulent. Injection flows may range from laminar to turbulent in nature. Recirculation is, therefore, a distinct possibility. The present study is designed to more closely model the flow conditions produced in clinical applications. The use of a Laser-Doppler Anemometer lifts the restrictions at like fluid injections and no recirculation. The model may then be described as a co-axial turbulent jet exiting into a laminar co-flowing stream. The use of the LDA system permits the study of recirculation regions and injections of polymer solutions into a co-flowing solvent. The objectives of this investigation are:

- 1) To provide an experimental model which closely approximates clinical angiographic procedures.
- 2) To study the modelled procedure as an injection of a solvent into a co-flowing like fluid with recirculation.
- 3) To also study the case in which the injectant is now a dilute polymer solution.
- 4) To obtain information on the differences in the resulting flow conditions for both injections.
- 5) To provide a description of the fluid dynamics of an angiographic injection and to determine the usefulness of long-chained drag reducing polymers in improving this procedure.

## CHAPTER II

## PRELIMINARY INVESTIGATION

As with any experimental investigation a certain amount of preliminary work is required. This chapter deals with the development of the flow model and the testing of the polymer parameters. Also included is some discussion of the early photographic and experimental results which lead to the final model configuration.

Development of the Flow Model

An exact model of an angiographic injection would be virtually impossible. The flow field is extremely complex. The catheter is not usually precisely parallel with the vessel wall and upon injection, the high momentum flux of the jet may cause violent motion of the catheter, a phenomenon known as catheter whip. To complicate matters the blood vasculature is not simple or consistent in physical properties. Arterial walls are flexible, yet not entirely elastic. The lumen, although circular in nature, is not truly circular. The entire system is a network of various angles and sizes along with numerous branches. At the injection site several of these physical properties may be neglected. There still remains, however, the problem of pulsatile flow. Because the flow is so complex, a simplified model must be devised. To obtain useful information, while still controlling the number of variables, the following restrictions were placed on the model:

- 1) Rigid walled tubing will be used for both the catheter and vessel model.
- 2) The flow will be modelled as being steady.
- 3) The catheter will be concentrically mounted in the flow to take advantage of axisymmetric considerations.

These restrictions reduce the problem to that of a confined jet exiting into a co-axial co-flowing stream. Although simplified, the model still maintains the basic flow geometry and flow conditions likely to be found in an angiographic. Because the basic similarities are maintained, useful information concerning the angiographic injection process may be expected.

At this point, it is necessary to obtain the similarity parameters which will make the model a relatively accurate representation of certain angiographic injections. For this study, the similarity parameters which will be used are the Reynolds number and Craya-Cuatet number at the catheter flow and the blood flow. The Reynolds number is expressed as:

$$Re = \frac{\rho UD}{\mu}$$

where  $\rho$  is the density of the fluid,  $\mu$  is the viscosity,  $U$  is the mean velocity of the flow and  $D$  is the diameter of the vessel. The second parameter is based on the ratio of momenta at the inner and outer flows. This may be expressed as (30)

$$C_t = \left[ \frac{M_o U_o}{M_c U_c - U_o} \right]^{1/2}$$

where  $M_o$  and  $M_c$  are the mass flow rates at the outer flow and the catheter flow, respectively; and  $U_o$  and  $U_c$  are the respective mean velocities.

#### Catheter or Injection Reynolds Numbers

The Reynolds numbers for angiograph injections are based on the catheter size used, the type of contrast agent injected and the rate of injection of this agent. Typical catheters employed in carotid angiography are of French size 6.0 and 7.0. The P6.0 catheter has an outside diameter of 2.00 mm and a lumen diameter of 1.19 mm. The P7.0 catheter has an outside diameter of 2.34 mm and lumen diameter of 1.27 mm (40). In the case of a percutaneous injection, an 18 gauge, thin walled, needle is used having a lumen diameter of 1.07 mm.

Several types of contrast agents are presently in use. For this model, the fluid properties of Renografin 76 and Renografin 60 were utilized. Renografin 60 has a viscosity ( $\mu$ ) at 4.0 cp at 37° centigrade and a density ( $\rho$ ) of 1.35 g/ml of 25° centigrade. Renografin 76 has a viscosity of 8.4 cp at 37°C and a density of 1.42 g/ml of 25°C (41). Before injection these contrast agents are usually heated to body temperature (approximately 37°C). Since variations in temperature have a negligible effect on the density of the agents, the value at 25°C is used in the Reynolds number calculations.

Rates of injection may vary considerably depending on the region under study and upon the personal preference of the operator. Injection rates of as high as 24 cc/sec have been reported in brachial arteriograms (42) Feild, et al. In cerebral studies, injection rates may vary from 8 to 10 cc/sec.

From the information given, Table 1 was computed. The mean velocity  $\bar{U}$  is based on the geometry of the catheter and the injection rates. The velocity,  $U_{\max}$  is based on Hagen-Poiseuille flow for Reynolds number less than 2500 and the  $1/\eta$  power law for Reynolds number greater than 2500. Although injection rates of 20 cc/sec are not usually used in cerebral angiography, rates this high have been used in peripheral angiography and for this reason such a rate should be included in the flow modeling. Because of the importance of turbulence on jet mixing the flow model shall be concerned with Reynolds numbers representative of turbulent flow.

Table 1. Possible Injection Reynolds Numbers

Contrast Agent	Catheter Size (cm)	Injection Rate (cc/sec)	$\bar{U}$	$U_{\max}$	Reynolds #
Renografin 76	.127	8	630	1260	1350
Renografin 76	.119	8	720	1440	1450
Renografin 76	.127	10	790	1580	1700
Renografin 76	.119	10	900	1800	1800
Renografin 60	.127	8	630	790	2700
Renografin 60	.119	8	720	900	2900
Renografin 60	.127	10	790	990	3400
Renografin 60	.119	10	900	1120	3600
Renografin 76	.127	20 *	1580	1970	3400
Renografin 76	.119	20 *	1800	2250	3600
Renografin 60	.127	20 *	1590	1970	6800
Renografin 60	.119	20 *	1800	2250	7400

\* Within the realm of peripheral angiography.

### Arterial Reynolds Numbers

Initial values for the Reynolds numbers possible in arterial flow are based on results obtained from animal studies at St. Joseph's Infirmary in Atlanta, Georgia. In these experiments, the thoracic aorta of a mongrel dog (approximately 40-50 lbs) was exposed. Measurements of mean flow rate were made using an electromagnetic flowmeter. Velocity profiles were obtained using a hot film probe. The traversing mechanism which supported the hot film probe was used to ascertain the lumen diameter of the vessel. This was accomplished by moving the hot film probe from one side of the vessel to the other. The total distance traversed in the vessel diameter, the mean flow rate was measured to be approximately 40 cc/sec with velocities varying from 10 cm/sec to 60 cm/sec (diastolic and systolic, respectively). The diameter of the aorta varied from 1.2 to 1.5 cm.

In the human, cardiac output varies from 330 cc/sec under extreme stress to 100 cc/sec of rest. This, plus the fact that the arterial lumen diameter variation 2.5-0.4 cms, allows for a wide variation of velocity throughout the vasculature, with the exception of flow to the brain. The mean arterial velocity varies from 40 to a few cm/sec depending on the location in the arterial tree. The larger arteries have, on the average a mean flow rate of, approximately 40 to 30 cc/sec, while the mean velocity in the arteries and capillaries drops from 20 to less than 4 cm/sec (43).

The flow rate to the brain is constant at approximately 750 cc/min (43). The majority of flow to the brain is via the carotid arteries.

In a healthy carotid, the approximate flow rate is 335 cc/min; with the flow diminishing to values of 100 cc/min or lower in subtotal atherosclerotic stenosis (44). Complete blockage may occur resulting in, of course, zero flow rate. The lumen diameter of a healthy common carotid artery approximately 0.7 to 1.0 cm. From this information, the mean velocity may vary from  $14\mu$  to  $28\mu$  cm/sec in a healthy carotid and from  $4\mu$  to  $8\mu$  cm/sec in the proximal region of a diseased carotid.

The density of blood is approximately  $1.06 \text{ gm/cm}^3$  (45). The viscosity of blood is, however, dependent on shear rate (if blood is non-Newtonian in nature). At high shear rates and  $37^\circ\text{C}$  the viscosity approaches a constant value of approximately 3.5 - 4.0 cp (dependent, in part, on the hematocrit). The non-Newtonian behavior is attributed to rouleaux formation at low shear rates. Rouleaux are aggregates of red blood cells forming chain-like structures. In most cases involving arterial flows the non-Newtonian behavior is minimal and the blood may be approximated as being Newtonian (for further explanation see Appendix IV).

Table 2 gives values of arterial Reynolds numbers which might be encountered in conjunction with angiographic injections. These were calculated using the representative flow rates and vessel diameters previously described and assuming that blood is a Newtonian fluid with a viscosity of 4.0 centipoise and a density of  $1.06 \text{ grams/cm}^3$ .

Table 2 indicates Reynolds numbers varying from laminar to just turbulent, based on a steady flow assumption. Turbulent flow regions can be realized in partially occluded vessels, and bifurcations but for the most part the arterial blood flow seldom becomes turbulent. For

purposes of experimentation and because of its central location in the range of Reynolds numbers possible, a Reynolds number of 1000 was chosen as representative of the outer flow similarity parameter.

#### Momentum Ratios

From the information provided in Tables 1 and 2 along with the fluid properties for blood and the contrast media, the corresponding Craya-Curtet numbers were calculated. The flow conditions corresponding to peripheral angiography (i.e. large vessels) produced values of  $C_T$  ranging from 1.0 to 0.3. Flow conditions corresponding to smaller vessel studies (e.g. carotid angiography) produced values of  $C_T$  ranging from 0.2 to 0.8. In both cases the  $C_T$  values are low enough to represent flows capable of producing a region of recirculation. In general, the values of  $C_T$  corresponding to an angiographic injection may vary from 1.5 to 0.05 depending on the specific procedure (i.e. injection site, contrast medium and injection rate). The final selection of the flow parameters for use in the flow facility should be based on these values as well as the Reynolds numbers.

Table 2. Possible Reynolds Numbers

Found in Arteries

Lumen Diameter	Mean Velocity	Reynolds Number
2.5 cm	40 cm/sec	2500
1.5 cm	25 cm/sec	938
1.0 cm	20 cm/sec	500
.5 cm	28 cm/sec	350
.7 cm	14.5 cm/sec	254
.5 cm	14.5 cm/sec	181

### Polymer Considerations

Development of the flow model must also consider any restrictions which may be incurred when using a long-chained drag reducing polymer. The polymer chosen for this investigation was Separan AP 30 (a poly acrylamide). Poly acrylamides in general have been shown to be excellent drag reducing polymers. They are strong enough to withstand high shear rates, easily dissolved in water and highly effective in low centerlines (22). The polymer was found to be effective over a wide range of concentrations, the most effective range being from 50 to 100 ppm. Because of the scope of this work, several injections had to be made in order to cover the various axial and radial positions presented. This required the preparation of several polymer solutions. To maintain accuracy when switching from one solution to the next, the effectiveness of the polymer solution was tested for each case.

The polymer tests were made under those conditions. All the tests were accomplished with the apparatus described in Chapter III. In each test, a sample of the polymer solution was removed from the flow system. The pressures required to expel the sample at rates of 20, 30, 40 and 45 cc/sec were compared with the pressures required to expel water at the same rates. The percentage of drag reduction (or effectiveness) was then calculated from the equation:

$$\% \text{ Reduction} = (1 - P_p/P_w) \times 100 ,$$

where  $P_p$  is the pressure required to expel the polymer solution and  $P_w$  is the comparable driving pressure for water.

In the first test the polymer solution is removed after leaving the holding but, before entering the catheter. The effectiveness is then calculated for the above mentioned flow rates. In the second test the polymer is pumped as quickly as possible through the system up to the a point just before the entrance to the catheter. In this way the maximum drag reduction before entry into the catheter is determined. The effectiveness is then measured at the various flow rates. Finally, the polymer is allowed to pass through the system where it is mixed with the outer flow of water. The system is allowed to operate at the flow model conditions until a representation sample of the mixture (injectant and outer fluid) is collected in the downstream reservoir. This downstream mixture is then tested for drag reducing effectiveness. This last test is perhaps the most important in that the total effect of the system on the polymer effectiveness may be determined including the reduced concentration due to dilution.

Over the period of these investigations several polymer solutions were prepared and tested. In each series of tests the overall polymer effectiveness varied from the mean by  $\pm 10\%$  or less. Maximum effectiveness was exhibited with the sample taken before entering the system. At 45 cc/sec the percent drag reduction was determined to be approximately 50% while a 40% reduction in drag was seen at 20 cc/sec. The downstream mixture exhibited an effectiveness of 40% at 45 cc/sec and 30% at 20 cc/sec, which was excellent for the now 25 ppm dilution. These tests provided assurance that the polymer solutions used were essentially the same and the results obtained would, therefore, have a high degree of reliability.

When a polymer is mixed with water, slight changes in viscosity may occur. This effect was also tested. By measuring the efflux time of a polymer solution versus the efflux time of water, a relative viscosity term was determined. The relative viscosities were found to be "approximately 1.03 for a 25 ppm solution, 1.13 for a 50 ppm solution and 1.37 for 100 ppm. In order to directly compare the injection of polymer solutions and of water, it is advisable to maintain momentum flux as well as Reynolds number. Since maximum effectiveness of the polymer was found to be in the range of 50 to 100 ppm and since the change in viscosity was much less for a 50 ppm solution than a 100 ppm solution, the most acceptable polymer solution was found to have a concentration near 50 ppm. For these reasons the injection of a 50 ppm solution of Separan AP30 was compared to the injection of water. All other parameters (flow rate, temperature and vessel sizes were held constant).

#### Flow Model Summary

In summary, the angiographic injection process is modelled as a co-axial jet exiting into a confined co-flowing stream. The co-flowing (or outer) stream has a Reynolds number of 1000. The jet (or inner) flow should have a Reynolds number which is representative of turbulent flow. Comparisons of pure solvent to dilute polymer solutions are to be made with a 50 ppm solution at Separan AP30.

#### Initial Flow Facility

The initial flow facility was designed to produce Reynolds numbers which correspond to those found in the arterial system and angiographic injections. Since the angiographic injection is to be modeled as a

concentrically mounted jet exiting into a confined co-flowing shear, such a system was constructed. The overall configuration is shown in Figure 1. A glass tube of 0.7 cm OD, .46 cm ID, 100 cm long is used to model the catheter, while the vessel is modeled by using a 223 cm long, 2.8 cm ID glass tube. The catheter is cantilevered from an adjustable ball point. The ball point can be moved up and down as well as rotated. This allows a variety of catheter positions, although in this investigation the catheter is centrally located.

The system itself is of a recirculating nature. Pumps are provided to deliver both the inner and outer flows. Flow rates are monitored by mechanical flow meters. The water feeding the outer flow enters the inlet box (A) and then proceeds through the outer flow tube to the constant bend, downstream reservoir (B). The catheter is fed directly from the pump. The water then mixes with the outer flow and travels to the downstream reservoir. It then travels from the overflow to the line which feeds the pumps (C) and the process is repeated. Temperature is monitored in the downstream reservoir; and when the temperature exceeds the set tolerance ( $23^{\circ}\text{C} \pm 1^{\circ}\text{C}$ ), sufficient water is replaced with cooler water to bring the temperature back within the specified limits. In experiments involving the LDA system, the water is seeded with silicon carbide particles (typically, 1.5 microns in diameter). For flow visualizations ink is injected into the line feeding the catheter flow. The total volume of water is changed frequently to minimize clouding of the recirculated flow with ink.

For polymer studies the model is basically the same. Since the polymer can be degraded by high shear rates, an electromagnetic flow

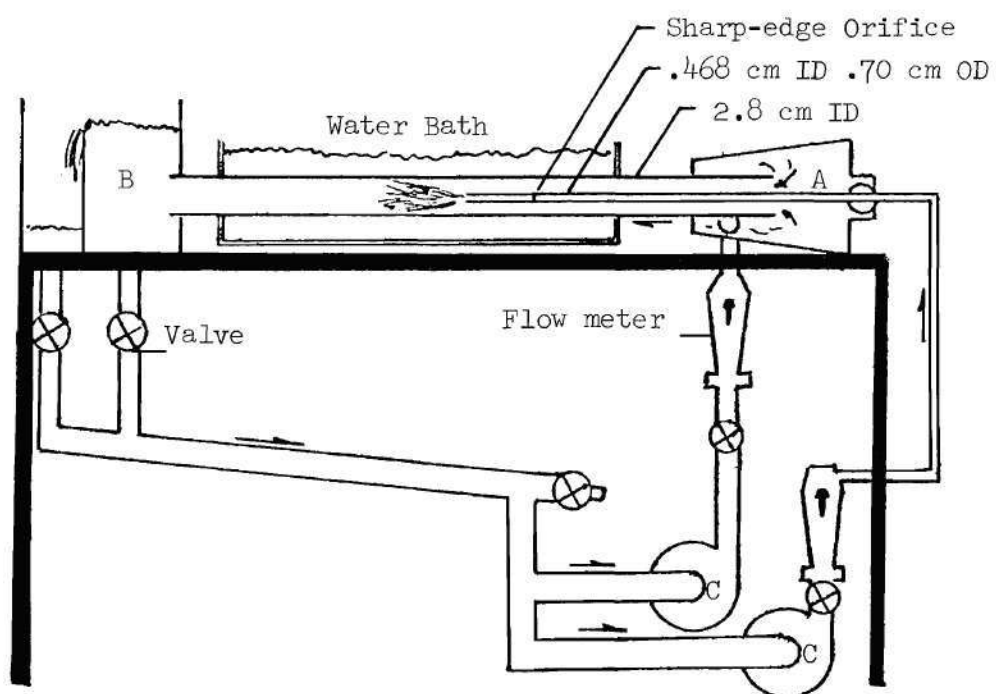


Figure 1. Flow Model - Recirculating System.

meter rather than the mechanical flow meter is employed to monitor the catheter flow rate. Also, to prevent recirculation of the mixture, a blowdown system as shown in Figure 2 must be utilized. Water feeding the outer flow enters the inlet box (A) from pumps (G) and (H) which are fed by a constant head upstream reservoir (D) and in later applications a seeding tank (E). The flow passes on to the downstream reservoir (D), and then to the drain (C). The catheter flow is fed by a 200 gal. polymer solution holding tank (F). The polymer solution passes through a booster pump, through the electromagnetic flow meter and on to the catheter. Flow rate is controlled by a compression clamp on the line feeding the catheter. The polymer exits into the outer flow where the two flows mix and then travel to the drain. For lower applications, the entire polymer solution is seeded prior to the experiment. For flow visualization ink was injected into the line feeding the jet.

#### Photographic Investigation

Photographs of the jet expansion were obtained at a variety of jet (or catheter) Reynolds numbers. In all investigations the outer Reynolds number was held constant at 1000. Photographs were made over a range of inner Reynolds numbers, with and without the presence of the drag reducing polymer. All photographs were printed on high contrast paper for maximum delineation of the flow characteristics. The arrangement of the photographic equipment is shown in Figure 3.

A single lens reflex camera is utilized in conjunction with an electronic flash. As seen in Figure 3, the flash is employed to illuminate a white screen. Since the deviation of the flash is approximately

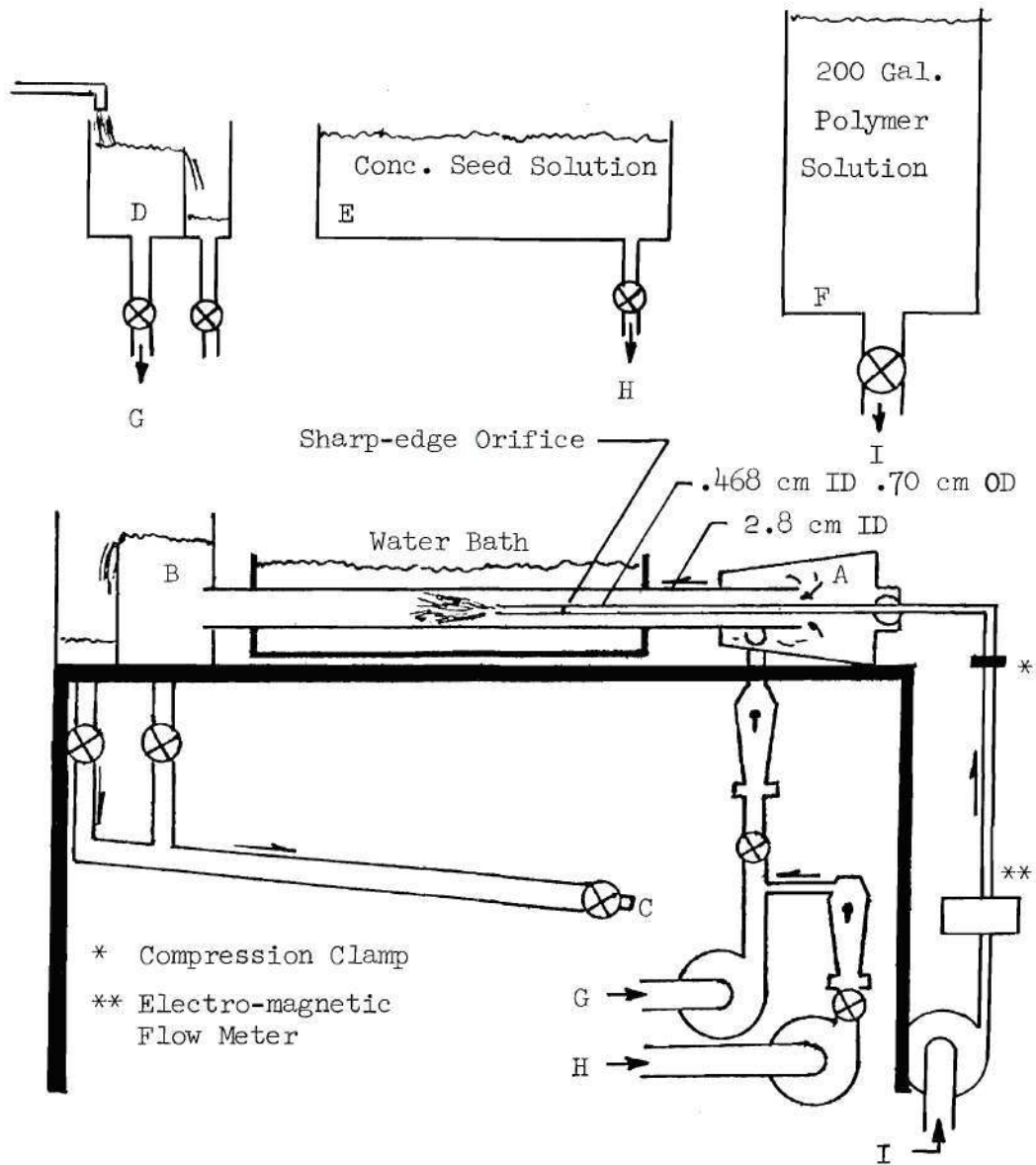
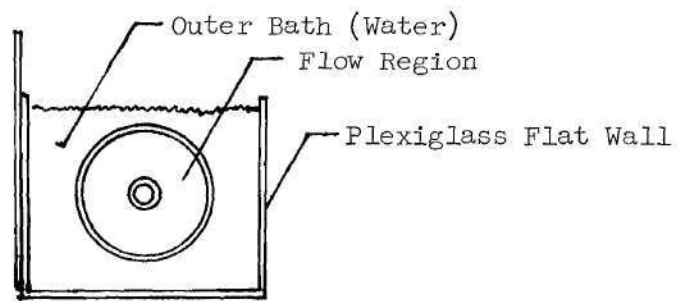
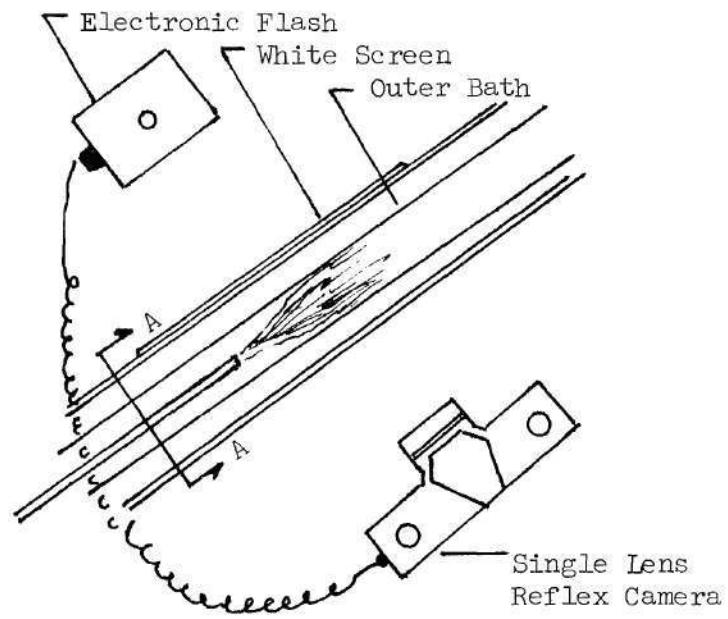


Figure 2. Flow Model - Blow Down System.



SECTION AA

Figure 3. Photographic Visualization.

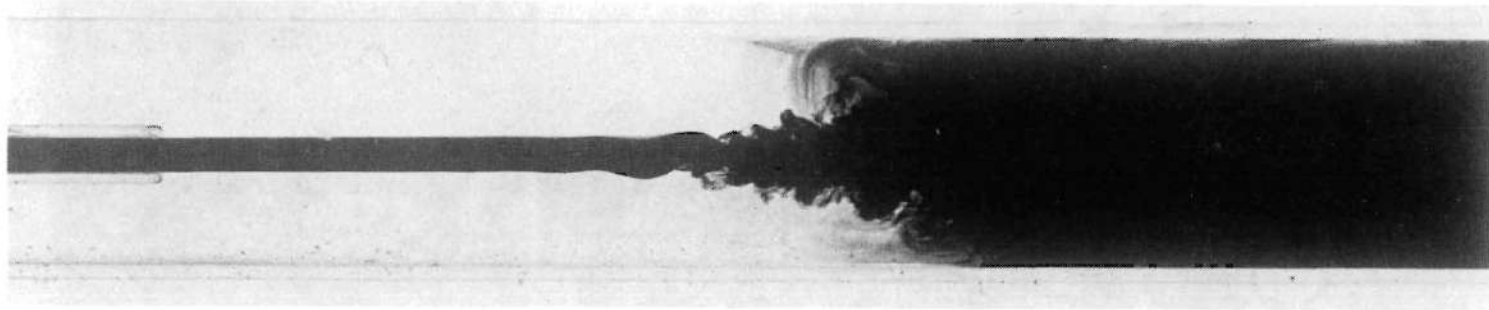
0.0001 second, a sharp "stop action" photograph can be obtained. In order that the jet be seen ink is added, by way of a syringe, to the inner flow. Since the flow is confined in a circular column, curvature effects tend to distort the image. To minimize this distortion, an outer water bath was employed. This greatly reduced the effect of curvature, and the resulting photographs were much more representative of the actual flow. From the photographic study, the final conditions for the flow model were obtained.

The information obtained from the series of photographs produced is highly qualitative, but extremely useful. At Reynolds numbers below 2500, the jet exited in an undisturbed stream which subsequently developed a helical instability. The jet appears to expand linearly once the instabilities begin to disintegrate into a smaller scale disorder. Figure 4 is a photograph of an injection with a Reynolds number of 2000. The helical instability is clearly visible. Measurements of the period of the instability along with the assumption of negligible expansion before the instability, enable an approximation of the frequency of the helix. The equations used are:

$$f = \frac{1}{T}$$

$$T = \frac{L}{U_{FR}}$$

where  $f$  is the frequency,  $T$  is the period,  $L$  is the length from peak to peak of the instability (measured from the photograph) and  $U_{FR}$  is the mean velocity based on catheter flow rate. For the injection in Figure 15 the frequency of the instability is approximately 37 Hertz. A Strouhal



Exit Plane	Helical Instability	Turbulent Expansion	

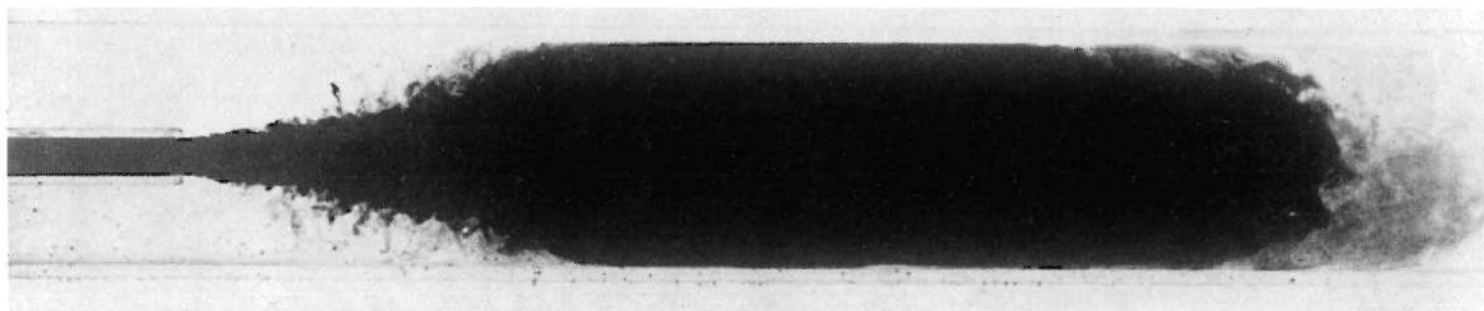
Figure 4. Injection of Water without BLT  $Re_c = 2000$ .

number ( $S_T$ ) based on the catheter diameter and the mean velocity of the catheter is found to be approximately .40, where

$$S_T = \frac{fD}{U_{FR}}$$

As the catheter flow rate increases the distance to the instability shortens and the region of turbulent mixing moves upstream. When the catheter Reynolds number exceeds transition the turbulent mixing region moves instantly from its downstream position to a new location near the exit plane. At this point the helical motion cannot be seen. There is, however, a short region of what appears to be undisturbed flow before the jet starts to expand. As the injection rate increases this region decreases in size. A possible explanation for the existence of this region may be due to the finite thickness of the catheter wall. This may result in a region of "dead water space" in which the velocity gradient is near zero (i.e. shear rate near zero). Before the turbulent mixing can occur, the velocity gradient must become high enough to produce shear rates necessary for turbulent mixing. As the Reynolds number increases and hence the velocity gradient near the catheter wall, less distance is required to overcome the effect of the catheter thickness. Also, as the Reynolds is increased the angle of expansion increases. For a catheter Reynolds number of 5000 the total included angle of spreading was approximately 186 degrees while a Reynolds number of 7000 produced a spreading angle of approximately 24 degrees. The case for a Reynolds number of 7000 is shown in Figure 5.

The photographs also disclose some information concerning the degree of turbulence in the mixing region, although this information is



\* |

Turbulent  
Expansion

|

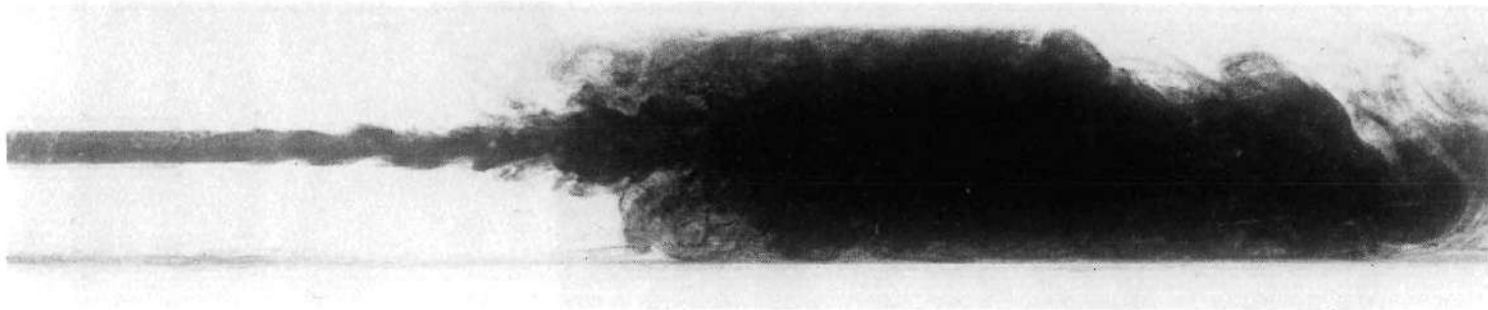
\* Exit Plane and Undisturbed Region

Figure 5. Injection of Water without BLT  $Re_c = 7000$ .

very qualitative and is actually only an indication of the intensity of the turbulence. Comparison of the mixing regions in the injections depicted in Figures 4 and 5 gives the impression of a larger scale of turbulence structure in the 2000 Reynolds number case than in the 7000 Reynolds number case. Integrals scale theory (46) suggests diminishing length scales for higher Reynolds numbers and although the photographs cannot produce the actual integral scale, the visible eddy size is an indication of the relative magnitude.

Next, a photographic study of the injection of a dilute polymer (50 ppm) solution was carried out. At low Reynolds numbers the polymer solution behaved essentially the same as the case for the water injectants. At a Reynolds number of approximately 2000 the frequency of the periodic instability was found to be approximately 31 Hertz with a resulting Strouhal number of approximately .34. The distance from the exit plane to the point of breakup occurred approximately 7 mm farther downstream for the polymer injection than for the water injection. This evidence tends to point to some form of damping section of the polymer.

The catheter Reynolds number was then increased to approximately 5000 (Figure 6). Although some delay in transition was expected (22), such an extensive suppression was surprising. Reynolds numbers in excess of 10,000 were required to produce what appeared to be turbulent jet mixing. At a Reynolds number of 5000, the resulting instability frequency and Strouhal number are calculated to be approximately 130 Hertz and .60. At a Reynolds number of 6500 the frequency was estimated at 210 Hertz with a Strouhal number of .71. It must be remembered that these values are only approximations and are provided to illustrate the



*	Helical Instability	Turbulent Expansion	* Exit Plane and Undisturbed Region
---	------------------------	------------------------	-------------------------------------

Figure 6. Injection of Polymer Solution without BLT  $Re_c = 4700$ .

effect of the polymer on the flow.

When inspecting the apparent eddy size there appears to be a noticeable difference in the turbulence structure produced by the polymer injection as opposed to the water injection for similar Reynolds numbers. The eddies produced in the polymer solution appear to be quite large compared to those of the water injections. This, again points out an effect of the long-chained polymer on the turbulent structure of a confined jet.

These photographs reveal dramatic effects of the polymer on the near field mixing region of the confined jet. For purposes of study, it was assumed that these may be divided into two categories: (i) effects of the polymer on the jet exit conditions which in turn affect the mixing and (ii) effects which occur exterior to the catheter and are due to altered rheological properties of the fluid. Clearly, these phenomena may be strongly coupled and a distinct separation is difficult in an experimental set-up. Within the scope of this research it was decided to concentrate on the near field region and thus try to achieve similar jet exit conditions for the water and polymer comparisons.

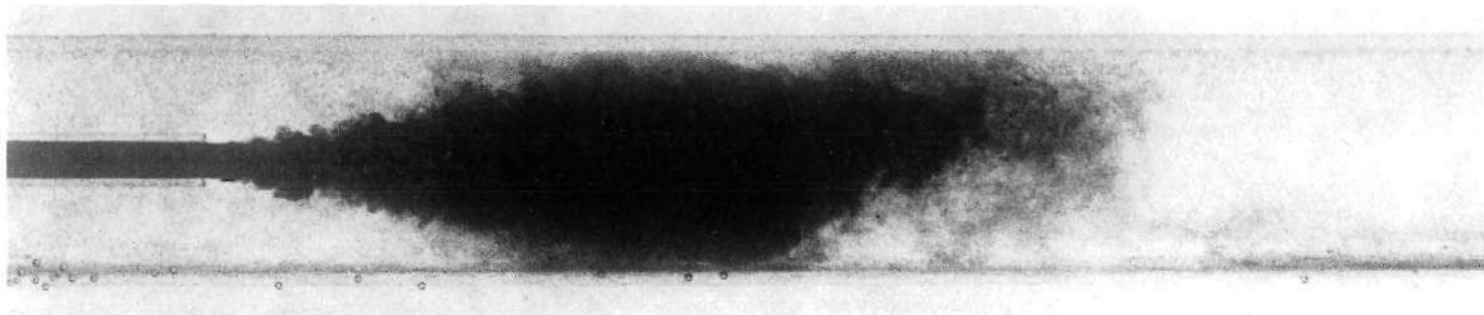
In order to move directly compare the polymer solution and water injections and yet stay within the range of physiological Reynolds numbers, the catheter flow had to be altered. This was accomplished by introducing a boundary layer trip (BLT) into the catheter. The BLT was a sharp-edge orifice placed 11.7 catheter diameter from the exit plane. The decrease in area was approximately 50% of the orifice. The BLT was employed to reduce the laminarizing effects of the polymer in the

catheter and yield similar exit conditions for the polymer and water injections. Thus, if both the polymer and water jets exit under similar turbulent conditions, it was expected that the dominant cause of any observed difference in the subsequent flow fields would be due to inherent effects of the polymer on the turbulence structure.

After insertion of the BLT a second series of photographs were produced with an injection Reynolds number of approximately 7000. The water injection did not appear to differ from the injection of water without the BLT. The polymer injection was greatly altered as can be seen in Figure 7. The jet now appears to behave more like a turbulent injection. By comparing Figure 5 and 7 it can be seen that polymer effects are still exhibited. In this case the gross spreading angle is determined to be approximately  $26^\circ$ , slightly larger than that for the water injection. Although not as pronounced as in the case without the BLT, the apparent eddy size was larger for the polymer solution than those found in either the water with or without the BLT.

It is emphasized that these observations are to be considered as only qualitative. Detailed measurements of the catheter conditions for the water and polymer injections will be presented subsequently. It will be shown there that, although the jet exit conditions are not identical for both cases, they are very similar. Thus, the BLT was deemed to be satisfactory for creating approximately the same turbulent exit conditions for both polymer and water flows.

Attempts were also made to employ the photographic technique to indicate the approximate upstream edge of the recirculation region. To



\*  
|  
|

Turbulent  
Expansion

|

\* Exit Plane and Undisturbed Region

Figure 7. Injection of Polymer Solution with BLT  $Re_c = 7000$ .

accomplish a visualization, the ink was allowed to enter the recirculation region before the photograph was taken. The resulting photographs provided the following information: for the water injections the most upstream part of the recirculation region was approximately .75 catheter diameter upstream of the exit plane; the polymer solution injection without the BLT was approximately 2.5 catheter diameters downstream of the exit plane and the polymer solution injection with the BLT was located at the exit plane.

Further attempts were made to obtain information from the photographs. In hopes of obtaining some information on concentration variations in the mixing region, an isodensitometer was utilized. Unfortunately, the quality control was not sufficient for meaningful comparisons. It is possible, however, that utilization of such a device with the proper photographic quality control could provide useful information on concentration profiles which would be of significant interest in angiographic injections.

A note of caution is necessary at this point. Although the photographic information suggests changes in mixing and perhaps increased spreading angle in the polymer solution injection with BLT, it should be remembered that the photographic information provided in this paper is at best qualitative. No strong conclusions should be based solely on the photographic evidence provided.

From the photographic investigation, it was concluded that for purposes of comparison, the flow model should incorporate the BLT. The Reynolds number chosen should be as high as possible without exceeding the physiological values computed earlier and the resulting Craya-Curtet

number ( $C_T$ ) should not be outside the range corresponding to angiographic procedures. The high value of Reynolds number is required to produce exit conditions which compare favorably. If the upper limit of 7000 is chosen the resulting Craya-Curtet number (.14 @ 23°C) falls within the range calculated for carotid investigations. Since a Reynolds number of 7000 would be more likely to produce similar exit conditions and, at the same time, closely correspond to the carotid investigations (via Craya-Curtet similarity), the catheter-flow was adjusted to produce such a value.

#### Final Flow Model

As a result of the investigation the final flow model was specified. It is designed to be a close approximation to an angiographic injection. The model is simplified to a concentric jet exiting into a confined co-flowing stream. The co-flowing stream Reynolds number of 1000 approximates a value which may occur in the human vasculature. The jet Reynolds number of 7000 approximates a value possible in an angiographic injection. The effect of a dilute polymer solution on the action of the jet is studied via the use of a 50 ppm solution of Separan AP30 as the jet fluid. Comparisons are made between a jet of water and a jet of dilute polymer solution. To facilitate comparisons at the relatively low Reynolds number of 7000 a boundary layer trip is introduced into the jet catheter. The model may, therefore, be restated as being a tripped concentric jet exiting into a confined co-flowing stream.

## CHAPTER III

### INSTRUMENTATION AND DATA REDUCTION

In this investigation, as with any experimental procedure, the instrumentation utilized is of great importance. The acquisition equipment in the present research may be subdivided into three groups, each dealing with a particular phase of the investigation: i) Data Acquisition Equipment, ii) Monitoring and Test Equipment, and iii) Data Reduction Equipment.

#### Data Acquisition Equipment

After the development of the model, acquisition of information concerning the flow field is necessary. Velocity measurements were made with a Laser Doppler Anemometer (LDA) system. The LDA has major advantages over other anemometers in that it is not dependent on the physical and thermodynamic properties of the fluid. It is, therefore, insensitive to changes in temperature, density, and mixing of unlike fluids. The LDA is also non-invasive and therefore non-interfering. These attributes make the study of injections of unlike fluids (e.g. polymer into solvent) possible. One drawback is the need for scattering particles in the flow. For the investigation silicon carbide particles of approximately 1.5 microns diameter were used. The LDA system used in this study was a DISA 55L Laser Doppler Anemometer Mark II. The system is composed of the following components:

1. Laser-Spectra Physics 120A with exciter.  
 $\lambda = 632.8 \text{ nm @ } 15 \text{ mW}$
2. Transducer - optics package
  - a. Beam splitter
  - b. Acousto - optic cell
  - c. Focusing lens
3. Photomultiplier with receiving lens
4. Doppler Signal Processor-Tracker
5. Range Translator.

The laser light is directed into the transducer and passes through a beam splitter. One of the resulting beams passes through an acousto-optic cell (Bragg cell) where the frequency is shifted by 40 mega Hertz (mHz). This shift in frequency allows measurement of both negative and positive velocity components. The second beam passes undisturbed through the optical unit. Both beams then proceed to a prism system where beam separations of 20, 40, and 80 mm may be selected. From there the beams pass through a focusing lens (12, 30, or 60 cm focal length). At the intersection of the beams an approximately ellipsoidal geometric sampling volume is produced. The size and shape of the sampling volume depend on the selected beam separation and the focal length of the lens. In this investigation, a 40 mm beam separation with a 12 cm lens was used. The resulting sampling volume in air is .12 mm by .72 mm. Because of differences in indices of refraction the sampling volume in water is approximately .12 mm by .96 mm. In this sampling, volume interferences fringes are established. As a scattering particle passes through the fringes the intensity of the light entering the photo multiplier is modulated.

This modulation corresponds to the shifted frequency (from the Bragg cell) minus the Doppler frequency,  $f_D$ . The velocity component being measured may be determined from the relationship,

$$v = f_D \lambda / 2 \sin(\theta/2)$$

where  $f_D$  is the Doppler frequency,  $\lambda$  is the wavelength of the laser light and  $\theta$  is the beam intersection angle.

To obtain  $f_D$ , the signal processor and range translator must be used. The signal from the photomultiplier is mixed with a signal from a local oscillator and the difference is fed into a preamplifier. The preamplified signal is then mixed with the output from a voltage controlled oscillator (VCO). The resulting output is kept centered in the middle of a narrow band pass filter by means of a fast servo loop that controls the VCO output. The output from the VCO is then subtracted from a set frequency (translator frequency). The resulting frequency is the Doppler frequency  $f_D$ . The Doppler frequency is then digitally processed and displayed as a mean velocity component. The Doppler frequency is also processed to give an analog output voltage which is proportional to  $f_D$  and thus the instantaneous velocity component (39,47). Further information may be found in Appendix II.

The laser system is arranged as shown in Figure 8. The sampling volume is moved via an x-y transversing table. Large axial displacements require movement of the table along the optical bench. As was the case with the flow visualization, an outer water bath is employed. The curvature effects are therefore minimized, increasing the signal to noise ratio of the receiving optics. Changes in sampling volume size, due to

change of medium, are shown schematically in Figure 9. A block diagram depicting the general operation of the LDA system is found in Figure 10.

#### Monitoring and Test Equipment

Consistent and repeatable experimentation depends largely on how well the flow is monitored. In this investigation, flow rate was of primary concern. For solvent into solvent studies, mechanical tube type flow meters were used to monitor the inner and outer flow rate. The flow meters are originally designed and calibrated for use with air at 14.7 psia and 70°F. Using the "bucket and stopwatch" method, these flowmeters were recalibrated for use with water. For the injection of a dilute polymer solution into the flow, a different type of flow meter is used. Since the long chain, drag reducing polymers are subject to degradation and loss of effectiveness in high shear regions, the inner or catheter flow rate was monitored by means of an electromagnetic flow meter (by Carolina Medical Electronics Incorporation Model 501) which was calibrated before each run by using the bucket and stopwatch method. Both types of flow meters were later used to check the accuracy of the LDA system. The velocity profile produced were integrated to provide flow rate values. Agreement was good considering the integration technique which was employed.

Other quantities were monitored besides flow rate. Temperature was recorded and held at 23°C ±1°. Doppler signal strength and instantaneous velocity were monitored using a dual trace oscilloscope and the LDA voltage out was read on a digital voltmeter.

When the drag reducing polymer is used, some method of testing the

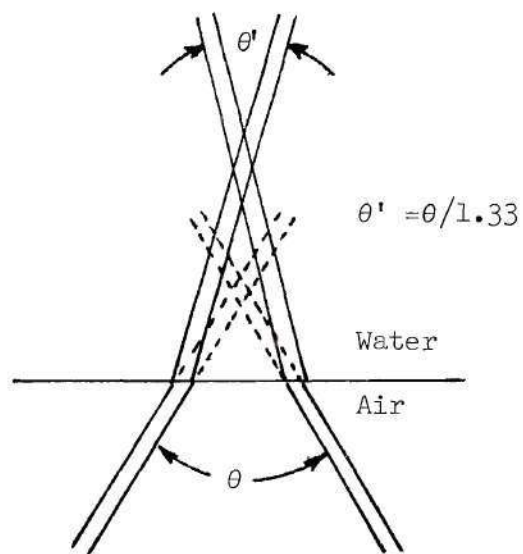
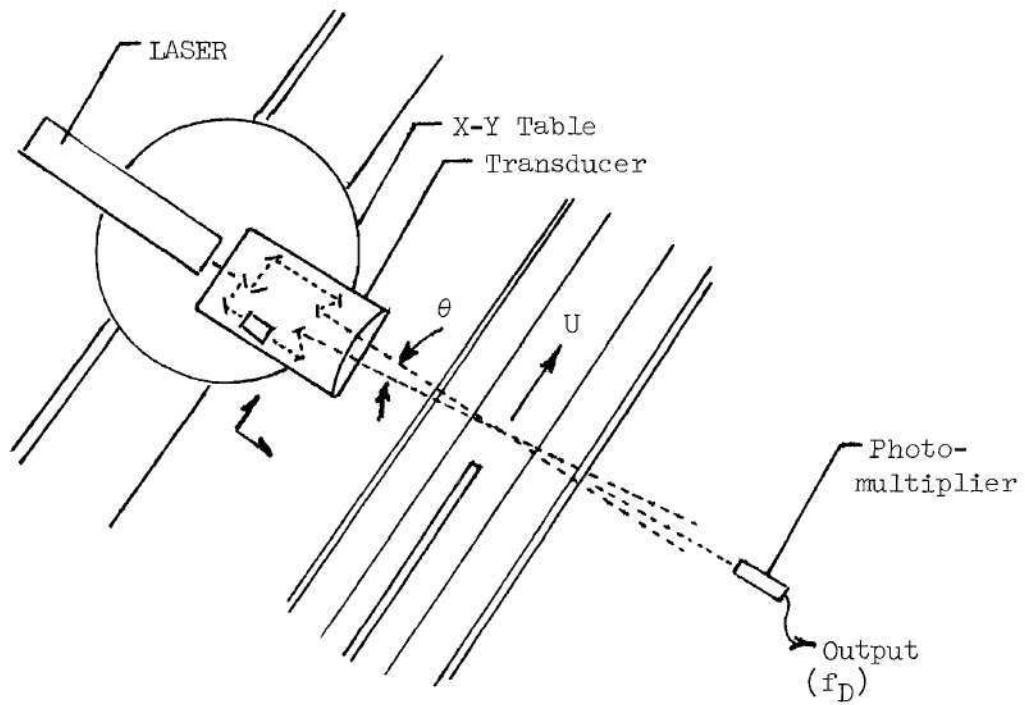


Table 9. Change in Sampling Volume Size due to Medium Change.

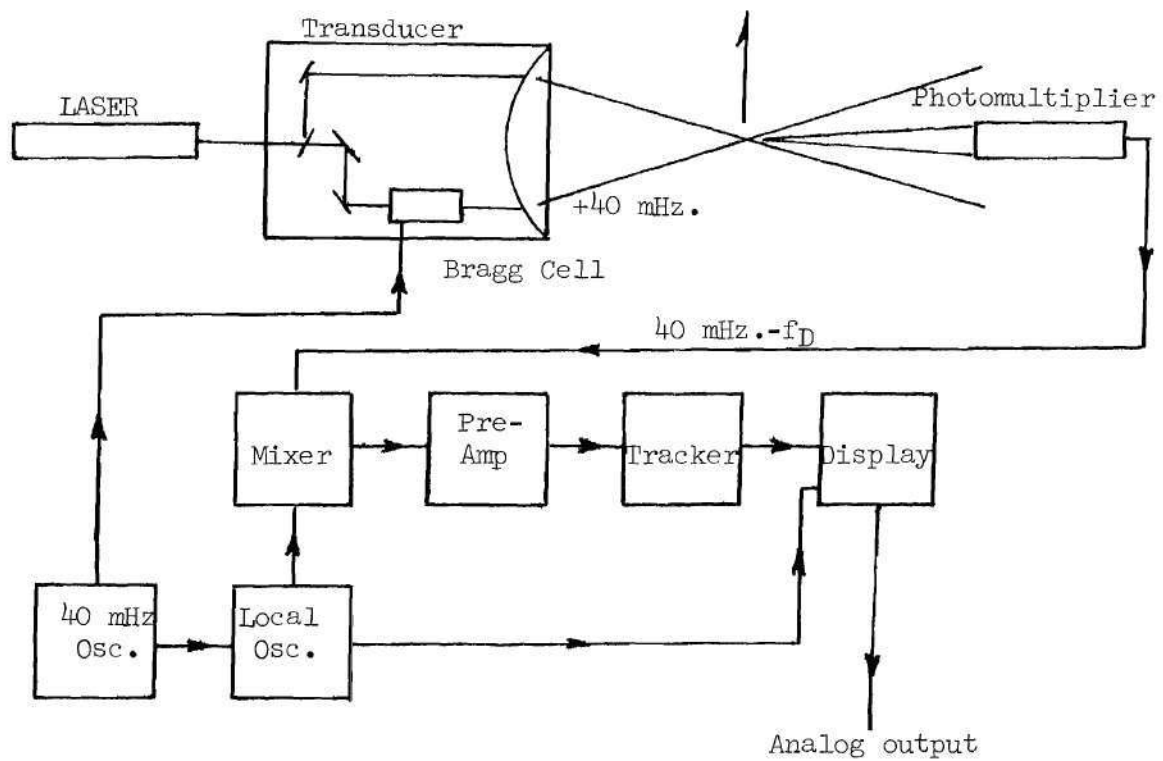


Figure 10. Block Diagram of LDA System.

effectiveness of the polymer solution is required. To accomplish this, a flow device was designed to measure the required driving pressure for a variety of flow rates. Comparisons were made of the pressure required for the polymer solution to that required for water at the same flow rates. The testing apparatus utilizes a VIAMONTE/HOBBS Injector model 2000 as a constant flow rate source and a Statham model P23 pressure transducer. A pressure tap is made at the upstream end of a long glass tube. The pressure required to drive the fluid of a set flow rate is recorded on a Hewlett-Packard strip chart recorder. Comparisons between water and polymer solution driving pressures are then made. The apparatus was calibrated with respect to flow rate by timing the piston travel. The pressure was calibrated by using a water column of known height. By determining the degree of reduction of necessary driving pressures, the effectiveness of the polymer solution was determined (see Chapter II, Polymer Considerations). The test apparatus is shown in Figure 11.

One last piece of test equipment should be described. Even though polymer concentrations are on the order of 50 ppm, viscosity may be changed appreciably. To test for a change in viscosity, a discharge flow system was devised. As seen in Figure 12, water or polymer solution is allowed to flow from a 100 ml reservoir through a small diameter catheter. Since the Reynolds number is so low polymer drag reduction effects are absent and the flow rate (or discharge time) is dependent on viscosity. By comparing discharge times of water and polymer solution at different concentrations, a relative viscosity may be obtained.

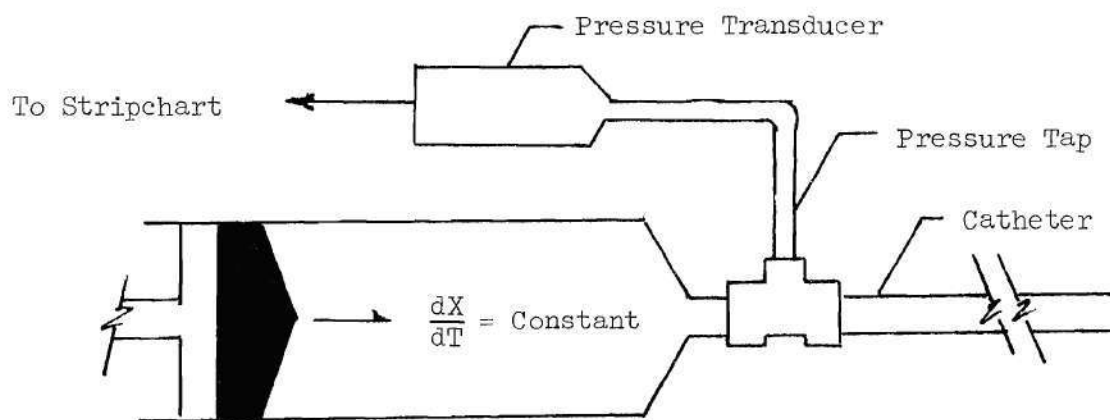


Figure 11. Polymer Effectives Test Apparatus.

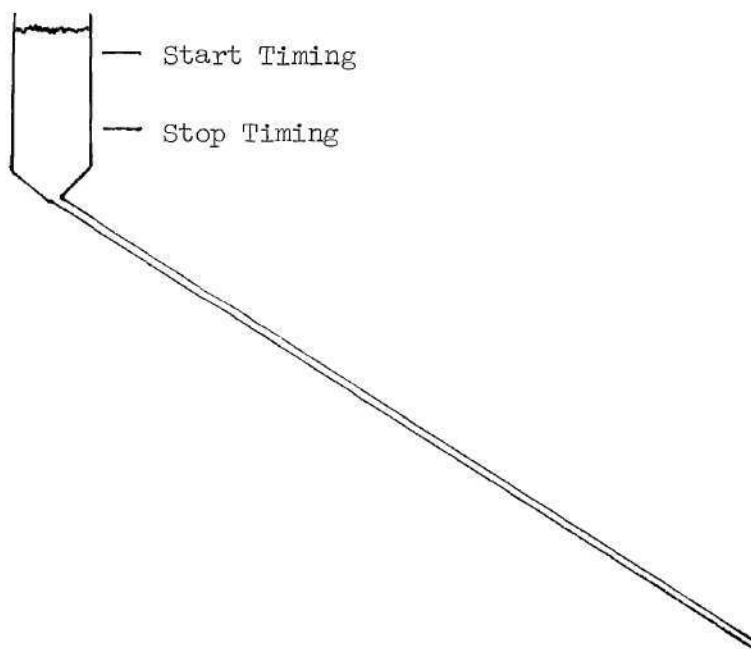


Figure 12. Relative Viscosity Test Apparatus.

### Data Reduction Equipment

Reduction of information obtained photographically required no special equipment. Attempts were made to further describe the flow by using an isodensitometer, but the photographic technique was not sufficiently sophisticated to allow useful comparisons. Primary data reduction dealt with analysis of the instantaneous velocity component produced by the LDA system.

The signal from the LDA system was fed directly to a Hewlett-Packard Fourier Analyzer (either the 5451A or the more advanced 5451B). The A System consists of the following units (48)

Model 180 AR/DR oscilloscope

Model 2100 Computer

Model 2752A Teleprinter

Model 5460A Display plug in unit

Model 5465A ADC plug in unit

Model 5475A Control unit.

The B model, although faster, is comparable to the A model in results and components. A Hewlett-Packard Moseley 135 x-y Recorder was used in conjunction with the Fourier Analyzer System, to obtain power spectral density graphs.

### Reduction of LDA Information

#### LDA Settings

The major thrust of data reduction was directed at processing the information obtained from the LDA system. The LDA tracks the frequency produced by a particle passing through the scattering volume. The frequency response of the system is dependent on the frequency range and

percent bandwidth selected. The translator allows utilization of a variety of frequency ranges. Various settings of range and percent bandwidth were compared to hot film data. Because the recirculation region is capable of producing variations in excess of  $\pm 35\%$  of the mean velocity, fast tracking capabilities were required. For this purpose the range setting of 1.5 MHz with a 1% bandwidth was selected. The resulting frequency response was 1.50 KHz. This high response was needed in regions where the mean velocity approached zero with high fluctuations in instantaneous velocity. For consistency, these settings were maintained throughout the investigation. Comparisons of the turbulence energy spectra produced by the LDA at these settings to hot film spectra showed agreement to about 150 Hz at low turbulence levels (see Figure 13 for comparison). The difference between the LDA and the hot film above 150 Hz was attributed to the optical limitations of the LDA system (54-57).

#### LDA Data Processing

The signal from the LDA system is fed into a Hewlett-Packard Fourier Analyzer, where it is digitized and processed. The Fourier Analyzer System performs analysis of time and frequency data containing frequencies from dc to 50 KHz (100 KHz optional). The system is capable of processing both continuous and transient data and may be programmed to perform a variety of operations on the incoming signal. The results may be displayed in a number of ways; oscilloscope, x-y plotter and point by point print out.

The first step in the processing is analog to digital conversion (ADC). The rate of conversion may be chosen in one of two ways. In the first method the maximum desired frequency ( $F_{\max}$ ) is chosen and the

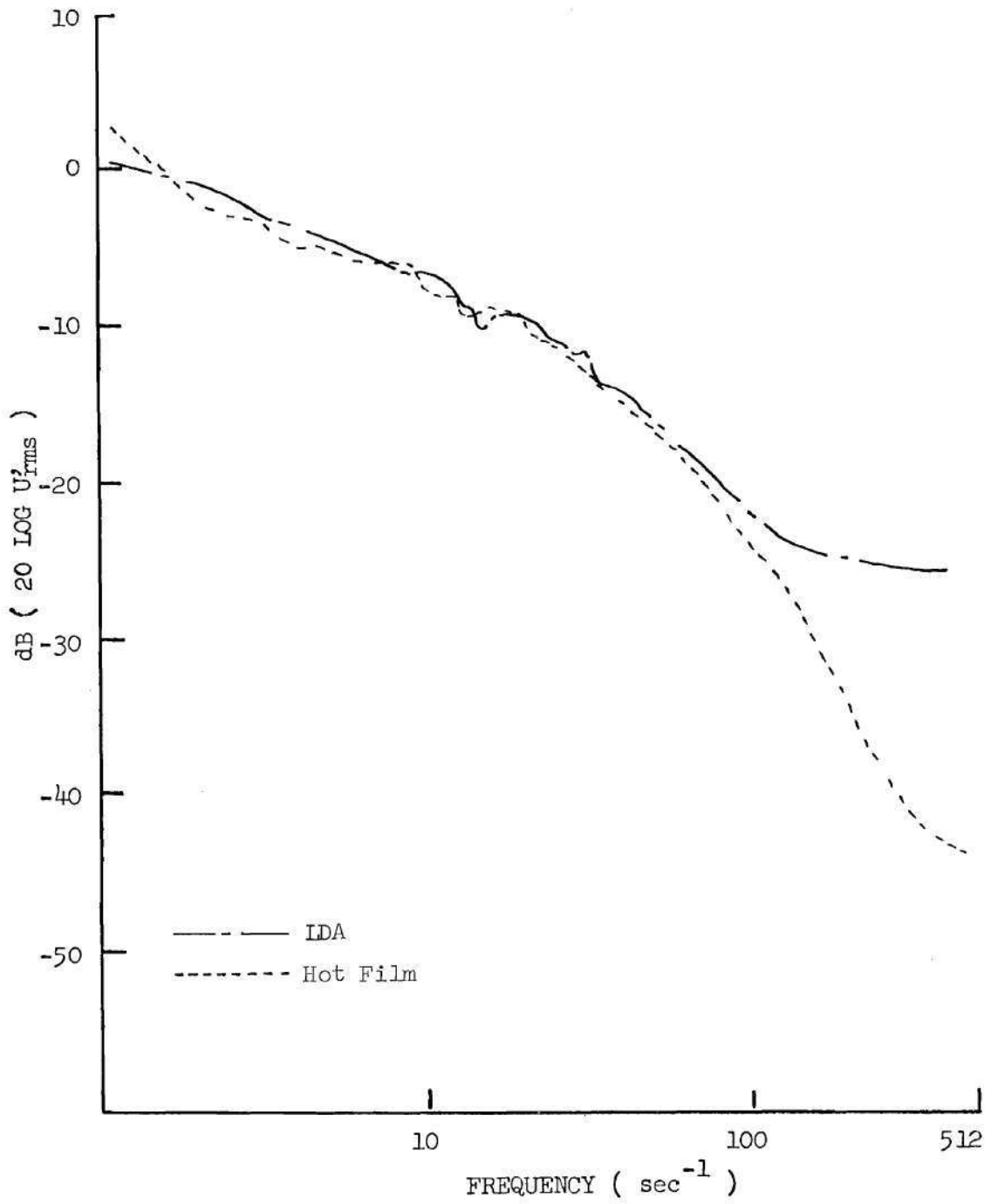


Figure 13. Comparison of LDA to Hot Film Spectra.

frequency resolution ( $\Delta f$ ) is dependent on the block size ( $N$ , number of data points in the record). This frequency resolution may be calculated from the equation:

$$\Delta f = 2 F_{\max} / N .$$

The record length ( $T$ ) may be computed by the equation

$$T = N / (2 F_{\max}) .$$

In the second method the desired frequency resolution ( $\Delta f$ ) is selected and the maximum frequency is dependent on the block size chosen. The maximum frequency is calculated by the equation:

$$F_{\max} = \Delta f N / 2$$

Since turbulence information may contain frequencies as high as 500 Hzs before being lost in noise,  $F_{\max}$  was chosen to be approximately 500. For convenience the second method was chosen. Because  $N$  is an integral power of two,  $F_{\max}$  was chosen to be 512. As can be seen from the equation for  $F_{\max}$ , the value of 512 may be acquired in a number of ways. The frequency resolution may be increased ( $\Delta f$  decreased) necessitating a large block size ( $N$ ) and therefore a longer record length ( $T$ ). To obtain optimum efficiency in calculation some compromise between  $\Delta f$  and  $T$  must be reached. To determine the minimum frequency resolution which may be employed without loss of information, comparisons of power spectra and intensities were made with different settings of  $\Delta f$ .  $F_{\max}$  was held constant in all cases. It was found that above a  $\Delta f$  of two Hertz, the agreement with higher resolution (lower  $\Delta f$ ) values become poor. In order

to minimize record length the frequency resolution of 2 Hertz was selected. For a maximum frequency of 512, the resulting block size was 512 with a record length of .5 seconds.

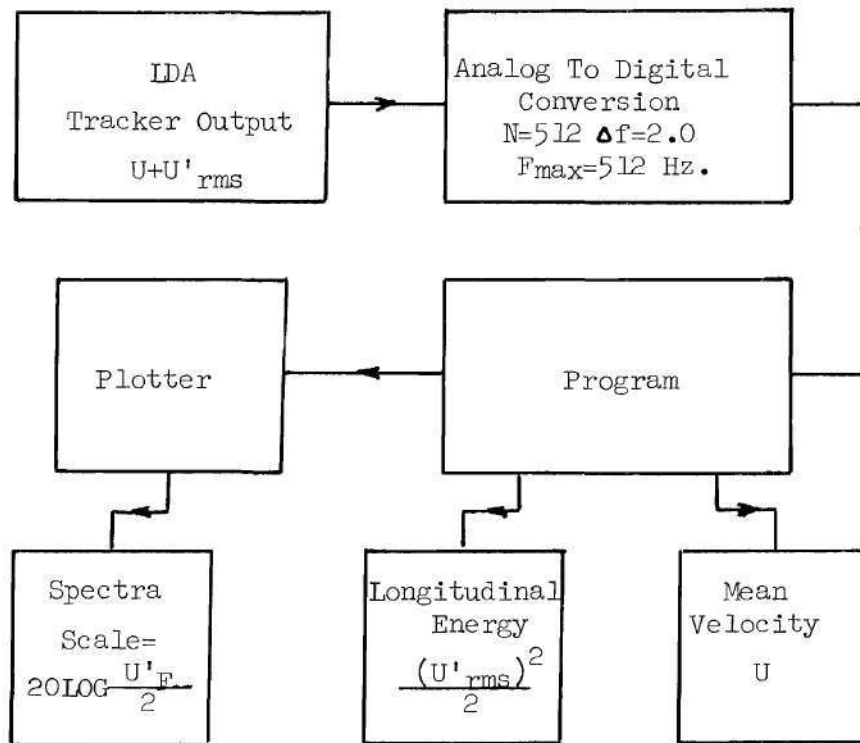
Because digital processing is employed, aliasing may be a problem. Since the LDA configuration has a frequency response of 1.5 KHz and the Fourier Analyzer set to have an  $F_{\max}$  of .512 KHz, aliasing will occur. A means of reducing the aliasing error is to filter out all frequencies above 512 Hertz. Filtering was attempted via a Kromhite action filter. Problems arose at voltages near zero. The d.c. offset in the filter was not accurate for small input signals. For this reason filtering was not possible for low voltages (velocities). For consistency in measurements filtering of the signal was abandoned. Comparisons between filtered and unfiltered data exhibited little difference, therefore demonstrating the effects of aliasing to be minimal for these studies.

After the signal was digitized, the information was processed to give the mean velocity, the power spectral density curve, and total energy. The mean velocity was produced by means of a time/ensemble average. The incoming record was summed 50 times (150 times in highly turbulent regions) and an average record was acquired. The average record was then integrated and divided by the block size (N). The last data point in the record is taken to be the mean velocity. Upon completion of the signal averaging the power spectral density is determined.

To obtain information concerning the lower frequencies (below KHz), the mean velocity record produced earlier is subtracted from the incoming signal. This removes the majority of the d.c. component of the spectra.

For this reason the mean velocity is subtracted and the entire spectrum is considered. The power spectral density produced in the Fourier Analyzer is actually a mean power spectral density. In this study, 50 power spectra are averaged for purposes of obtaining a good statistical representation. At a maximum frequency of 512 with a frequency resolution of two Hertz, the mean spectrum consists of a d.c. component (in this case the remainder after subtracting the mean velocity component) and 256 data points each with a two Hertz frequency bandwidth. Restated, aside from the d.c. component, each data point represents a rise in frequency by two Hertz. The value stored in each data point past d.c. (or zero) is given as: the signal amplitude squared divided by four. Since the Fourier transform is taken without reference to the effective bandwidth set by the ADC sampling controls, the spectrum can be normalized to unit bandwidth by dividing by  $\Delta f$ . The resulting spectrum has amplitudes which now correspond to the root mean squared (rms) velocity squared divided by two. The power spectrum produced in this investigation, therefore, has an amplitude of the rms velocity squared divided by four. The spectra produced in this manner are then plotted on a log-log scale. A flow chart describing the LDA Data Reduction is given in Figure 14.

Total longitudinal turbulence energy is produced by summing the energy content of all frequency components. In the Fourier Analyzer this summation can be accomplished by integrating the power spectral density. The resulting value is expressed as the total energy divided by two. For clarification see the flow chart in Figure 14. The total energy given is actually the mean total energy based on an average over



$U$  = Mean Velocity

$\frac{(U'_{rms})^2}{2}$  = Total Longitudinal Energy

$\frac{(U'_F)^2}{4}$  = Longitudinal Energy /  $\Delta f$

Figure 14. Flow Chart of LDA Data Reduction.

50 samples. Samples of the programs utilized in this investigation have been reproduced in Appendix III.

## CHAPTER IV

## DISCUSSION OF RESULTS

LDA Investigations

In order to gain information of a more quantitative nature, the flow model was studied with the aid of the LDA Fourier Analyzer system described in Chapter III. The axial velocity component and the corresponding longitudinal fluctuations and spectra were measured over a range of radial positions at various axial stations. Based on the photographic information the following axial stations were selected for study: -0.1, 0.1, 0.5, 1.0, 2.0, 3.0, 4.0, 5.0 and 10.0 inches from the exit plane. Translated into catheter diameters these stations are  $X/D = -0.54, 0.54, 2.71, 5.42, 10.85, 16.28, 21.71, 27.14,$  and  $54.27$ . For centerline decay measurements additional axial locations corresponding to  $32.56, 37.99, 43.42$  and  $48.85$  catheter diameters were included.

Centerline Decay

Measurements of the mean centerline velocity decay were produced for the cases of water injections with and without the BLT and polymer solution injections with and without the BLT. For consistency all values of the mean velocity components were nondimensionalized by the mean catheter velocity based on flow rate ( $U_{FR}$ ). The axial locations are given in terms of catheter diameters ( $X/D$ ). Prior to presenting the results of the centerline measurements, the initial conditions of each flow case are discussed.

Initial Conditions. The catheter velocity profiles were produced and compared with the  $1/6^{\text{th}}$  and  $1/7^{\text{th}}$  power law as well as the laminar profile (49). The results are shown in Figures 15 and 16. The profile in each case do not compare exactly with the turbulent flow theories but are much closer to the turbulent case than to the laminar. The only exception to this is the polymer solution injection without the BLT. This profile is, in actuality, not too far removed from the laminar profile. This is probably due to a delay in transition caused by the polymer.

The lack of agreement with the turbulent theory (power law profile) may be the result of several factors. Because of the small size of the catheter in the flow model, a 5% error in the diameter measurements can produce an error of 10 percent in the final velocity ratio. Also because of its size, accurate measurement of the diameter is difficult. Secondly, the Reynolds number used is somewhat low for the application of a power law profile to be precisely accurate. Turbulent flow behavior in a regime close to transition is subject to large variances. To check the accuracy of the profile produced by the LDA, a comparison of the known flow rate and the integrated velocity profile was conducted. Using a trapezoidal technique for integrating the measured profile, the calculated flow rate varied by less than 2% from the measured value. Although improved agreement with the power law could be obtained at higher Reynolds numbers, the value of 7000 most nearly approximates the upper clinical Reynolds number limit. For this reason the Reynolds number of 7000 was maintained.

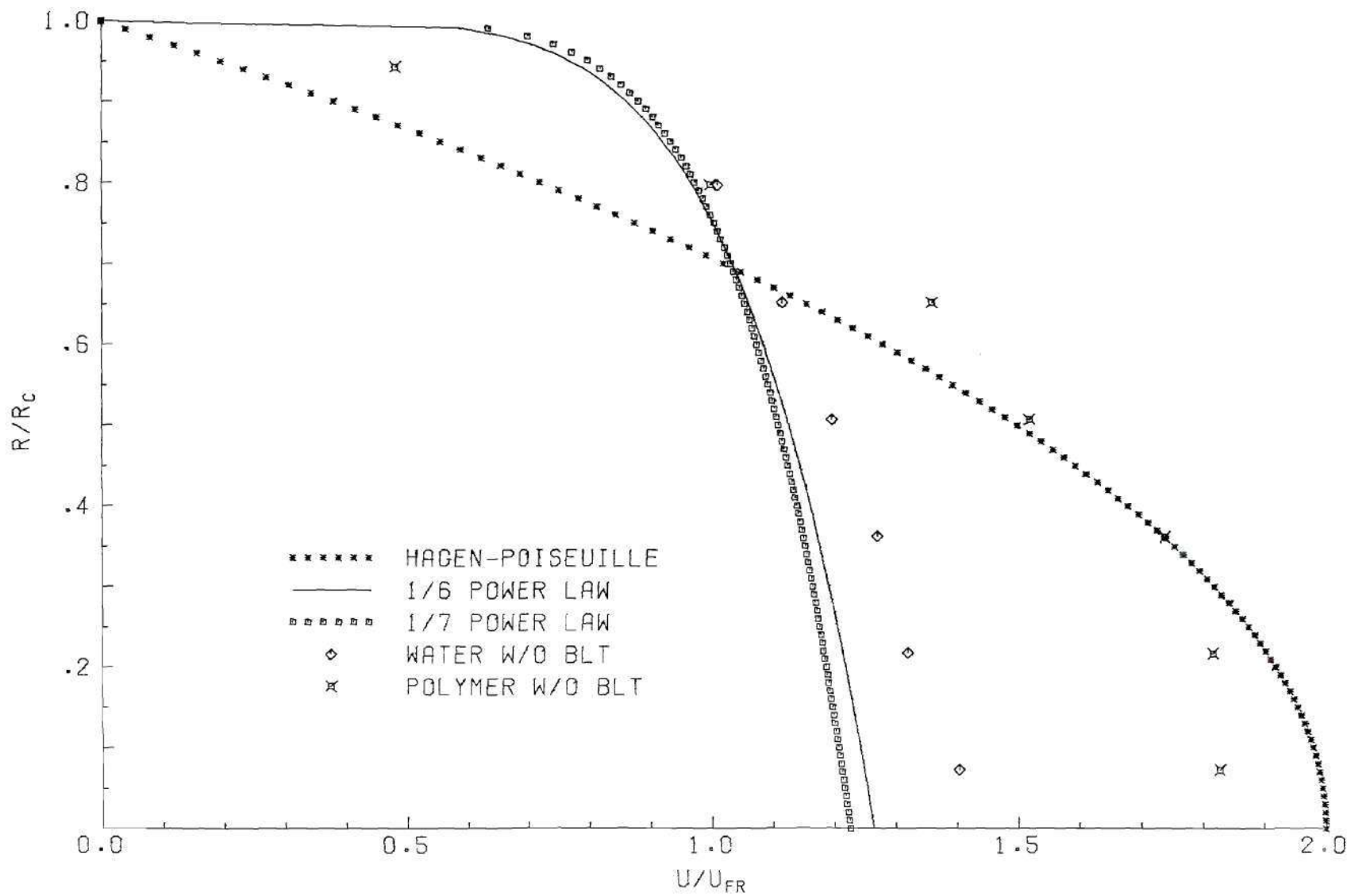


Figure 15. Comparison of Catheter Velocity Profiles to Theory,  $Re = 7000$ .

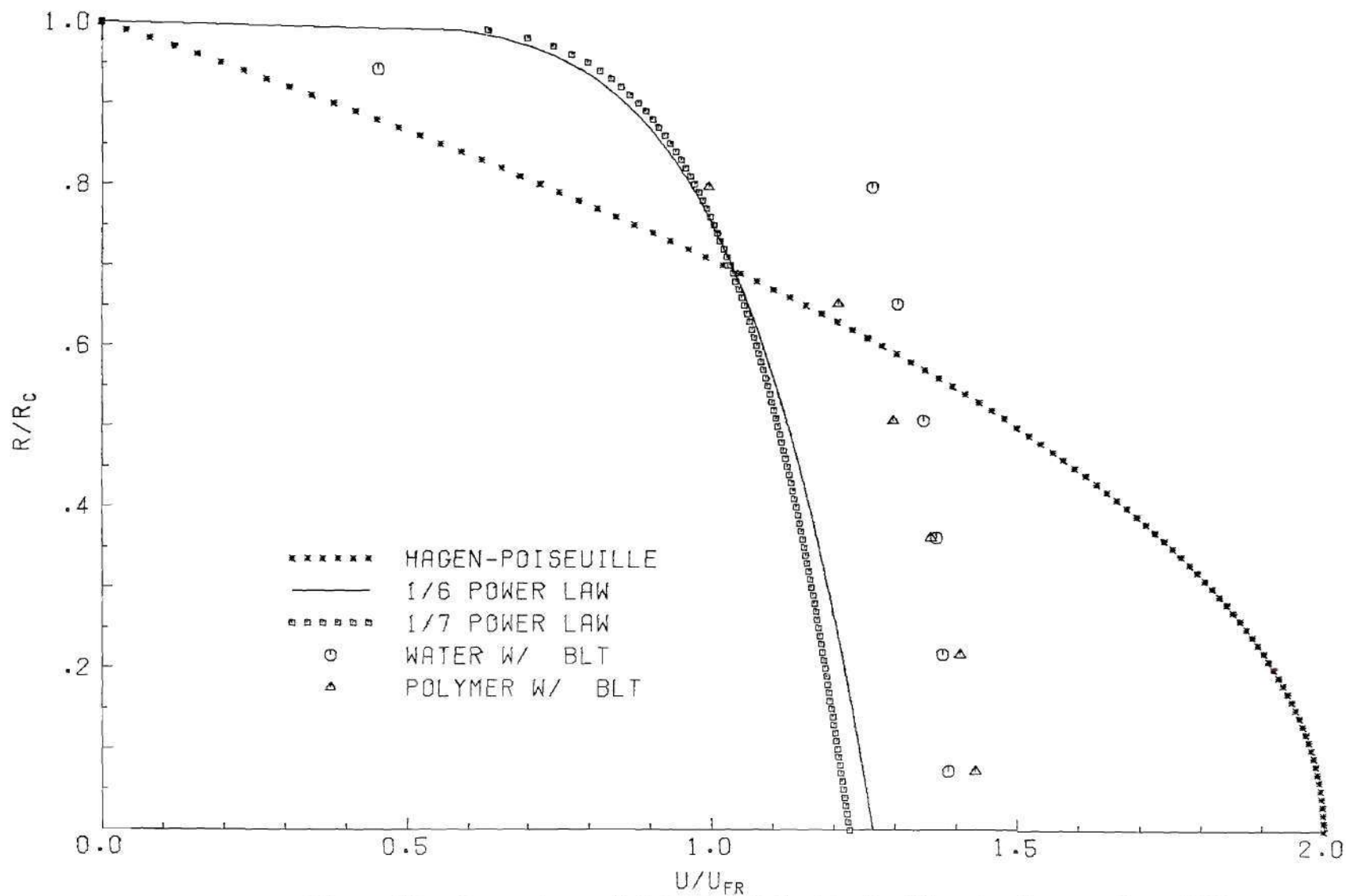


Figure 16. Comparison of Catheter Velocity Profiles to Theory,  $Re = 7000$ .

Centerline Velocity Decay. The nondimensionalized centerline velocities were plotted against the axial stations ( $X/D$ ). The results are shown in Figure 17. The most obvious result can be seen in the value of the nondimensional velocity component near the exit plane which is  $X/D = 0.0$ . Three of the curves appear to start at approximately the same point (1.4 - 1.45); while the fourth curve (Polymer without the BLT) begins at a value near 1.8. This large difference in initial values is attributed to the delay in transition caused by the presence of the polymer. The fact that the polymer solution with the BLT has an initial value near those for the water injections points out the effectiveness of the BLT in creating a turbulent flow despite the presence of the polymer.

Comparison of the water injection without the BLT to that of water with the BLT indicates that the velocity decay is greater for the BLT case. This suggests a higher turbulence kinetic energy which contributes to the mixing of the jet with the co-flowing stream. Comparison of water without the BLT to polymer without the BLT shows that even though the polymer solution exits in a "pseudo"-laminar form, the decay of velocity exceeds the water case. In fact the polymer without the BLT has a lower velocity after about 11 catheter diameters. This suggests a strong effect of the polymer on the turbulence and the mixing. Comparison of water with the BLT to polymer with the BLT shows similar but less dramatic results. In this case the polymer has a lower velocity after approximately one catheter diameter. It is also interesting to note both polymer cases approach the data stream velocity from along similar curves. The same holds for the water cases. That is to say, that regardless of

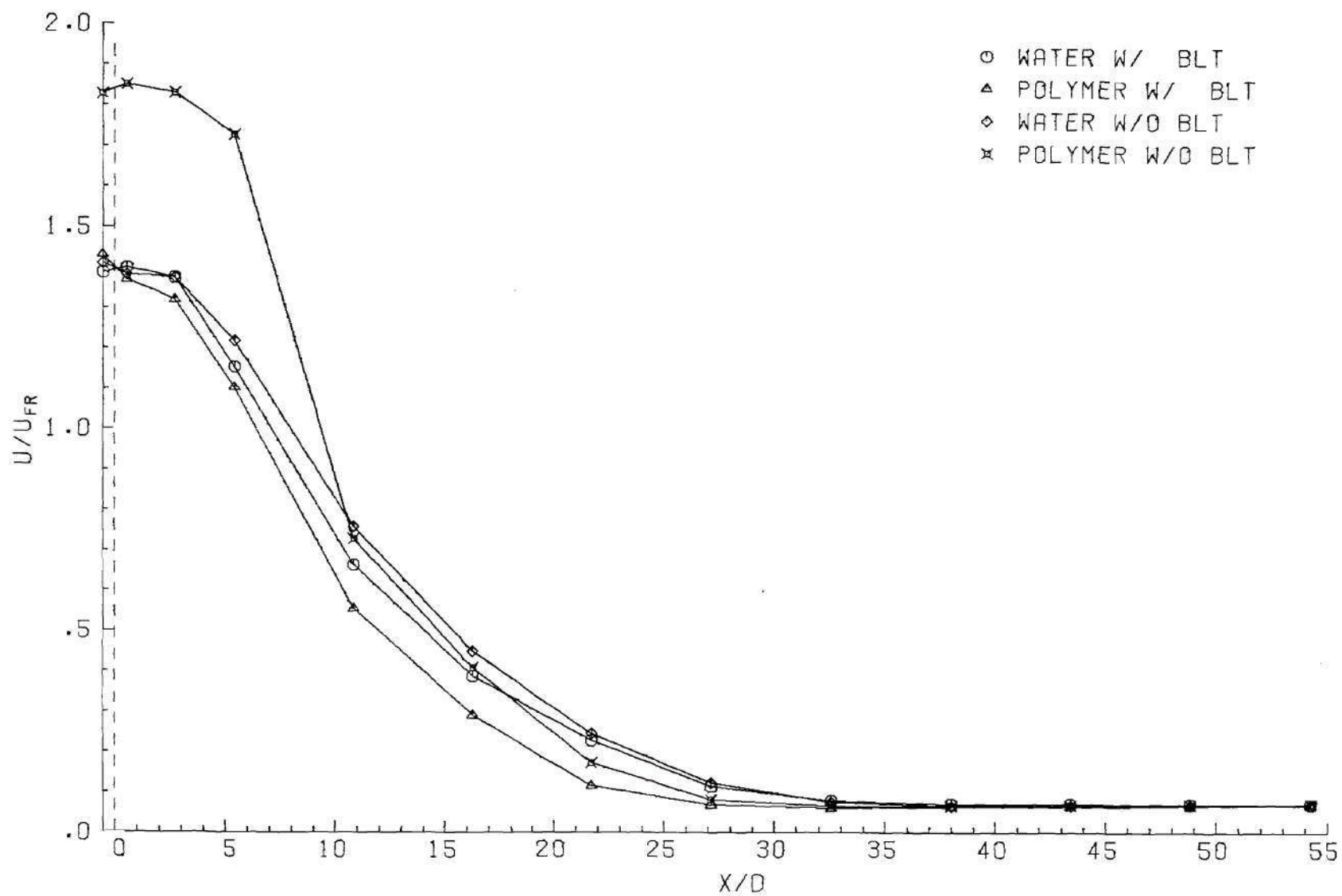


Figure 17. Centerline Decay of Velocity.

of whether or not the BLT is employed, the polymer solution approaches the downstream velocity more rapidly than the water injectant.

Centerline Fluctuation Measurements. The velocity fluctuations were also obtained for each axial location. The values of the fluctuations ( $U'_{rms}$ ) were calculated from the longitudinal turbulence energy computed by the Fourier Analyzer. In order to produce a nondimensional velocity fluctuation plot, the values for  $U'_{rms}$  were divided by the mean velocity based on flow rate of the injection ( $U_{FR}$ ). The resulting plots are shown in Figure 18.

Comparison of the two water injections produces several interesting observations. Both injections begin with approximately the same degree of fluctuation (turbulent intensity). However, shortly after two catheter diameter, the BLT water injection fluctuations begin to surpass those of the projection without the BLT. The major portion of this difference appears to take place over a range of approximately 14 catheter diameters. Afterwards, the two curves compare relatively well. This, again, indicates a change in the mixing due to the presence of the BLT alone and is consistent with the centerline decay results in Figure 17.

Comparison of the polymer solution injection without the BLT to the comparable water injection exhibit a large variation. The fluctuations for the polymer solution injection initially parallel the water case at a slightly lower level. Then after approximately three catheter diameters, the fluctuations increase to a level of almost 2.5 times the level of the water fluctuations. At  $X/D = 16.28$  a very large velocity fluctuation is observed. If compared to the photographic information provided, this corresponds to the approximate position at which the

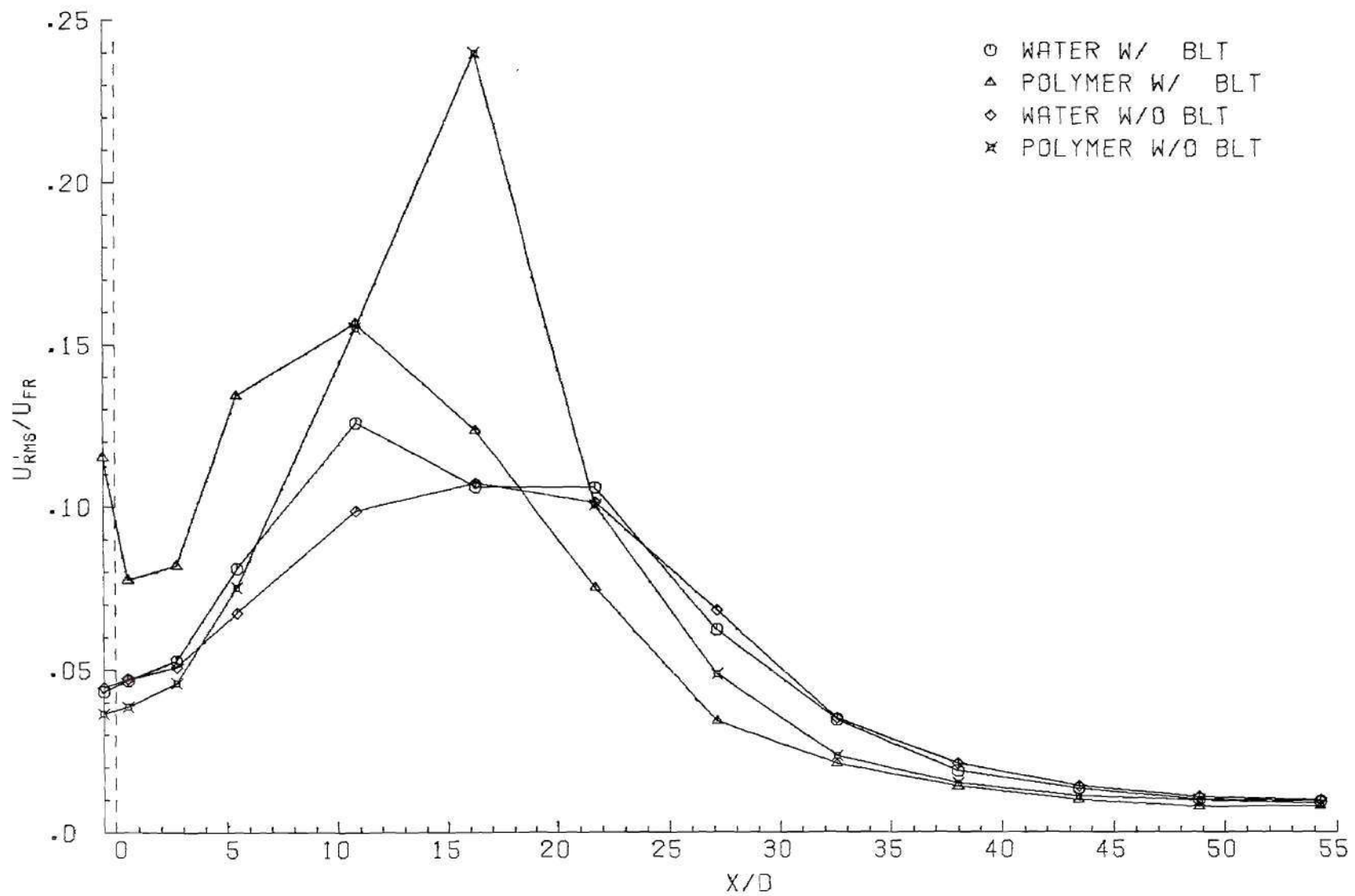


Figure 18. Centerline Variation of  $U'_{rms}/U_{FR}$ .

helical instability begins to break into turbulent mixing. After this point the level of the fluctuations then rapidly decreases to a point which is, once again, below that of the water injection case. This large degree of fluctuation may be the result of two possible changes in the flow conditions. The first possible cause may be attributed to the change in the conditions at the exit plane due to the delay in transition caused by the presence of the polymer. The second explanation for the observed behavior is the possible effect of the polymer on the turbulent structure in the mixing region. It is not unlikely that the high fluctuations observed are a product of both these conditions. By comparing the BLT injections (water vs. polymer solution), some separation of the two possible effects is possible.

By contrasting the two BLT injections (water and polymer) it becomes apparent that the changes in the initial conditions are partly responsible for the large fluctuations seen in the polymer solution injection without the BLT. However, there appears to be an effect which may be considered a result of an altered mixing region. Although the polymer solution exhibits a higher fluctuation level due to the BLT, the resulting plot parallels the water case up to about 10 catheter diameters. After this point the polymer solution fluctuations drop to a level below all the other cases. It is interesting to note at this point that the two polymer injections again approach the downstream asymptote more rapidly than the two water injections. This fact strengthens the assumption of an altered turbulent mixing due to the presence of the polymer in the fluid.

Further normalization may be accomplished by dividing the resulting fluctuations by the local mean velocity ( $U_L$ ) instead of the mean velocity based on flow rate. The results of such a nondimensionalization are presented in Figure 19. The most obvious result in the method of reduction is an apparently stronger correlation of the data. The two water injections differ only slightly. While the two polymer solution injections are similar with respect to the turbulence intensity variations. Contrasting water to polymer solution injections, the peak rms fluctuations (or deviation from the local mean) of the polymer solution case is greater than and occurs before the peak rms fluctuation for the water case. This is consistent with the observations of Vlasov *et al.* (35) concerning the increased turbulence due to the presence of a drag reducing polymer in a submerged jet. It is this increased level of turbulence which is believed to be responsible for the more rapid decay of the centerline velocities of polymer solutions.

Centerline Spectra. Further information concerning the centerline decay of the velocity fluctuations (and, hence, the turbulence structure) may be obtained through the study of the resulting centerline power spectral densities. Since the power spectral density is a distribution of energy (or  $(U'_{rms})^2$ ) over a range of frequencies, variations in the curve shape will be directly related to the changes in the distribution of energy and, therefore, the turbulent nature of the flow. Complete centerline spectra for each case are provided in Appendix V. The spectra resulting from the two water injections displayed a high degree of correlation and for this reason, figures comparing water and polymer injections employ only one water spectrum.

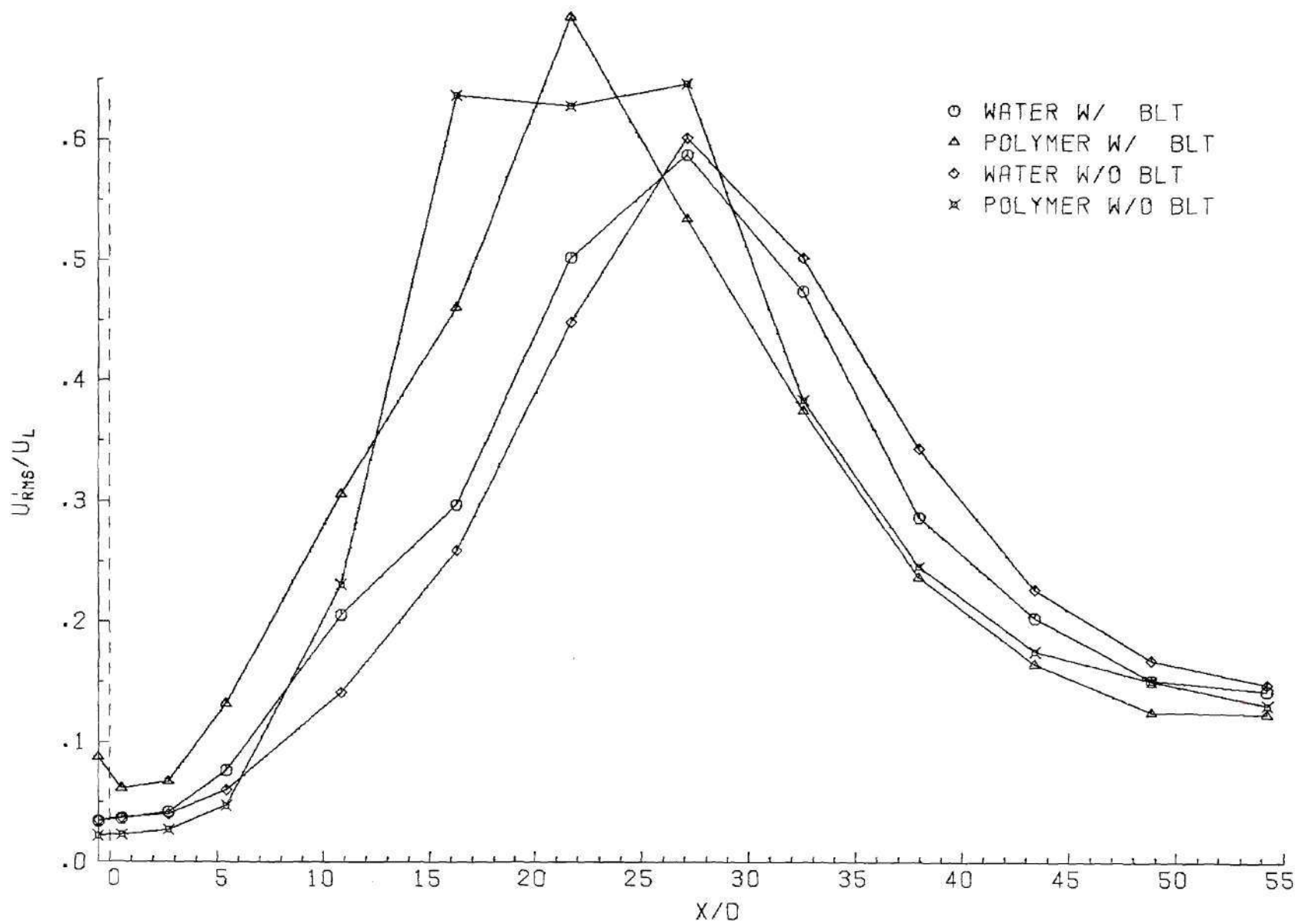


Figure 19. Centerline Variation of  $U'_{rms}/U_L$ .

As was seen from the variation of the velocity fluctuations along the centerline, the total longitudinal energy exhibits an increase followed by a decrease in magnitude. The general centerline flow field may, therefore, be described by two regions; one of increasing total longitudinal energy and one of decreasing energy.

Spectra representative of the near field or increasing energy region may be found in Figure 20. When compared to the water spectrum both polymer spectra display behavior which is different from that produced by the water injection. The energy distribution for both polymer injections exhibits a lower relative magnitude in the higher frequencies (above 20 Hz) and higher magnitudes in the lower frequencies. Although the near-exit centerline velocity of the polymer solution without the BLT appears in the photographs to be a "pseudo"-laminar flow, the resulting spectra are not characteristic of laminar flow, nor do they represent turbulent flow. At an  $X/D$  of 2.71 the spectrum exhibits a "spike" which has a center frequency (230 Hz) corresponding very closely to the frequency of the helical instability described in the Photographic Investigation section of Chapter II (see Figure 21). This close agreement reaffirms the importance of the photographic investigation in providing guidance for the interpretation of the detected flow field measurements.

The near field spectrum for the polymer solution with the BLT exhibits an overall elevation of the turbulence energy content, with the major increase being found below 100 Hz as seen in Figure 20. Above 100 Hz the energy content is elevated only slightly. At other axial locations in the region of increasing fluctuations, this general behavior is still seen. It is possible, therefore, to attribute the increased

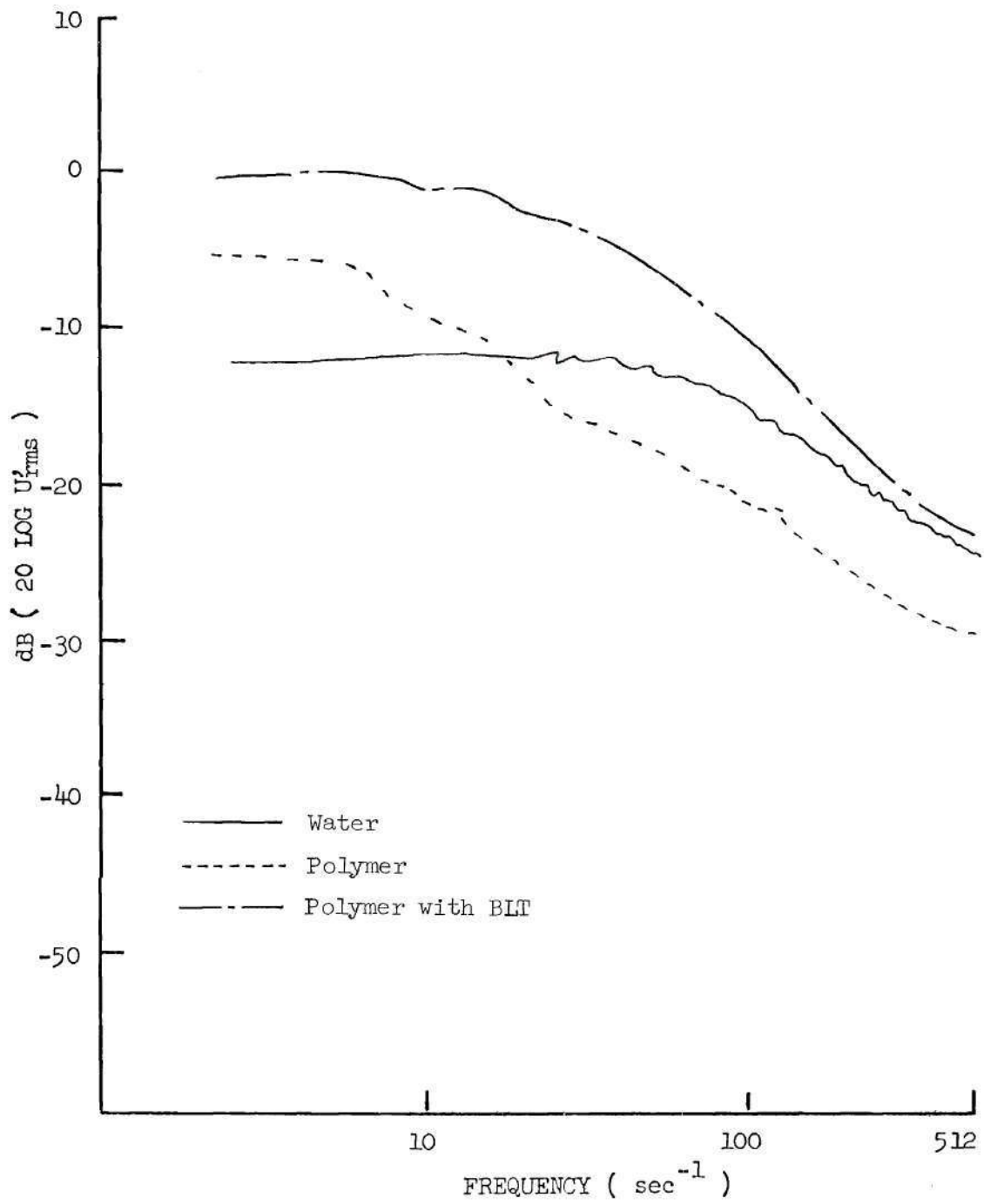


Figure 20. Comparison of Centerline Spectra at  $X/D = -.54$ .

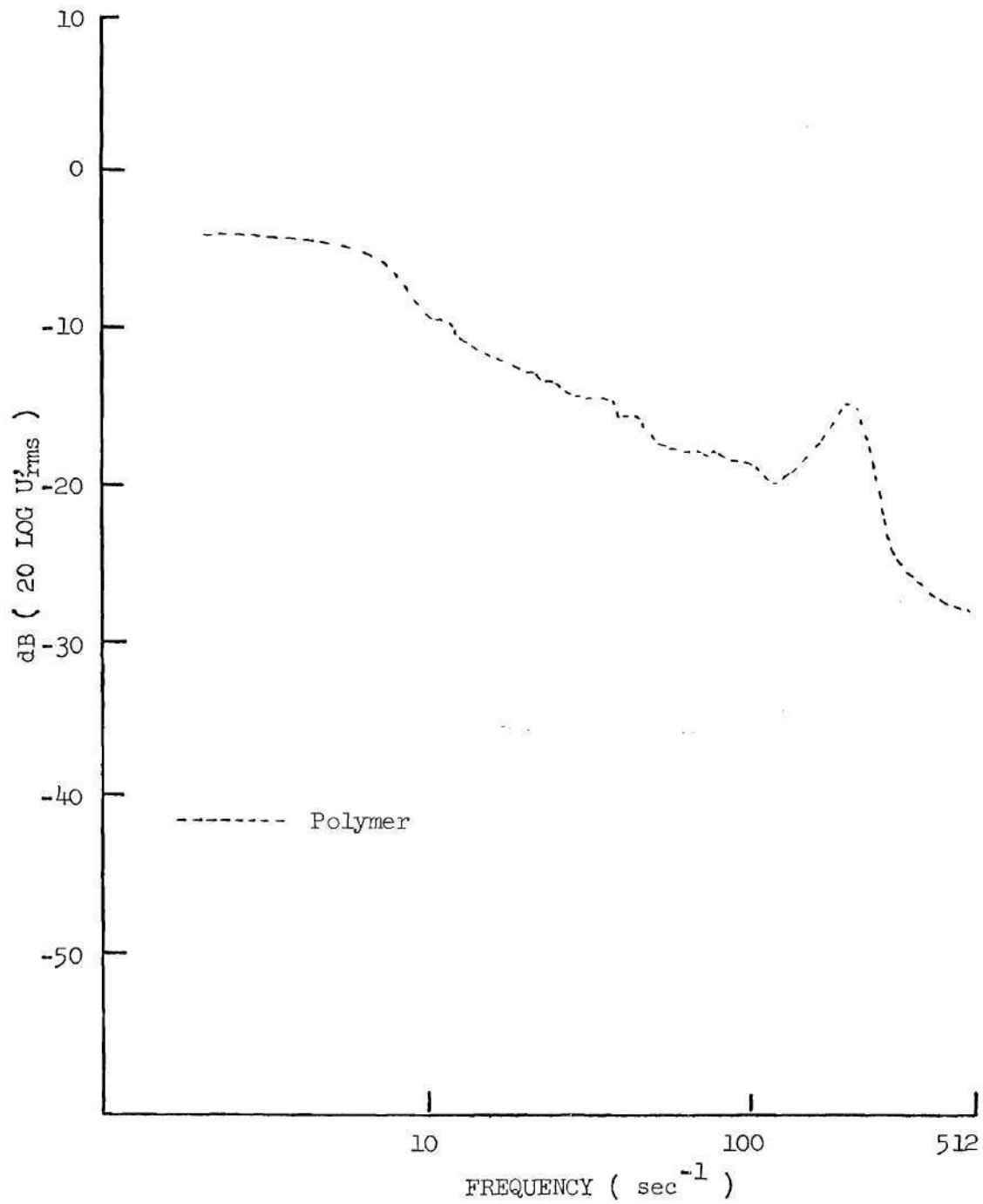


Figure 21. Spectrum Displaying Helical Instability,  $X/D = 2.71$ .

total longitudinal energy seen for both polymer injections (with and without the BLT) to an increase in the energy content of the lower frequencies. This suggests a larger energy content in the larger eddies and is consistent with the visual impression inferred from the photographs.

In the region of decreasing velocity fluctuations both polymer solution injections exhibit a similar behavior. A representative comparison is shown in Figure 22. In this figure both polymer injection spectra indicate the more rapid decay in energy discussed earlier. Also seen is the different distribution of energy with respect to frequency. Both polymer spectra have slopes which indicate that the majority of energy is contained in the lower frequencies to a greater extent than in the water case.

#### Radial Variations

Although valuable information can be obtained from the study of centerline results, the overall description of the flow would be lacking without a comprehensive examination of the radial variations of the velocity and turbulent energy. Because the polymer solution with the BLT has an initial behavior more similar to that of the water injection with the BLT, radial variations of the axial velocity components, the fluctuations and power spectral densities are presented and compared for each case (water vs. polymer).

Water with the BLT. The variations of the mean velocity components ( $U$ ) are presented in the form of radial profiles at different axial stations. The fluctuation ( $U'_{rms}$ ) profiles may be found in Appendix V. The axial development of the profiles is illustrated by plotting

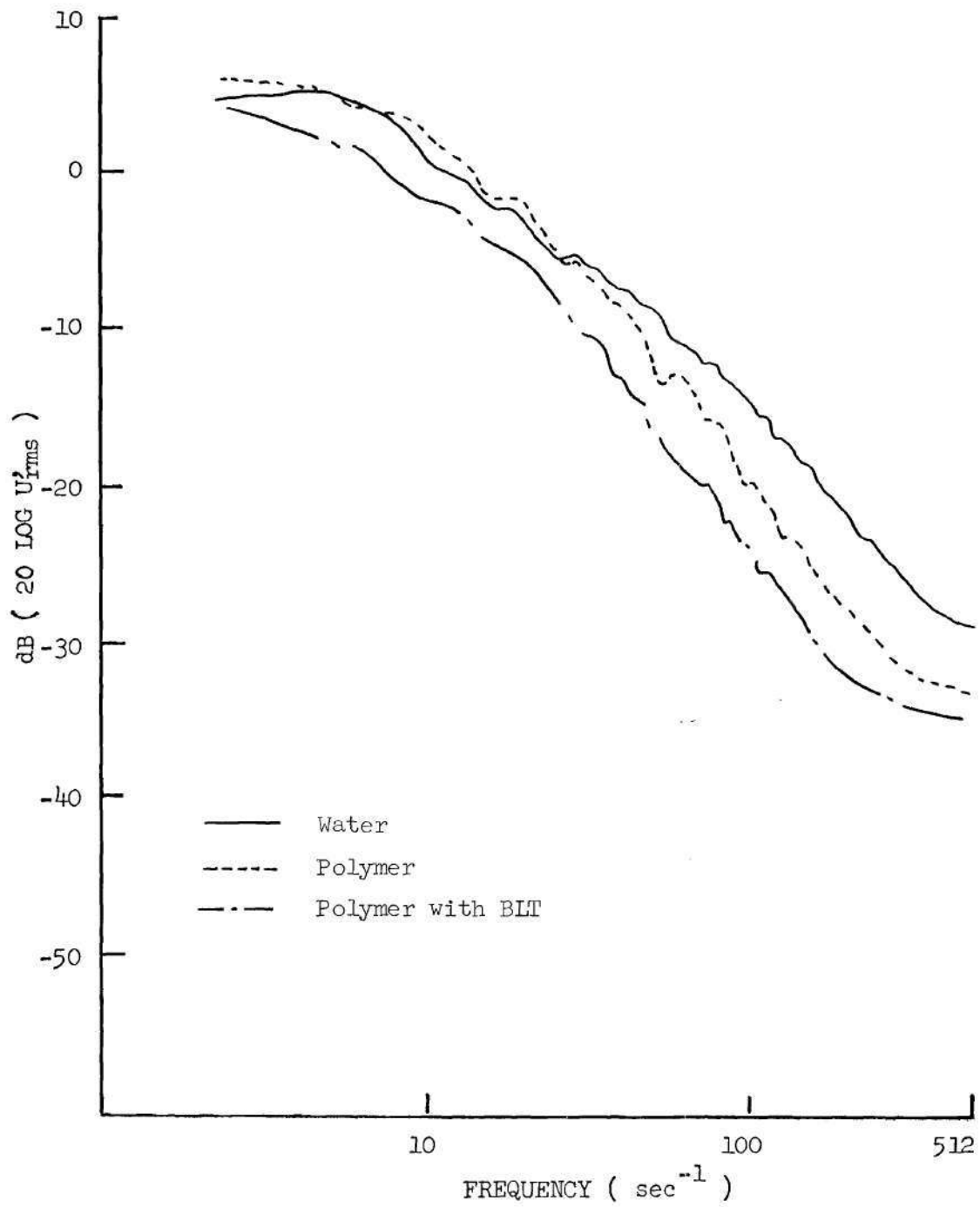


Figure 22. Comparison of Centerline Spectra at  $X/D = 21.71$ .

several profiles on the same figure. Because nine axial stations are to be represented, two figures are utilized to present the information without excessive overlap. The first of the two figures exhibits the profiles at the axial stations from  $-.54$  to  $10.85$  catheter diameters, the second from  $10.85$  to  $54.27$ .

The velocity profiles are presented in Figures 23 and 24. Normalization of the velocity component is accomplished via the mean catheter velocity ( $U_{FR}$ ) based on flow rate. The radial location ( $R$ ) is normalized with the radius of the outer tube ( $R_o$ ). The spreading of the jet is evidenced by the increasing velocities at radial positions away from the catheter and by decreasing velocities near the wall and at the centerline. Because of the large difference between the jet and co-flowing momenta, a recirculation region is produced. Evidence of this region is exemplified by the negative velocities at stations  $10.85$  and  $16.28$ . As the jet continues to decay, this region of negative velocities (or retrograde flow region) diminishes until the entire flow is again positive. At the  $54.27$  diameter station the profile is essentially flat. Subsequently, as the flow continues downstream, the profile begins its evolution toward a fully developed laminar state, due to the low Reynolds number of the total flow (approximately 2000).

Polymer with the BLT. The radial variations of the mean velocity component ( $U$ ) and the corresponding fluctuations are presented in the same fashion as the water information. Again, the axial stations are displayed on two figures to provide an overview of the injection process. The first of each set of figures covers the axial stations from  $-.54$  to  $10.85$  catheter diameters, the second from  $10.85$  to  $54.27$ . Normalization

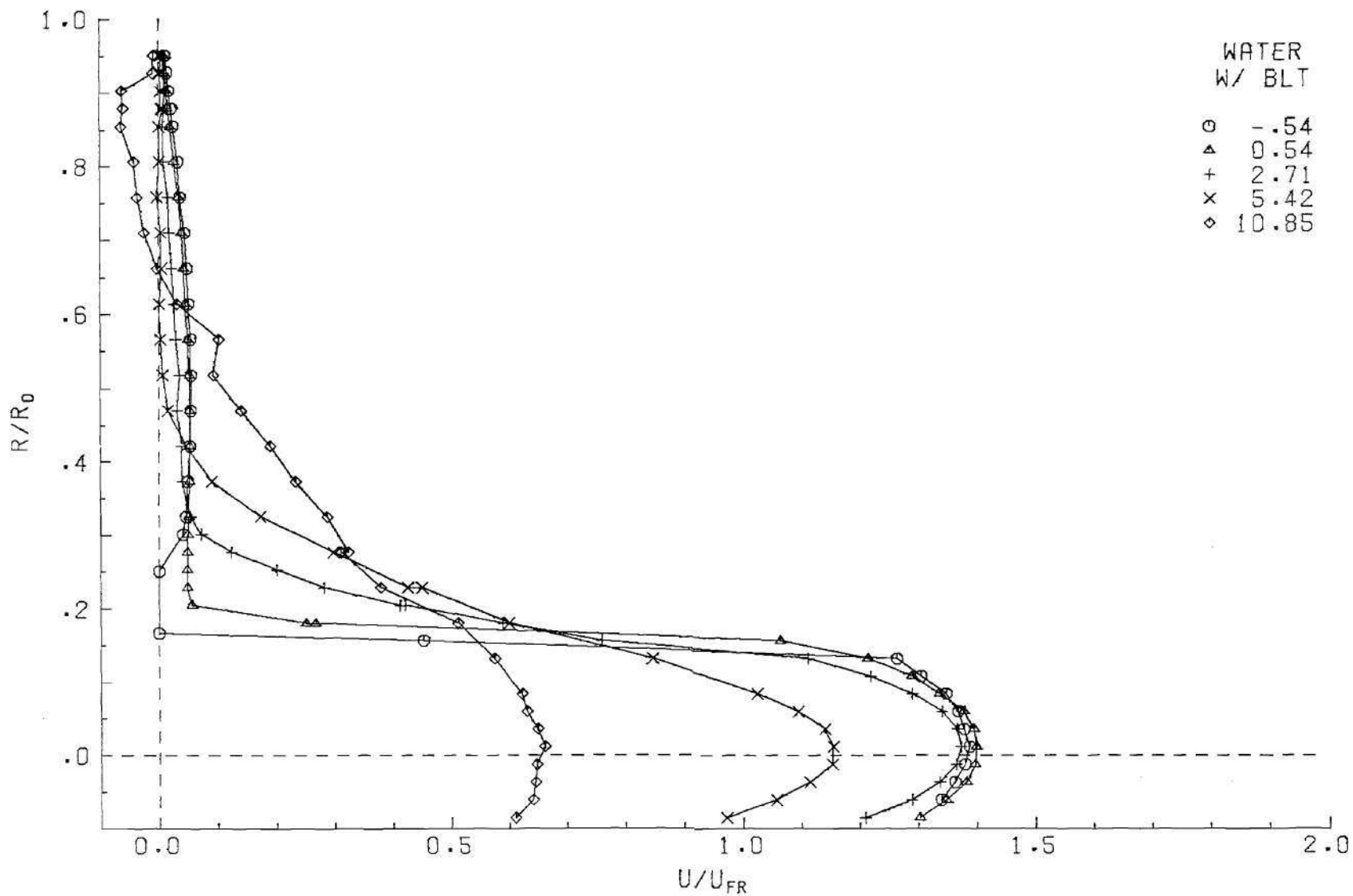


Figure 23. Velocity Profiles, Water with BLT,  $X/D$  from -0.54 to 10.85.

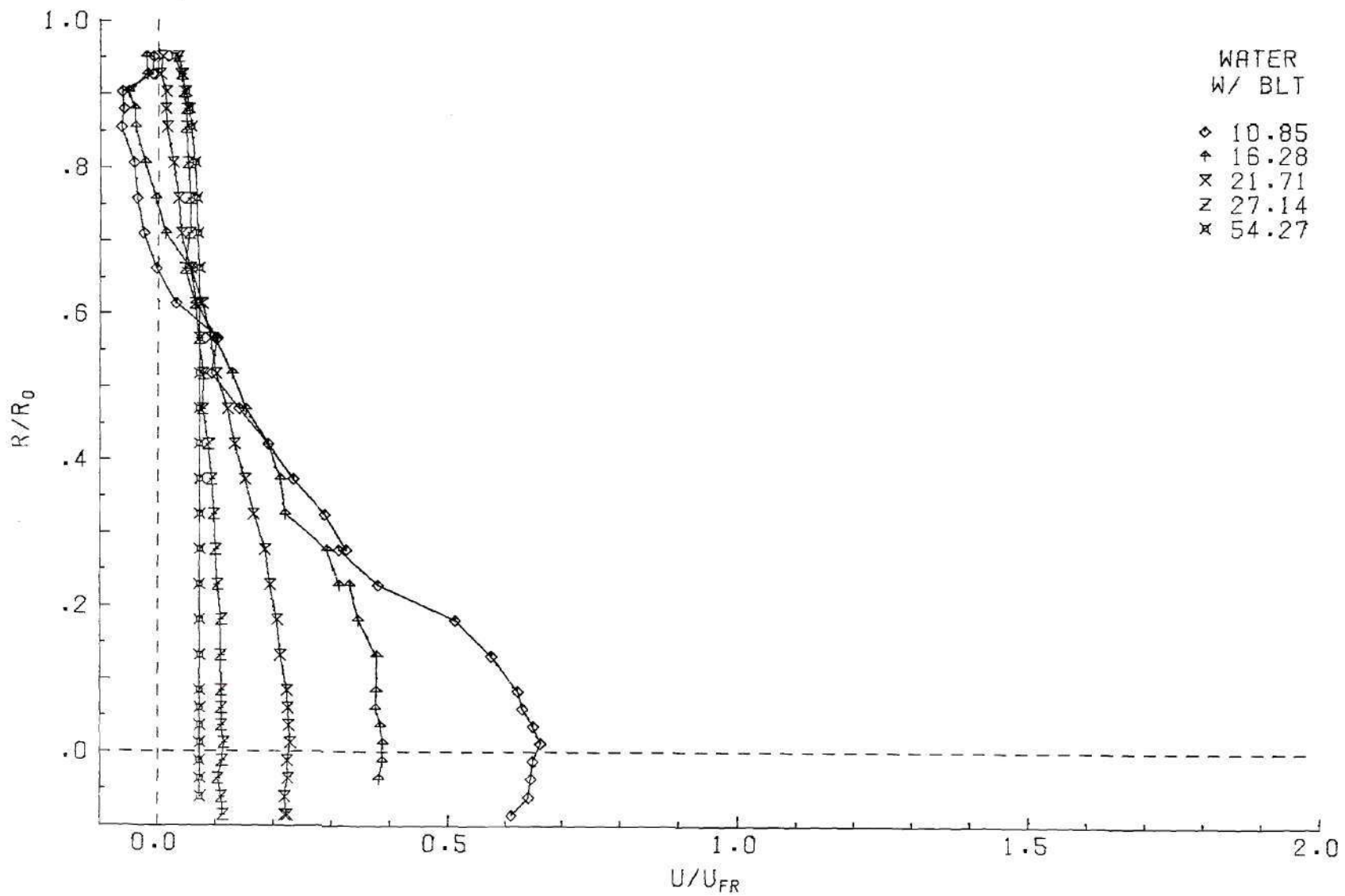


Figure 24. Velocity Profiles, Water with BLT, X/D from 10.85 to 54.27.

of the resulting velocities ( $U_L$  and  $U'_{rms}$ ) is accomplished in same manner as the water case.

The velocity profiles are presented in Figures 25 and 26. When direct comparisons between the two injections are made, however substantial differences are seen.

Comparisons. Direct comparisons of the mean velocity and the fluctuations are presented at various axial locations. Further comparisons may be found in Appendix V.

Figures 27 through 29 represent the near exit plane conditions. A difference in the catheter profiles is perhaps the most obvious result. Although the water case exhibits a more turbulent profile, the polymer solution features a larger overall fluctuation ( $U'_{rms}$ ). As seen earlier in the centerline decay study this effect is primarily contained in the lower frequencies of the turbulence power spectra. The outer flow regions appear to be very similar. The slight differences in profiles may be attributed to small errors in alignment of the flow facility and in flow meter readings. The fluctuations in the water flow are, however, essentially comparable.

Figures 30 through 32 are important in that they present the almost immediate effect of the jet on the outer flow. Little difference in the outer flow is evident in Figure 30 but Figures 31 and 32 provide strong evidence that the outer flow region is less effected initially by the polymer solution jet. This is seen in the increased fluctuations in the water case as opposed to the polymer solution case. In fact, the polymer solution fluctuations lag the water injections in the near wall region until recirculation (see Figures 39 and 40) occurs. Figure 31 and

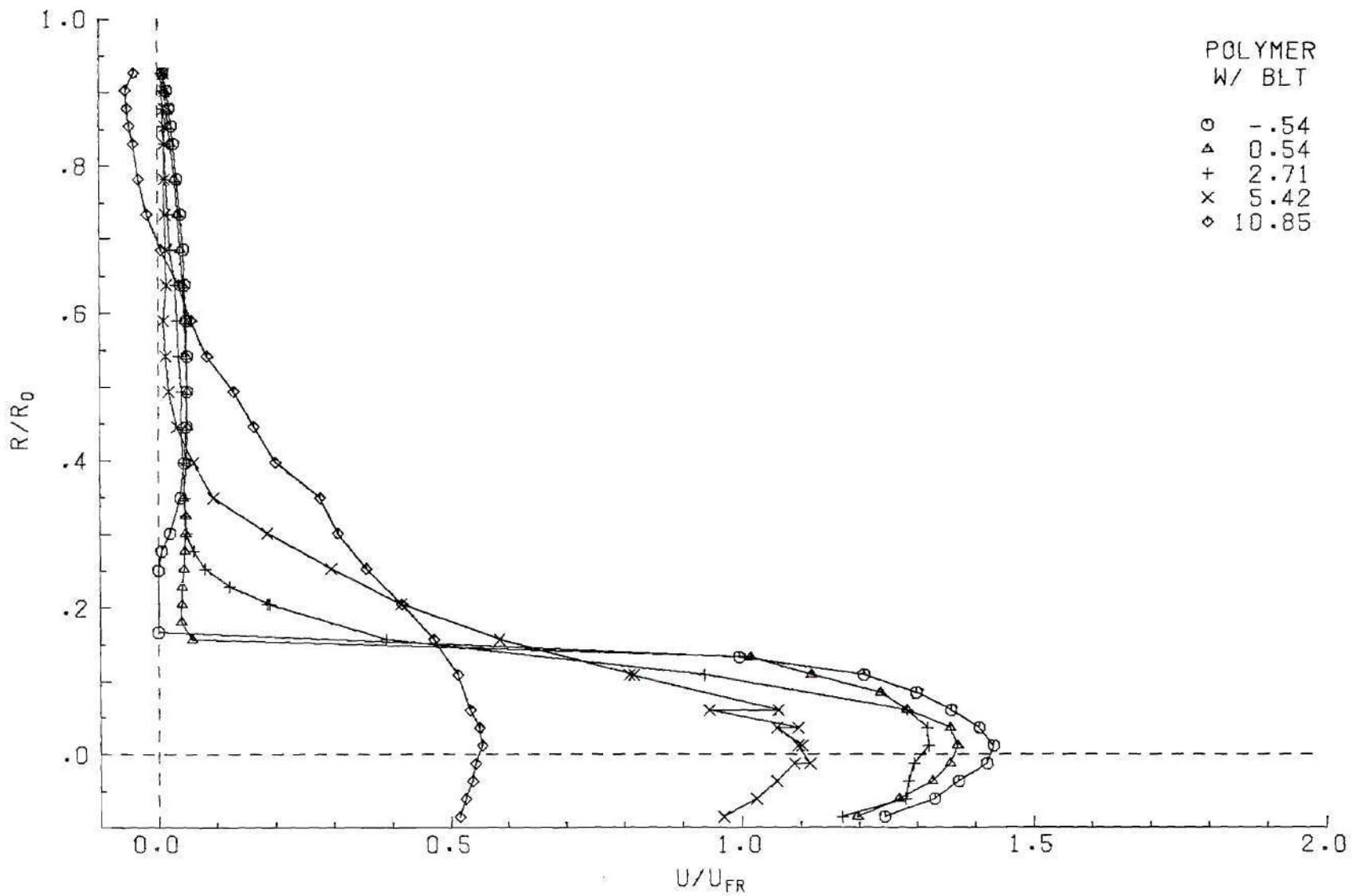
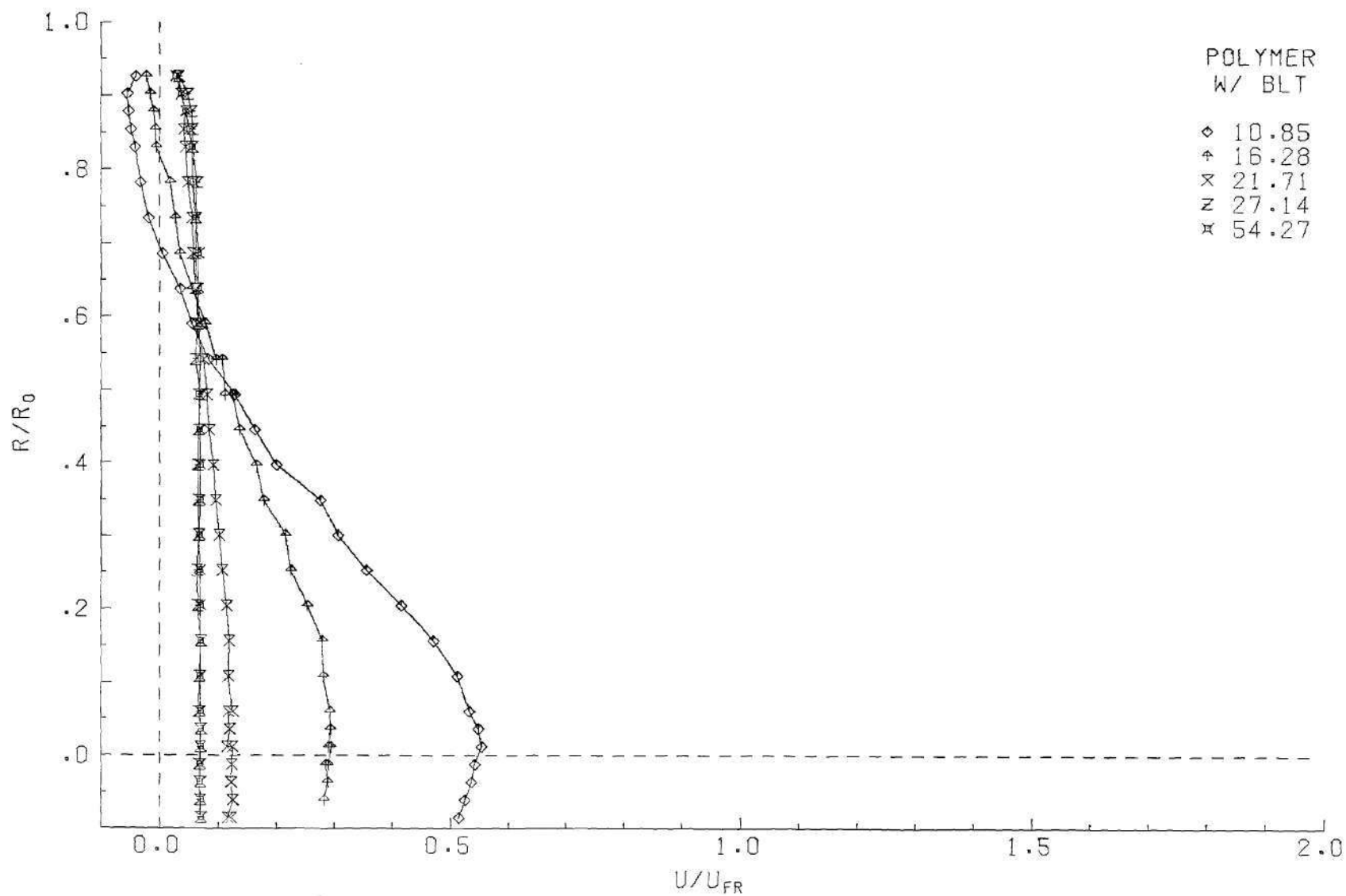


Figure 25. Velocity Profiles, Polymer Solution with BLT,  $X/D$  from  $-.54$  to  $10.85$ .



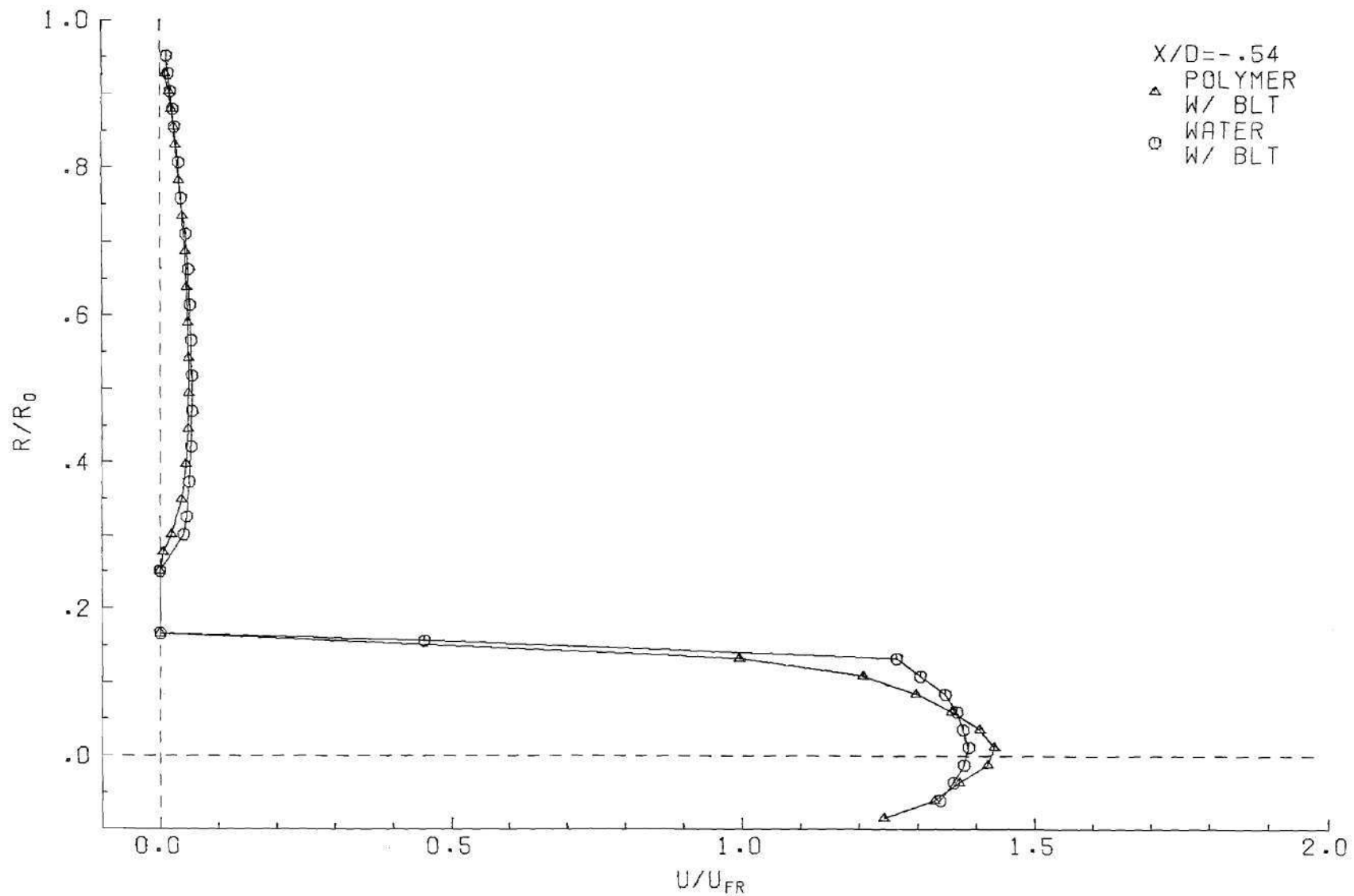


Figure 27. Comparison of Polymer Solution to Water, Velocity Profile,  $X/D = -0.54$ .

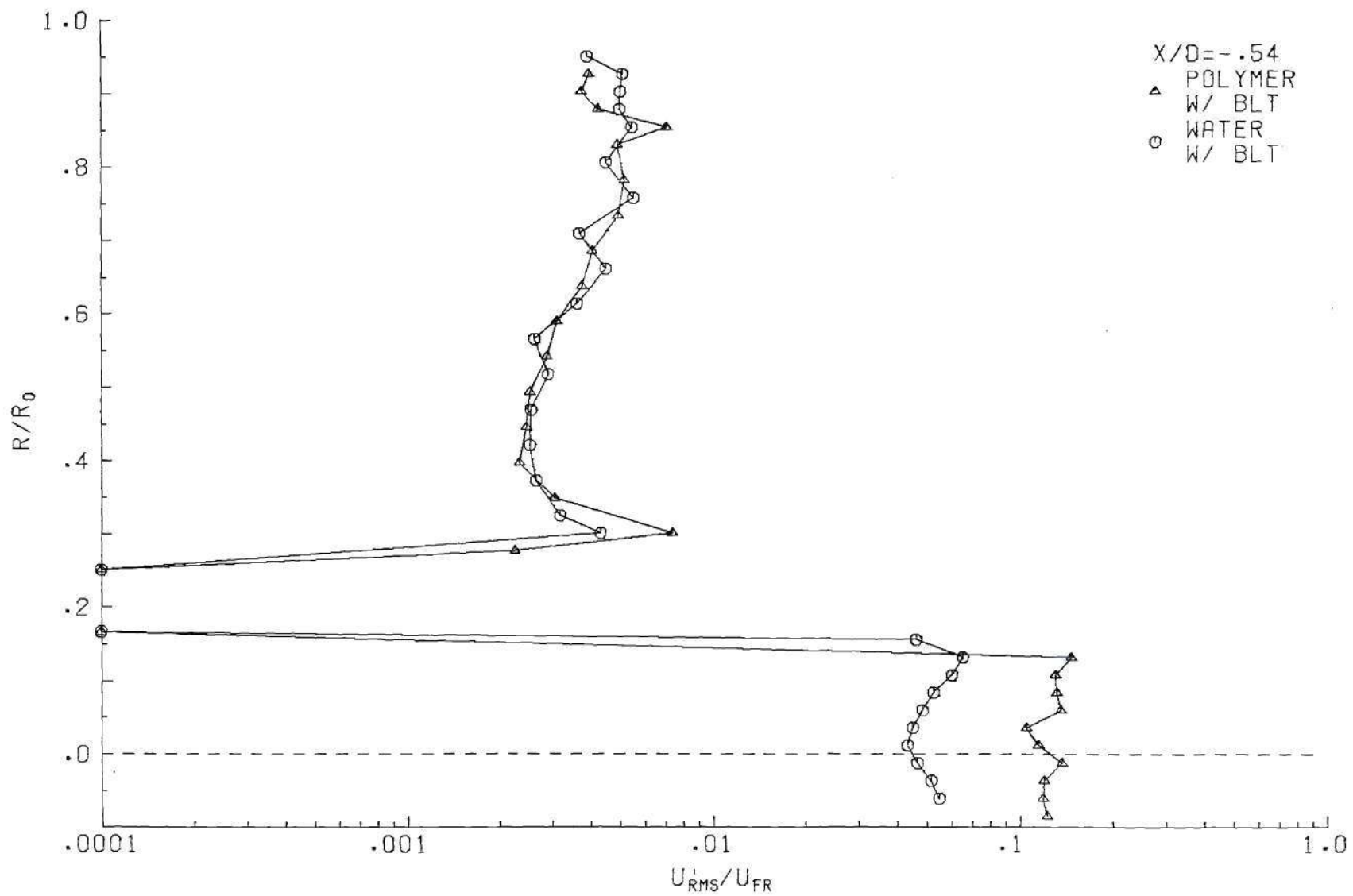


Figure 28. Comparison of Polymer Solution to Water Fluctuation Profile  $X/D = -0.54$ .

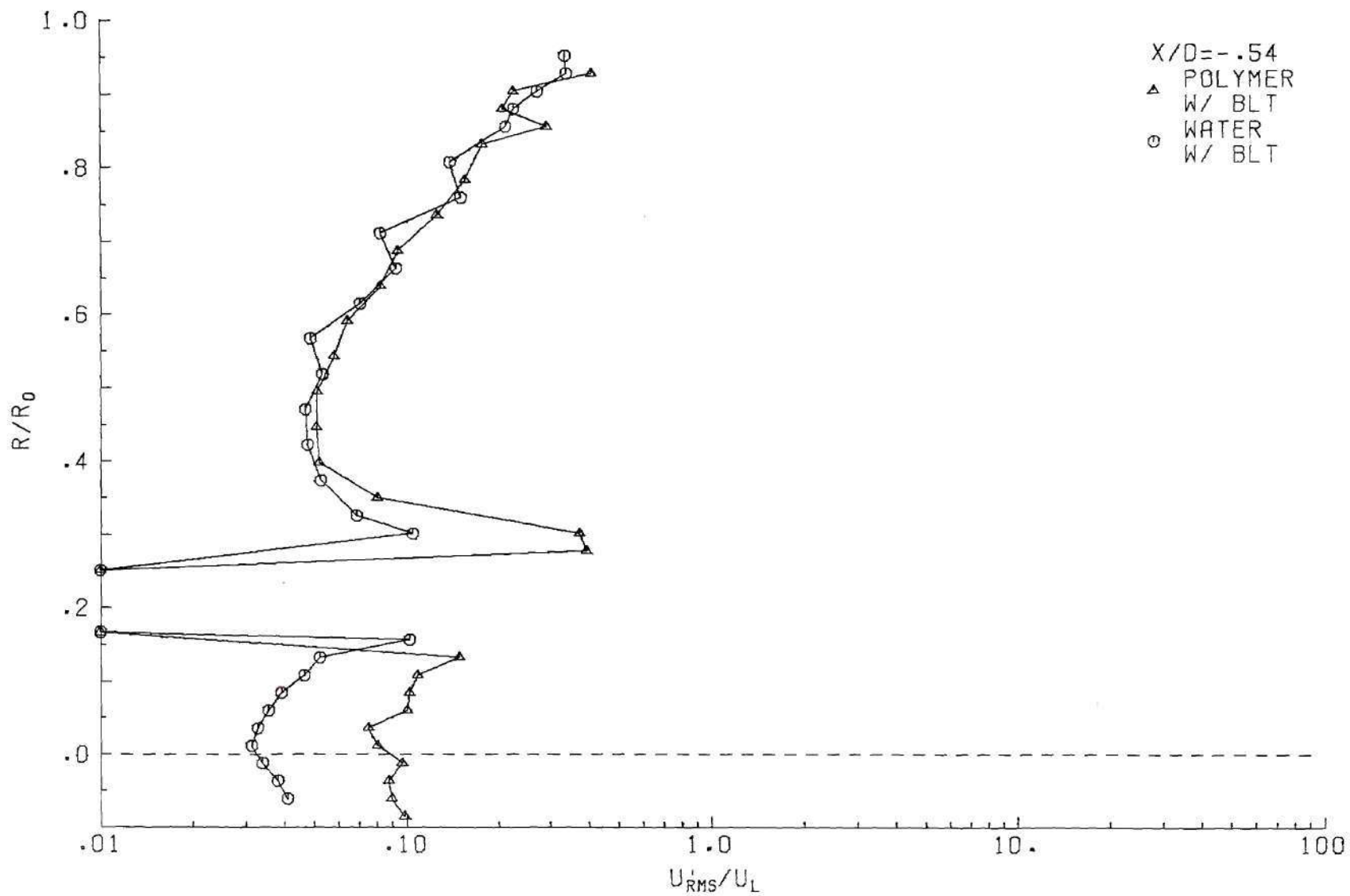


Figure 29. Comparison of Polymer Solution to Water Intensity Profile,  $X/D = -0.54$ .

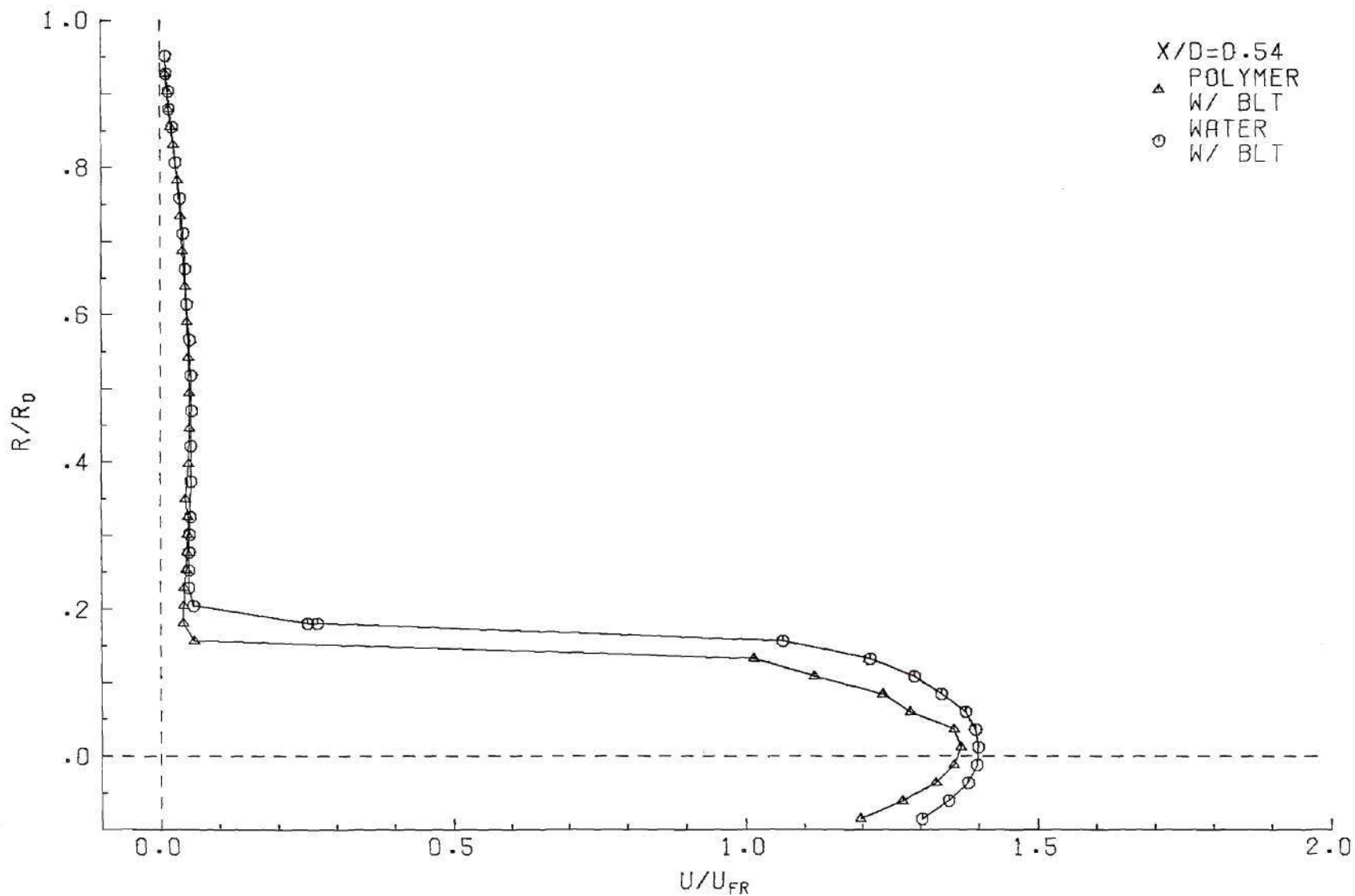


Figure 30. Comparison of Polymer Solution to Water Velocity Profile, X/D = 0.54.

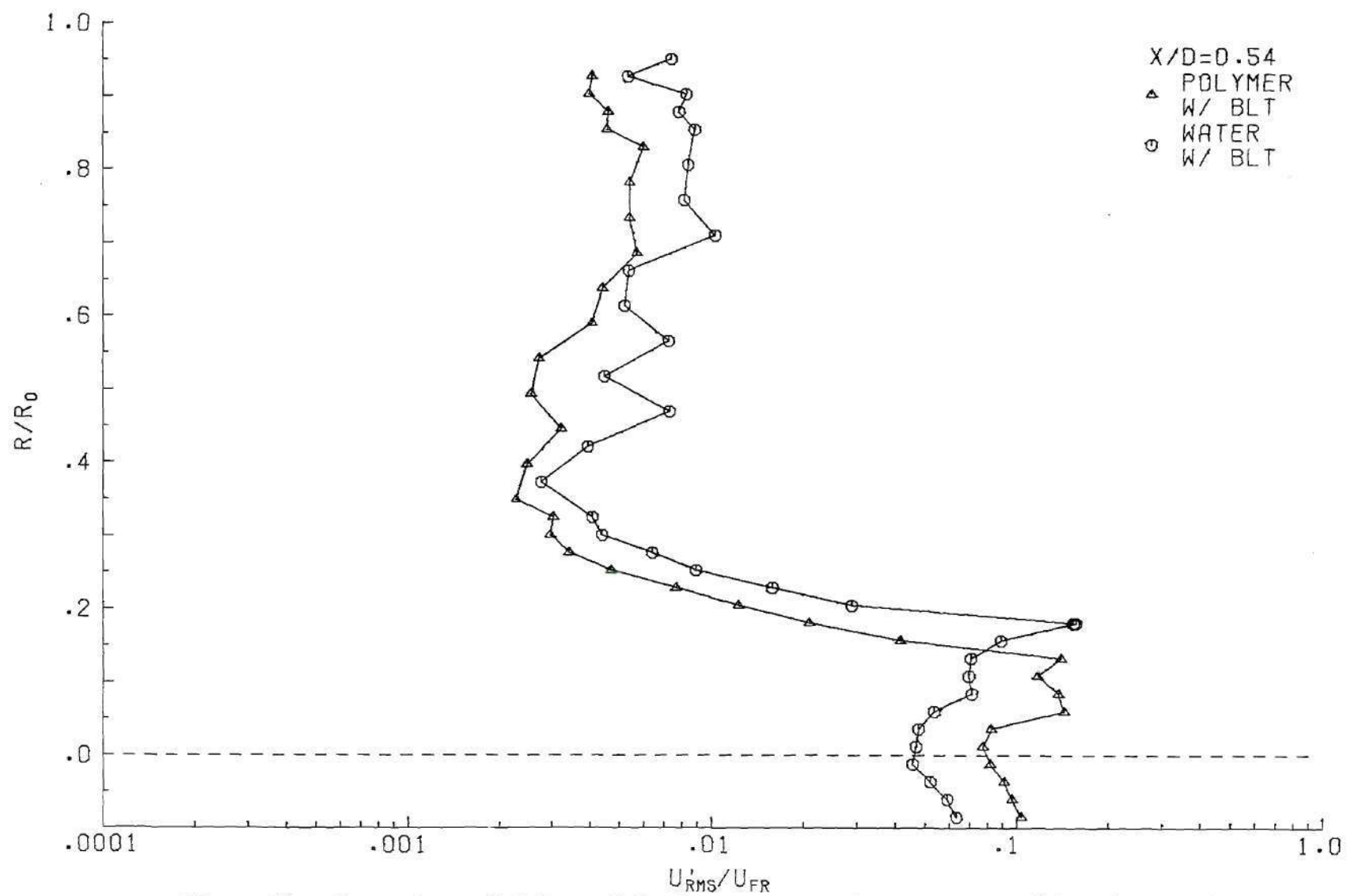


Figure 31. Comparison of Polymer Solution to Water Fluctuation Profile X/D = 0.54.

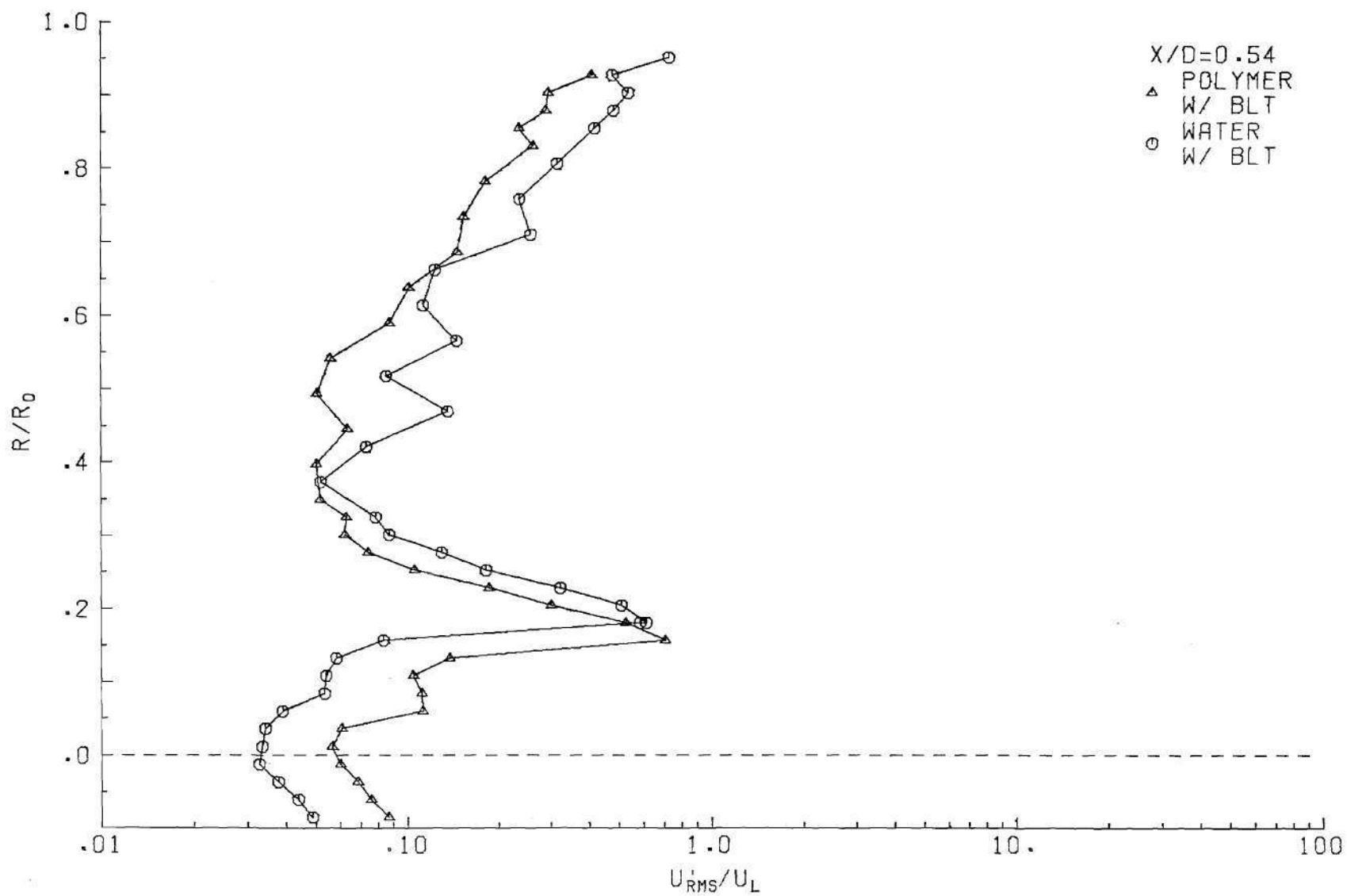


Figure 32. Comparison of Polymer Solution to Water Intensity Profile, X/D = 0.54.

32 also provide near jet information which tends to suggest an altered transfer of energy from the jet edge. This is seen as a wider region of high value fluctuations near the centerline for the water case and is probably the result of the difference in velocity gradients (Figure 30).

From the centerline studies, the polymer solution exhibits a more rapid decay of centerline velocities representative of increased jet spreading. However, from the velocity profiles this does not appear to be exactly the case. The polymer solution displays a more rapid decay at centerline values but a less rapid initial dispersion of the profile into the outer region. This delayed initial spreading may be seen in Figure 36 as a plot of the radial location, at which half of the peak velocity ( $U_p$ ) may be found. That is

$$U(R_{1/2}/R_o) = \frac{1}{2} U_p$$

Near an axial location of 10 catheter diameters, the polymer jet is found to show a substantially more rapid spreading. In the near jet region, the delayed spreading and the increased centerline decay of velocity suggest a possible discrepancy in the flow field. Since the total flow rate is constant, this discrepancy must be compensated elsewhere in the flow. Because the system is cylindrical and axisymmetric small changes in velocity near the outer wall can produce considerable changes in the centerline values. Evidence of differences near the wall becomes most apparent at axial stations just before, during and after recirculation (Figures 37 - 45). The polymer solution fluctuations in the outer region

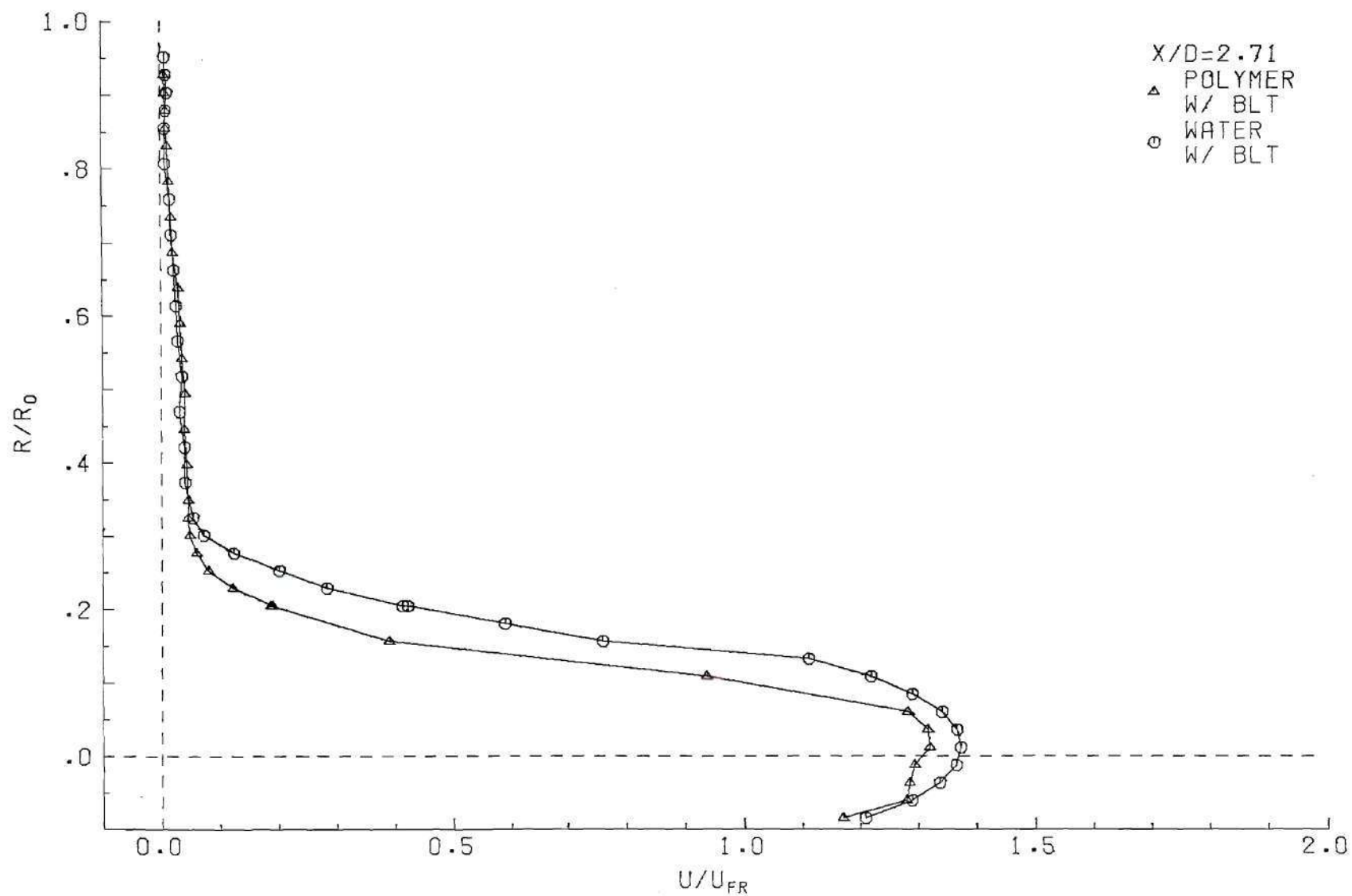


Figure 33. Comparison of Polymer Solution to Water Velocity Profile,  $X/D = 2.71$ .

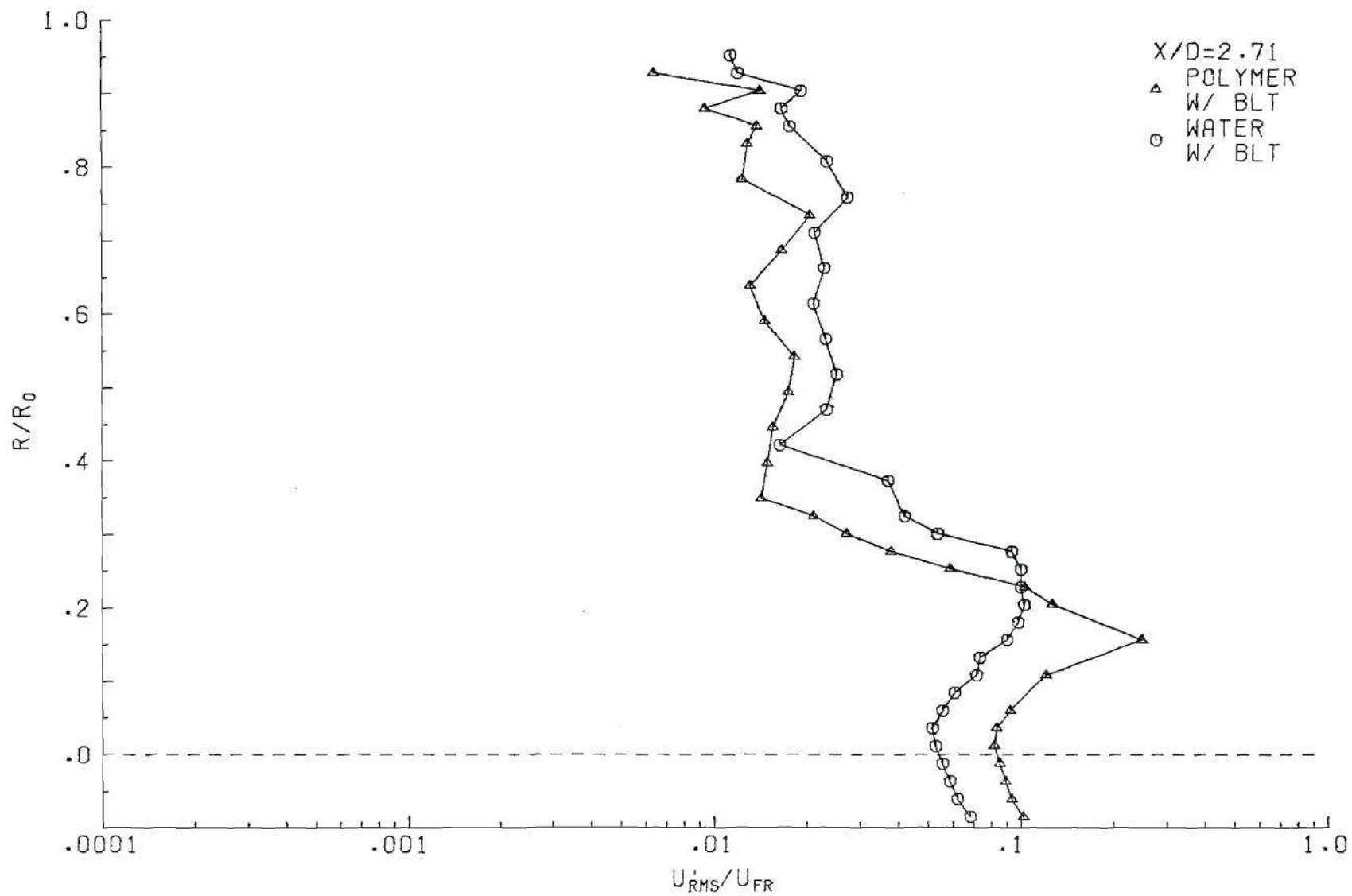


Figure 34. Comparison of Polymer Solution to Water Fluctuation Profile, X/D = 2.71.

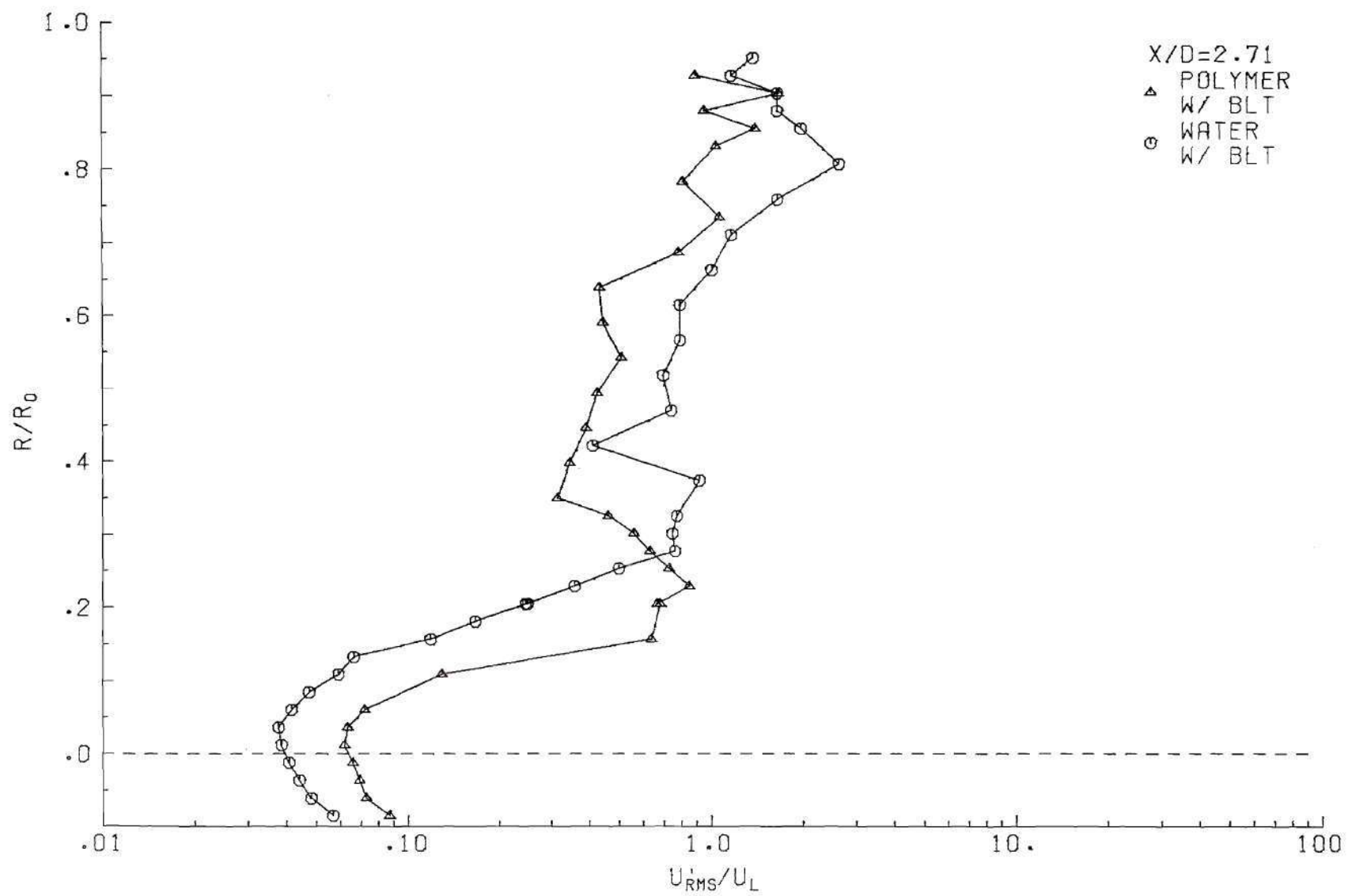


Figure 35. Comparison of Polymer Solution to Water Intensity Profile, X/D = 2.71.

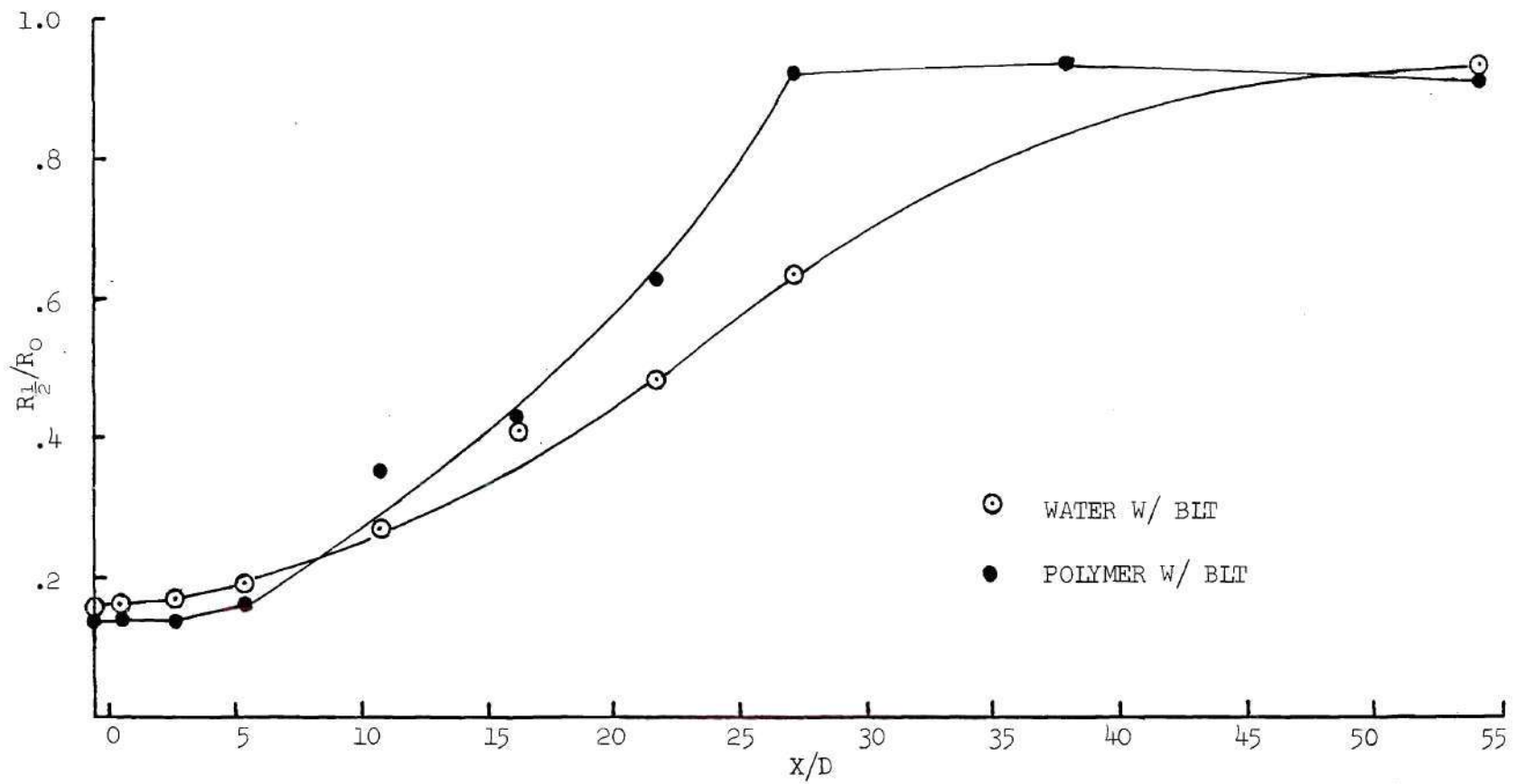


Figure 36. Jet Spreading Using Half Velocities.

still lag the water case until an  $X/D$  of 10.85 is reached (recirculation) (see Figure 41).

Figures 37 through 39 represent the axial location with an  $X/D$  of 5.42, just before recirculation. As can be seen in Figure 37 the outer flow region for the water case is almost zero from an  $R/R_0$  of .55 to 1.0. The polymer solution does not display any velocities very near zero until the wall is reached. Since conservation of mass for the tube cross-section must be satisfied, this explains the decreased centerline value of the polymer accompanied by lower apparent dispersion into the outer flow region. Figure 38 again shows the elevated fluctuations near the centerline and the lagging fluctuations near the wall for the polymer solution injection. The differences are, however, becoming less than those found farther upstream. Figure 39 presents, perhaps, a clearer comparison of the two situations. Because the velocities are near zero in the outer region for the water injection, the resulting nondimensional intensities are much higher than for the polymer. The centerline values again display the increased energy for the polymer jet.

Figures 40 through 42 represent two stations in the region of recirculation. Figure 40 ( $X/D$  equal to 10.85) displays a marked difference in the sizes of the retrograde flow regions. Also of interest is the similarity of the velocity profiles in the outer region. The necessary result is the region confined near the centerline in which the water displays a higher velocity value. Similar results are seen in Figure 42 ( $X/D$  of 16.28). The velocity fluctuations or energy content show essentially the same behavior across the flow when compared to water. The

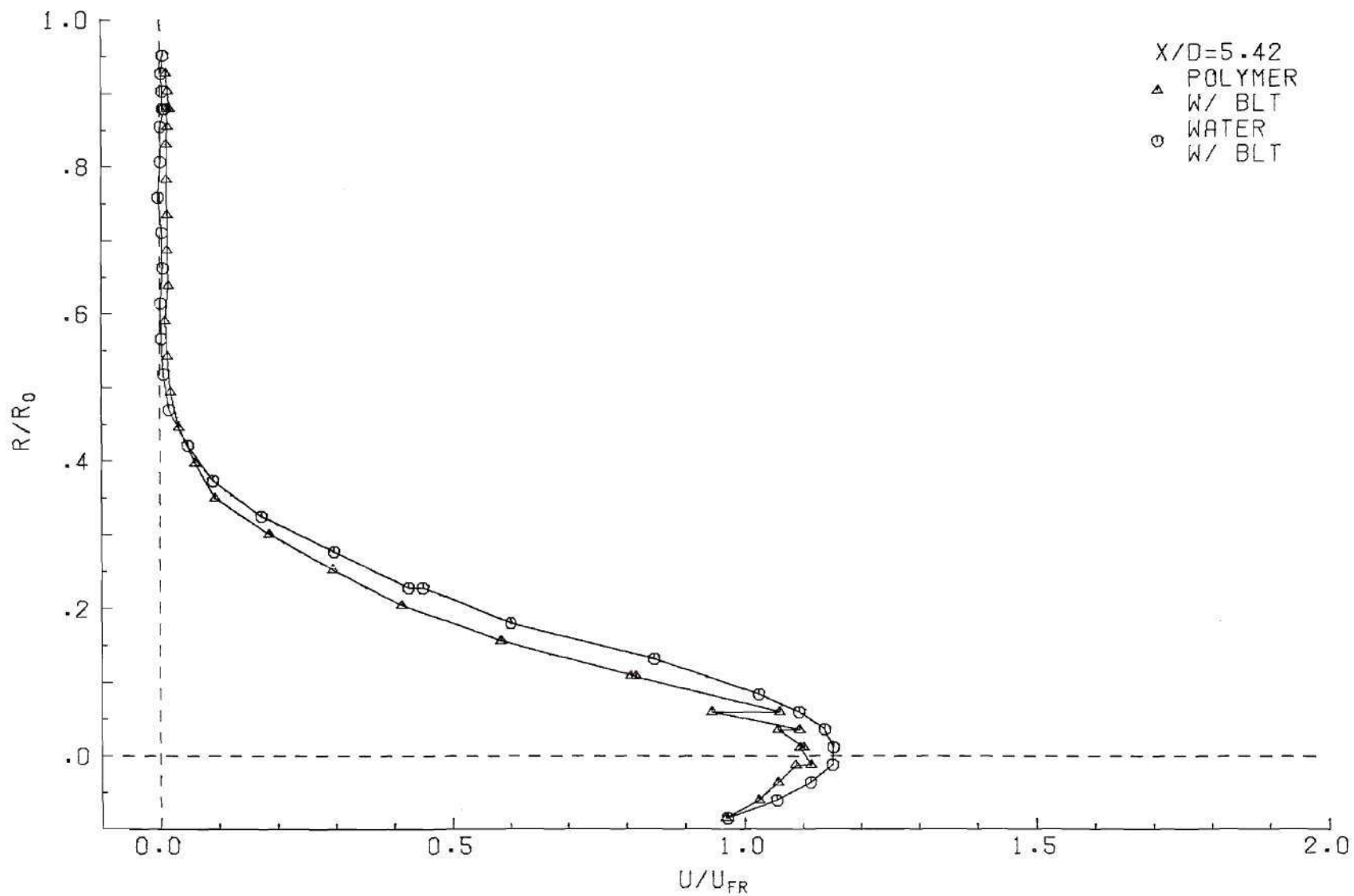


Figure 37. Comparison of Polymer Solution to Water Velocity Profile, X/D = 5.42.

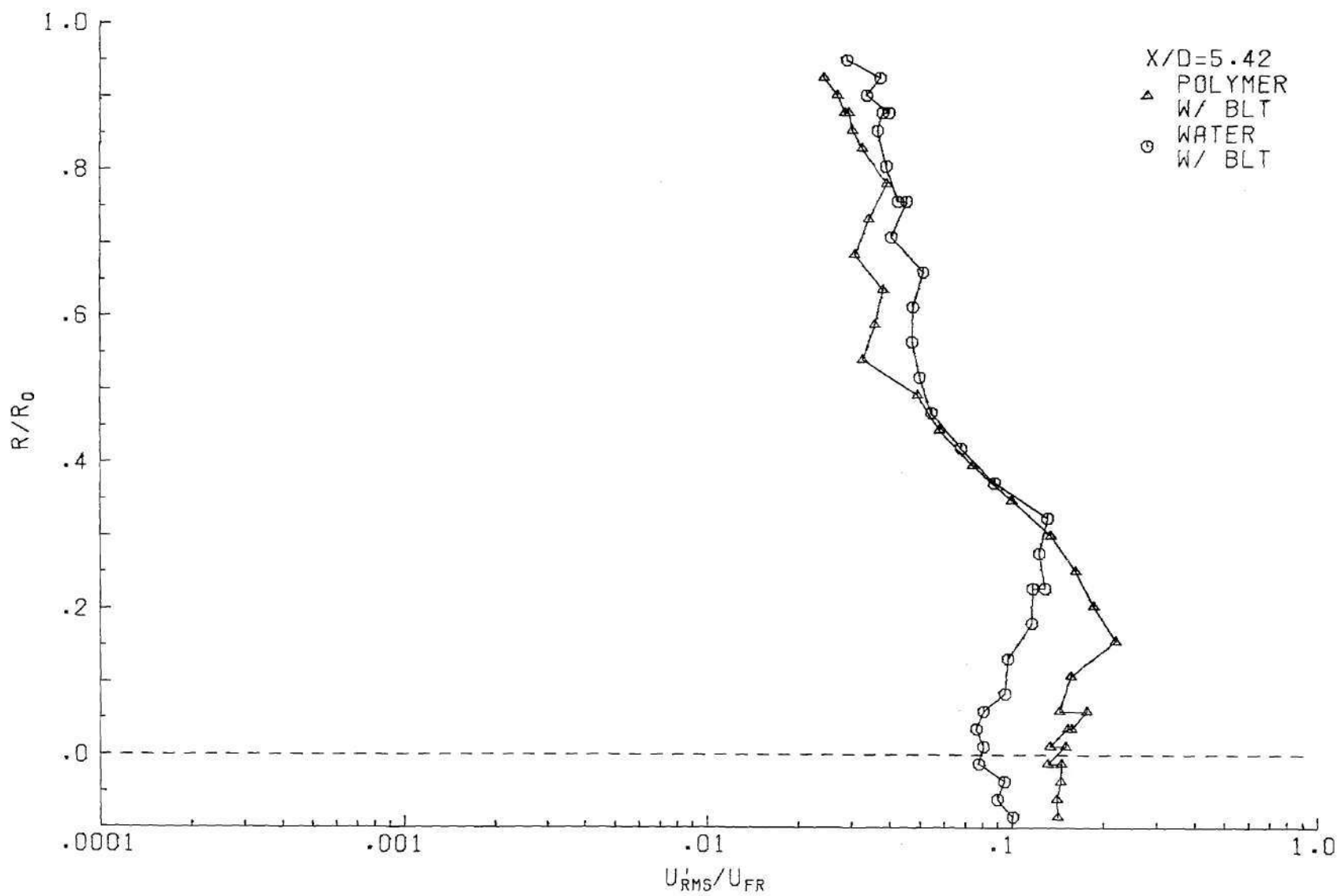


Figure 38. Comparison of Polymer Solution to Water Fluctuation Profile, X/D = 5.42.

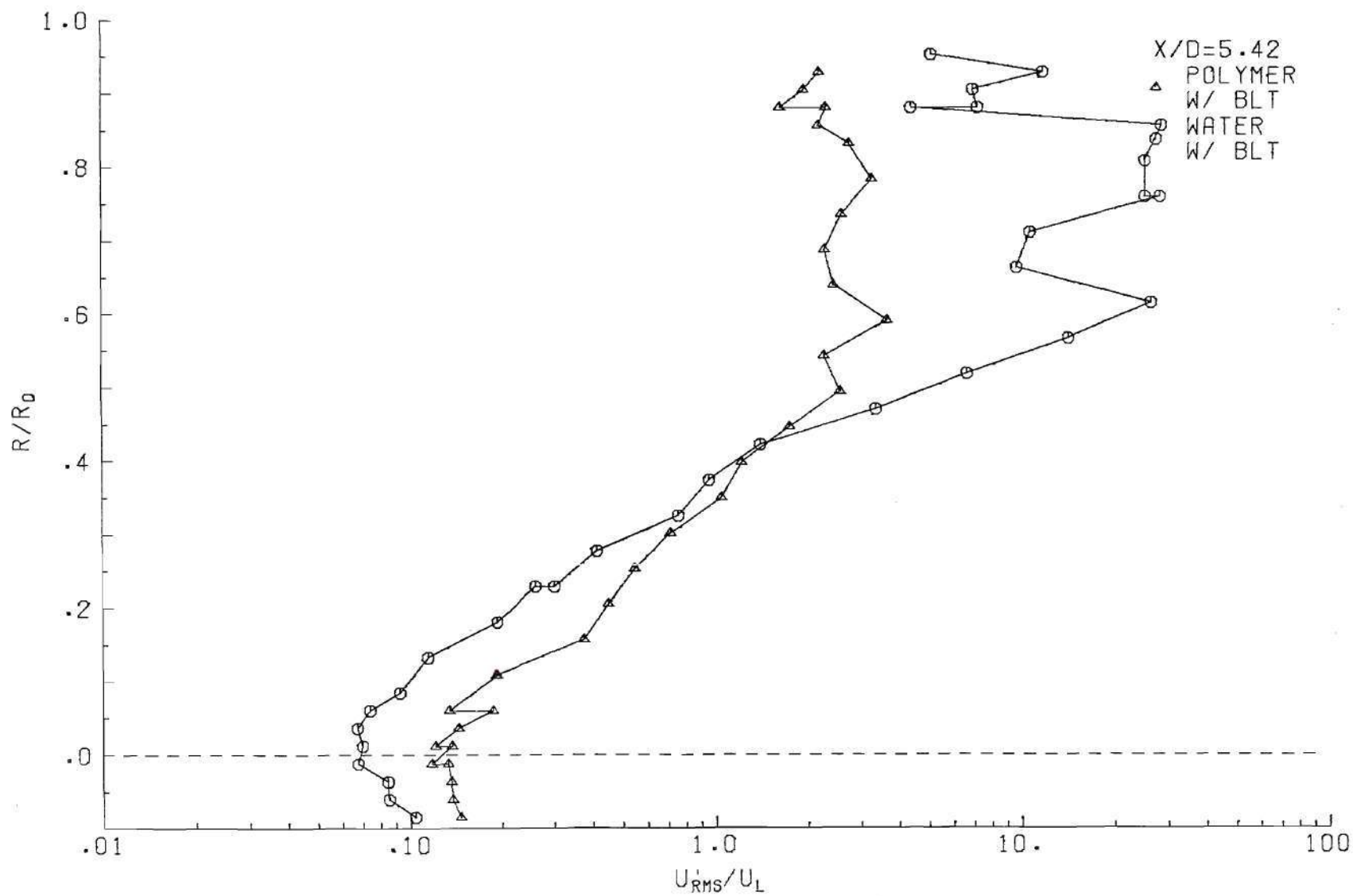


Figure 39. Comparison of Polymer Solution to Water Intensity Profile,  $X/D = 5.42$ .

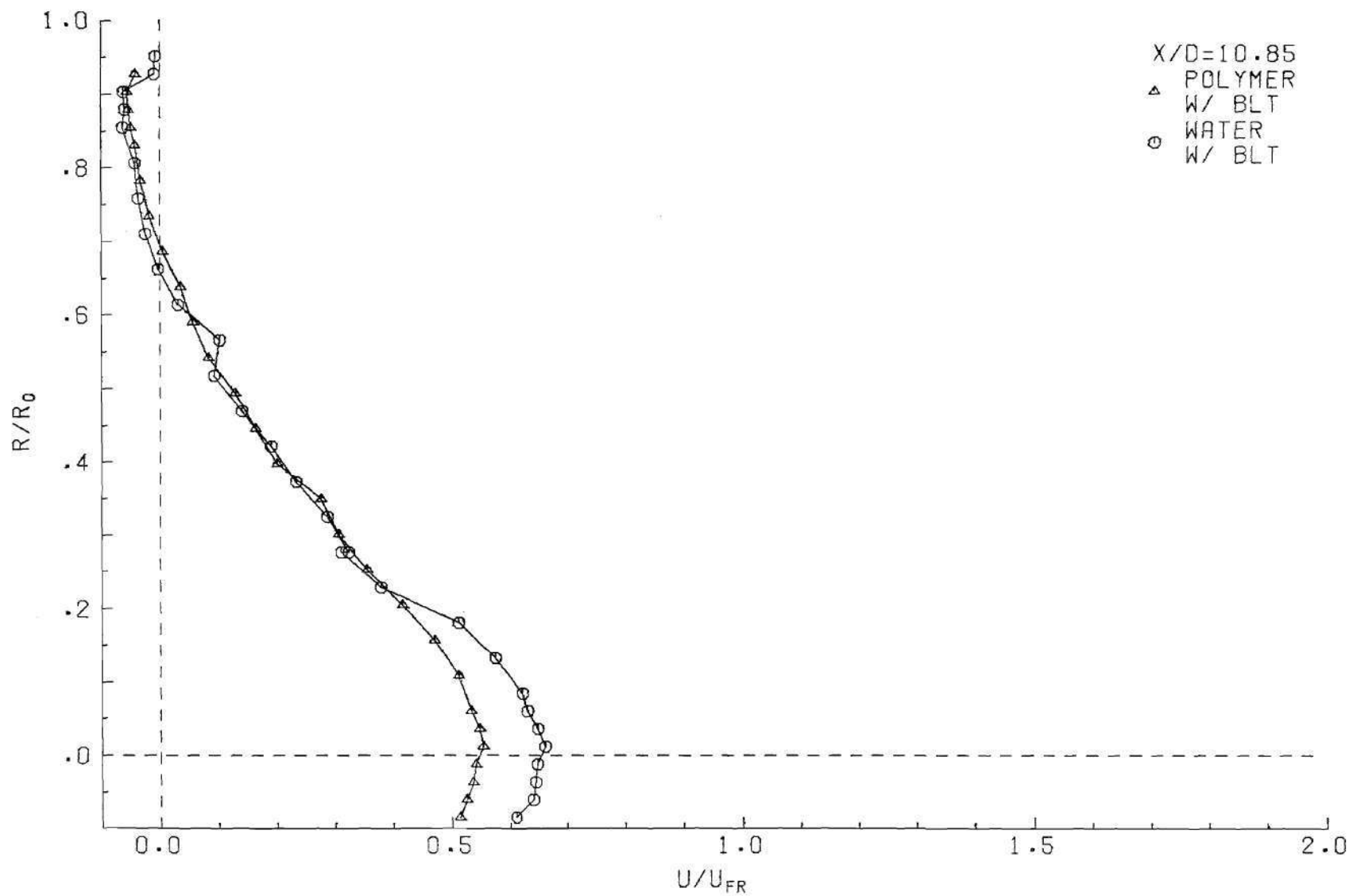


Figure 40. Comparison of Polymer Solution to Water Velocity Profile,  $X/D = 10.85$ .

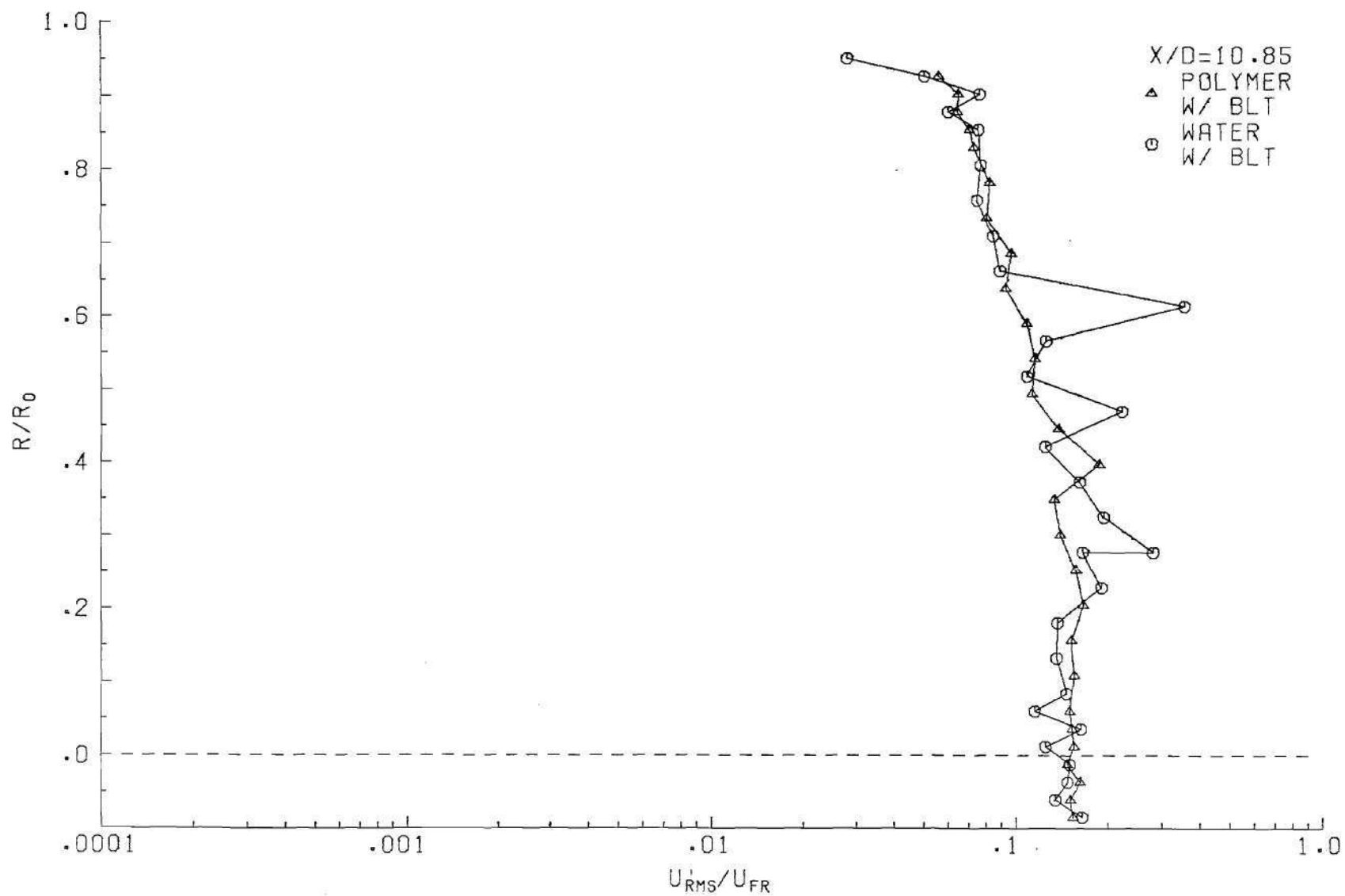


Figure 41. Comparison of Polymer Solution to Water Fluctuation Profile, X/D = 10.85.

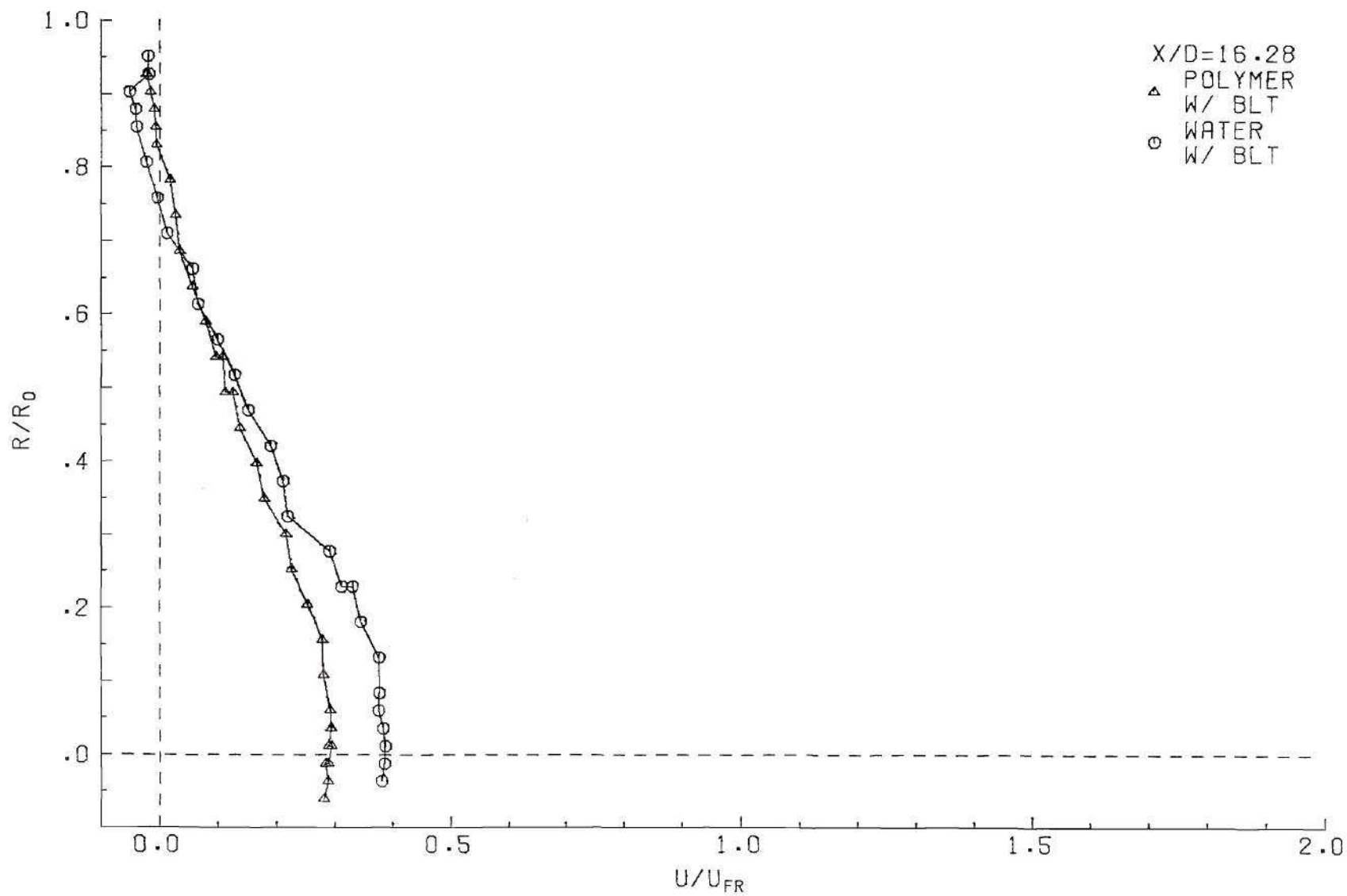


Figure 42. Comparison of Polymer Solution to Water Velocity Profile, X/D = 16.28.

intensities for each case also appear to be of the same order although the water case does display a higher degree of scatter. Additional figures corresponding to this region may be found in Appendix V. From the information in Figures 40 and 42 the region of retrograde flow and thus, probably the recirculation region appear to be thinner for the polymer solution case. A thinner region of recirculation occurs and the entrainment requirements, and therefore the mixing properties of the polymer solutions injections, must be different from the water case, the higher overall entrainment of the polymer jet suggesting a more efficient mixing.

Figures 43 through 45 provide information on stations downstream of the recirculation region. The quick recovery of the velocities in the outer flow region for the polymer case again suggests the smaller recirculation region in the polymer injection. The first instance in which the polymer injection exhibits lower total energy (or fluctuation level) throughout the field is found at an  $X/D$  of 21.71. However, when the intensity is considered, the polymer solution still lags near the wall and leads near the centerline. When the flow has reached an axial station of  $X/D$  equal to 27.14 the velocity profiles are nearly the same (Figure 43). When comparing the energy involved (represented by  $U'_{rms}/U_{FR}$ ), the polymer solution again displays a lower energy than the water case. The turbulent intensity is also found to be lower, suggesting a more efficient dissipation of energy in the polymer solution injection.

As seen in Figure 44 the velocity profiles are approximately the same at  $X/D = 54.27$ . The total energy, as well as the intensities, are found to be slightly lower for the polymer solution case. Radial profiles

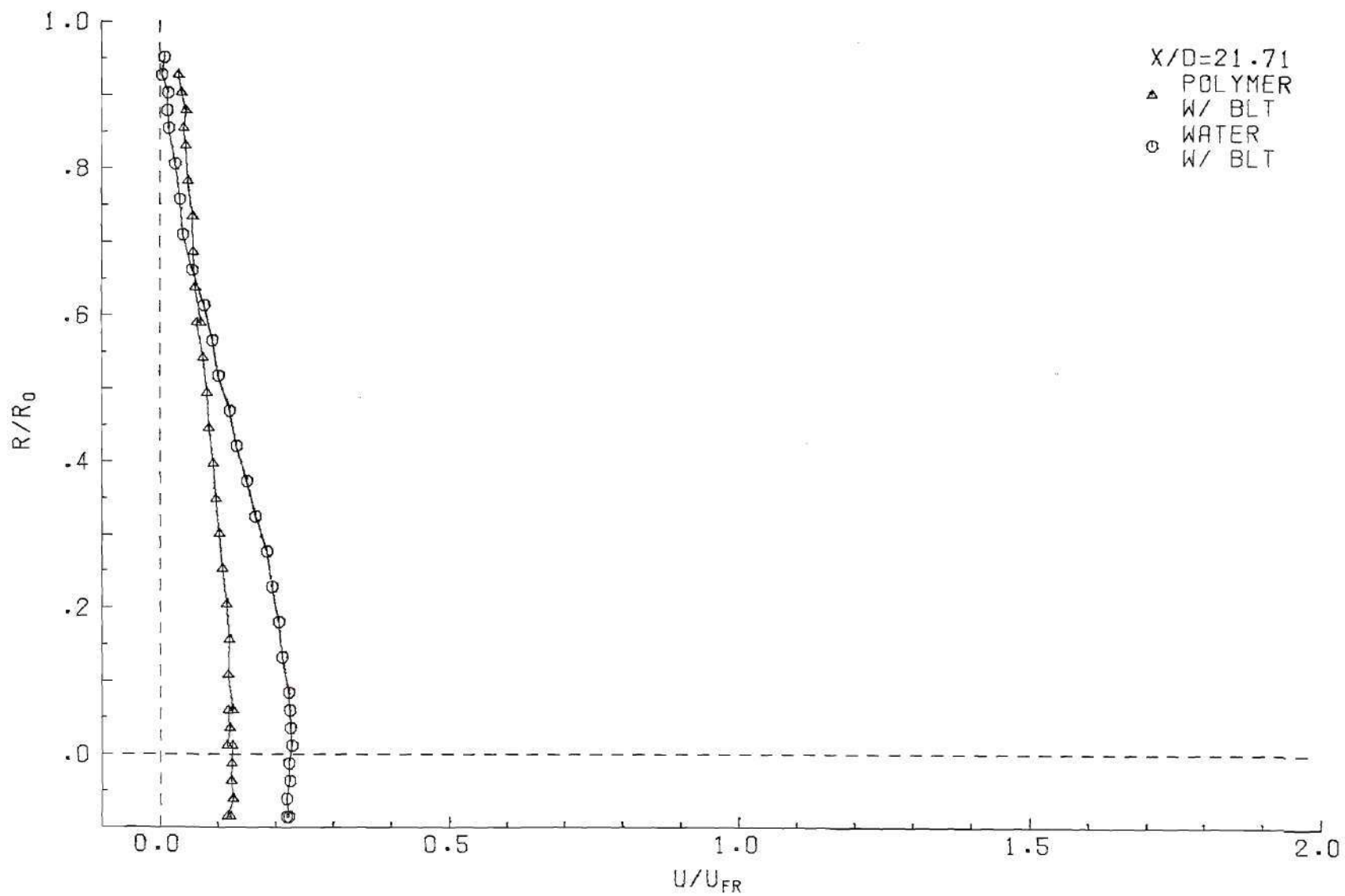


Figure 43. Comparison of Polymer Solution to Water Velocity Profile, X/D = 21.71.

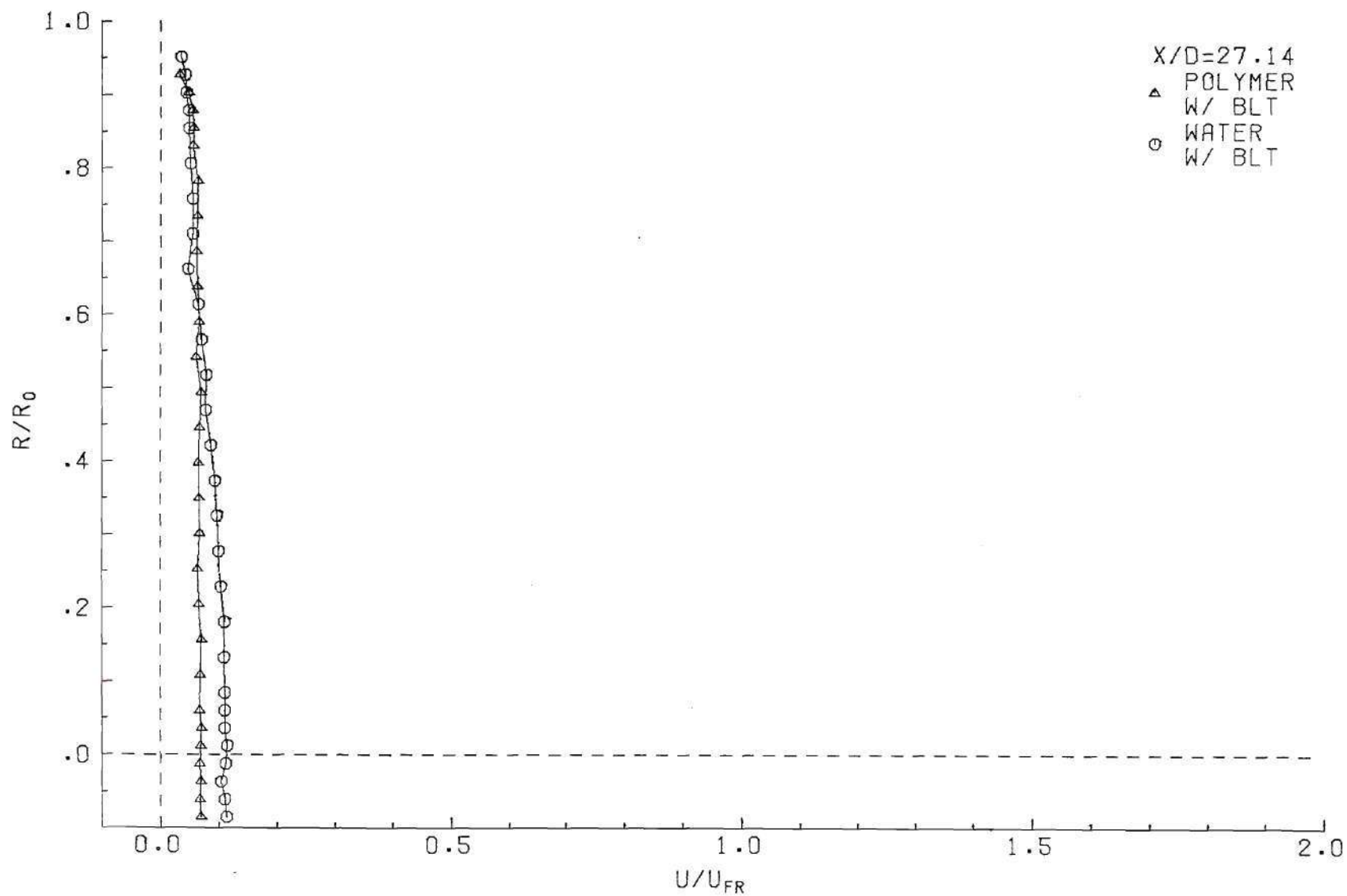


Figure 44. Comparison of Polymer Solution to Water Velocity Profile,  $X/D = 27.14$ .

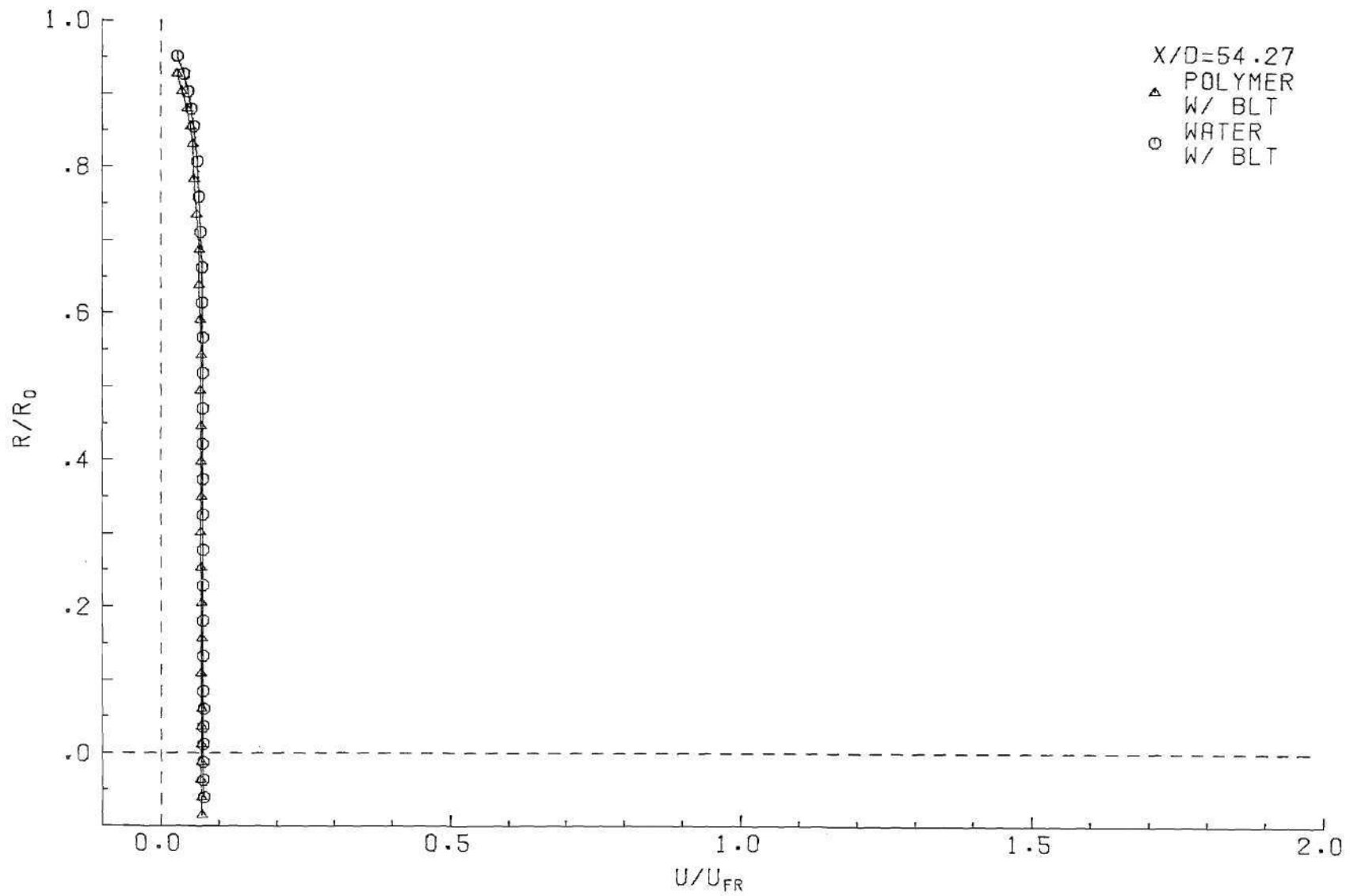


Figure 45. Comparison of Polymer Solution to Water Velocity Profile,  $X/D = 54.27$ .

of the energy and intensity corresponding to the above may be found in Appendix V.

Retrograde Flow Region. Because the recirculation region appeared to be effected by the presence of the polymer, some value representative of the location of the recirculation region should be determined for not only the BLT cases but for the non-BLT cases as well. Since the recirculation region consists of positive as well as negative velocity components, the actual shape of this zone is difficult to map. If the geometry of the flow system had allowed measurement of the radial as well as the axial components of the velocity, velocity vectors could be determined which would display the overall shape of the recirculation region. Unfortunately, radial components could not be measured with any reliability due to the small radius of curvature of the flow facility tubing. In order to obtain some information concerning the size of the recirculation region, an alternate method was employed. The axial length of the near wall retrograde flow region was measured as an indication of the size of the recirculation. To accomplish this, the LDA transducer was traversed axially along the wall, as closely as the resolution of the sample volume would permit, until the upstream and downstream zero velocity locations were determined (points of sign change).

Because of the high fluctuation, long averaging times were necessary and the measurements were repeated to check reliability. The results of these measurements are shown in Figure 46. As can be seen from this figure both injections using the polymer solution resulted in a smaller near wall retrograde flow region. This, combined with information found in Figures 40 and 42, suggests the production of smaller

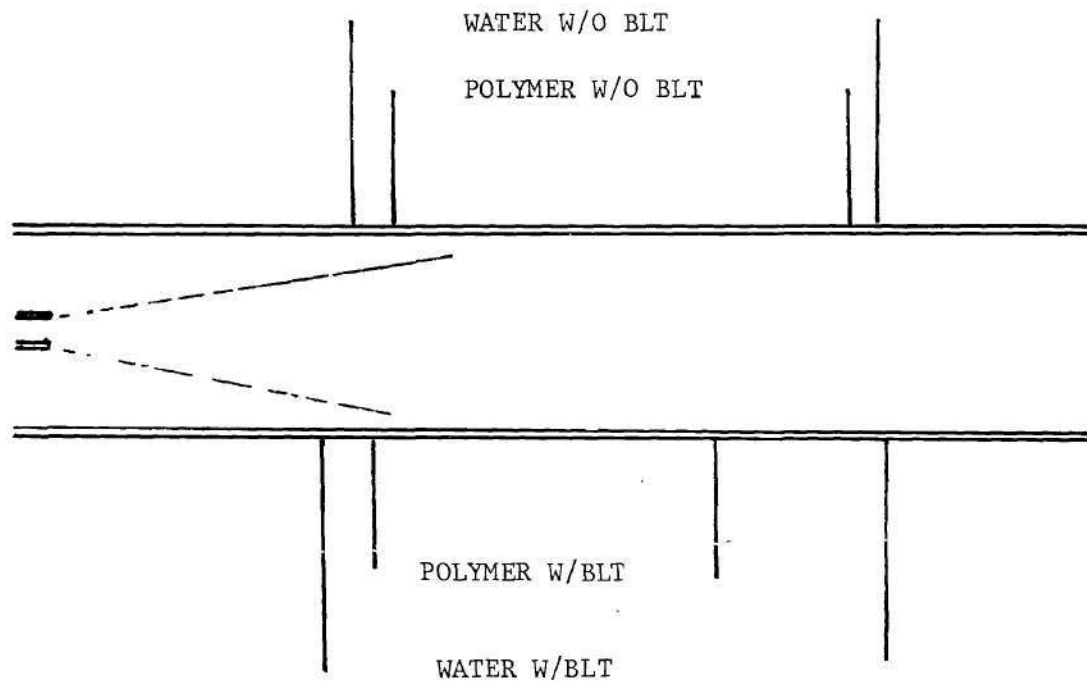


Figure 46. Lengths of Near Wall Retrograde Flow Regions.

recirculation regions. When comparing both the water injections, the presence of the BLT appears to produce only a very slight change in the size of the recirculation region. The presence of the BLT in the polymer injections has quite a marked effect with the resulting recirculation region being much smaller in size for the BLT case. The exact reasons for the large differences in recirculation sizes are not fully understood but the initial conditions as well as the altered turbulent mixing are believed to have an effect on the recirculation size and location.

Spectra. Additional information concerning the injection process and the resulting turbulent mixing may be obtained through a study of the various power spectral densities produced at different locations in the flow. Representation of the overall radial variation of the power spectral densities at each axial station is produced by plotting several radial locations on the same figure.

The water injection with the BLT is represented by Figures 47 through 55. Where possible, the spectra at or near the radial positions ( $R/R_0$ ) of .012, .11, .30, .52, .76 and .88 are presented.

Figure 47 represents the radial variation of the spectra at an axial location of -0.54 catheter diameters. Spectra of the outer flow region ( $R/R_0$  equal to .30 through .88) display energy levels so low as to be obscured by the noise and ambiguity in the system. This is not unusual in that the outer flow is very nearly laminar with the majority of the energy being contained by the mean flow (and hence, low frequencies). The catheter spectra demonstrate a decrease in the energy contained by the lower frequencies as the centerline is approached. Figure

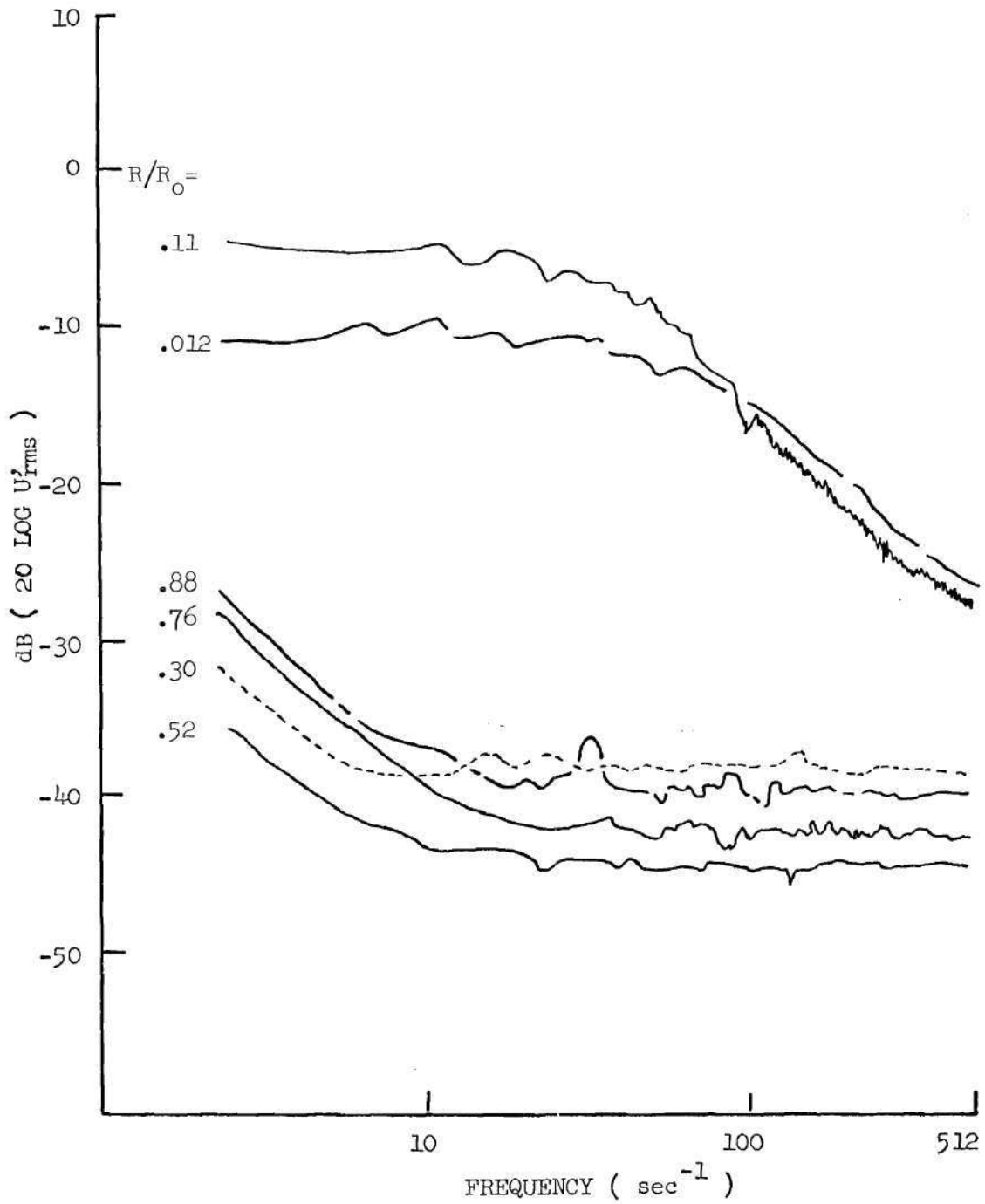


Figure 47. Radial Variation of Spectra, Water Injection,  $X/D = -0.54$ .

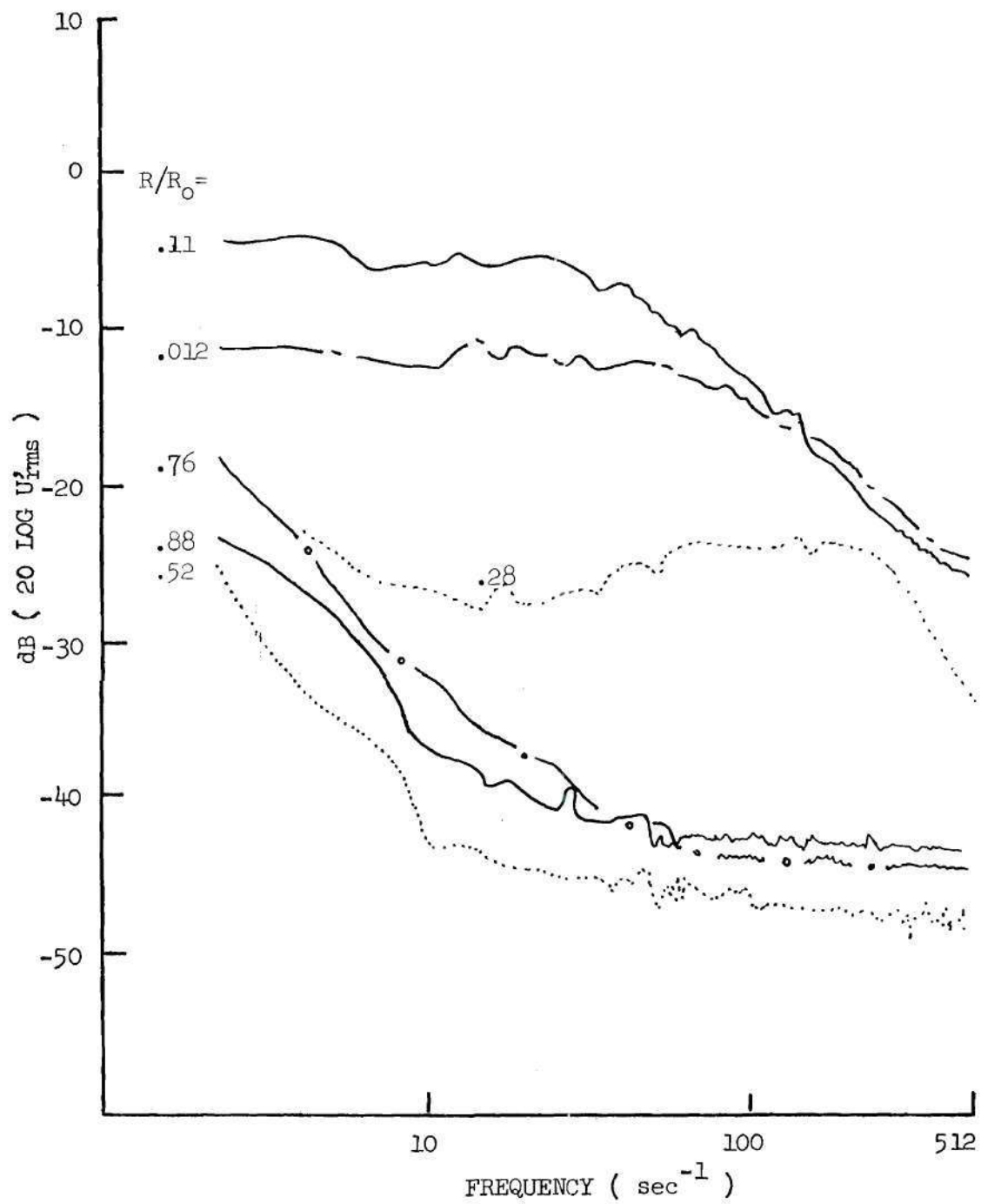


Figure 48. Radial Variation of Spectra, Water Injection,  $X/D = 0.54$ .

48 ( $X/D$  equal 0.54) displays approximately the same behavior. However, at an  $R/R_0$  equal to .28 the behavior of the spectra displays a strong deviation. A wide band region of increased energy over frequencies from approximately 30 to 500 Hertz is evident. A more detailed representation of this region is shown in Figure 49 which displays the power spectral densities at radial positions from an  $R/R_0$  of 0.18 to 0.42 at an  $X/D$  of 0.54 catheter diameters. The catheter lip covers the radial positions from 0.17 to 0.25 and may be considered as a possible factor contributing to the spectral distribution. At the radial position of  $R/R_0$  equal to .42 the spectral distribution is near that of the pseudo-laminar outer flow. Moving toward the centerline (decreasing  $R/R_0$ ) the disturbance (hump in the spectrum) increases in magnitude with a decrease in the overall frequency range. The center frequency of this disturbance also increases as the centerline is approached. Cassanova (50) reported a similar increasing of frequency for vortex shedding after a stenosis. Also noteworthy is a relatively unaffected range of lower frequencies apparent in the spectra. It is not until the radial location is in the region distal to the catheter lip that the lower frequencies begin to show a marked increase in energy content. Finally, when the radial position is very near the inner flow region, the disturbance appears to be dispersed by the higher turbulence flow.

Figure 50 represents the flow at an axial station of 2.71 catheter diameters. From the information provided the energy content in the outer flow is seen to be increasing. This is manifested as an increase in the frequencies below 110 Hertz. At the same time the inner flow

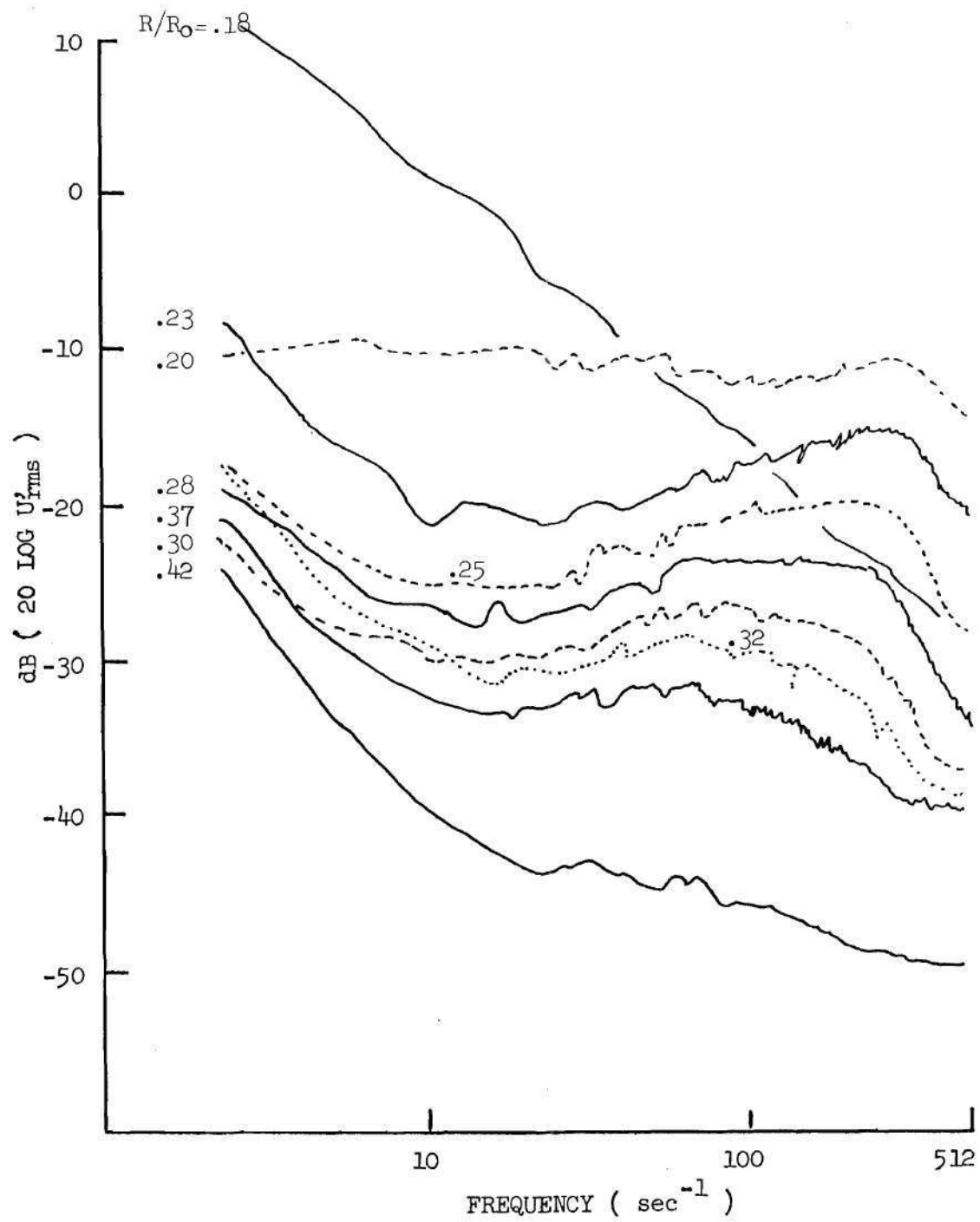


Figure 49. Radial Variation of Spectra Water Injection.

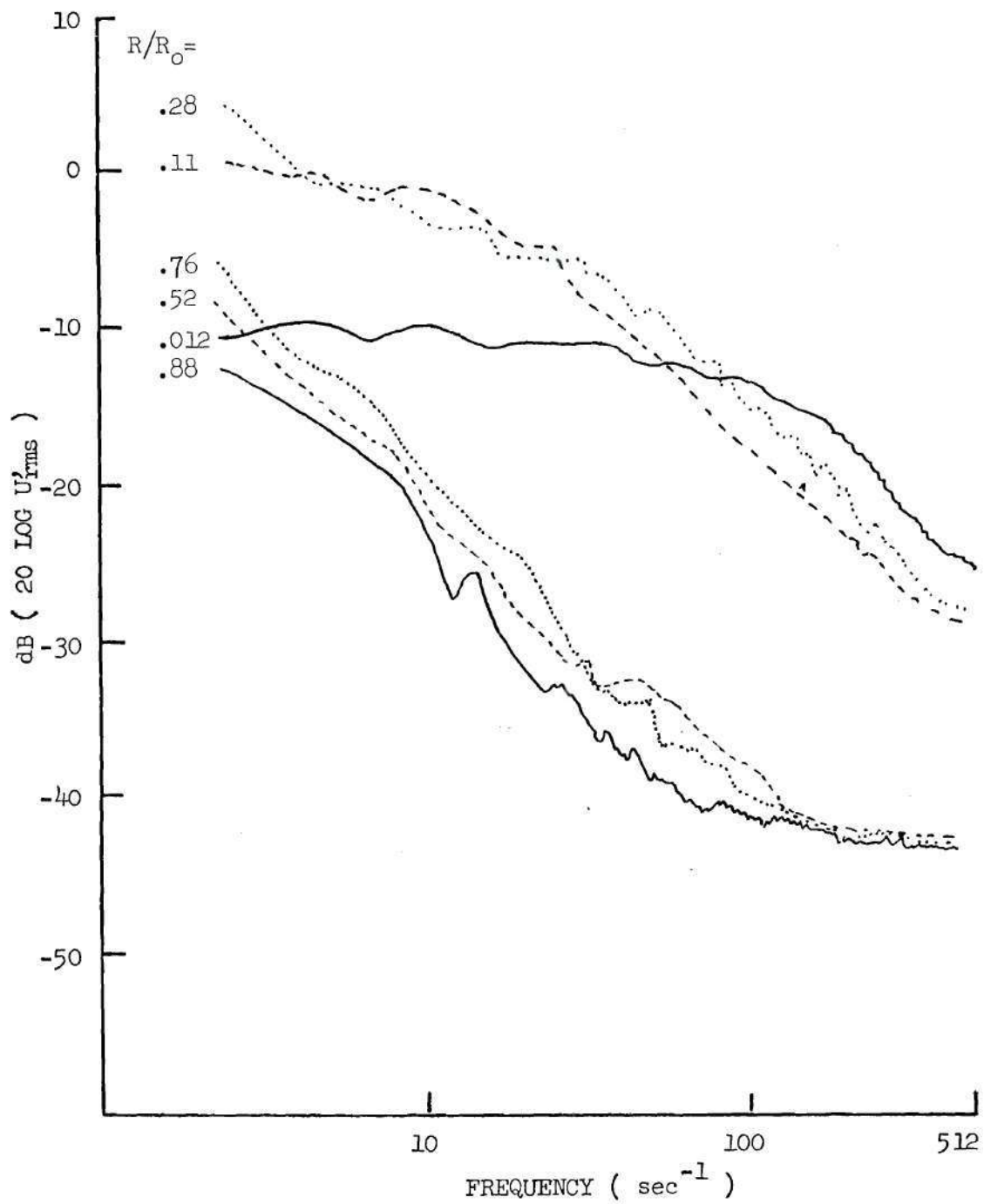


Figure 50. Radial Variation of Spectra, Water Injection,  $X/D = 2.71$ .

region away from the centerline is also displaying an increase in energy contained in the lower frequencies. Because a disturbance was detected in the spectra at  $X/D = 0.54$ , the developing region at the present location was also studied. The resulting power spectral densities are found in Figure 51. Although relatively lower in magnitude than the remainder of a spectrum, the disturbance can still be seen over the radial positions from an  $R/R_0$  of 0.28 to 0.52. The center frequency is now located at a lower value than previously and suggests that the frequency of the disturbance decreases axially as well as radially.

At this point it is necessary to account for the broadband peaked disturbance seen in the turbulence power spectra. Because of the low outer velocity, there are some similarities between the present confined jet and the cases of free jets and stenosed flows. In these latter cases the disturbance seen in the spectra could be attributed to vortex shedding. For flow through a stenosis the resulting Strouhal number is found to vary from 1.0 near the jet to less than 0.6 just before the breakup at the vortex. The value of .6 is found at a location whose spectrum provides a maximum disturbance intensity (50). Crow and Champagne (19) found similar results for a turbulent free jet. Becker and Messaro (18), in their study of a variety of free end confined jets, found that, for a Craya-Curtet number of .35 and a Reynolds number of 7000, near jet Strouhal numbers of approximately 1.0 were produced. In the present flow the Strouhal numbers calculated ranged from 1.0 at an  $X/D$  of 0.54 to 0.20 at an  $X/D$  of 2.71. Since the overall disturbance agreed so well with the behavior that would result from vortex shedding of the jet, it is not

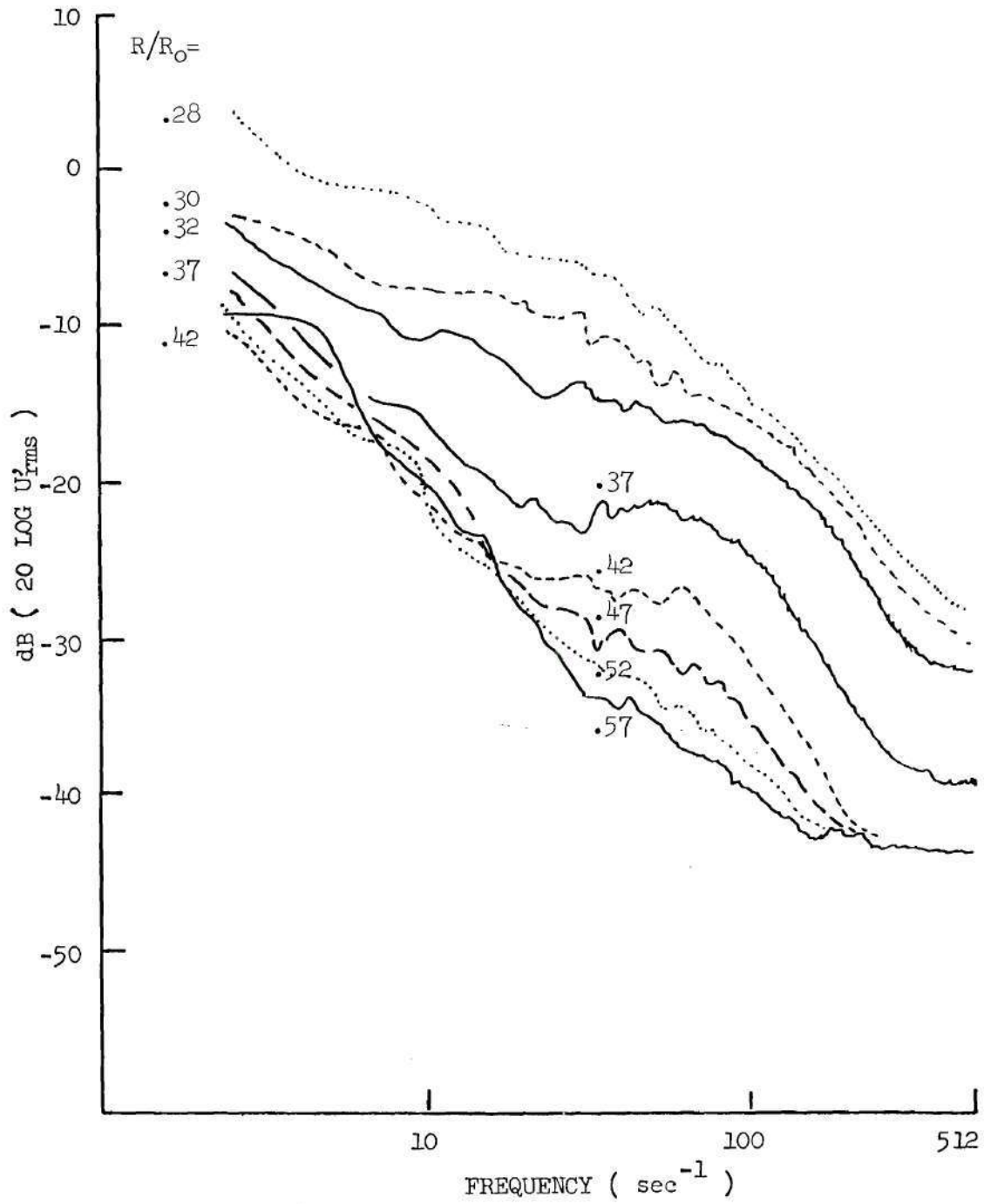


Figure 51. Radial Variation of Spectra, Water Injection,  $X/D = 2.71$ .

unlikely that the disturbances seen in Figure 49 and 51 originated from this phenomenon. The extent of the downstream propagation of the disturbance also tends to substantiate this conclusion.

In frequency space, the Kolmogorov theory for isotropic turbulence suggests a power spectral density in which the predominant slope is  $-2$  when a log-log plot is employed. Kolmogorov-like spectra (slope of  $-2$ ) have, however, been observed in meteorological flow conditions which exhibit little isotropy. In fact, it is not uncommon for turbulent flows to exist which do not meet the Kolmogorov criterion but still exhibit the  $-2$  slope ( $-5/2$  in wave number space) (51). In the present study the data are plotted on a log-log scale in which the ordinate covers twice the number of decades per unit length as the abscissa. For this type of plot, the slope of a spectrum with a Kolmogorov-like distribution would have an apparent slope of  $-1$  or an inclination of  $-45^\circ$ .

Figure 52 represents the axial station corresponding to 5.43 catheter diameters. When compared to the near exit plane conditions ( $X/D = -.54$ ), the spectra at all radial positions have increased in total energy content. The outer flow spectra have been shifted out of the noise with the spectral shape retaining the same slope for low frequencies. The inner flow region has spectra with high frequencies of essentially the same value as those at  $X/D = -.54$ . The energy content of the frequencies below approximately 110 Hertz shows an increasing trend. The overall slopes at the inner and out flow regions are approaching similar values. The higher frequencies of the spectra for the inner flow region and the lower frequencies of the spectra for the outer flow

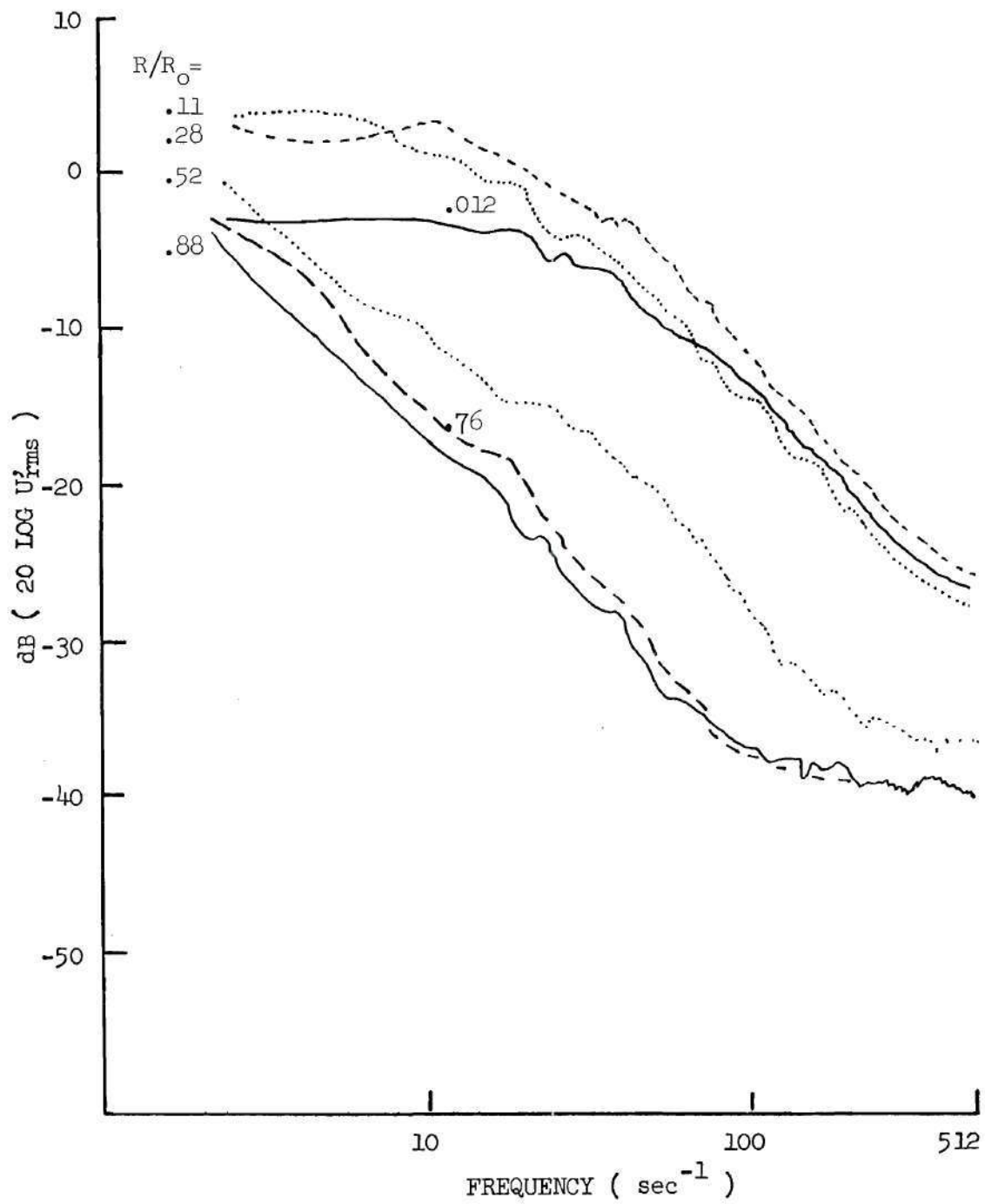


Figure 52. Radial Variation of Spectra, Water Injection,  $X/D = 5.42$ .

region display an inclination angle of approximately  $-45$  degrees.

At an  $X/D$  of 10.85 (Figure 53), the longitudinal turbulence energy contained by the outer flow has shifted the spectra closer to that of the inner flow. The energy content of the inner flow region appears to have dropped only slightly. The slope over a range of frequencies from approximately 10 to 100 Hertz is maintained at  $-2$  (for these plots  $-1$  or  $-45$  degrees). At an  $X/D$  of 16.28 the spectra are more closely correlated with a slight drop in energy levels for the inner flow. A slope of  $-2$  is now only seen over a region between approximately 45 and 200 Hertz. The spectra corresponding to an  $X/D$  of 21.71 and 27.14 catheter diameters differ from the previous case with the exception of an overall decrease in the energy content of all the spectra.

At an  $X/D$  of 54.27 diameters the spectra show an overall loss of turbulent energy. The slope is no longer Kolmogorov-like in distribution. The higher frequency energy content has dropped below the noise and ambiguity of the system. The spectra do show a high degree of correlation consistent with the flat velocity profile and a uniform distribution of energy described in the previous section.

The polymer spectra were reduced in a similar fashion and are presented in Figure 56 through 64. The spectra produced by the flow at  $X/D$  equal to  $-0.54$  are shown in Figure 56. As expected, there is essentially no difference in the outer flow spectra when compared to the comparable water case. However, the inner flow produces spectra that are different from the water case. The overall level of energy is higher for the polymer solution especially in the lower frequencies.

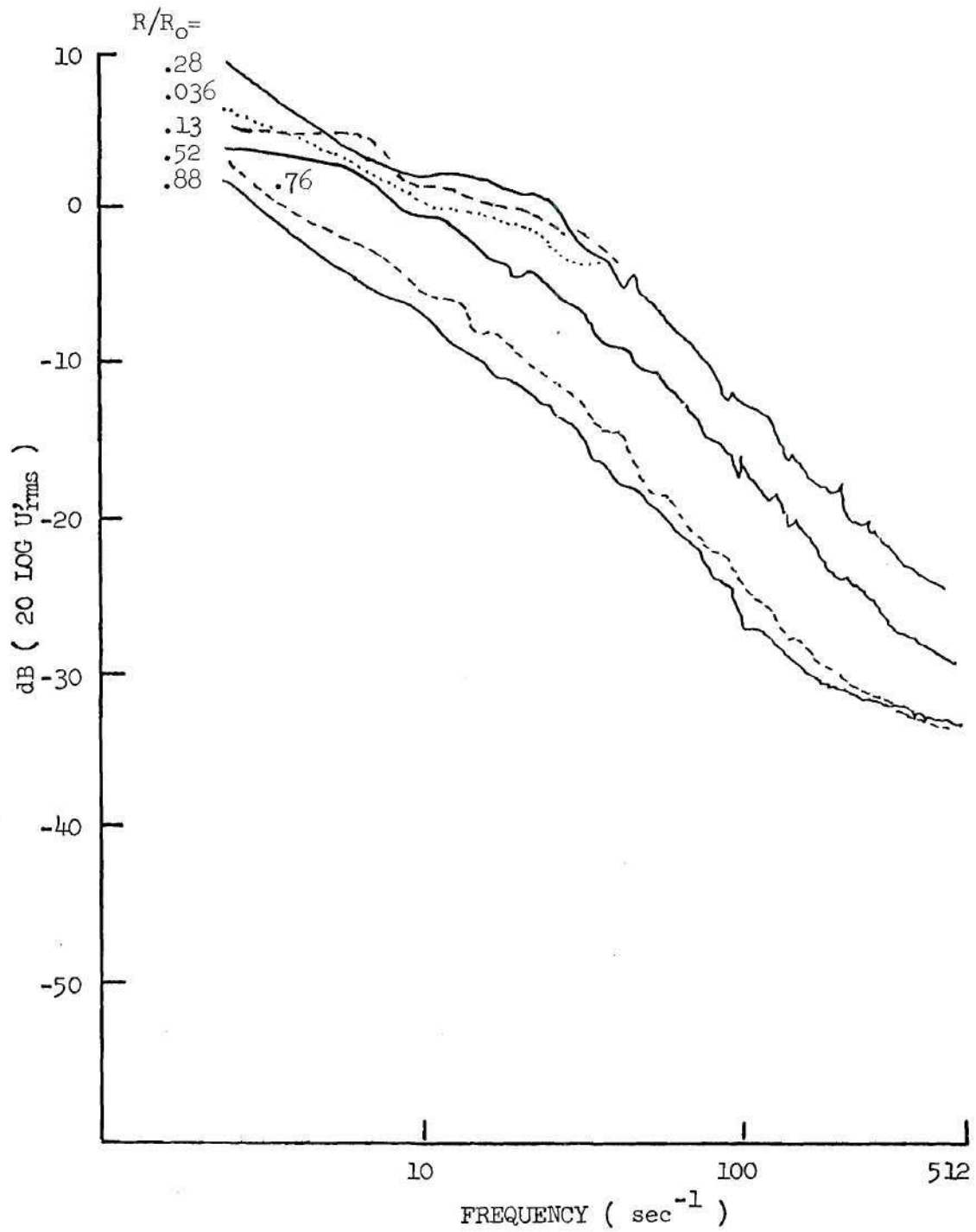


Figure 53. Radial Variation of Spectra, Water Injection,  $X/D = 10.85$ .

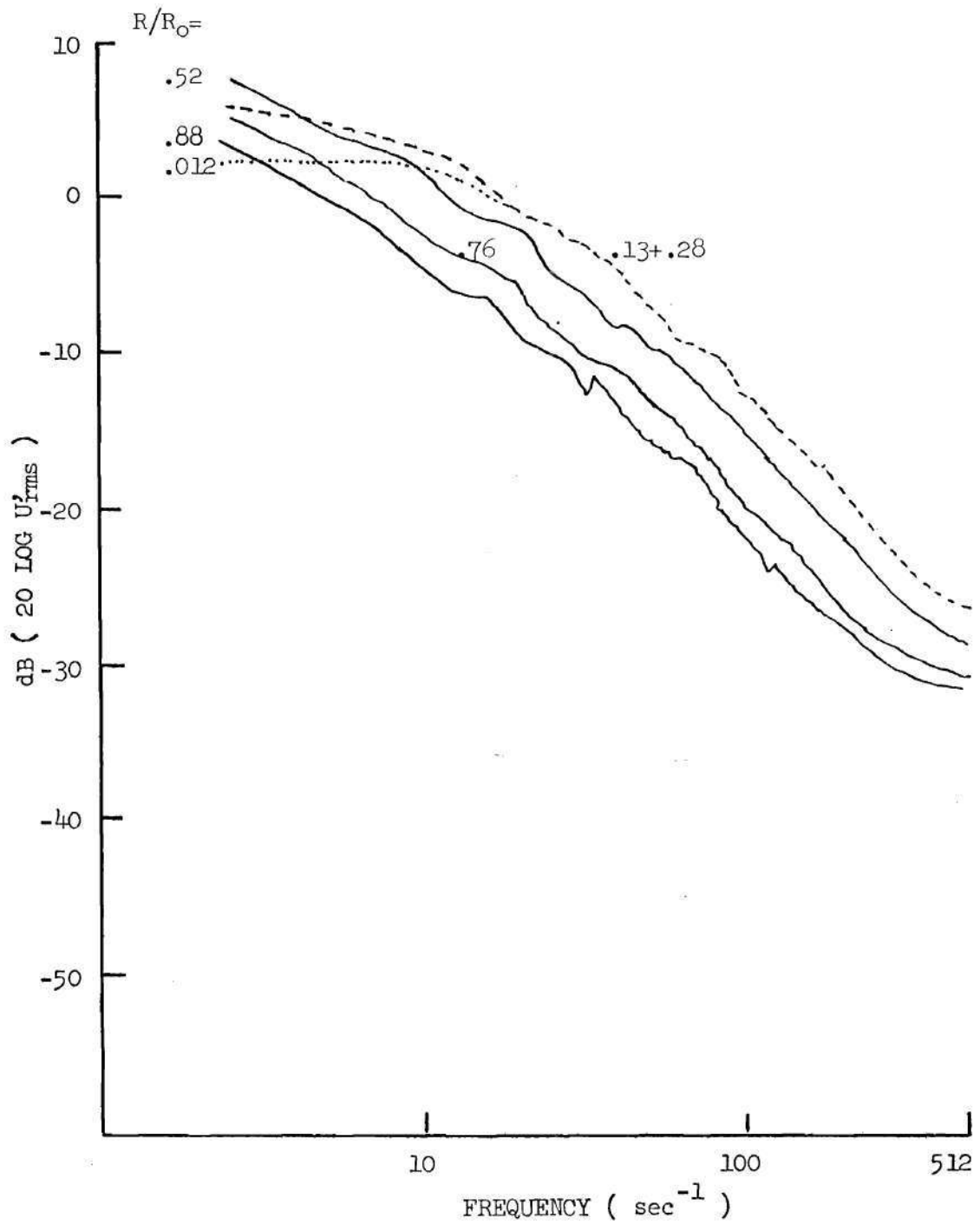


Figure 54. Radial Variation of Spectra, Water Injection,  
 $X/D = 16.28$ .

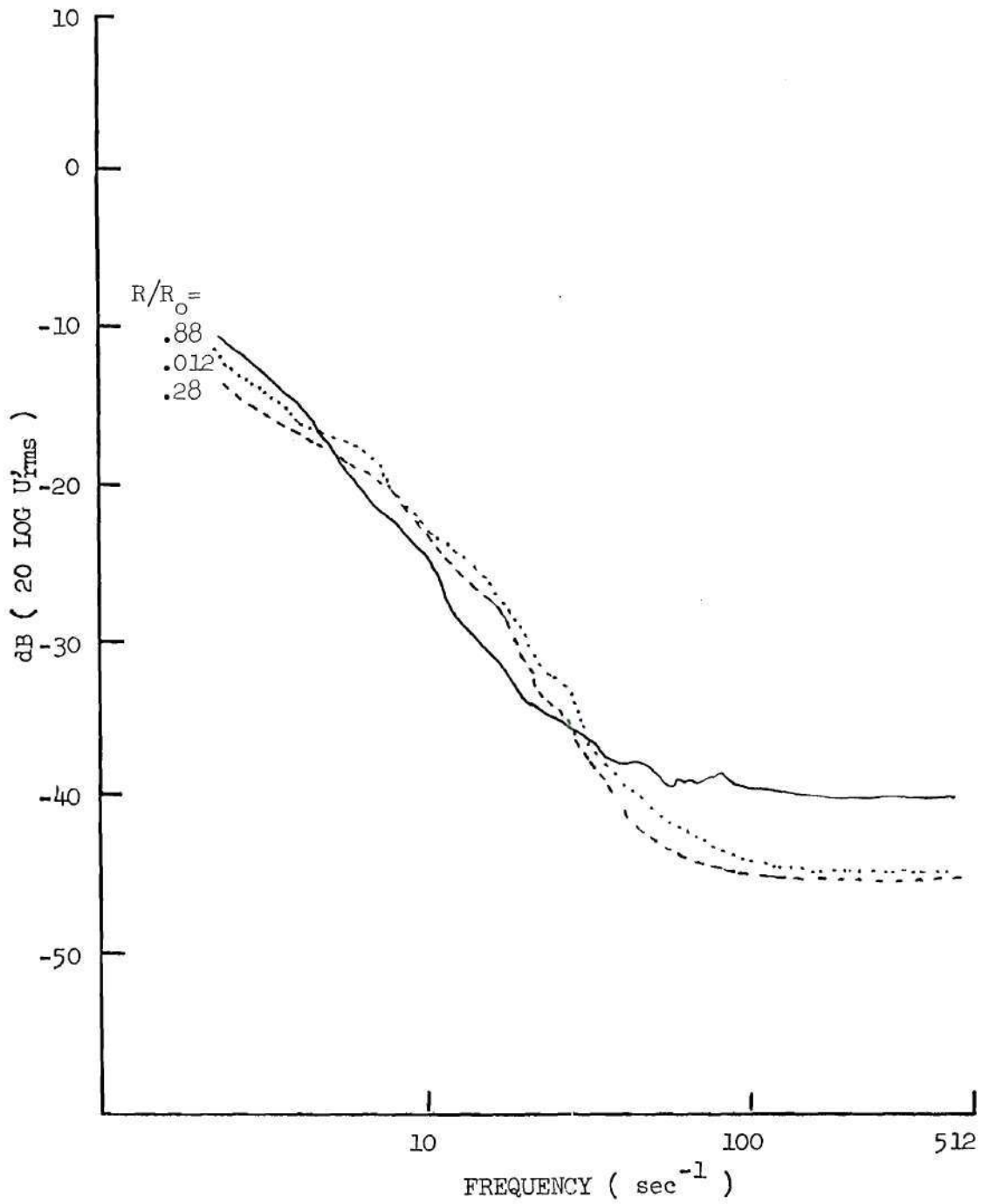


Figure 55. Radial Variation of Spectra, Water Injection,  
 $X/D - 54.27$ .

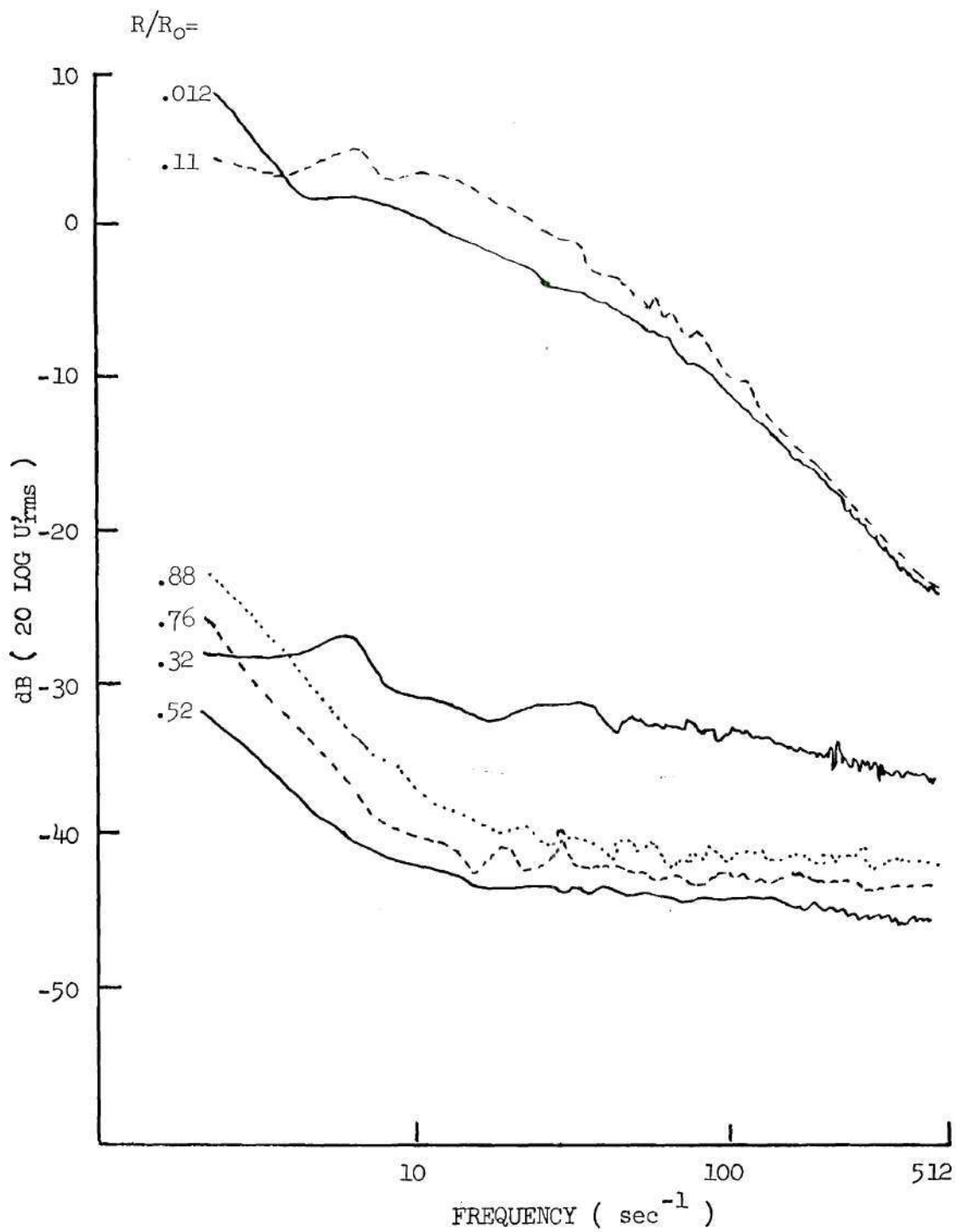


Figure 56. Radial Variation of Spectra, Polymer Solution,  
 $X/D = -0.54$ .

At the axial station equivalent to  $X/D$  equal to 0.54 (Figure 57) the inner flow is affected only slightly by the presence of the polymer. This effect is noticed in the frequencies below 100 Hertz. The near centerline spectrum loses some energy while the spectrum at a  $R/R_0$  of 0.11 shows a slight increase in energy. The outer flow region is of greater interest, however. A phenomenon comparable to the water case is evident at an  $R/R_0$  of 0.30 (i.e., vortex shedding). The outer spectra of the outer flow show little change over those found at comparable radial locations for an  $X/D$  of 0.54.

Figure 58 represents the power spectral densities associated with the vortex shedding at an  $X/D$  of 0.54 catheter diameter. The radial locations range from an  $R/R_0$  of 0.18 to 0.44. When compared to results from the water injection, several differences can be seen. The overall levels of the turbulence energy contained in the spectra are lower for the polymer injection at all the radial positions depicted. Secondly, the disturbance bandwidth is not as large for the polymer case indicating a lower fluctuation about the center frequency. The center frequency was determined to be approximately 290 Hertz, not too different from the water injection case.

Figures 59 and 60 represent results from the axial station with an  $X/D$  of 2.71 catheter diameters. At this point, the near centerline spectrum ( $R/R_0 = 0.012$ ) shows a slight elevation of energy in the higher frequencies. The outer region has changed significantly. At an  $R/R_0$  of 0.25 the turbulence energy content of the higher frequencies is essentially the same as the inner flow region. The radial positions from 0.49 to 0.86 show a strong elevation of the energy contained at the frequencies

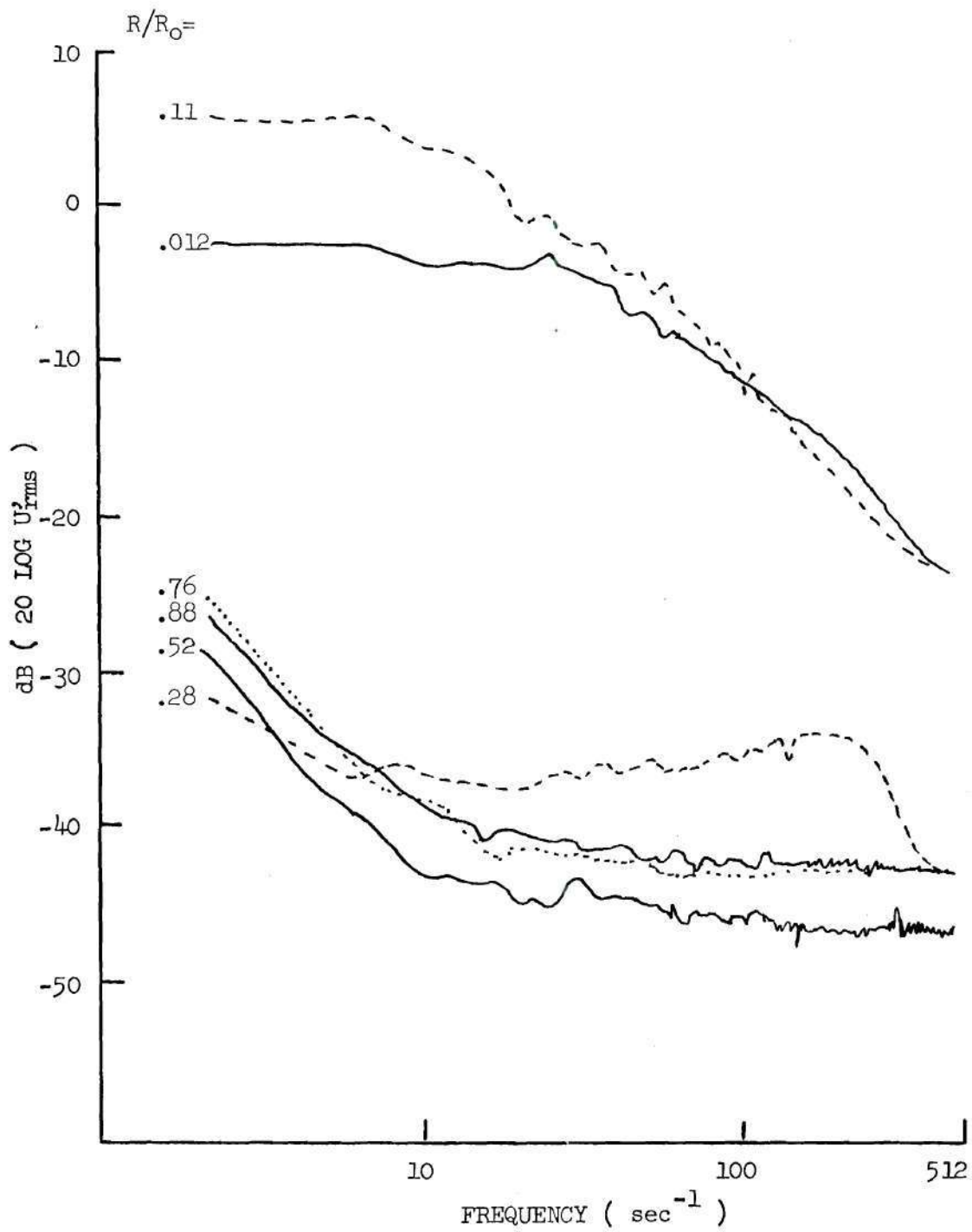


Figure 57. Radial Variation of Spectra, Polymer Solution,  
 $X/D = 0.54$ .

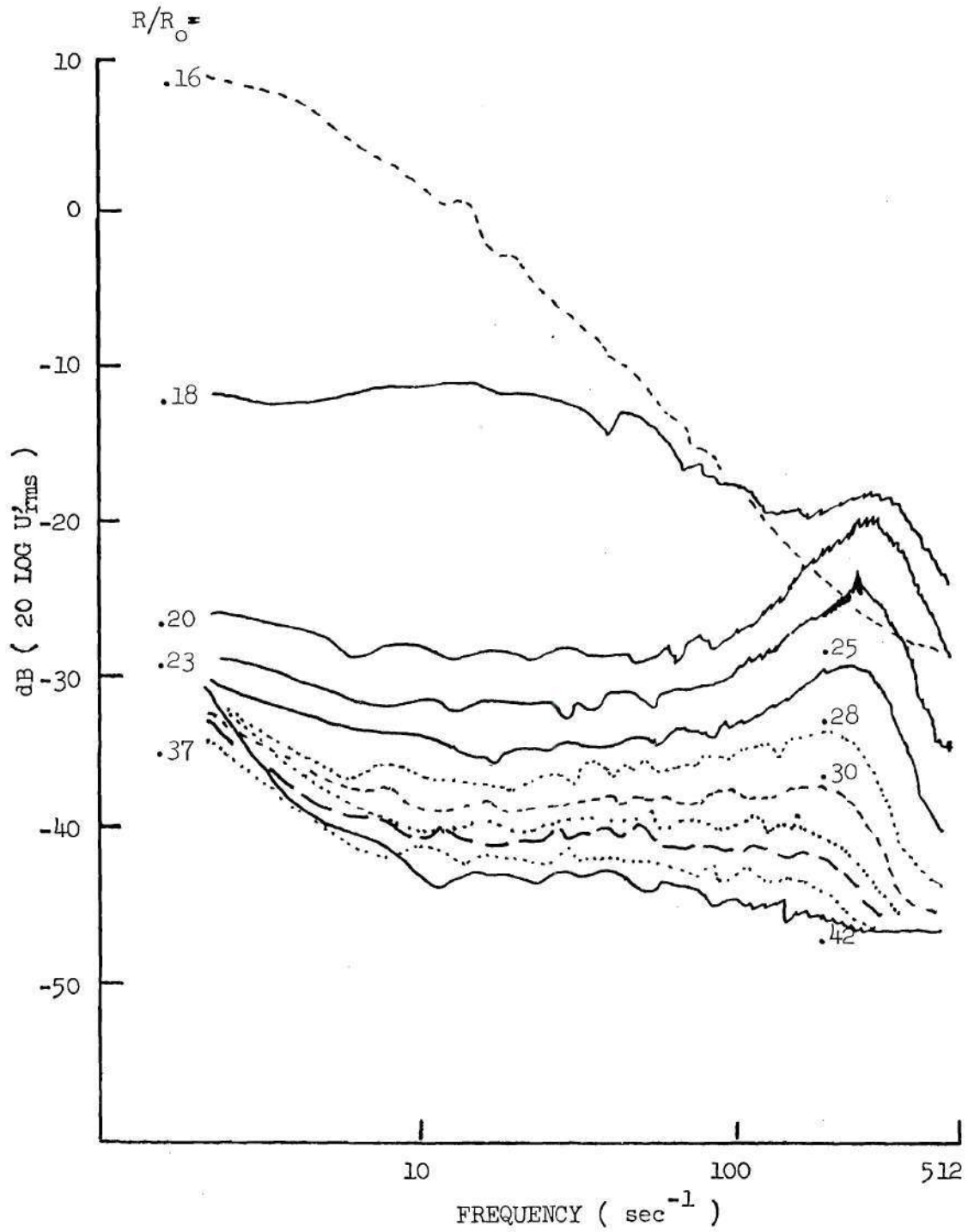


Figure 58. Radial Variation of Spectra, Polymer Solution,  $X/D = 0.54$ .

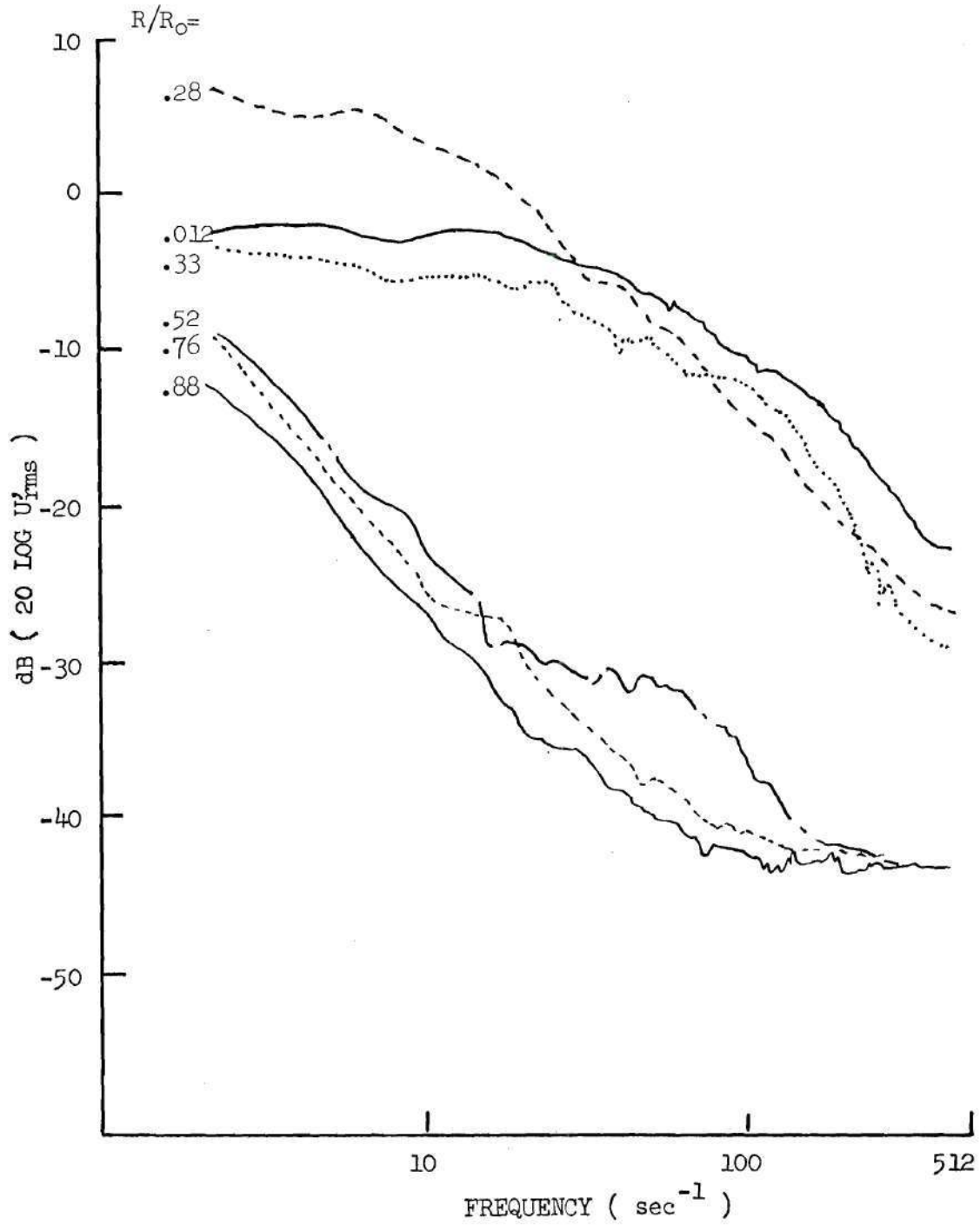


Figure 59. Radial Variation of Spectra, Polymer Solution,  $X/D = 2.71$ .

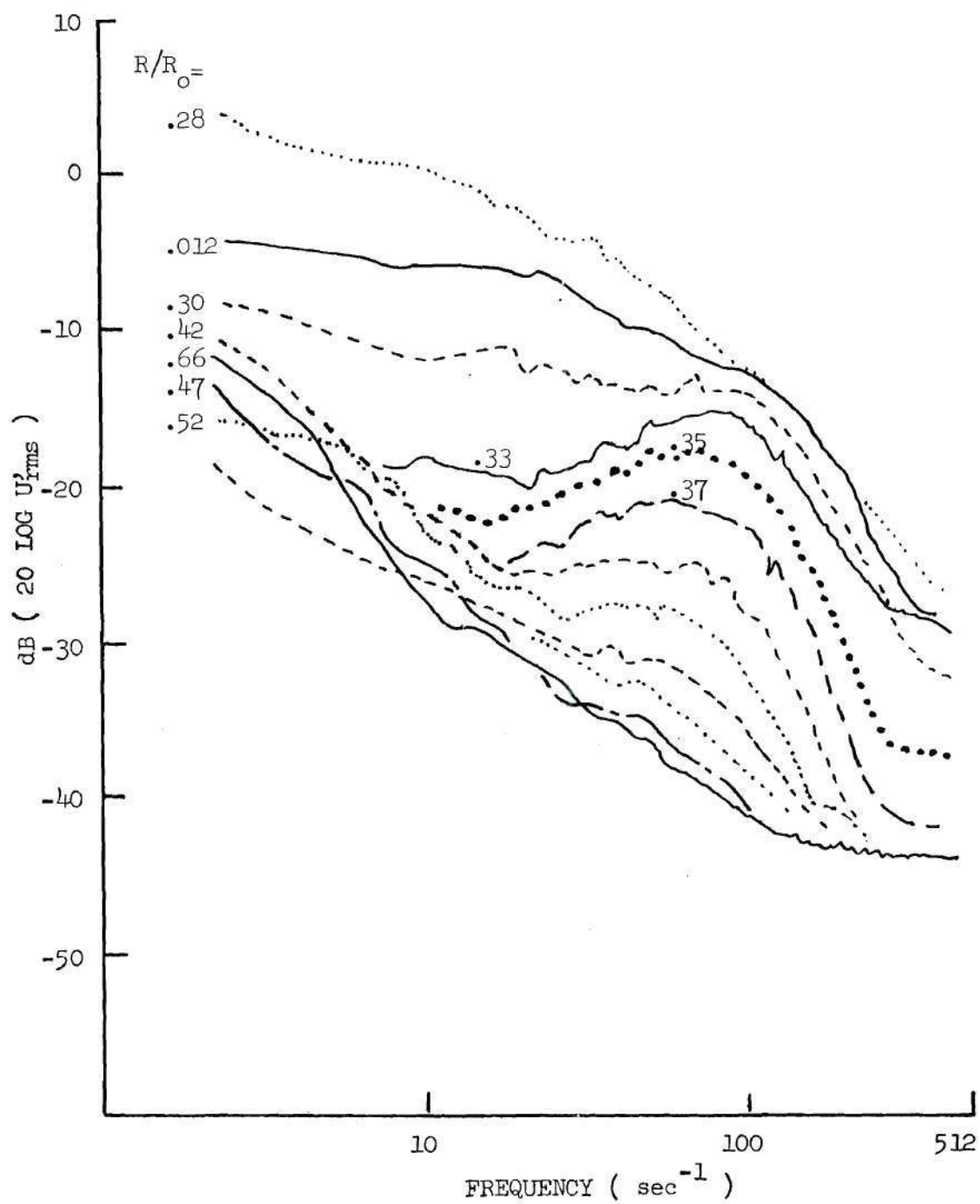


Figure 60. Radial Variation of Spectra, Polymer Solution,  
 $X/D = 2.7$ .

below 110 Hertz. Compared to the spectra for the water injection at this axial station, the outer flow spectra are essentially the same while the polymer injection exhibits higher energy content at the lower frequencies. The progression of the vortex is shown in Figure 60. The presence of the vortex is seen over a range of positions from an  $R/R_0$  of 0.25 to 0.64. When compared to the water injection, the vortex formed by the polymer solution is seen to have traveled farther into the outer flow. The center frequency is seen to be approximately 95 Hertz as opposed to the 60 Hertz seen in the water case. The total bandwidth appears to be approximately the same. These observations when linked with the conditions at an  $X/D$  of 0.54, tend to suggest a more well-defined and adherent vortex being produced by the polymer solution injection.

Figure 61 is representative of measurements taken at the axial location  $X/D$  equal to 5.43. The inner flow ( $R/R_0$  of 0.012 and 0.13) is depicted by a single spectrum because of the high agreement between the two locations. The spectra at  $R/R_0$ 's of 0.76 and 0.88 representing the outer flow also show a high level of agreement. The effect of the vortex may show a high level of agreement. The effect of the vortex may still be seen at the radial station  $R/R_0$  equal to 0.52. The spectrum is shifted upward as a result of the vortex action on the mixing. When compared to the near initial conditions ( $X/D = -0.54$ ), the outer flow spectra are seen to have shifted by a large amount, especially in the lower frequencies. The inner flow spectra are essentially the same. Comparison with the comparable water injection shows strong similarity in the outer flow region and slightly higher energies in the lower frequencies for the polymer solution in the inner flow region. The polymer solution appears

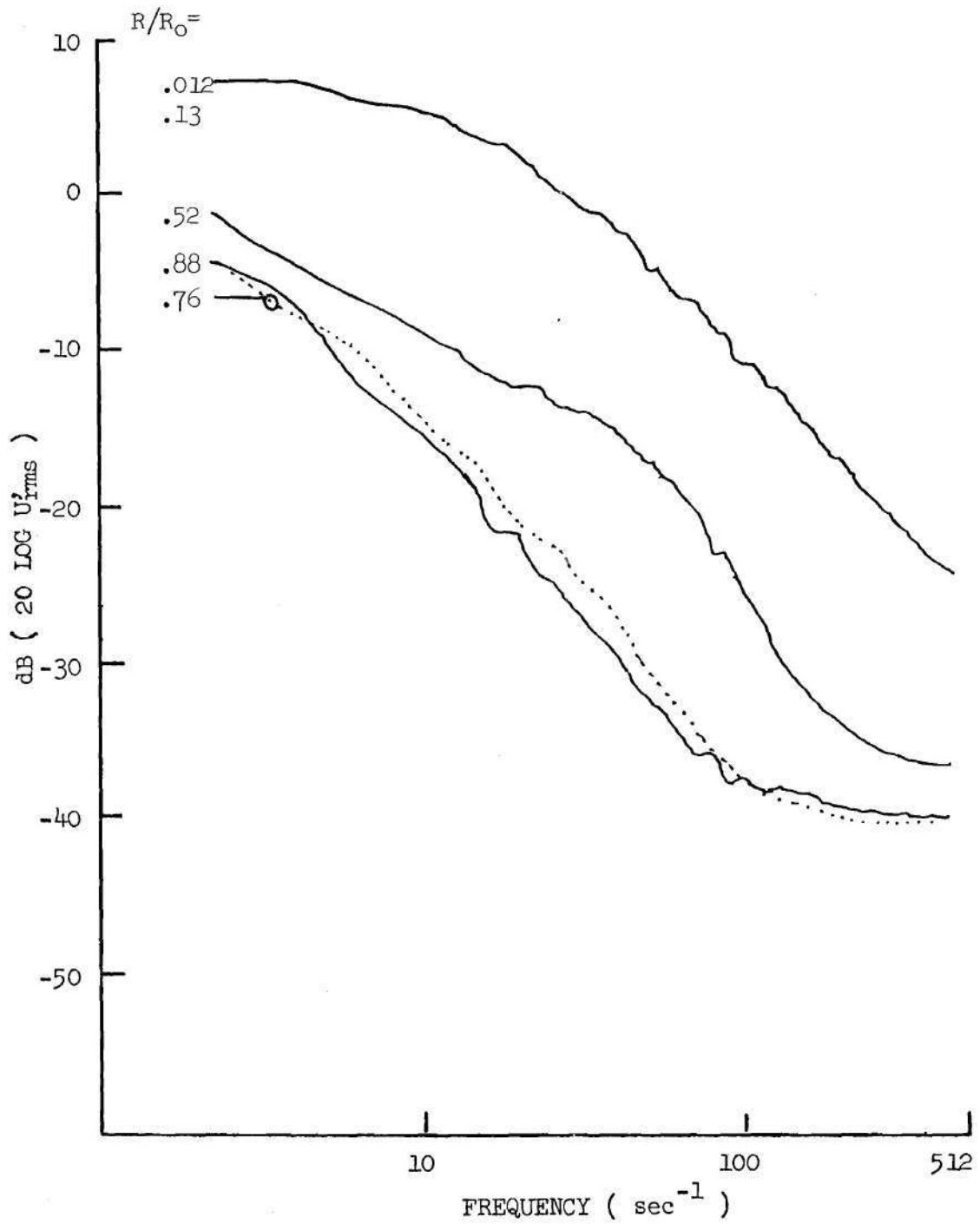


Figure 61. Radial Variation of Spectra, Polymer Solution,  $X/D = 5.43$ .

to produce a Kolmogorov-like spectrum from approximately 250 Hertz on for the inner flow; however, no such spectrum is found in the outer flow region.

At an X/D of 10.85 (Figure 62) the spectra show the trend toward higher agreement as seen in the comparable water case. The outer flow region is exhibiting higher energies while inner flow region is declining slightly in energy. Comparison to the water case shows slightly higher energies for the polymer case with a little more separation between the inner and outer flow region spectra. Also of interest is the fact that the polymer solution does not exhibit any region which produces a Kolmogorov-like spectral distribution. The apparent slope is steeper suggesting a more rapid decay of the higher frequencies.

At an X/D of 16.28 (Figure 63) the polymer solution injection still differs from the water case. The resulting spectra have approximately the same level of agreement (closeness) as do the water spectra but the higher frequencies seen in the polymer solution spectra contain a much lower amount of energy. The resulting slope of the polymer spectra (although not entirely linear) is therefore steeper than that for the water case. Again, the inner and outer spectra for the polymer solution case are more closely related than the previous axial stations and a drop in energy is seen at all radial positions.

At an axial location of 21.71 catheter diameters the inner and outer flow regions produce spectra which are not too different in distribution, with the outer regions displaying slightly lower energy than the inner flow region. The total energy is less than that found at the previous axial location. The spectra produced by the polymer injection

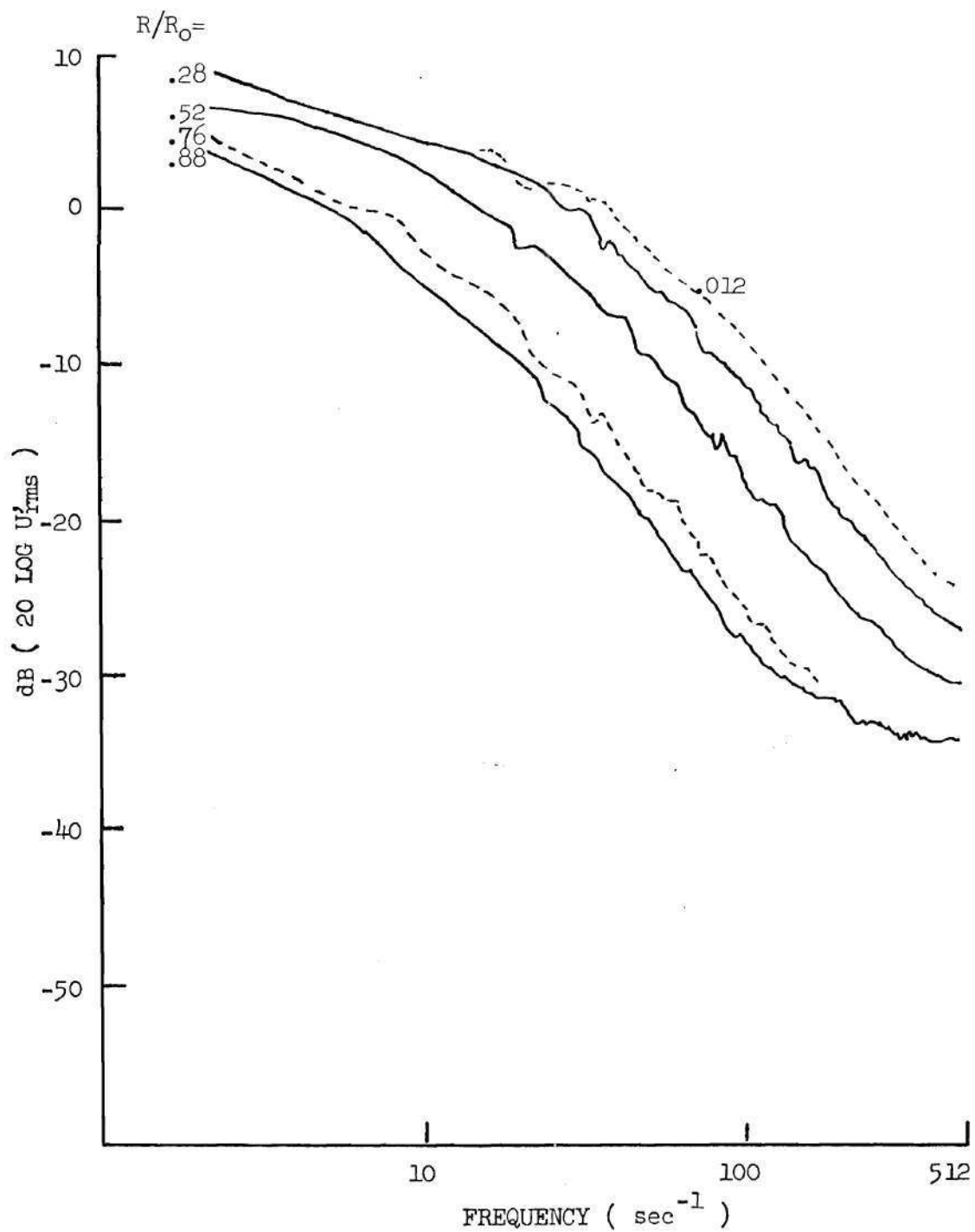


Figure 62. Radial Variation of Spectra, Polymer Solution,  $X/D = 10.85$ .

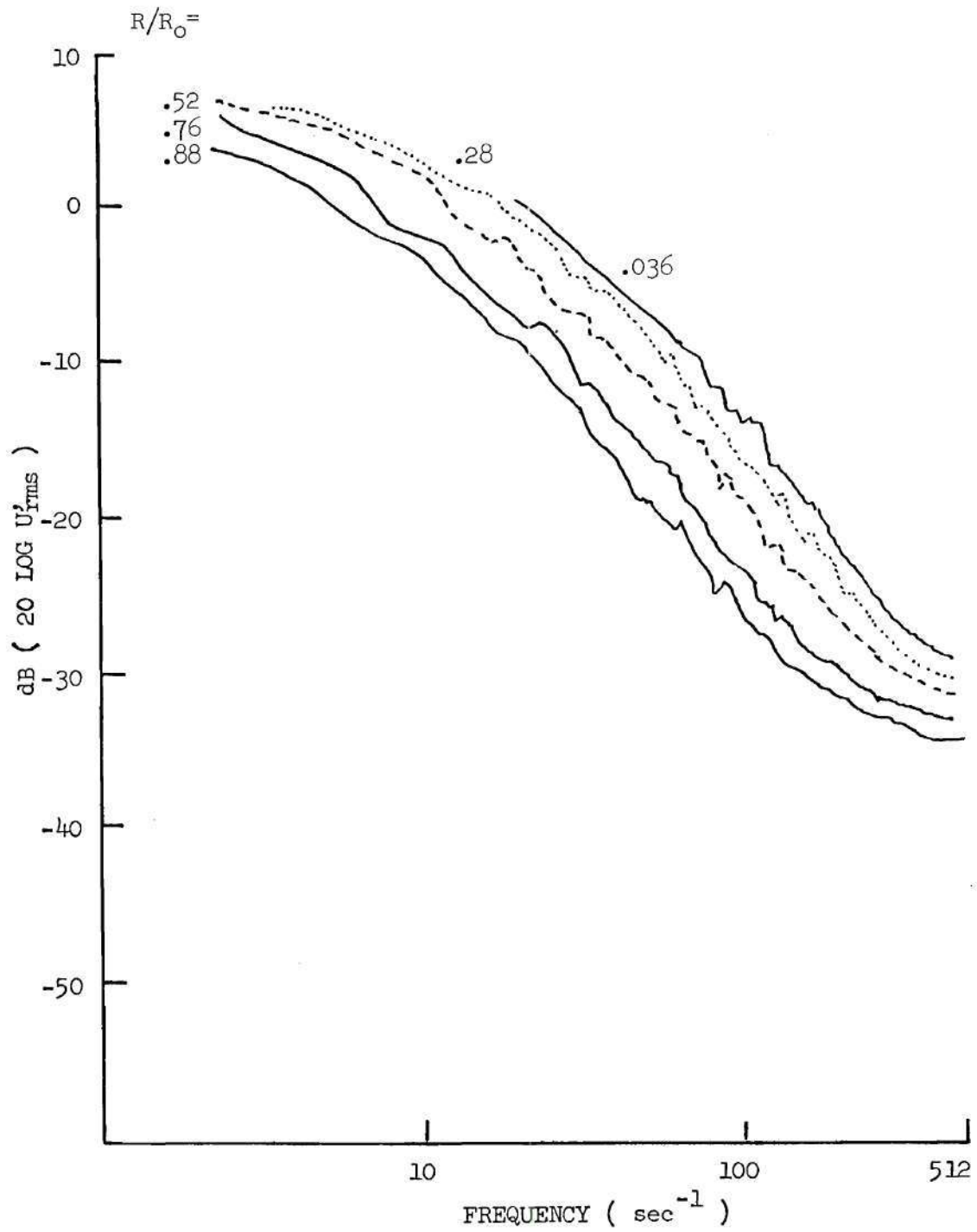


Figure 63. Radial Variation of Spectra, Polymer Solution,  
 $X/D = 16.28$ .

are not similar in distribution to the water injection spectra. The polymer spectra are of lower total energy (corresponding to the results described earlier) with the energies in the high-frequencies lagging far behind the comparable energies in the water case. The result is a spectral slope which is much greater for the polymer case than for the water. This difference tends to suggest an enhanced viscous dissipation of energy from the smaller scale eddies.

At an X/D of 27.14 catheter diameters similar results are seen. The polymer energy content is less with an energy distribution deficient in the higher frequencies. The resulting slope is again steeper than that for the water case. At 54.27 catheter diameters (Figure 64), the resulting spectra are essentially the same as those produced for the water injection, the total energy in the polymer spectra being slightly lower in magnitude. The basic spectral distributions are, however, the same, indicating an end to the polymer effect on the spectral distribution of the energy and thus the flow. It is to be remembered that the downstream flow will eventually become laminar and that the polymer effect has been seen only at high Reynolds numbers (22) (i.e., turbulent flow). Additional spectra may be found in Appendix V.

Primary Mixing Region. From the photographic study, the approximate location of the jet initial mixing region was determined. The location of this region was found to correspond to the axial and radial positions which displayed a vortex disturbance in the power spectra. If the region over which the vortex disturbance is considered to be an indication of the mixing region, an approximation of the thickness may be obtained from the spectra. This is accomplished by noting the thickness

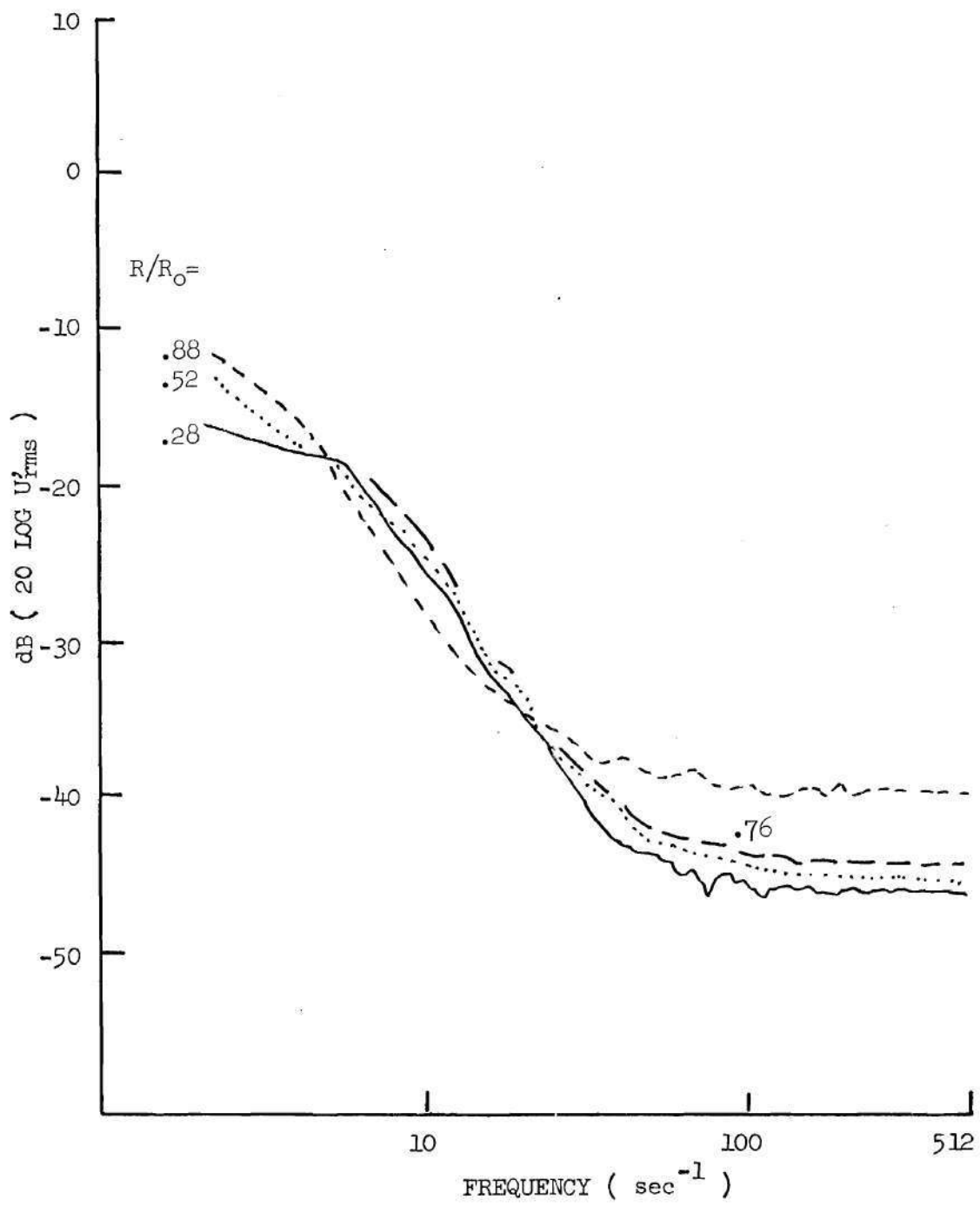


Figure 64. Radial Variation of Spectra, Polymer Solution,  
 $X/D = 54.27$ .

over which the effects of the vortex are visible. The radial variations for the axial locations of 0.54 and 2.71 diameters were shown in Figures 49 and 51 for water and 58 and 60 for the polymer solution. From the spectra the thickness of the primary mixing region is shown to be only slightly greater for the polymer solution at an  $X/D$  of 0.54. At an  $X/D$  of 2.71 catheter diameters the polymer solution mixing zone is approximately 36 percent greater than that for the water case. This increased thickness of the primary mixing region for the polymer case is in agreement with the increased eddy size seen in the photographic investigations.

## CHAPTER V

## CONCLUSIONS AND RECOMMENDATIONS

An experimental model of angiographic injections has been studied. The model utilized was that of a concentrically mounted jet exiting into a confined co-flowing stream. The Reynolds numbers and momenta of the inner and outer flows were set to correspond to actual injection parameters. Dilute solutions of a drag reducing polymer were studied as an alternate injectant and compared to a water injection. The outer flow consisted of water for both cases. Because of the low Reynolds number and the apparent delay in transition caused by the polymer, the catheter flow was altered through the use of a boundary layer trip in an effort to achieve similar jet exit conditions. The model was studied via photographic techniques and Laser Doppler Anemometry.

Summary of ResultsPhotographic Investigations

The photographic investigation provided a visual description of the changes resulting from variations in the catheter Reynolds number and the type of injectant (water or polymer). The effect of the BLT on the jet expansion was also studied.

The observations made without the BLT are listed below.

- 1) At Reynolds numbers below 2500, which corresponds to transition in the catheter, the water injection displayed a helical instability

before the jet began to break into a smaller more random structure characteristic of turbulent mixing. The same effect was observed for the polymer solution injection.

2. As the Reynolds number was increased to near transition, the water injectant produced a jet configuration similar to the lower Reynolds number cases described above. This jet was, however, very sensitive to any form of disturbance and would immediately start to break up near the exit plane at the slightest change in conditions. The jet often resumed its lower Reynolds behavior just as quickly as the turbulent catheter jet behavior was produced.

3. The recirculation region was also strongly visible in the photographic investigation. After addition of ink to the catheter flow, the ink could be seen first in the expanding jet. A large portion was, however, mixed into the recirculation region allowing an adequate visualization of a portion of the region.

4. As the Reynolds number was increased above transition, the water injectant produced a jet which began to break up into turbulence almost immediately downstream of the exit plane. The helical instability was no longer visible although a small section of apparently undisturbed flow existed just downstream of the injection plane.

5. At Reynolds just above transition the polymer solution showed no apparent change from the Reynolds numbers below transition. At a Reynolds number of 7000 the jet still displayed a region of helical instability followed by the breakup and expansion of the jet, suggesting a strong delay of transition in the catheter flow.

6. The eddy size at comparable Reynolds numbers appeared to be larger for the injection of the polymer solution than for water.

Because of the apparent delay in transition and in order to obtain more similar exit conditions between the polymer solution and water injections, a boundary layer trip was introduced into the catheter. Photographs were produced with an outer flow Reynolds number of 1000 and an inner flow Reynolds number of 7000. The following observations were made.

1. The apparent spreading and turbulence structure of the water injection was approximately the same as the non-BLT case.

2. The polymer injection was much more turbulent in nature, when compared to the non BLT polymer injection. The helical instability was no longer visible and jet appeared to break up in a manner similar to the water cases.

3. The overall spreading angle for the polymer jet was only slightly greater than the water case, suggesting a possible increase in mixing.

4. There was, again, an apparent suppression of the small scale eddy structure in the polymer case.

5. An attempt was made to obtain the upstream location of the recirculation region for an injection with a Reynolds number of 7000 with and without the BLT; polymer and water. The outer Reynolds number was held at 1000. Both water injections produced a recirculation region which appeared to start approximately .75 catheter diameters upstream of the exit plane. The polymer injection with the BLT produced a recirculation region which appeared to start approximately .75 catheter diameters

upstream of the exit plane. The polymer injection with the BLT produced a recirculation region which appeared to start at the exit plane, while the injection without the BLT has a recirculation region beginning approximately 2.5 diameters downstream of the exit plane.

#### LDA Investigations

The Laser Doppler Anemometer (LDA) measurements were obtained from two studies. The first study was the centerline decay of the longitudinal components of the flow field for polymer and water injections with and without the BLT. Included in this study was the determination of the initial condition of the catheter velocity profile. The second study was a comprehensive investigation of radial variation of the longitudinal velocity component for injections of water and polymer with the BLT only. The results of these experiments are given below.

1. The study of the initial catheter velocity profiles provided information concerning the effect of the BLT on the polymer and water injections. Without the BLT the polymer displayed a velocity profile which appeared to be very nearly laminar. This "pseudo"-laminar behavior is attributed to a delay in transition due to the presence of the polymer in the fluid. The addition of the BLT to the catheter produced a velocity profile which was much more turbulent in appearance. The BLT had a slight effect on the water case, the profile with the BLT being somewhat flatter.

2. The centerline decay of the axial velocity component was found to be more rapid for both polymer cases compared to either water injection. This increased decay in the centerline velocities suggests the possibility of a more rapid spreading of the jet. In each case where the BLT was

used the velocity decay was more rapid than the non BLT case.

3. The variation of the longitudinal turbulent energy along the centerline indicates a higher initial turbulence for the polymer with the BLT when compared to any other case studied. Both polymer cases exhibited a more rapid rise to a higher turbulent energy as the axial distance from the jet exit increased. After the peak value was reached, the turbulent energy was found to decay more rapidly in the polymer case as well. When normalized by the local velocity the axial variation of the turbulent intensities appeared to be approximately the same for similar injectants. The polymer cases produced a more rapid rise to a higher intensity level followed by a more rapid decay.

4. Polymer centerline spectra indicate higher energy content in the lower frequencies than the water cases at the same axial location. The polymer spectra were shown to decay more rapidly than the comparable water cases, the loss of energy being most rapid in the higher frequencies. The spectral distribution of the polymer with the BLT appears to lie somewhere between the spectra of the polymer without the BLT and the water spectra with (or without) the BLT.

The radial distribution studies produced the following results (BLT cases only):

1. In comparison with the polymer injection, the water injection had a more immediate effect on the outer flow or near wall region.

2. The near centerline longitudinal turbulence energy was found to be higher for the polymer case up to about 21.71 catheter diameters.

3. The near wall turbulence energies produced by the polymer solution injection continued to be lower than the values evident in the

water injections for all axial stations studied.

4. Although the centerline velocities decayed more rapidly for the polymer case, the overall velocity profile showed less dispersion into the outer flow region. To satisfy continuity the near wall velocities are necessarily greater for the polymer injection case.

5. The apparent size of the recirculation region was found to be much less for the polymer injection than for the water injection (again, the effects near the wall were less for the polymer injection). The lower centerline velocities for the polymer case may be a result of the smaller region of recirculation, which creates a venturi-like effect.

6. Energy spectra for both injections produced a peak at axial positions of 0.54 and 2.71 diameters. The resulting center frequency of this local maximum was found to be approximately 300 Hertz and is attributed to vortex shedding. The bandwidth of the "spike" was found to be much less for the polymer solution injection.

7. The overall decay of the turbulent energy with respect to axial distance in the flow field was found to be much more rapid for the polymer injection. In addition, the most rapid loss of energy occurred in the higher frequencies of the spectra. Low frequency energy content was found to be higher for polymer than water cases. The water injection, on the other hand, displayed regions in the flow in which the power spectra exhibited a Kolmogorov-like distribution. The polymer injections exhibited no such distribution.

8. The location of the mixing region was approximated from the photographic information. These resulting positions corresponded well to those radial locations which demonstrated a transition from

characteristic innerflow spectral shape to those more representative of the outer flow region. From the spectra produced the thickness of the mixing region was found to be approximately the same for the two cases at an X/D of 0.54 (near the exit plane). At an X/D of 2.71 the apparent thickness was found to be some 36 percent greater for the polymer case, again suggesting large scale turbulence lengths.

Although the initial conditions were not found to be exactly the same, the majority of the differences observed are believed to be a result of the presence of the polymer in the flow. Evidence for this assumption may be found throughout the flow field. The near field or initial conditions indicate greater differences between the water injections with and without the BLT (velocity profiles) than is apparent in the water and polymer injections with the BLT. The resulting flow fields are, however, very similar for the water injections but quite different for the water and polymer (BLT) injections. In the far field the two polymer injections (with and without the BLT) behave very much the same although the initial conditions are very different. From these observations and others, the effects of the initial conditions appear to be overshadowed by the effects of presence of the polymer in the flow field.

#### Conclusions

From the various observations made during the course of the investigation certain statements or conclusions may be drawn concerning the behavior of the concentric confined jet, polymer effectiveness, and this application to angiographic injections. From these observations, statements concerning the altered behavior of the jet due to the presence of

small amounts of a drag reducing polymer are derived and are listed below.

1. At Reynolds numbers above those causing transition in water the polymer solution exhibits a catheter velocity profile and jet spreading corresponding to near laminar flow, suggesting a delay in transition.

2. Placement of a 50 percent sharp edged orifice in the catheter nearly eliminates the laminar-like behavior of the polymer jet at Reynolds numbers near 7000.

3. The eddy size resulting from the polymer injection gives the appearance of being coarser or larger than that produced by the comparable water injections.

4. Near wall fluctuations are found to be lower for the polymer injection while the near centerline intensities are higher.

5. Because the injection into a laminar co-flowing stream is highly elliptic in nature, the exact behavior at the jet is coupled with the upstream conditions. The resulting recirculation region is found to be smaller for the polymer injection than that for the water injection. The existence of the recirculation region affects the upstream conditions (especially near the wall) and thereby alters the apparent jet spreading.

6. Since the exit plane conditions are very nearly the same, the difference in the size of the resulting recirculation regions is thought to be primarily due to the presence of the polymer in the jet fluid. The exact mechanism for the reduced size of the recirculation region is not understood but the effect of the polymer on mixing is believed to play an important role.

7. The results from the investigation provide useful information concerning applied angiography and the potential of drag reducing polymers in the procedure. The experimentation produced the following conclusions concerning the angiographic procedure:

a) There exists an extensive region of high turbulence intensities and presumably high Reynolds stresses in the angiographic injection flow field. The region up to about 25 catheter diameters is potentially dangerous due to either high jet velocities, high turbulence intensities or a combination of both.

b) Although a concentric model was used the actual injection procedure is seldom aligned in such a manner. In some instances the catheter may impinge on the wall. The resulting stagnation pressures and catheter whip could be hazardous, especially in cases of atherosclerosis.

c) Upon injection a recirculation region may be produced which is capable of "trapping" a portion of injectant until the injection is terminated.

d) Use of drag reducing polymers in conjunction with angiography is not a promising consideration.

e) Possible improvements may, however, be possible through improved catheter design. For example, by employing a BLT the near field mixing of injections at low flow rates may be improved by reducing turbulence prior to the jet exit.

8. The polymer used in this research was Separan AP-30. It was found to be an excellent drag reducing polymer for experimental research. It strongly resists shear stress degradation and is easily dissolved in water. The good repeatability of the polymer mixture studies was due,

for the most part, to this polymer.

#### Discussion and Recommendations

As has been pointed out, the long-chained drag reducing polymer greatly affects the development and turbulent structure of a confined jet exiting into a confined co-flowing stream. Generally, the alterations of the flow field would prove to be adverse if applied to the clinical situation, and therefore these polymers do not appear to offer any significant usefulness in angiographic injection procedures for the conditions studied here. Although driving pressures would be reduced, the effect of the polymer solution on the total flow field would be adverse. Unless the Reynolds numbers of the injections were highly turbulent (above 15,000) the polymer would delay the transition to a turbulent velocity profile. If mounted concentrically no major drawback would be incurred. However, the catheter seldom, if ever, is capable of being aligned. Frequently, the catheter lies near the wall. If the jet were to impinge on the wall, the local stagnation pressures could exceed non polymer injections by as much as 60% (based on peak velocities for fully developed laminar and turbulent flows). If a boundary layer trip is introduced this effect would be lessened. However, the polymer exhibits higher turbulence intensities near the centerline whether or not the BLT is employed. These higher fluctuations could be of concern if the catheter lies near the wall. Also, because of the high flow rates employed, the problem of catheter whip would not be alleviated by the use of the polymer. All evidence indicates that the use of a drag reducing polymer in an angiographic procedure could have potentially adverse effects without showing any

significant benefits. From the effects brought about by the insertion of the BLT, it is believed that improved angiographic techniques may result from altered catheter design. It is, therefore, recommended that future research dealing with angiography be concentrated in the realm of catheter design, with emphasis on altering the injection configuration to improve mixing in the near field.

Because of the dangers inherent in the angiographic procedure, care should be exercised in the choice of the injection rate and the location of the catheter in the vessel. Since high fluctuations, as well as high centerline velocities are possible up to approximately 25 catheter diameters, great care should be made in the placement of the catheter to minimize trauma to healthy and, especially, diseased vessels.

Because the effects of the drag reducing polymer were not found beneficial in angiographic injections by no means suggests that continued research into the behavior and effects of the polymer be curtailed. The mechanizing for the polymers effectiveness in drag reduction and turbulent mixing are not well understood. It is evident from this research that the turbulent nature of the flow has been altered by the presence of the polymer and that larger scale turbulence is indicated. The characteristic length of the polymer has been shown to be much smaller than the smallest length scale encountered in turbulent flow and could not directly interfere with the eddies. However, it is not unlikely that the polymer alters the ability of eddies to interact, thereby changing the turbulence structure of the flow. This has been hypothesized by Lumley (27) for the counter-rotating vortices near the wall, and is believed to

be a factor in the mixing region of the expanding jet. Further research into the effects of the long-chained drag reducing polymer on various turbulent flows may lead to a better understanding of the mechanism which alters the turbulent structure.

## APPENDIX I

## PERIPHERAL ANGIOGRAPHY: HISTORY AND COMPLICATIONS

History

The historical outline given in this appendix is based, for the most part, on a review paper by Wendth (1).

- 1890 - Professor Authur Goodspeed (University of Pennsylvania) produces images of coins on photographic plate while using a Crooke's tube. No report made.
- 1895 - Roentgen first observed new unknown beam of energy, x-rays, November 8.
- 1896 - Haschek and Lindenthal, using amputated limb, perform first femoral arteriogram. Teichman's mixture used as radiopaque dye.
- 1896 - Codman reports cadaveric opacification of the aorta and its branches by using mercury salts.
- 1912 - Belichroder performs first in vivo insertion of a catheter into an artery. Procedure was not diagnostic. Procedure was to treat puerperal sepsis by infusing an antiseptic solution into the uterine arteries from a catheter passed from the femoral artery.
- 1920's - (mid-late) Dr. Reynoldo Dos Saatos discovers low morbidity in the puncturing of major vessels of the abdomen.

1929 - Dos Saatos uses translumbar approach to treat tuberculous peritonitis, patient died due to respiratory complications. Necropsy examination revealed aorta puncture scarcely visible. Later used translumbar technique to obtain visualization of aorta and major branches. Procedure painful requiring local anesthesia. 100% Sodium Iodide was used as contrast medium. By 1937 over 1,000 cases done with some serious complications including four fatalities.

1937-1953 - Many advances in contrast agents - newer, water soluble, less toxic.

Dr. Pedro Farinás initiates near procedure. Femoral artery is surgically exposed and rubber catheter is inserted into femoral and moved to area to be visualized.

Procedure improved in 1949 by Radner. Guide wire placed inside catheter to stiffen catheter thus improving accuracy of location.

1949 - Freeman suggests use of Valsalva method to decrease cardiac output and thus facilitate counter current injection into femoral artery via simple percutaneous puncture.

1951 - Pierce uses 12 - 15 gauge needle to puncture artery.

Catheter then fed through the lumen of the needle. Only straight catheters may be used.

1953 - Seldinger (2) describes a percutaneous procedure combining several techniques. Not too dissimilar from many of today's procedures. Needle with outer diameter the same as catheter is used to puncture the vessel wall. A guide wire is fed

into the artery through the needle. The needle is then removed leaving the guide wire. At this point the catheter is slipped over the guide wire and fed into the artery. The procedure allows insertion of large catheters without increasing the size of the puncture wound.

1953 - Present - Improvements to basic techniques and catheter design are made.

#### Complications

Although a widely utilized procedure, angiography is not without complications. In the review paper by Wendth (1) the complications may arise from four major factors: angiographic instrumentation, vascular or hematologic reactions, effect of the contrast agent and infection. Wendth provided further detail for the first three factors. The angiographic instrumentation may cause vascular perforation of the artery, intermural passage the guide wire or catheter, intimal tear or detachment by the needle or catheter tip, subintimal or extravascular injection and possibly catheter or guide wire fracture with a resulting foreign body embolism. Complications of a vascular or hematologic nature were presented as delayed bleeding, local hematoma upon catheter removal, uncontrollable pericatheter bleeding, thrombosis at the arteriotomy site, peripheral embolism of pericatheter thrombus, peripheral embolism of the detached artheromatous plaque(s), pseudo-aneurysm formation and rupture of the aneurysm. The contrast agent is capable of producing the following complications; nephropathy, neurogenic (cord and vasovagal syncope), cardiogenic (tachycardia, arrest) and histamine type reaction (see Wendith especially p. 388).

## APPENDIX II

## ADDITIONAL INFORMATION ON THE DISA 55L LDA SYSTEM

The information included in this appendix provides a more in depth explanation of the DISA LDA system. The majority of discussion is based on information found in the DISA operation manual (47) and other references (52,53).

Basic Concepts

Before any description of the LDA system can be given, several basic concepts dealing with the physics of lasers and electronics must be understood. These concepts include properties of laser light, interference fringes, heterodyning, definition of a Schmitt triggers, integrating circuits and filters. For the most part a "black box" approach is utilized.

Laser Light

The laser is not new to the scientific community. Because of its unique physical properties, it has been utilized in many types of instrumentation. Generally, laser light may be described as having four basic properties:

1. Laser light is very nearly monochromatic, i.e., one wavelength is present.
2. Laser light is highly collimated, i.e., there is very little dispersion of the beam.

3. There is little phase difference present in the beam.  
The beam is coherent.
4. The laser may be operated in a mode which results in Gaussian variation in intensity across the beam.

### Interference Fringes

Because the laser beam is a coherent light source, mixing of two beams will produce interference fringes or lines. The production of these fringes is due to constructive and destructive interference. In the LDA system two beams are focused together at a point. At the intersection of these beams an interference fringe is produced (see Figure A-1). If both beams have the same frequency, a stationary fringe pattern will be produced. The distance between fringes is directly related to wave length of the beams and the intersection angle. If, however, one beam is of slightly different wave length, a moving fringe pattern results. The speed of the fringes will be directly related to the difference in wave lengths (frequency). Because both beams have a Gaussian distribution, the resulting sampling volume (or fringe region) will also have a Gaussian distribution.

### Heterodyning

In its simplest terms, heterodyning is the mixing of two signals. If two signals,  $f$  and  $f + \Delta f$ , are mixed, the resultant signal will be comprised of two frequencies,  $2f + \Delta f$  and  $\Delta f$ . This may be described mathematically by the equation:

$$\sin((f)t + \phi) \cdot \sin((f + \Delta f)t + \beta) = \frac{1}{2} \sin[(2f + \Delta f)t + \phi + \beta] + \frac{1}{2} \sin[(\Delta f)t + \phi - \beta]$$

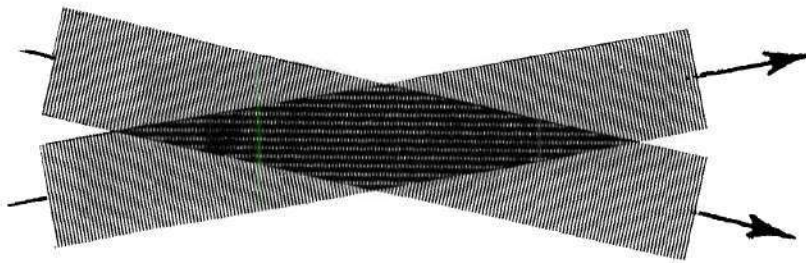


Figure A-1. Formation of Interference Fringes.

where  $\phi$  and  $\beta$  are phase constants. By using selective filtering either frequency may be obtained. The fringe pattern produced by the mixing of two beams of laser light is the result of optical heterodyning. There are three aspects of electronics which should be discussed before entering the discussion of the tracker itself. These are the Schmitt trigger, a simple integrating circuit, and the voltage controlled oscillator (VCO).

#### Schmitt Trigger

A Schmitt trigger is an electronic circuit which will produce a pulse of set amplitude and duration when an input voltage increases above a certain threshold value. The trigger will not fire again until the voltage has dropped below and then risen above the threshold value (see Figure A-2).

#### Integration Circuit

In electronic systems, most analog integrators employ some type of resistive capacitive network. The time constant associated with this network is based, in part, on how quickly the capacitor can be charged and discharged ( $t = 1/R_c$ ). This time constant restricts the integration to a certain range of frequencies. This fact requires different time constants (e.g. different capacitance values) for accurate integration of different frequencies. Generally, optimum integration is achieved when the network is tuned for an individual frequency.

#### Voltage Controlled Oscillator

A voltage controlled oscillator or VCO is a device which produces a frequency output which is directly proportional to the voltage applied. The ranges of the VCO used in the DISA trackers may be found in Table A-1.

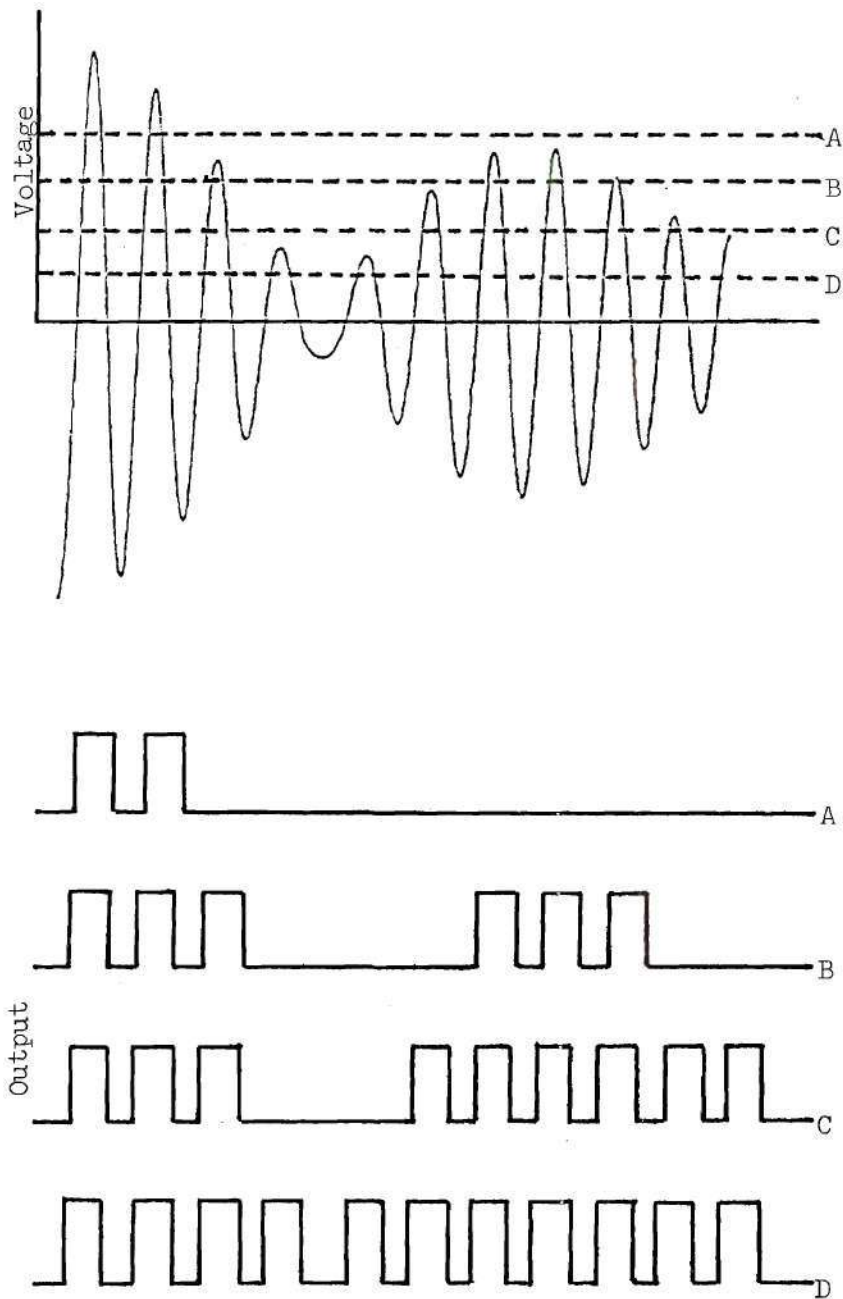


Figure A-2. Pulses from Schmitt Trigger with Various Threshold Values.

### Basic DISA Tracker Design

The DISA 55L Laser Doppler Anemometer Mark II is built around the earlier Mark I system. For this reason, the Mark I system is discussed first. The system can be separated into two parts, production of the Doppler frequency and tracking or following of the Doppler frequency to produce a velocity signal.

#### Production of $f_D$

In the Mark I system, a laser beam passes through a beam splitter to produce two separate beams. The two beams are then focused to a point to form a sampling volume. Since the beams are of equal frequency, the resulting fringe pattern is stationary. As a particle passes through the fringes, the light scattered from the particle varies in amplitude with a frequency of  $f_D$ . Where  $f_D$  is determined from

$$V = \frac{f_D \times \lambda}{2 \sin \theta/2} \quad (A-1)$$

with  $V$  being the normal velocity component of the particle passing through the fringe,  $\lambda$  being the wavelength of the laser beam and  $\theta$  being the intersection angle of the two beams (see Figure A-3).

To change the light amplitude variation into an electric signal, a photomultiplier with receiving optics is used. This signal is both amplitude and frequency modulated. The amplitude modulation is a result of variations in seeding concentration. The frequency modulation is, of course, a result of variations in the velocity component being measured.

#### Tracking of $f_D$

The frequency tracker is built around an automatically tracking

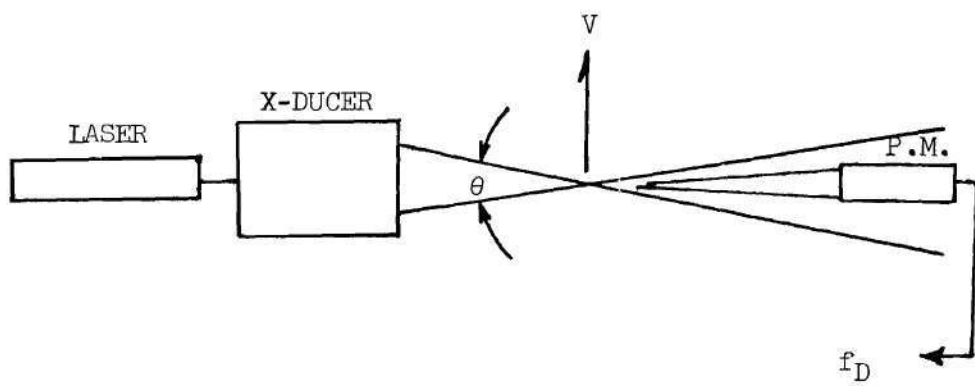


Figure A-3. LDA Geometry, Differential Mode.

variable oscillator. For use in a wide variety of flows the tracker has been designed to cover Doppler frequencies varying from 2.25 KHz to 15 MHz. To maintain accuracy of lower frequencies, the tracker provides seven overlapping ranges as shown in Table A-1. Each range has a dynamic range of approximately 6:1. By using this system, turbulence variations up to  $\pm 35\%$  about any mean Doppler frequency between 3KHz and 11 MHz may be followed within one of the ranges.

The tracker or frequency follower is shown in a block diagram in Figure A-4. The Doppler signal is fed into a mixer where the  $f_D$  signal is mixed with a second frequency ( $f_{VCO}$ ) from a voltage controlled oscillator. When tracking, the resulting frequency ( $f_T$ ) is near  $f_{IF}$ . A narrow band filter (IF/A) is then employed to remove as much as possible. From there, the signal passes to the first limiter (Limiter I). The limiter consists of a Schmitt trigger with an adjustable threshold level. In this way, the inherent amplitude modulation is removed and a constant amplitude square wave is produced. This signal is then fed to the discriminator which produces a feedback voltage that controls the VCO and maintains the mixed frequency  $f_T$  near  $f_{IF}$ .

The discriminator consists of a second narrow band pass filter, a second limiter and a phase comparator. The signal coming from Limiter I is fed through the second narrow band filter (IF/B also centered at  $f_{IF}$ ) to remove all the higher harmonics in the signal. The result is a sinusoidal signal. The signal is then passed through Limiter II to produce a second square wave signal at  $f_{IF}$ . This second IF stage is designed, however, to produce an output that lags the output of Limiter I by  $90^\circ$  if  $f_T = f_{IF}$ . The signal lags by less than  $90^\circ$  (to  $0^\circ$ ) if  $f_T < f_{IF}$  and

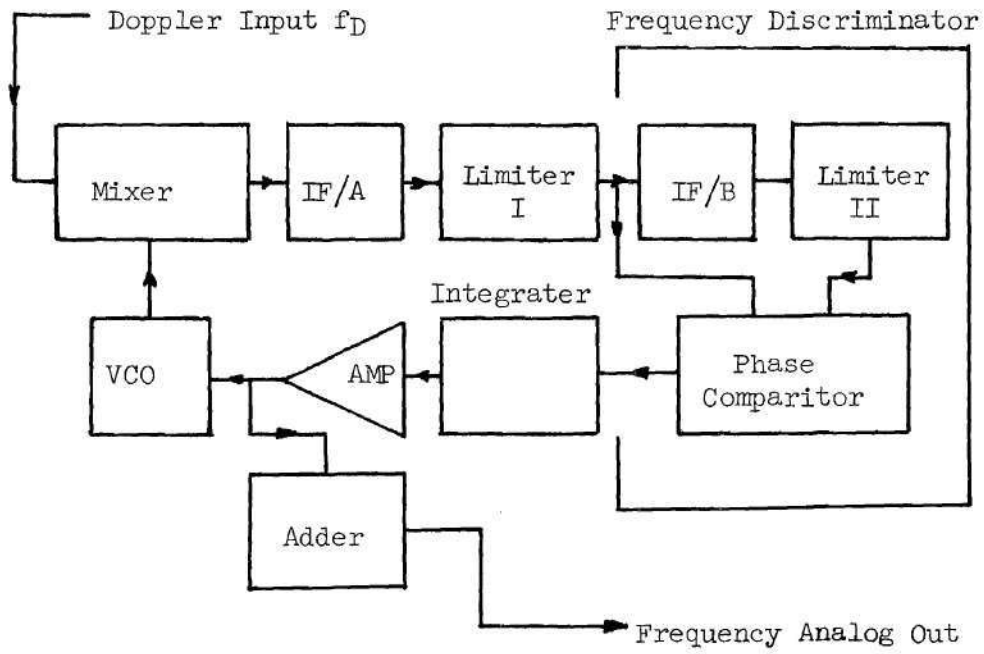


Figure A-4. Block Diagram of LDA Tracker.

by more than  $90^\circ$  (to  $180^\circ$ ) if  $f_T \neq f_{IF}$ . This signal and the signal from Limiter I are then compared by way of a phase comparator. The comparator performs a simple analog multiplication and its output is therefore  $2f_{IF}$ . The Mark space/time ratio varies with the phase difference of the inputs. This signal is then integrated to produce a dc voltage which varies with phase difference (the difference between  $f_{IF}$  and  $f_T$ ). This correction voltage is amplified and fed to the voltage controlled amplifier. As a result of this feedback, the oscillator frequency tracks that of the Doppler signal with the difference between the oscillator and the Doppler frequency being held nearly constant at  $f_T$ .

Restated,  $f_T$  is held very nearly equal to  $f_{IF}$ . How well  $f_T$  equals  $f_{IF}$  is dependent on the feedback loop gain. As the loop gain is increased the difference between  $f_T$  and  $f_{IF}$  is decreased. There is, however, an upper limit to the loop gain, above which the circuit will oscillate. For this reason, the gain is set at a value which will provide close tracking without oscillation.

The correction voltage applied to the voltage controlled oscillator is by definition directly proportional to  $f_{VCO}$ . By monitoring this voltage an analog signal proportional to the Doppler frequency may be obtained. This is accomplished by subtracting the voltage which corresponds to  $f_D$  (as constant). The following relations may aid in understanding the basic mixing.

$$f_D \text{ mixed with } f_{VCO} \rightarrow f_T$$

$$f_T \text{ compared to } f_{IF} \rightarrow \text{correction to VCO}$$

$$\text{VCO to change } f_{VCO} \text{ so that } f_T - f_{IF} \sim 0$$

$$f_{VCO} - f_D = f_T \cong f_{IF} = \text{cst}$$

$$f_{IF} \cong f_{VCO} - f_D$$

$$f_D \cong f_{VCO} - f_{IF}$$

$$f_{VCO} \propto \text{voltage applied to VCO.}$$

In order to follow different velocity ranges, the center frequencies of both narrow band filters and limiters are set to a new  $f_{IF}$ , as in Table A-1. For proper integration, the integration components must also be changed. The total effect of the narrow band filter and the necessary integration factors places a limit on how fast the tracker can follow a signal. The tracking speed can be improved by changing the width of the band pass filters. This is accomplished by changing the position of the percent bandwidth setting. Increasing the bandwidth may, however, reduce the signal to noise ratio of the signal entering into the discriminator section of the tracker. The tracker is equipped with five bandwidth settings (.5, 1, 2, 4, 8 percent of the frequency range).

#### Present Tracker

The early system had two major drawbacks which restricted its usefulness. The first drawback is that at low velocities only  $\pm 35\%$  of the Doppler frequency could be followed. In most applications this affords no hindrance. However, in recirculation regions, velocities may be quite near zero (on the average) with fluctuations in excess of 100%. This would be impossible for the Mark I tracker to follow. The second drawback is a result of the interference fringes produced since the fringe is stationary, a particle traveling in a "negative" direction will produce a Doppler frequency equal to that produced by a particle with equal velocity

traveling in the positive direction. This effect is known as sign ambiguity (common in heat transfer type anemometers). Although not a serious drawback, treatment of recirculation regions would be more accurate if direction could be determined.

Both drawbacks have been alleviated in the Mark II model system. This was accomplished by producing a moving fringe pattern. To produce a moving fringe pattern, the beams producing the fringe must be of different frequencies. To shift the frequency of one of the beams, an acousto-optic (or Bragg) cell is used. After the laser light has entered the optical package (or transducer) the beam is divided by a beam splitter into two beams. One beam passes through the transducer unaffected. The other beam enters a Bragg cell where the frequency is shifted by a value determined by the acoustic excitement of the cell (39). The basic operation of this cell is shown in Figure A-5. In this system the Bragg cell is driven at 40 MHz to produce a beam shifted by +40 MHz (1st order beam). The 0<sup>th</sup> order beam is blocked from leaving the optics package. If the photomultiplier is positioned as shown in Figure A-6, the frequency detected by the photomultiplier will be greater than 40 MHz for "negative" flow and less than 40 MHz for positive flow.

Because the tracker is designed to operate only in the frequency ranges shown in Table A-1, the signal from the photomultiplier must be processed to give a signal which will be within the range of the tracker. This is accomplished through the use of a range translator. The range translator is a local oscillator capable of producing frequencies from 0 to 50 MHz in steps of 10 kHz. To provide maximum stability the oscillator is driven from the same 40 MHz oscillator used to drive the Bragg cell.

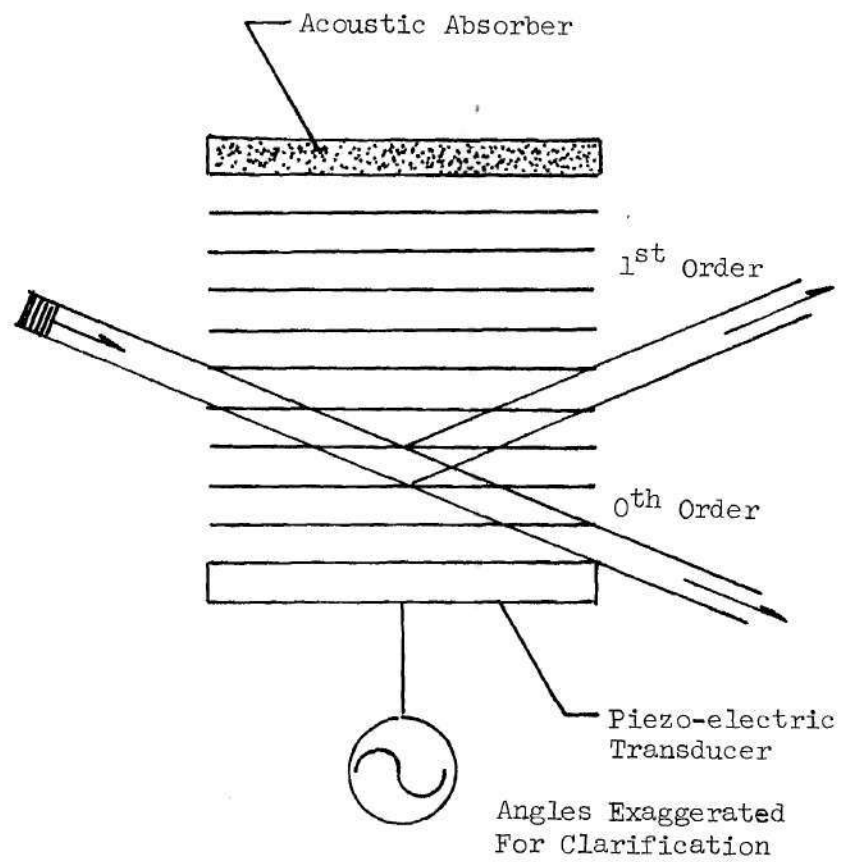


Figure A-5. Operation of Bragg Cell.

The signal produced by the local oscillator ( $f_{LO}$ ) is mixed with the signal coming from the photomultiplier. The resulting frequency ( $f_T$ ) is then fed into a tracker system similar to that in the Mark I system. This tracker frequency  $f_T$  is defined as:

$$f_T = f_D + f_{LO} - 40 \text{ mHz}$$

If  $f_{LO}$  is set equal to 40 mHz, the tracker frequency is equal to the Doppler frequency  $f_D$  and the tracker becomes essentially the same as the Mark I system.

In order to track a negative velocity, the photomultiplier signal must be mixed with a local oscillator (range translator) signal which is greater than 40 mHz. This results in a tracker signal  $f_T$  within one of the ranges. As now becomes apparent in Table A-1, the versatility of the tracker has been greatly enhanced. By selecting a range which is higher than the range needed to track a signal in the Mark I system and the translating the signal to a frequency that can be handled by that range, larger fluctuations (greater than 35%) in velocity can be followed. Tracking is exactly the same as for the Mark I system except the frequency being tracked is now followed in a higher frequency range, thus allowing for greater frequency fluctuations. Conversely, by mixing the photomultiplier signal with a local oscillator signal less than 40 mHz, a signal of low variation may be tracked in a lower frequency range (compared to the range necessary in the Mark I system). In this way the frequency ranges originally designed to handle various velocity ranges may now be considered as ranges of variation, lower ranges handling the lower

variations in velocity (or  $f_D$ ) and higher ranges handling higher fluctuations. Of course, there is some danger in increasing the noise entering the system by using the higher frequency range which requires a wider bandpass filter.

Also of consideration is the use of the percent bandwidth setting, which can also change the width of the bandpass filter. The choice of which settings to use becomes, at times, a compromise. For example using a frequency range of 500 kHz with an 8% bandwidth will result in a frequency response of approximately 4kHz while a frequency range of 5 MHz with a 1% bandwidth will produce a comparable 5 kHz frequency response (see Table A-2). The choice of setting to be used would depend largely on the position which allows the optimum tracker response.

Since the tracker is now following some fluctuation  $f_T$ , the signal processing for an analog output must be changed. In Mark I system the VCO was controlled by a fast servo loop to maintain the difference between  $f_D$  and  $f_{VCO}$  constant at  $f_T$  (which very closely approximated  $f_{IF}$ ). The same configuration is used in the Mark II system. The difference between  $f_T$  and  $f_{VCO}$  is held constant at  $f_T$  which very closely approximates  $f_{IF}$ . The frequency of the bandpass filters may be described by the following equation:

$$f_{IF} = f_{VCO} - f_T = f_{VCO} - f_D - f_{LO} + f_o \quad (A-2)$$

where  $f_{VCO}$  is the voltage controlled oscillator output,  $f_D$  is the Doppler frequency,  $f_{LO}$  is the frequency from the range translator and  $f_o$  is the 40 MHz shift from the Bragg cell. Since  $f_{IF}$ ,  $f_{LO}$  and  $f_o$  are all constant,

$f_{VCO}$  varies only because of the Doppler frequency  $f_D$ . In order to simplify processing, the range translator provides a second signal. This signal is the difference between  $f_o$  (40 MHz) and the translation frequency  $f_{CO}$  given is:

$$f'_{LO} = |f_{LO} - f_o| \quad (A-3)$$

since  $f_{LO}$  and  $f_o$  are both constant  $f'_{LO}$  is also a constant. Using equation (A-3), equation (A-2) may be rewritten as

$$f_{IF} = f_{VCO} - f_T = f_{VCO} - f_D - f'_{LO}$$

or

$$f_D = f_{VCO} - f_{IF} - f'_{LO} \quad (A-4)$$

The three frequencies on the right hand side of equation (A-4) are counted digitally to produce a digital display of the mean velocity. Since  $f_{IF}$  and  $f'_{LO}$  are constants, the counting time used is constant and independent of the integration time selected. The VCO signal ( $f_{VCO}$ ), however, is counted for a period of time dependent on the integration time selected. After completion of counting, the digital value is multiplied by the correction factor determined from equation (A-1) and then displayed.

The analog signal is also processed in manner different from the Mark I system. The Mark II system operates on the basis of equation (A-4). The frequencies  $f_{VCO}$  and  $f'_{LO}$  are fed into separate frequency to voltage converters and subtracted. Since  $f_{IF}$  is constant and does not

change with translation as does  $f'_{LO}$ , no frequency to voltage converter is necessary. The digital unit provides a dc voltage which is directly proportional to  $f_{IF}$ . This voltage is also subtracted. The result is a voltage which is directly proportional to  $f_D$ . In order that the analog signal produced be equal to the velocity component of the flow, an adjustable gain amplifier is provided. The resulting signal may then be processed by any method desired.

### Frequency Response

The frequency response of the tracker with respect to the various bandwidth and range settings is shown in Table A-2. The entire LDA system is limited, however more by the optics and flow than by the electronics. This optical frequency limit is a result of the ambiguity inherent in LDA systems (54-57). The ambiguity generally causes a spectral broadening and is produced by several factors:

1. Since the sampling volume is finite in size and scattering particles are necessary to reflect the laser light, the signal received is a combination of many frequencies which have various durations and amplitudes. This mixture of signals represents all the velocities present in the sampling volume and because of destructive and constructive interference the signal may not truly represent the flow.

2. A second source of ambiguity is a result of the focused laser beam. As seen in Figure A-7 the angle between the two beams is  $\theta \pm \alpha$ . Because of this variation the frequency seen by the photodetector also has a variance as is seen from the Doppler equation.

$$f_D = \frac{\lambda U}{2 \sin \left( \frac{\theta \pm \alpha}{2} \right)}$$

Table A-1. Frequency Ranges for LDA Tracker

Range	( $f_T$ )	( $f_{IF}$ )	( $f_{VCO}$ )
15 kHz	2.25 - 15 kHz	1.5 kHz	3.75 - 16.5 kHz
50 kHz	7.50 - 50 kHz	5 kHz	12.5 - 55 kHz
150 kHz	22.5 - 150 kHz	15 kHz	37.5 - 165 kHz
500 kHz	75 - 500 kHz	50 kHz	125 - 550 kHz
1.5 mHz	.225 - 1.5 mHz	150 kHz	.375 - 1.65 mHz
5.0 mHz	.75 - 5 mHz	500 kHz	1.25 - 5.5 mHz
15 mHz	2.25 - 15 mHz	1.5 mHz	3.75 - 16.5 mHz

Table A-2. Frequency Response as Value of Percent Bandwidth

Range % BW	15 kHz	50 kHz	150 kHz	500 kHz	1.5 mHz	5.0 mHz	15 mHz
8	120 Hz	400 Hz	1.2 kHz	4.0 kHz	12 kHz	40 kHz	120 kHz
4	60 Hz	200 Hz	600 Hz	2.0 kHz	6 kHz	20 kHz	60 kHz
2	30 Hz	100 Hz	300 Hz	1.0 kHz	3 kHz	10 kHz	30 kHz
1	15 Hz	50 Hz	150 Hz	500 Hz	1.5 kHz	5 kHz	15 kHz
0.5	7.5 Hz	25 Hz	75 Hz	250 Hz	.75 kHz	2.5 kHz	7.5 kHz

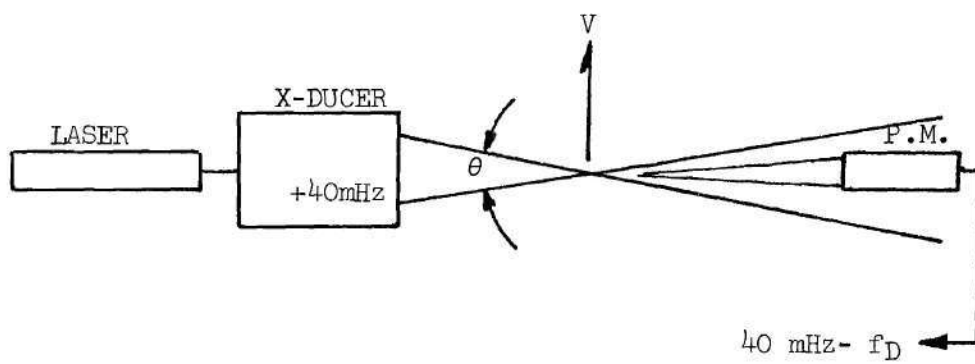


Figure A-6. LDA Geometry, Differential Mode, 40 mHz Shift.

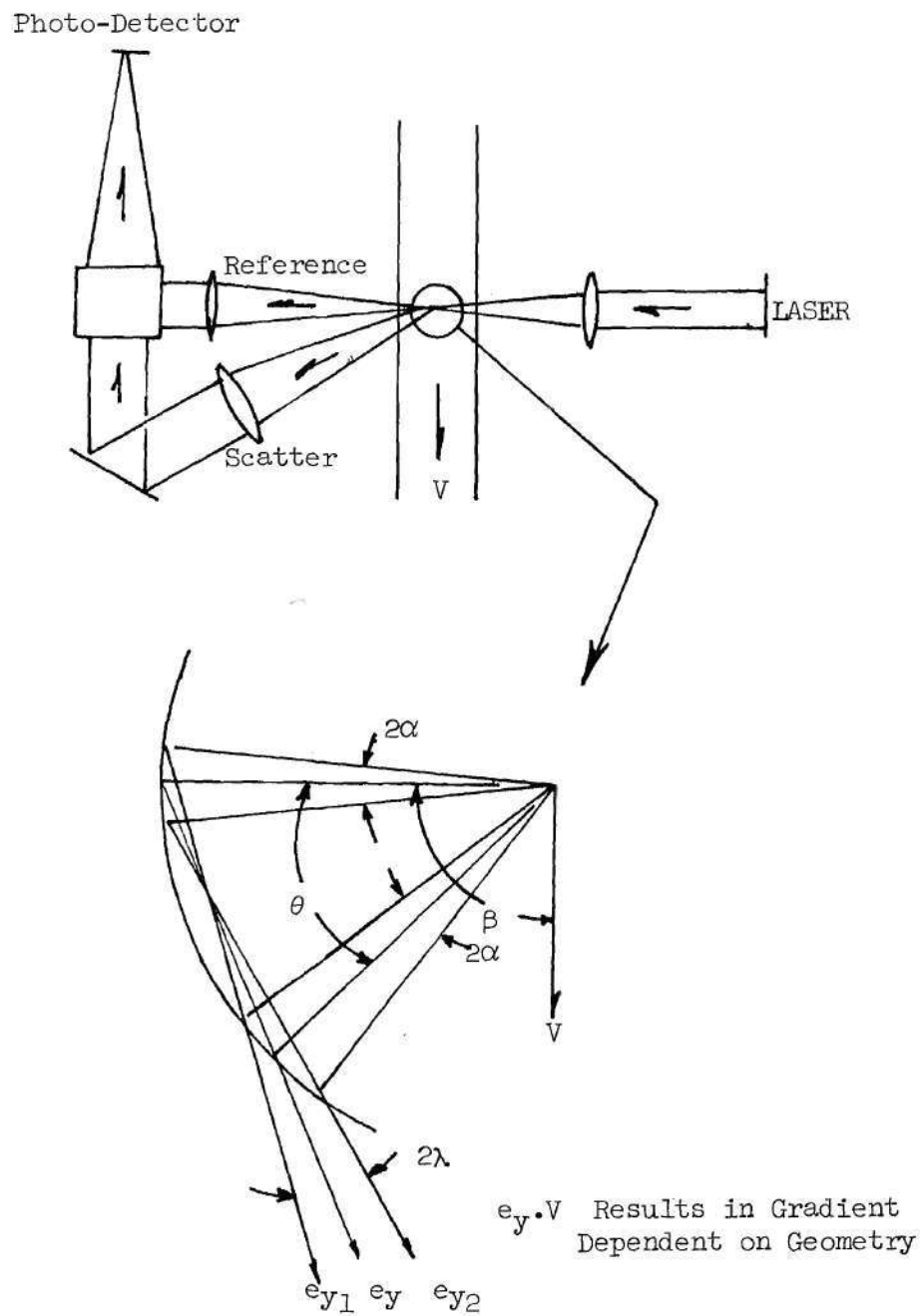


Figure A-7. Production of Ambiguity, Reference Beam Mode.

The end result is an apparent velocity gradient produced by the optics alone.

3. Ambiguity may also result from transient Doppler data as a result of finite transit time, frequency modulation, and Brownian motion.

Although a problem, ambiguity does not greatly limit the usefulness of the LDA to any great extent. At high turbulence levels the spectral broadening appears to be minimal and agreement with hot film data is very good.

## APPENDIX III

## SAMPLE PROGRAM

The sample programs are given in Figures A-5 and A-6 and apply to the Hewlett Packard B model Fourier Analyzer.

1 L	10		
4 CL	1		
7 CL	2		
10 L	11		
13 RB	0	2	
17 A+	2		
20 X>	2		
23 #	11	50	0
28 :	2	50	
32 \$	2		
35 :	2	512	
39 -	2	511	
43 CL	2	1	512
48 \$	2		
51 L	12		
54 RB	0	1	
58 A-	2		
61 F			
63 SP			
65 #	12	50	0
70 X<	1		
73 TL			
75 .			
77 X<	2		
80 W	0	512	
84 X<	1		
87 \$			
89 W	0	256	
93 .			
95 J	10		
98 .			

Figure A8. Sample Program Number I.

100 L	20		
103 CL	1		
106 CL	2		
109 L	21		
112 RB	0	2	
116 A+	2		
119 X>	2		
122 #	21	150	0
127 :	2	150	
131 \$	2		
134 :	2	512	
138 -	2	511	
142 CL	2	1	512
147 \$	2		
150 L	22		
153 RB	0	1	
157 A-	2		
160 F			
162 SP			
164 #	22	50	0
169 X<	1		
172 TL			
174 .			
176 X<	2		
179 W	0	512	
183 X<	1		
186 \$			
188 W	0	256	
192 .			
194 J	20		
197 .			

Figure A9. Sample Program Number II.

## APPENDIX IV

## CASSON MODEL

The viscous properties of blood have been compared mathematically to the Casson model for oil based inks (58). In the Casson model the following assumptions are made:

1. Attractive forces between individual particles are postulated.
2. Individual particles tend to chain together to form long rods.
3. The particles are suspended in a Newtonian Fluid.
4. Energy dissipation of a single rod is determined by its action in the fluid.
5. Interactions between rods are neglected.
6. Rod motion depends on its initial orientation.
7. Brownian motion is neglected.
8. Viscosity is determined by summing energy dissipation.
9. Break of rods is related to tension developed as motion occurs.

In the final result the Casson model may be written as:

$$\tau^{1/2} = \tau_y^{1/2} + (\mu \dot{\gamma})^{1/2} \quad \tau \geq \tau_y$$

$$\dot{\gamma} = 0 \quad \tau < \tau_y$$

where  $\tau$  is the shear stress,  $\tau_y$  is the yield stress of the fluid,  $\mu$  is the viscosity (varying with temperature and Hematocrit only), and  $\dot{\gamma}$  is the shear rate. Since the Casson model is considered to be accurate when

applied to blood (59), it was employed to check the Newtonian approximation. Using a value of  $.04 \text{ dynes/cm}^2$  as the yield stress of a hematocrit of 40 (59) and a viscosity of 4 cp, direct comparisons of Hagen-Poiseuille (Newtonian) and Casson (non Newtonian) flows can be made. Figure A-10 shows the comparison using a mean velocity of 40 cm/sec and a vessel diameter of 2.5 cm ( $Re = 2500$ ). Figure A-11 compares the Casson and Hagen Poiseuille flows using a mean velocity of 25 cm/sec and a vessel diameter of 1.5 cm ( $Re = 940$ ). In Figure A-12 the comparison is based on a mean velocity of 14.5 cm/sec and a lumen diameter of .5 cm ( $Re = 180$ ). As is immediately apparent, there is very little difference between the non-Newtonian and Newtonian velocity profiles in Figures A-10 through A-12. The two models (Casson and Hagen Poiseuille) agree quite well for  $R/R_0$  greater than about .5. In this region  $U/U_{FR}$  is slightly greater for the Casson model. In the region for  $R/R_0$  between .5 and 0 the velocity of the Casson model drops off, the error in the worst case being less than 4%. From the equation for the Casson flow, there should be a core region in the flow. In each case this core region is confined within very small radius from the centerline to an  $R/R_0$  of less than .007 in the first two cases and .004 as the last example. Based on this information, it is justifiable to use a Newtonian approximation for the experimental model. Water may therefore be used in the flow facility.

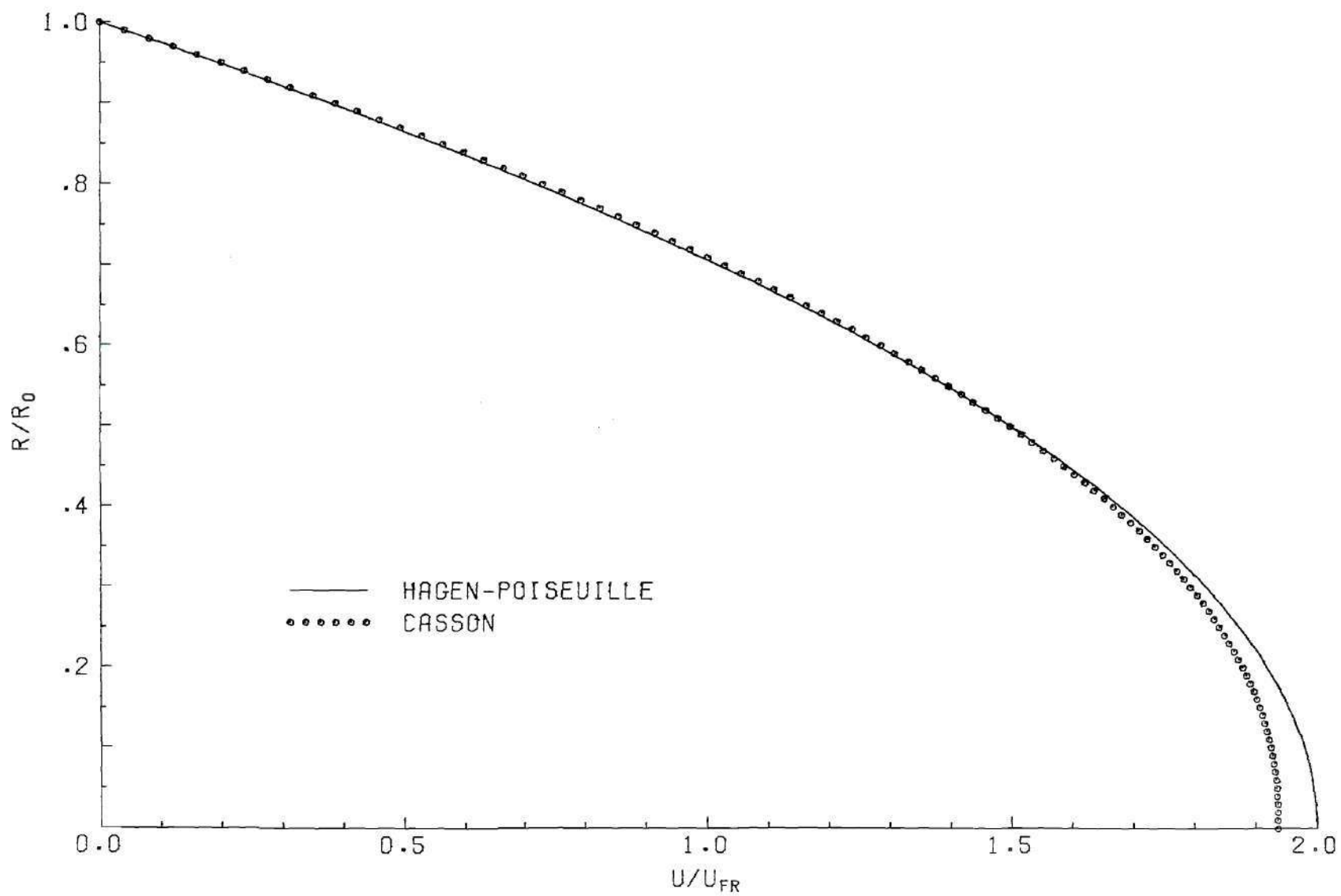


Figure A-10. Comparison of Casson to Newtonian,  $U_{FR} = 40$  cm/sec  $R_0 = 1.25$  cm.

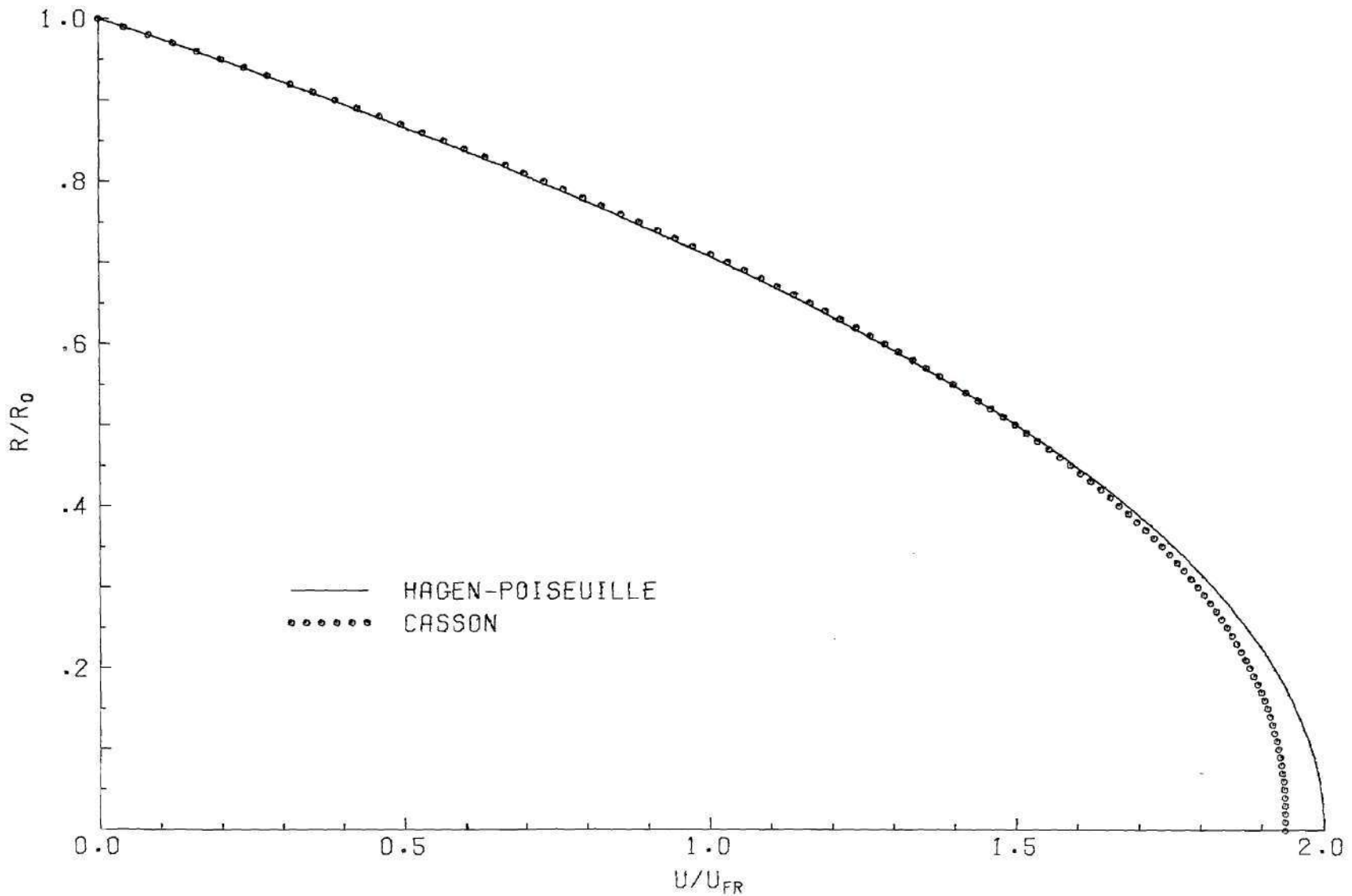


Figure A-11. Comparison of Casson to Newtonian,  $U_{FR} = 25$  cm/sec  $R_0 = .75$  cm.

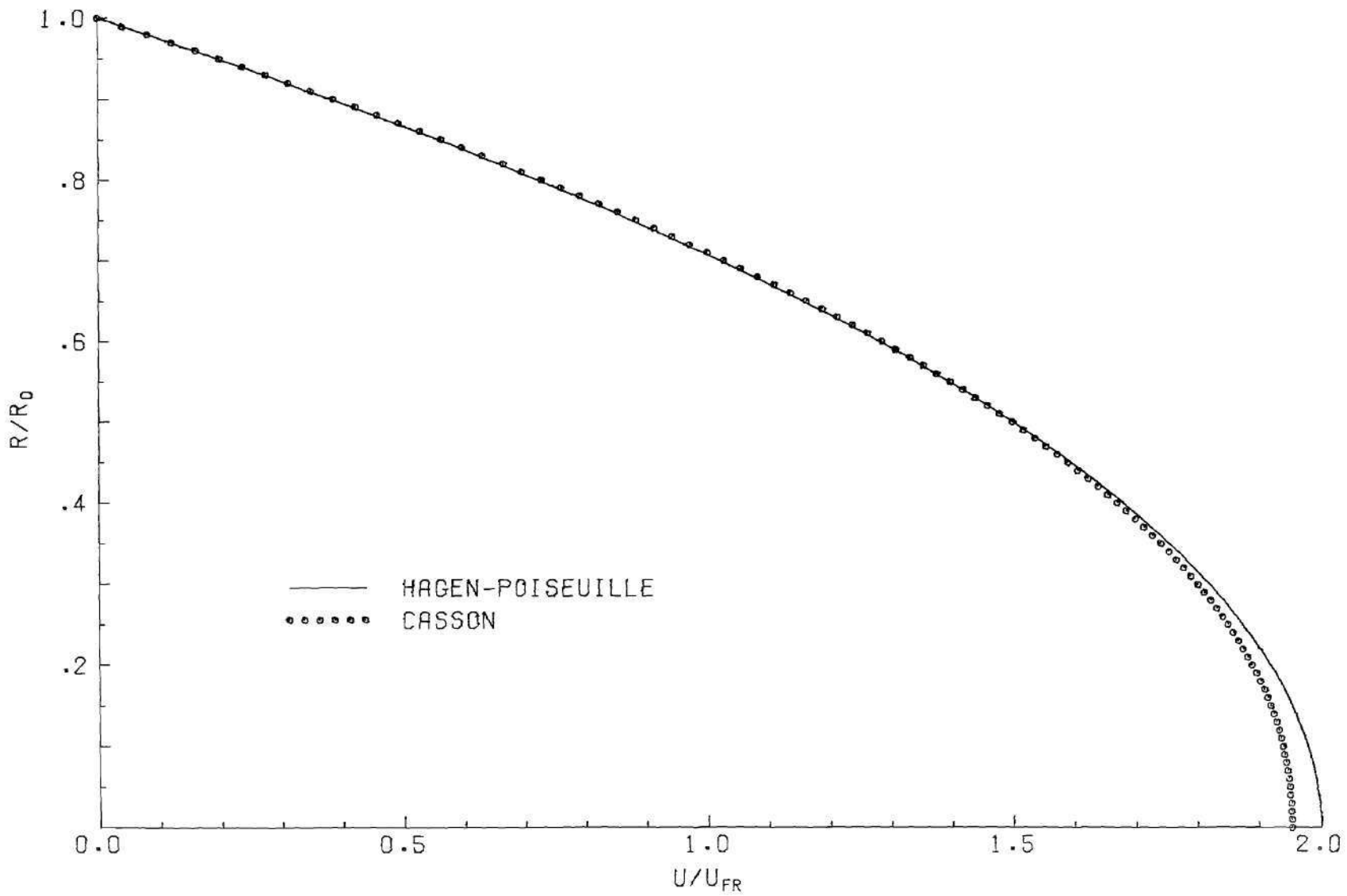


Figure A-12. Comparison of Casson to Newtonian,  $U_{FR} = 14.5$  cm/sec  $R_0 = 0.25$  cm.

## APPENDIX V

## ADDITIONAL RESULTS AND DISCUSSION

In Chapter IV several plots and figures were not included so that the overall presentation would be less confusing. For completeness the remaining figures are included in this appendix, along with descriptions when necessary. The information is presented under the same headings used in Chapter IV.

Centerline Spectra

Centerline spectra for all four cases (water and polymer solution with and without the BLT) are presented in this section. To minimize overlap, each case consists of two figures, i) increasing energy spectra and ii) decreasing energy spectra. Spectra for water without the BLT are presented in Figures A-13 and A-14. Figures A-15 and A-16 correspond to the injection of water with the BLT. The two water cases agree quite well. The major difference is found in the lower frequencies (less than 10 Hz) at an axial station 10.8 catheter diameters downstream of the exit plane. At this station the case with the BLT exhibits an elevation of the lower frequency energy. The BLT spectra are also slightly elevated at the axial stations -.54 to 10.8 catheter diameters. The decreasing energy spectra for both water cases are approximately the same. Spectra for the polymer solution injections are produced in a similar fashion in Figures A-17 and A-18 for the injection without the BLT and Figures A-19 and A-20

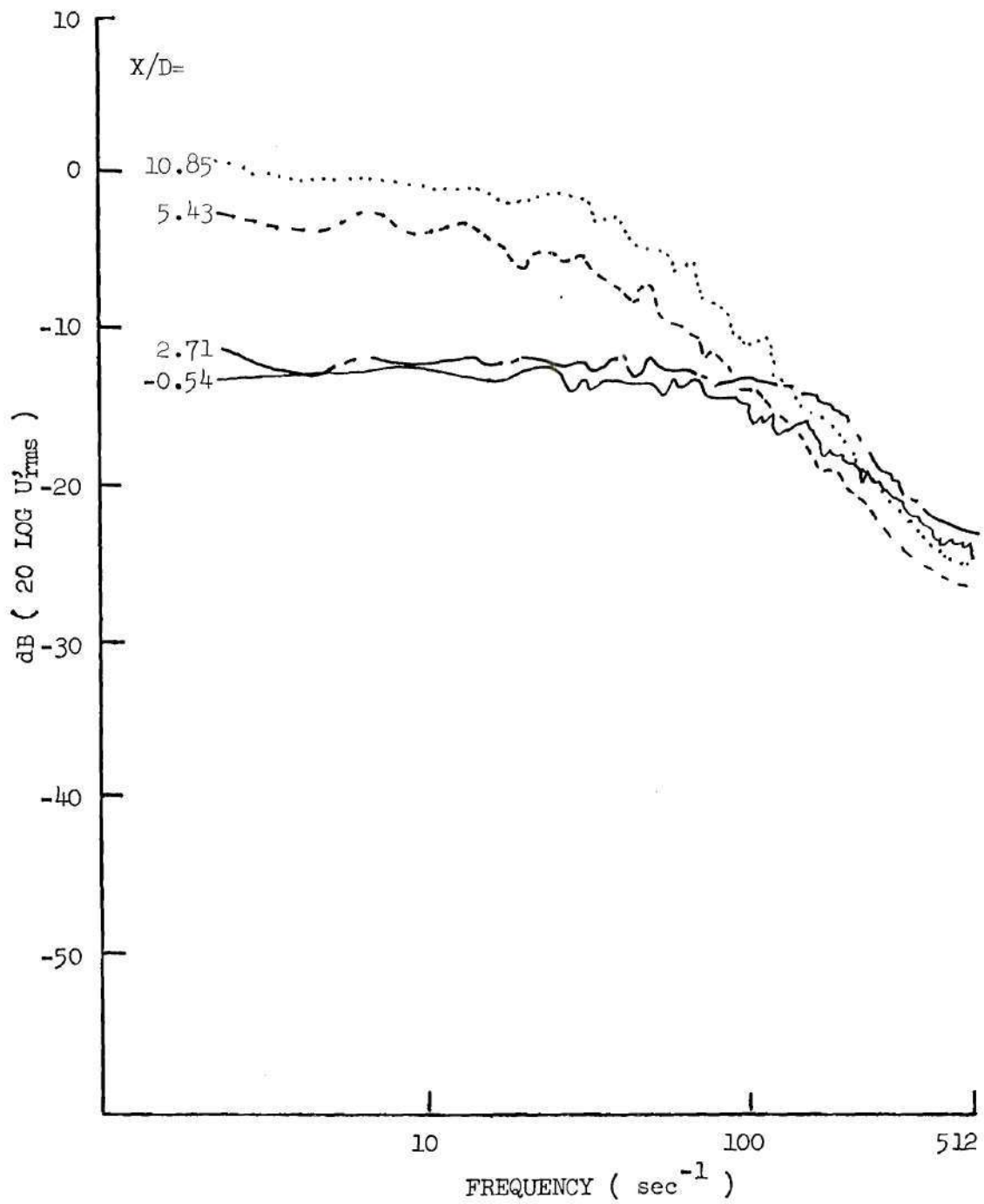


Figure A-13. Centerline Variation of Energy Spectra, Water Without BLT.

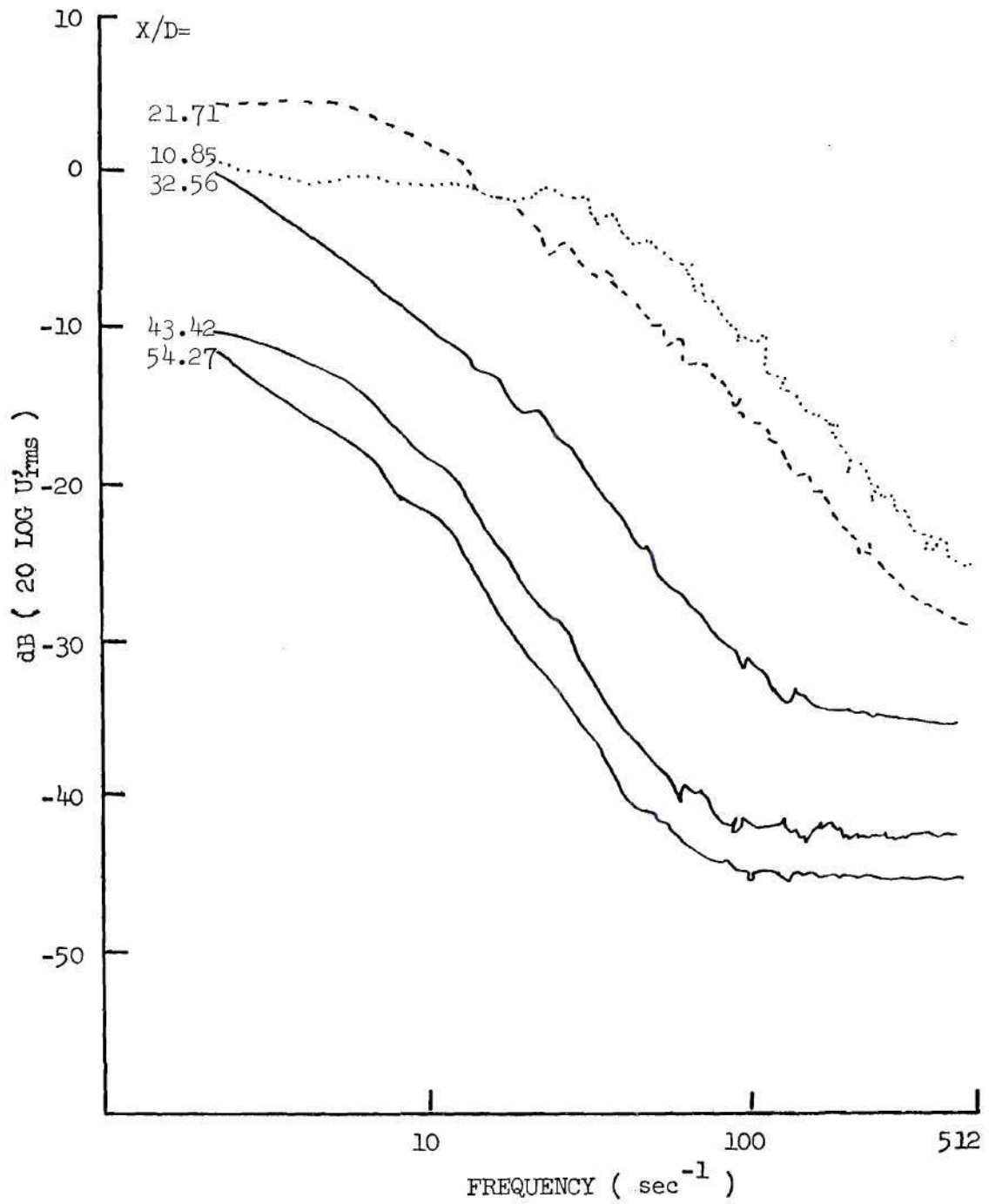


Figure A-14. Centerline Variation of Energy Spectra, Water Without BLT.

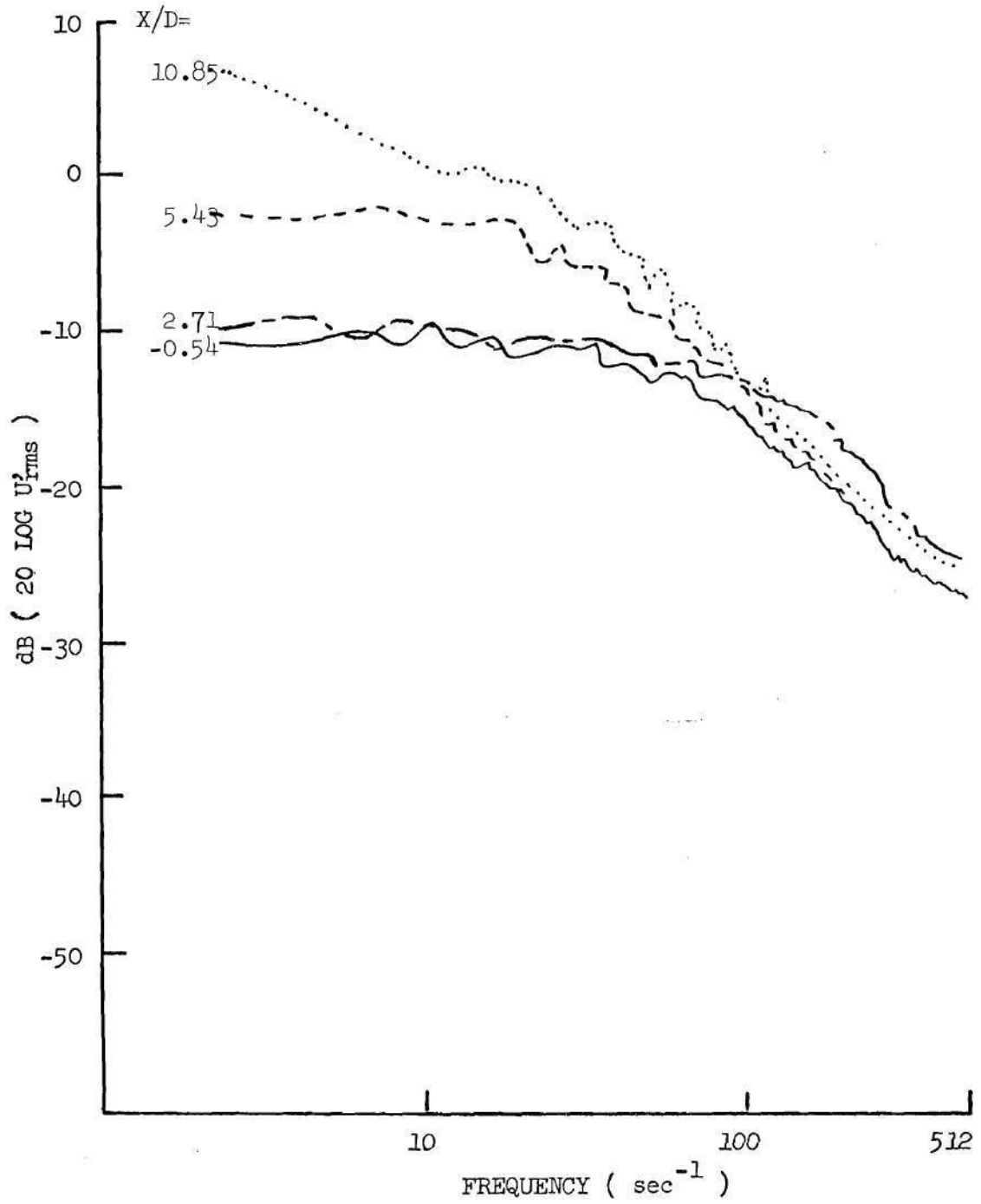


Figure A-15. Centerline Variation of Energy Spectra, Water with BLT.

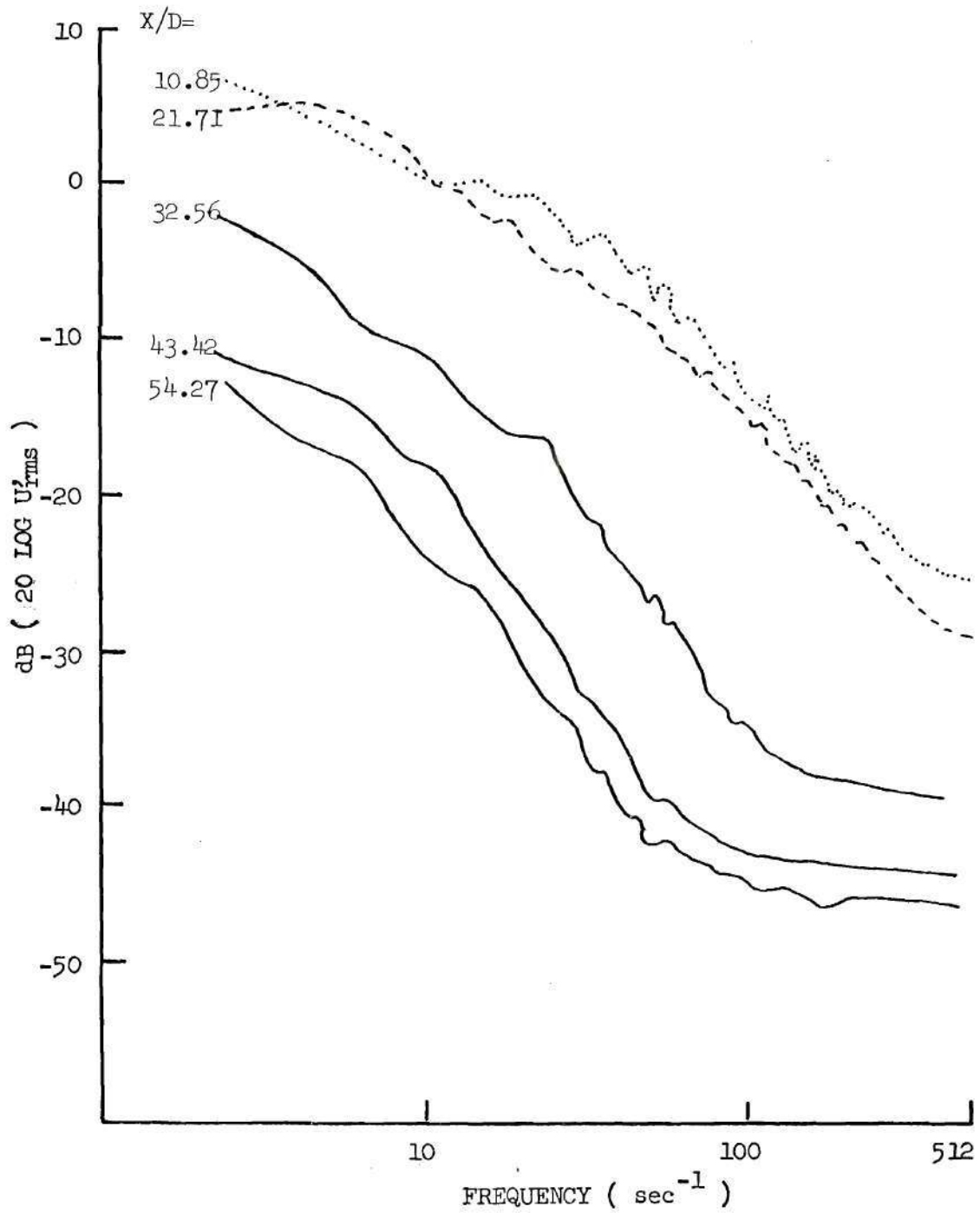


Figure A-16. Centerline Variation of Energy Spectra, Water with BLT.

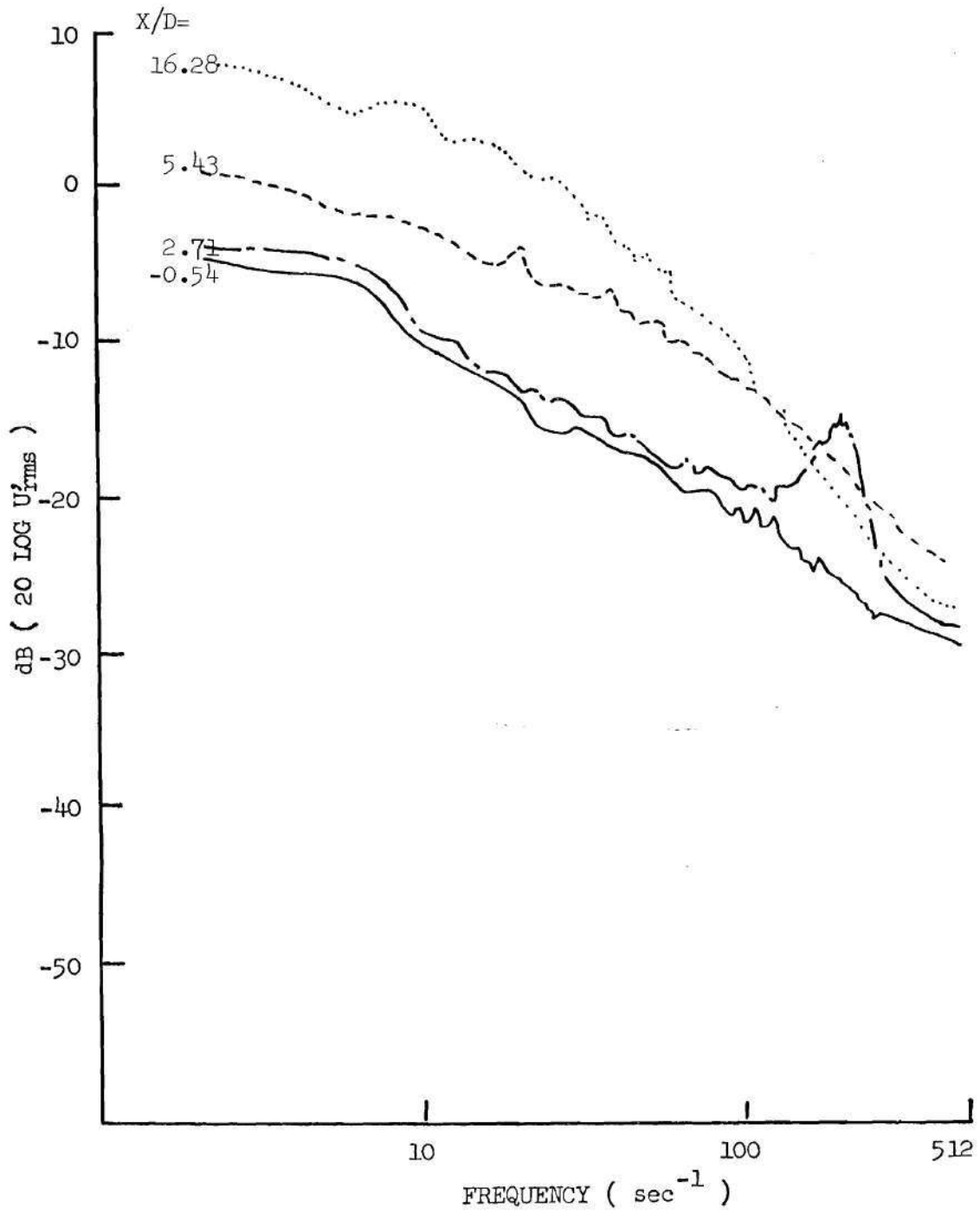


Figure A-17. Centerline Variation of Energy Spectra, Polymer Solution without BLT.

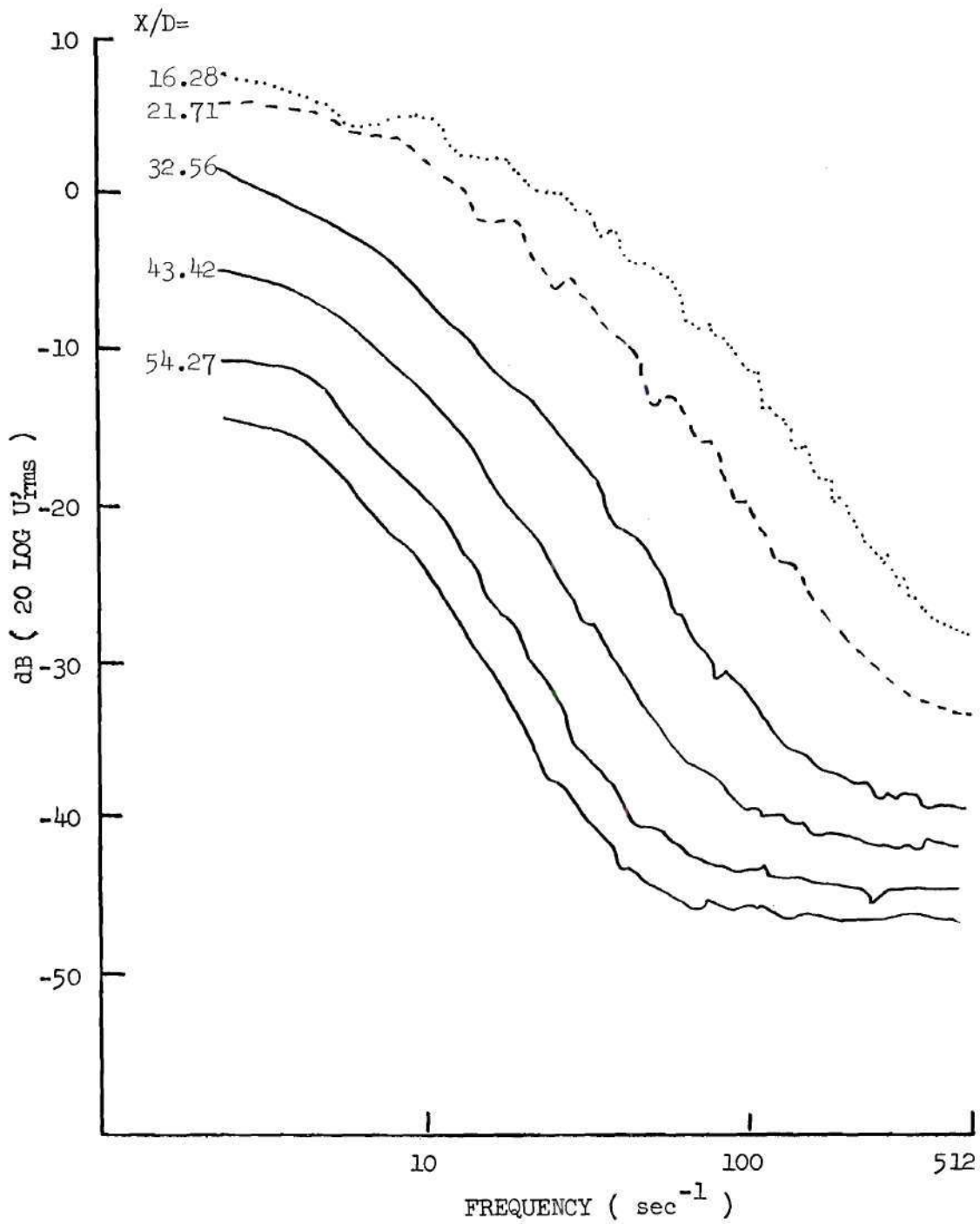


Figure A-18. Centerline Variation of Energy Spectra, Polymer Solution without BLT.

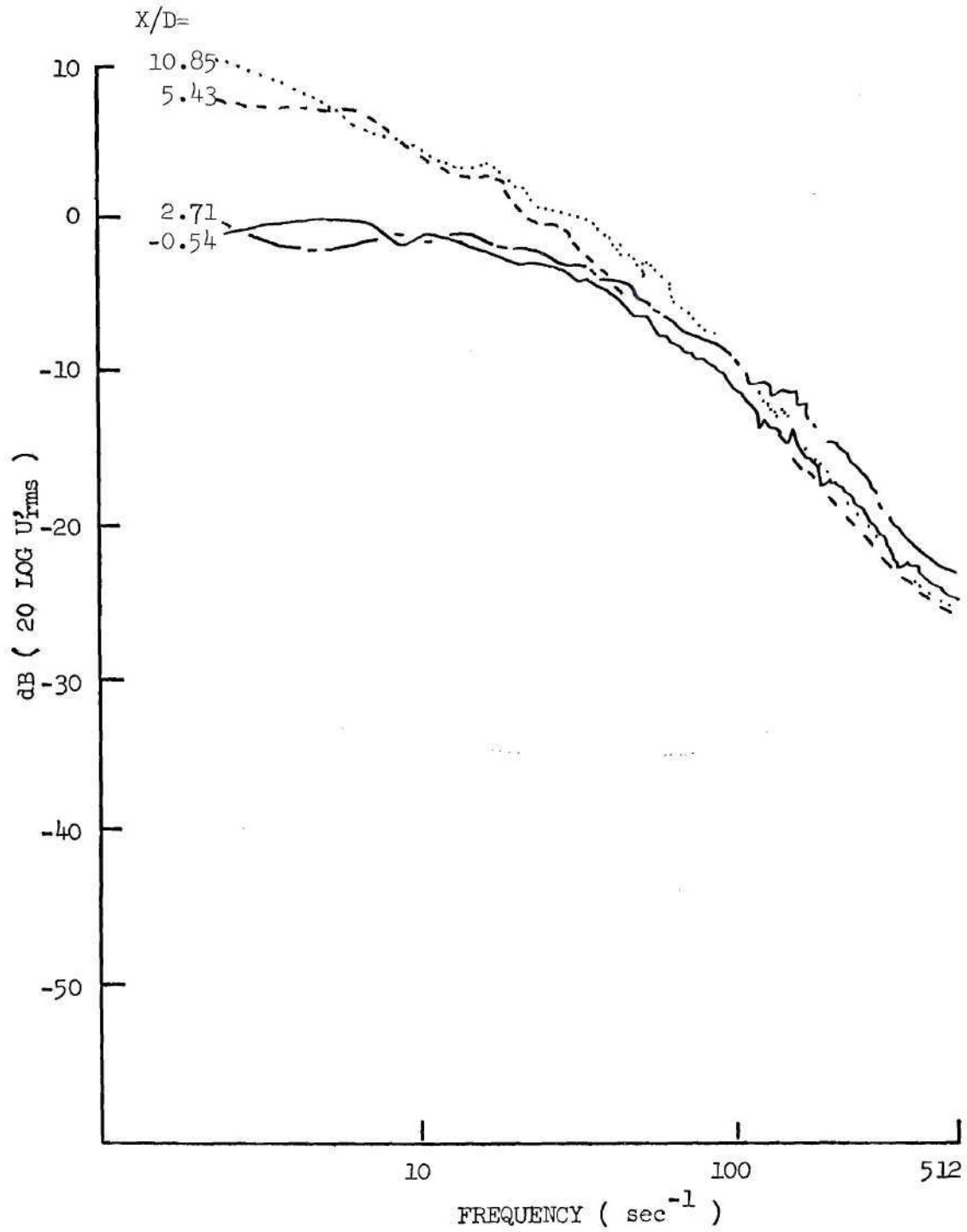


Figure A-19. Centerline Variation of Energy Spectra, Polymer Solution with BLT.

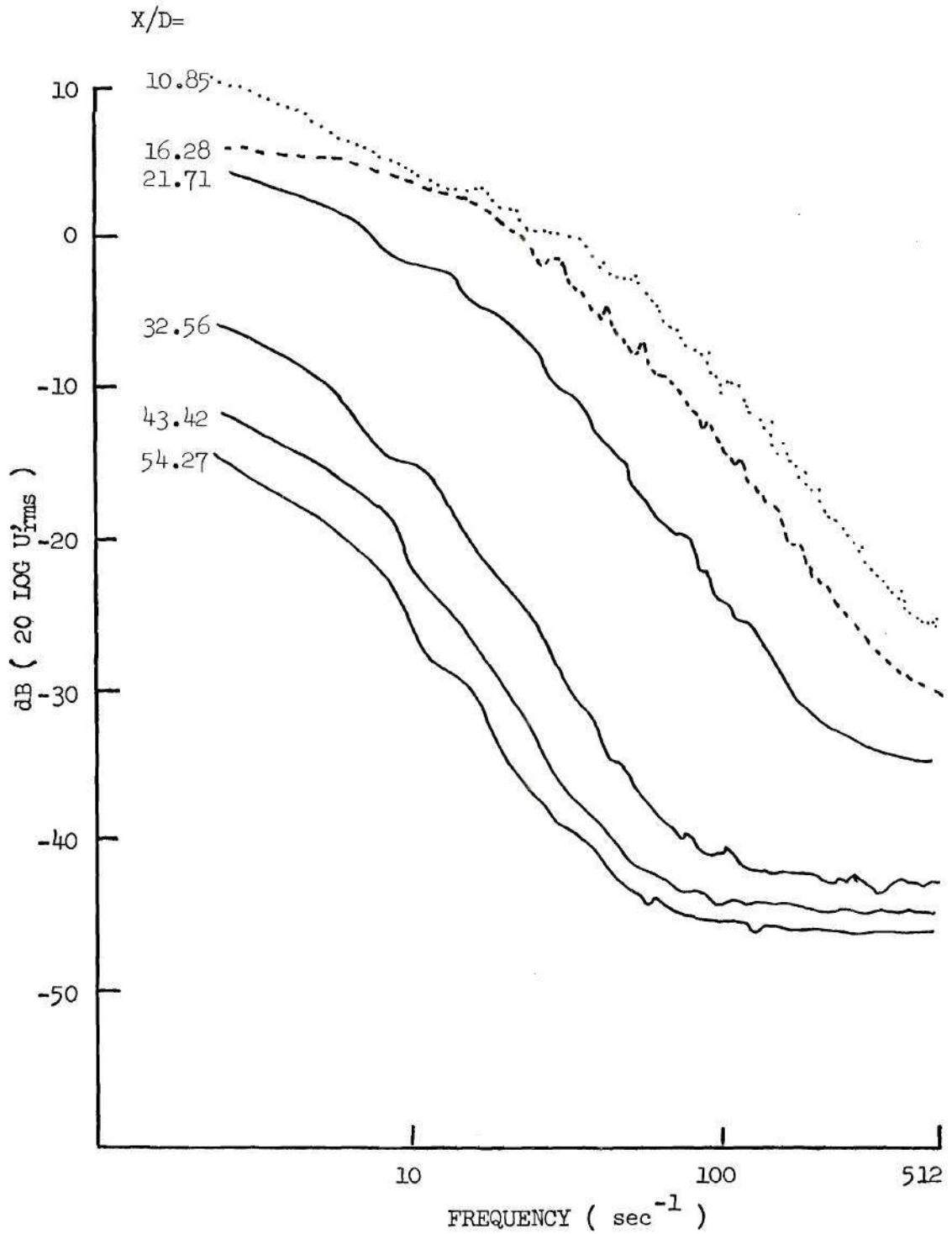


Figure A-20. Centerline Variation of Energy Spectra, Polymer Solution with BLT.

for the BLT case.

#### Radial Variations

The velocity fluctuations ( $U'_{rms}$ ) are presented in Figures A-21 through A-24. The fluctuations are non-dimensionalized by the mean catheter velocity ( $U_{FR}$ ), Figures A-21 and A-22, and by the local mean velocity ( $U_L$ ), Figure A-23 and A-24. In regions where  $U_L$  is negative the absolute value of  $U_L$  is employed. The resulting fluctuations are related to the U-component of turbulent energy ( $U'_{rms}/U_{FR}$ )<sup>2</sup> and intensity ( $U'_{rms}/U_L$ ) at a point. Figures A-21 and A-22 indicate a rise and then a fall of the turbulent energy at each radial position as the flow moves downstream. It is interesting to note the outer flow is effected by the jet at less than one catheter diameter distal to the exit plane. The radial distribution of the turbulent energy becomes essentially uniform after 16.28 diameters or near, reattachment. Figures A-23 and A-24 also present a rise and fall of the radial intensity distribution at increasing axial stations. Again the almost immediate effect on the outer flow is apparent. The strong peaks found at 10.85 and 16.28 diameters are the result of  $U_L$  approaching zero. A generally uniform intensity profile is obtained after 21.74 diameters.

The polymer profiles are presented in a similar fashion. At first glance the polymer development does not appear to be two different from the water injection. Some immediate differences are, however, obvious. The velocity fluctuations in the outer flow region are not as strongly effected in the early development of the jet, the early development of the velocity fluctuations in the center region is not as rapid, and,

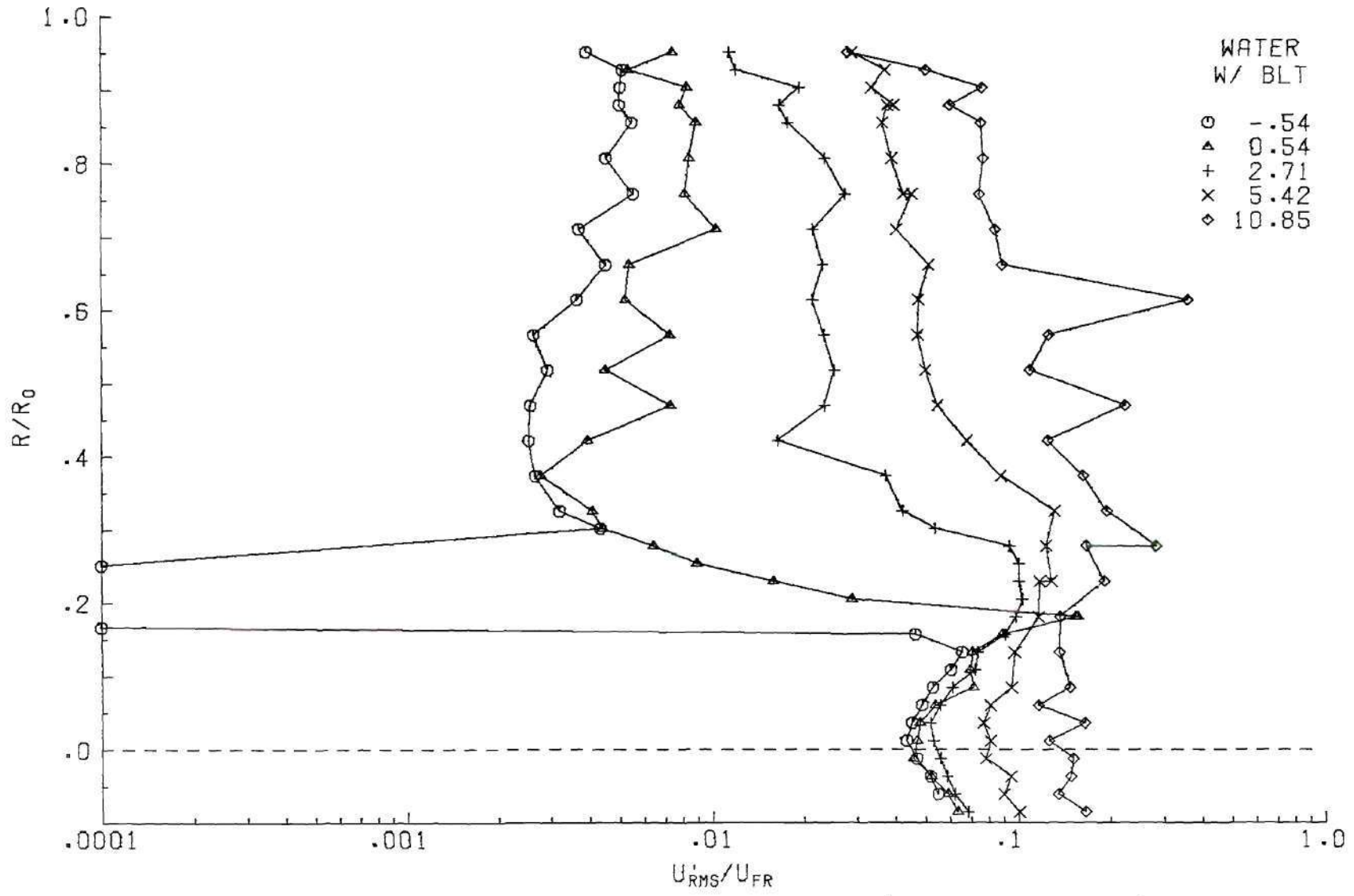


Figure A-21. Fluctuation Profiles, Water with BLT, X/D from -0.54 to 10.85.

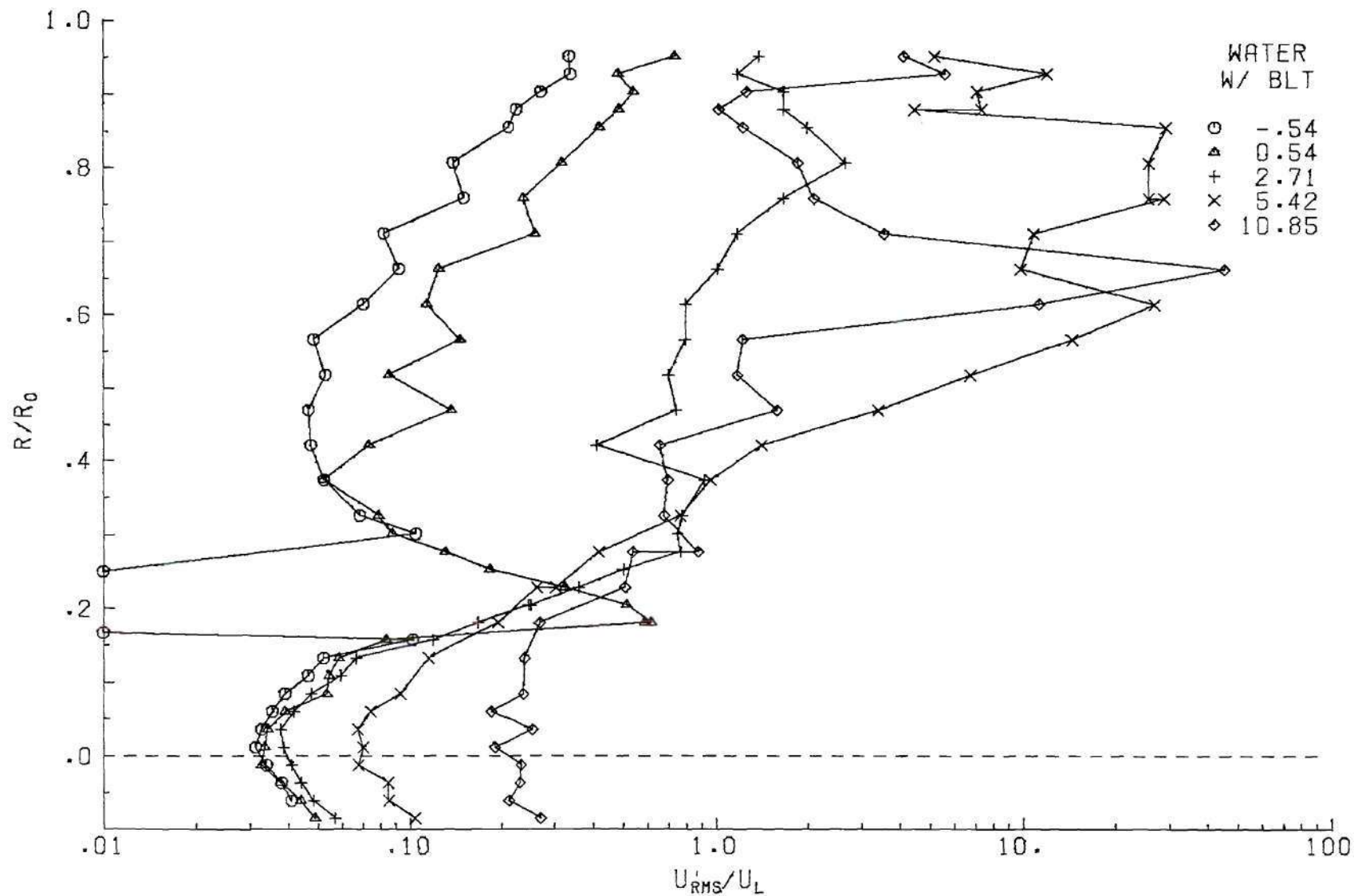


Figure A-22. Fluctuation Profiles, Water with BLT, X/D for 10.85 to 54.27.

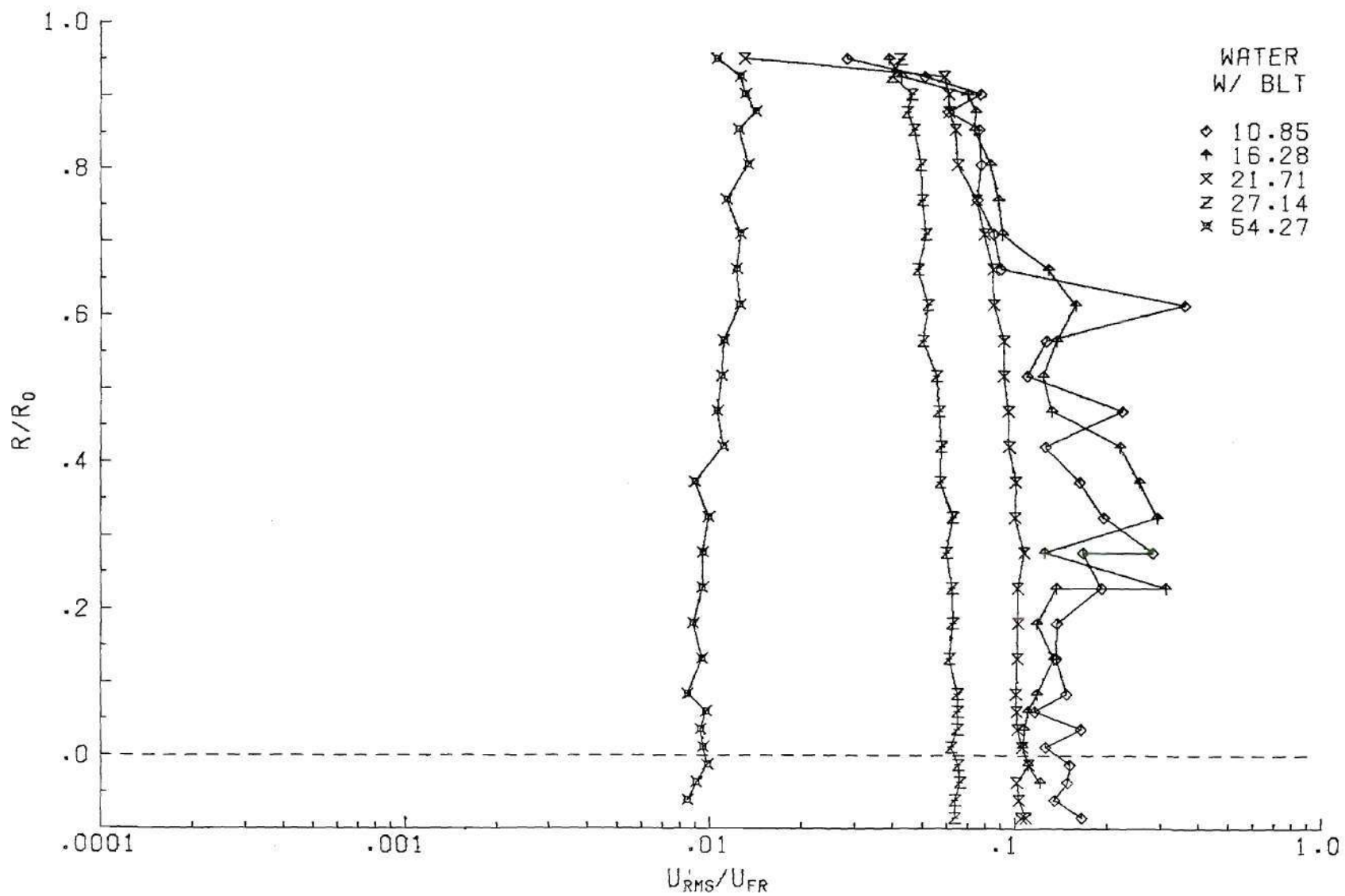


Figure A-23. Intensity Profiles, Water with BLT, X/D from -0.54 to 10.85.

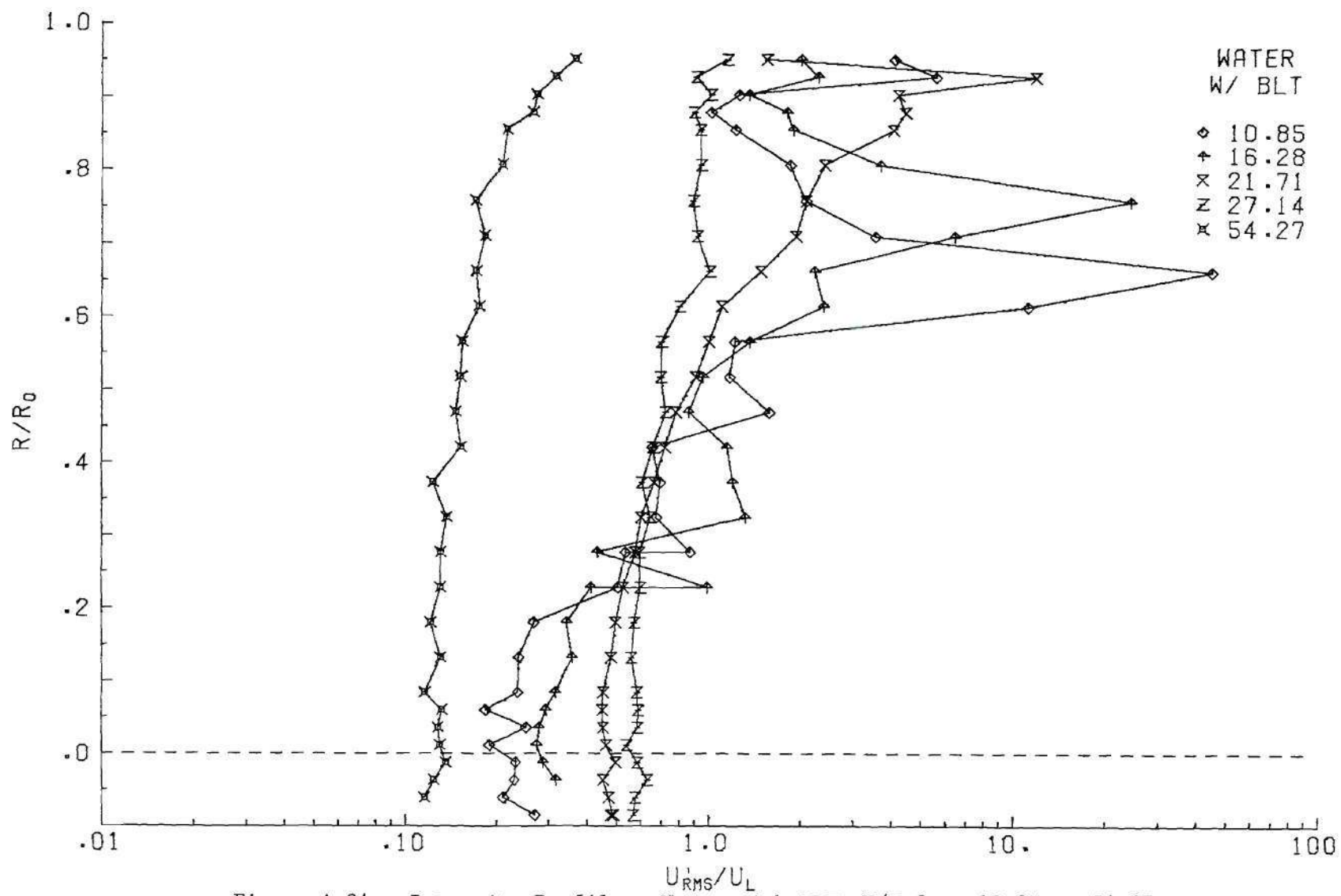


Figure A-24. Intensity Profiles, Water with BLT, X/D from 10.85 to 54.27.

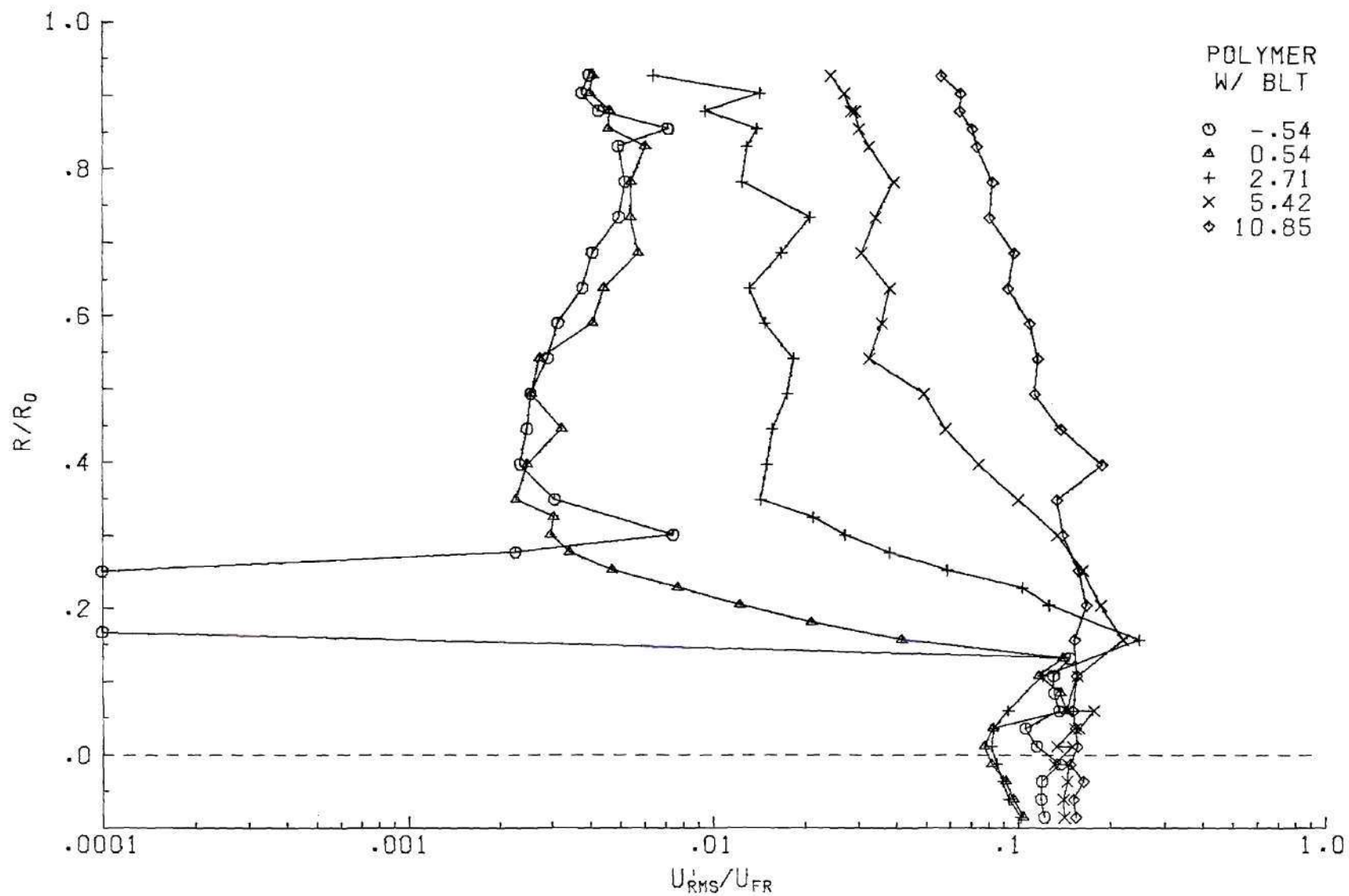


Figure A-25. Fluctuation Profiles, Polymer Solution with BLT, X/D from -0.54 to 10.85.

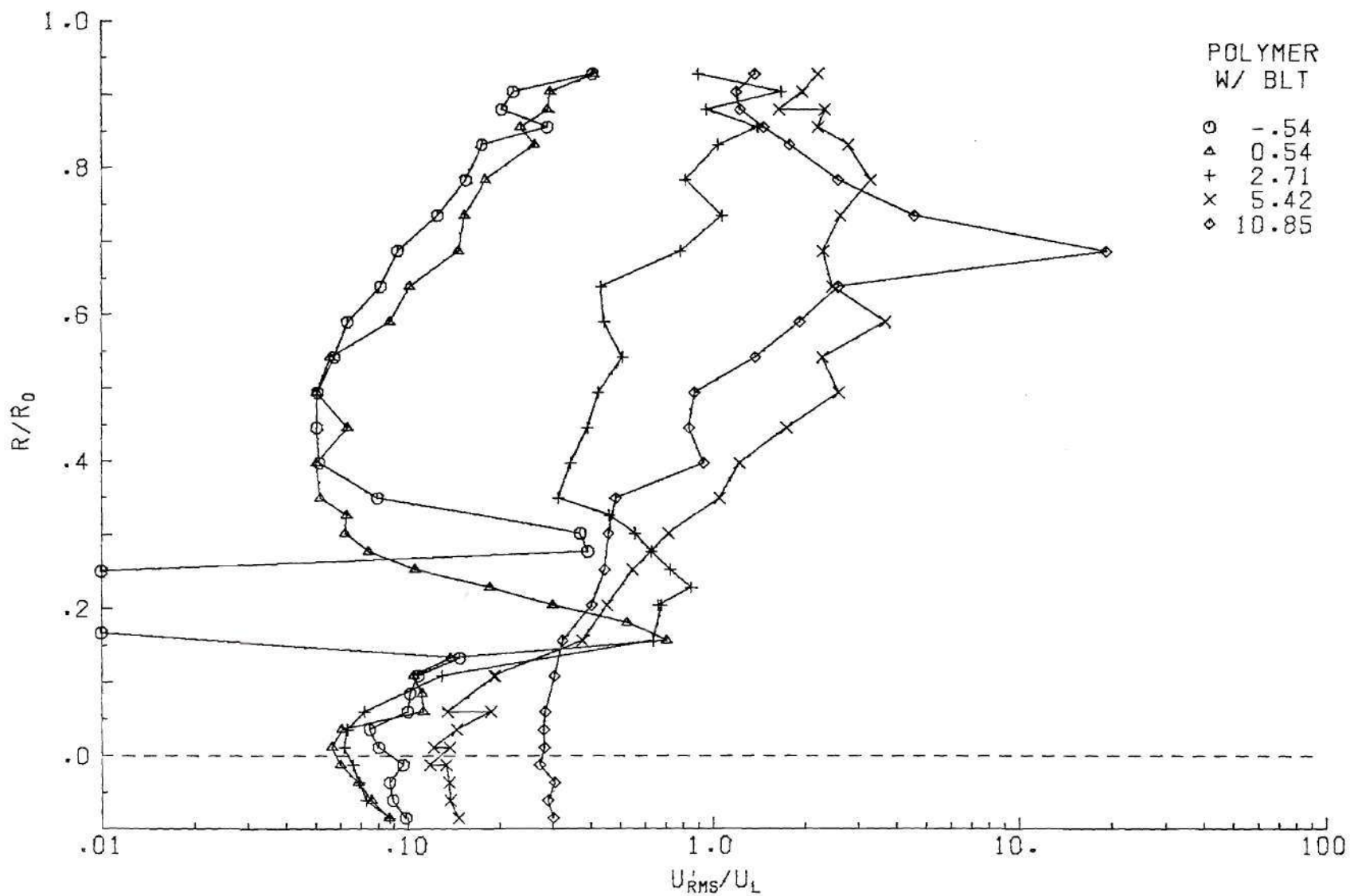


Figure A-26. Fluctuation Profiles, Polymer Solution with BLT, X/D from 10.85 to 54.27.

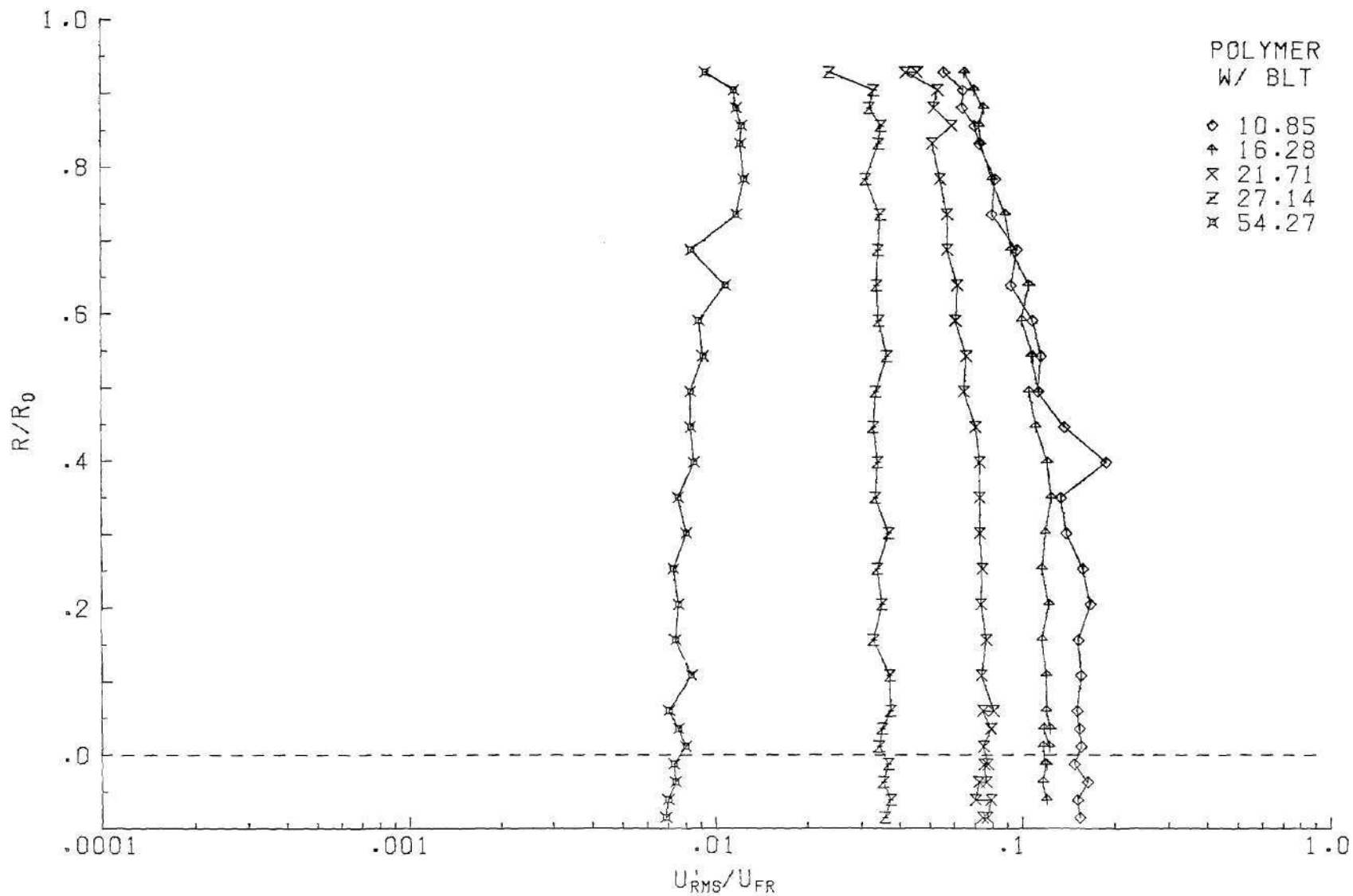


Figure A-27. Intensity Profiles, Polymer Solution with BLT, X/D from -0.54 to 10.85.

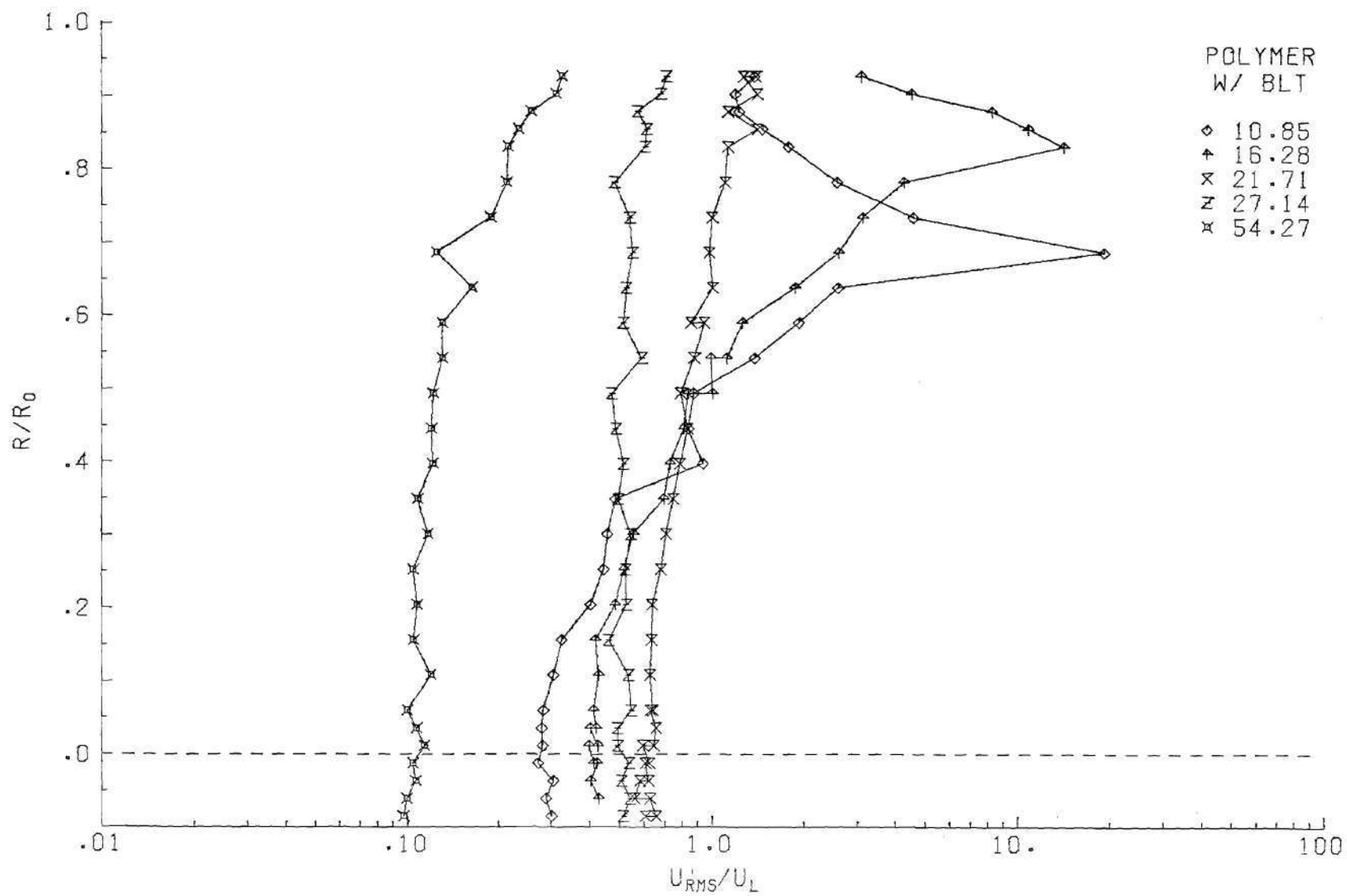


Figure A-28. Intensity Profiles, Polymer Solution with BLT, X/D from 10.85 to 54.27.

finally, the radial distribution appears to become more rapidly uniform in terms of  $U'_{\text{rms}}/U_{\text{FR}}$ .

#### Comparisons

The following plots correspond to the axial locations mentioned in the discussion concerning the direct comparison between the water and polymer injections using the BLT (Figures A-29 through A-38).

#### Spectra

The spectra in Figures A-39 through A-41 correspond to the axial locations mentioned in Chapter V.

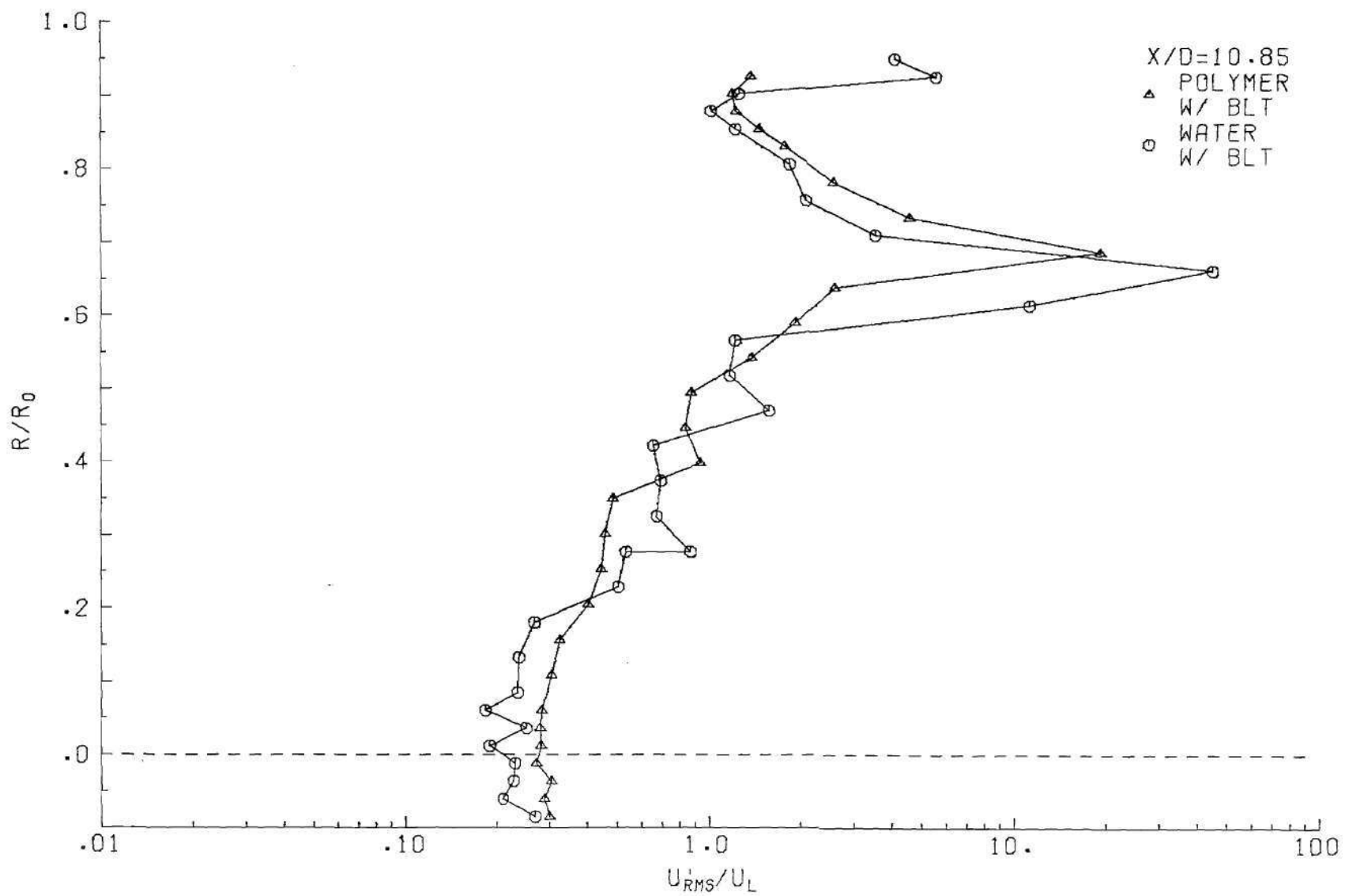


Figure A-29. Comparison of Polymer Solution to Water Intensity Profile,  $X/D = 10.85$ .

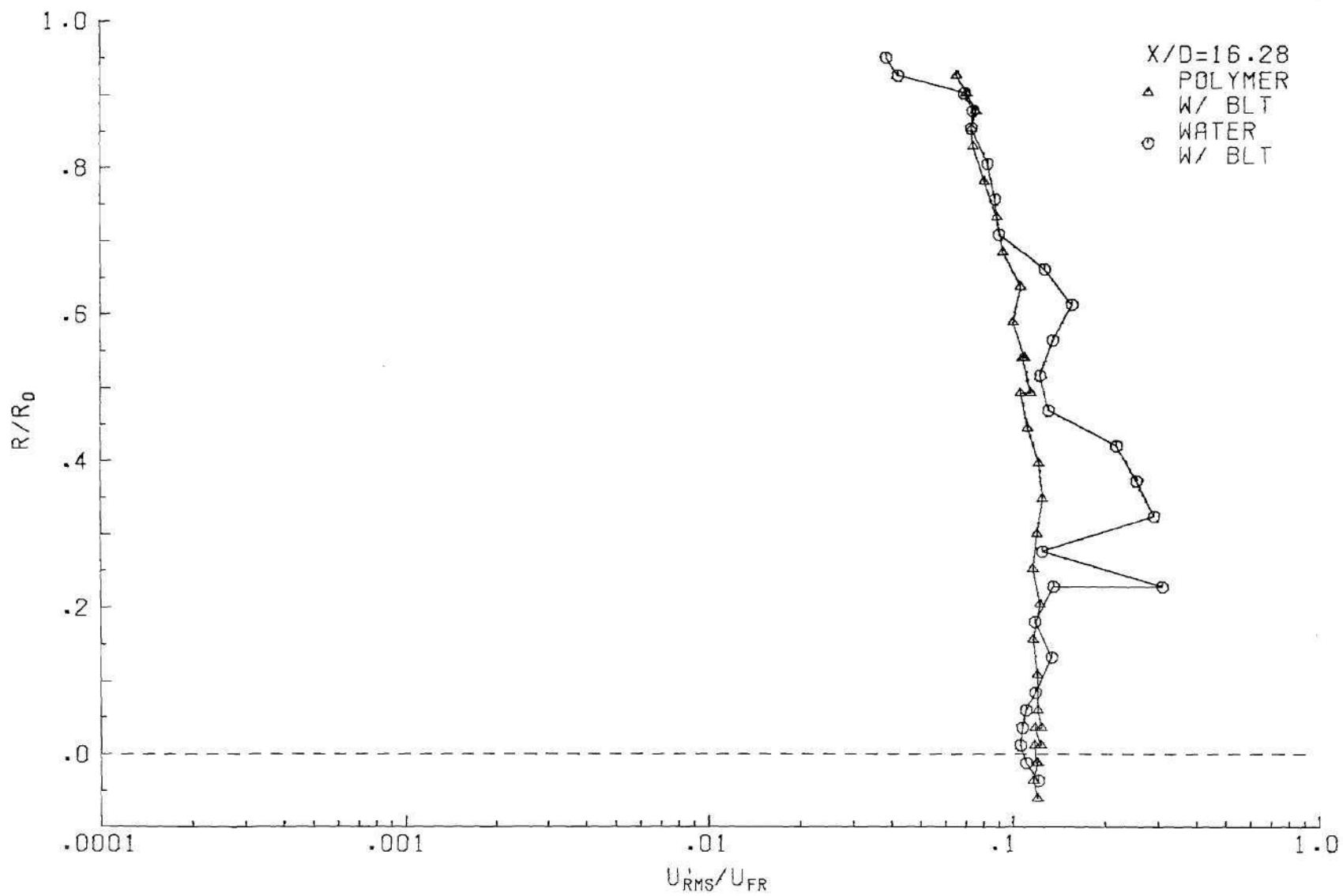


Figure A-30. Comparison of Polymer Solution to Water Fluctuation Profile, X/D = 16.28.

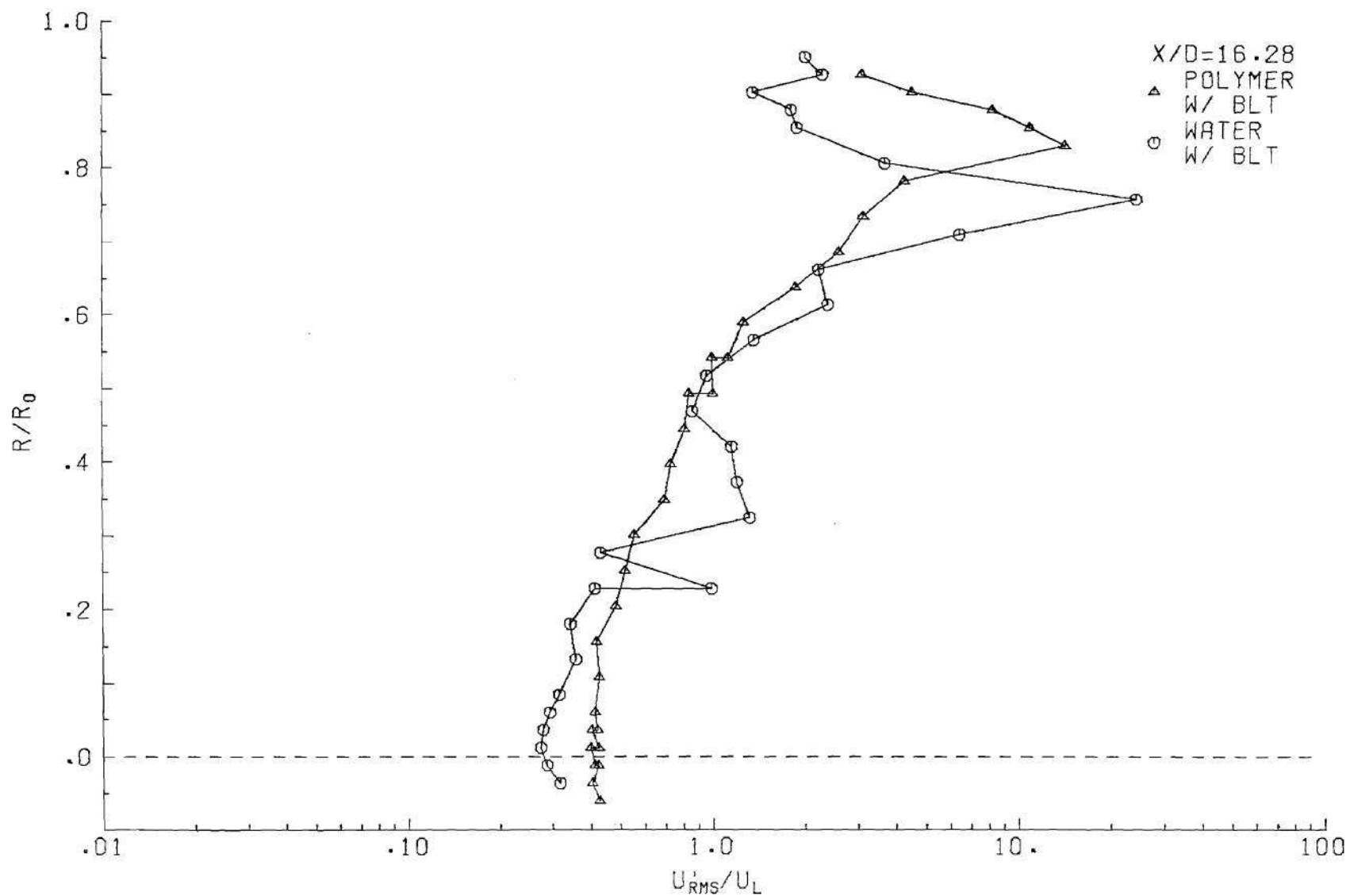


Figure A-31. Comparison of Polymer Solution to Water Intensity Profile,  $X/D = 16.28$ .

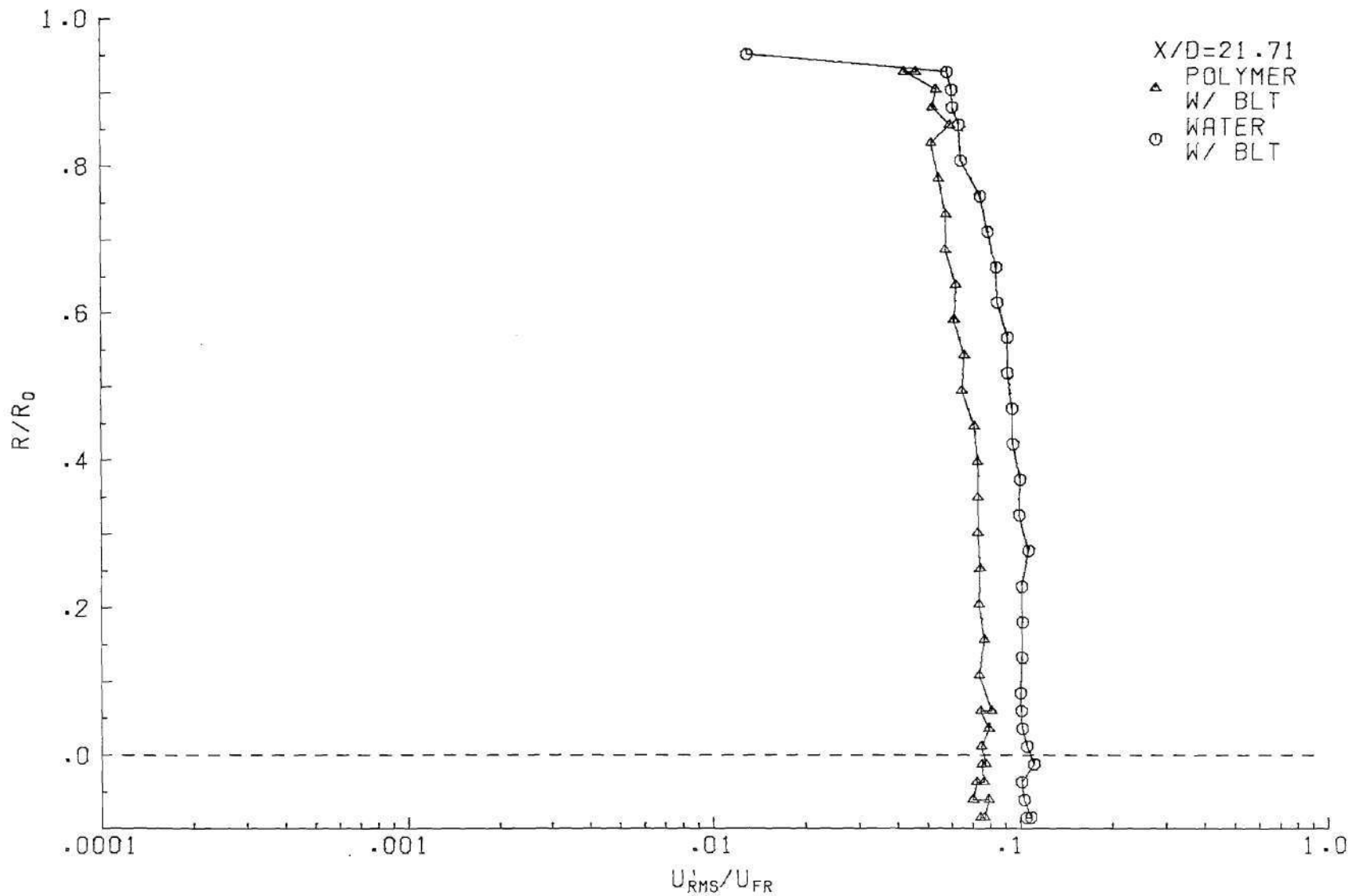


Figure A-32. Comparison of Polymer Solution to Water Fluctuation Profile, X/D = 21.71.

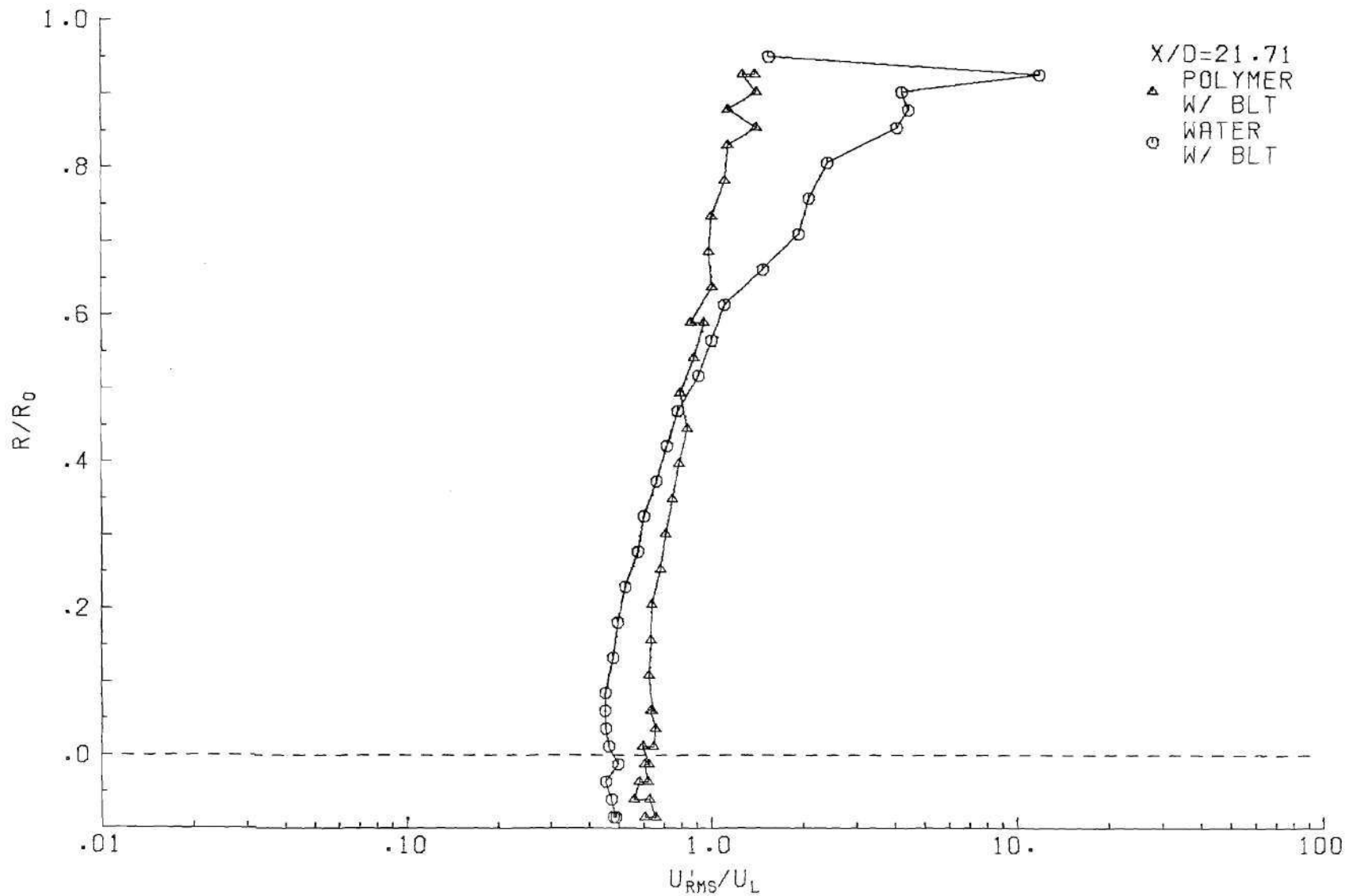


Figure A-33. Comparison of Polymer Solution to Water Intensity Profile,  $X/D - 21.71$ .

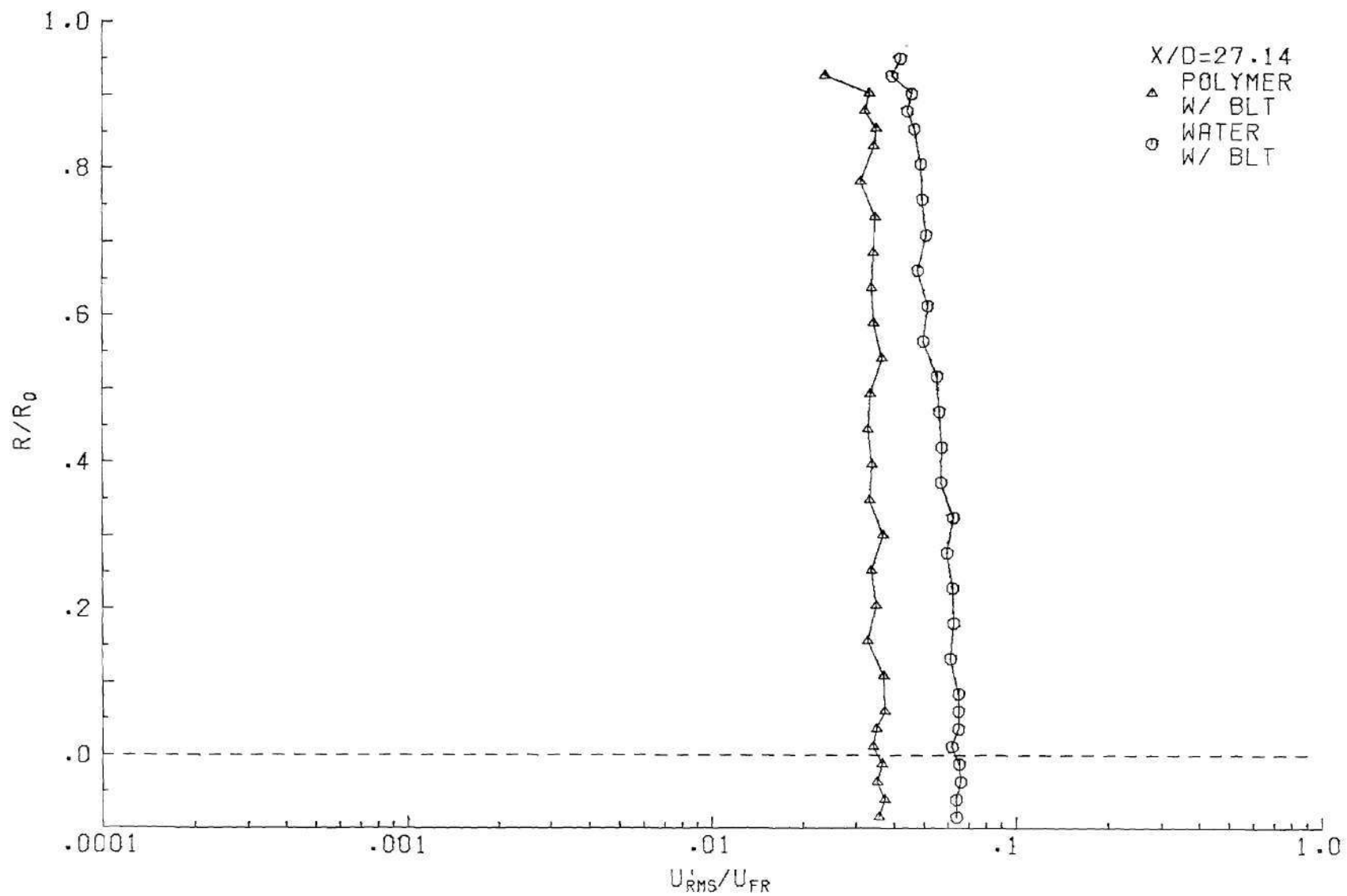


Figure A-34. Comparison of Polymer Solution to Water Fluctuation Profile, X/D = 27.14.

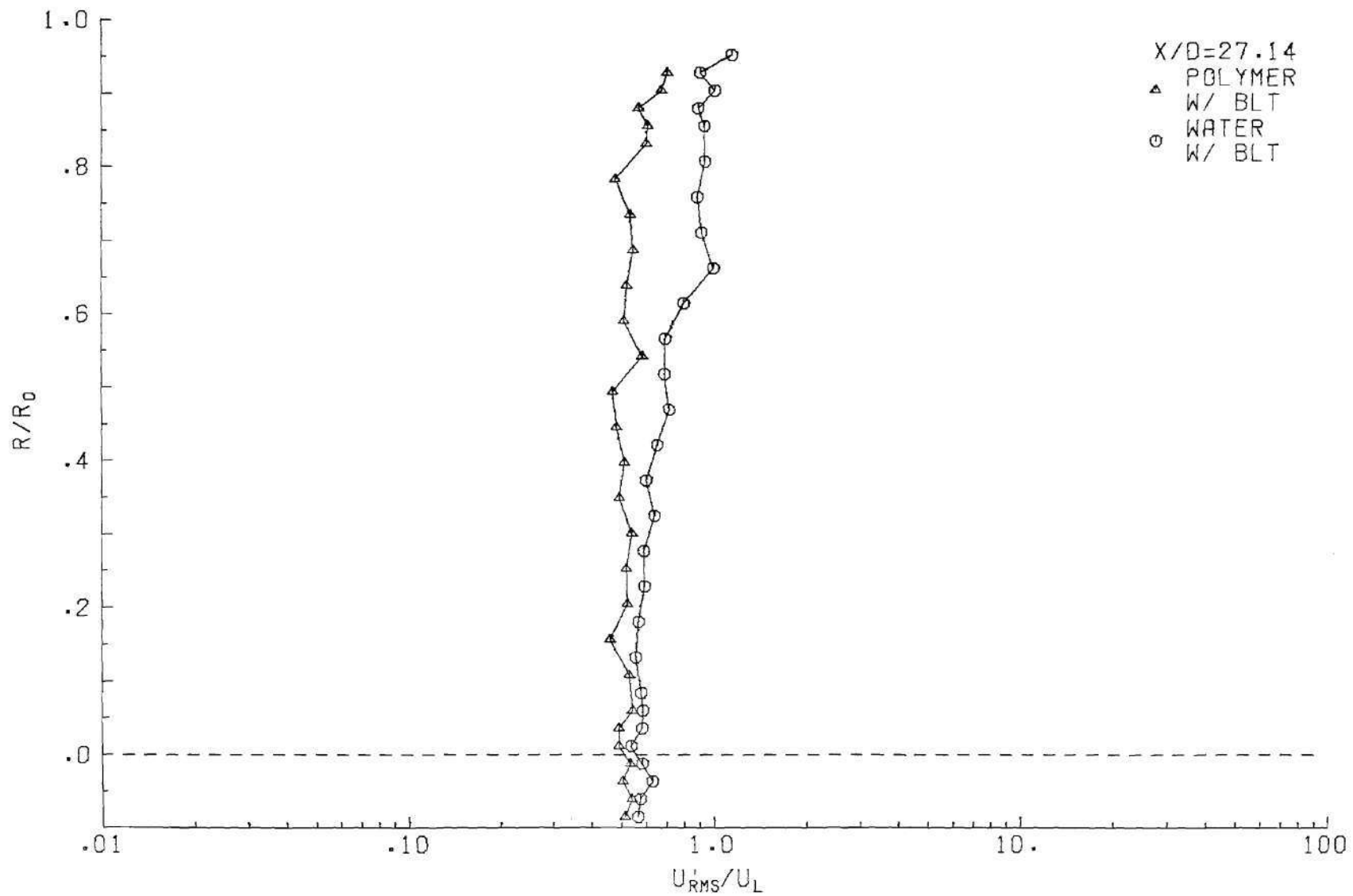


Figure A-35. Comparison of Polymer Solution to Water Intensity Profile,  $X/D = 27.14$ .

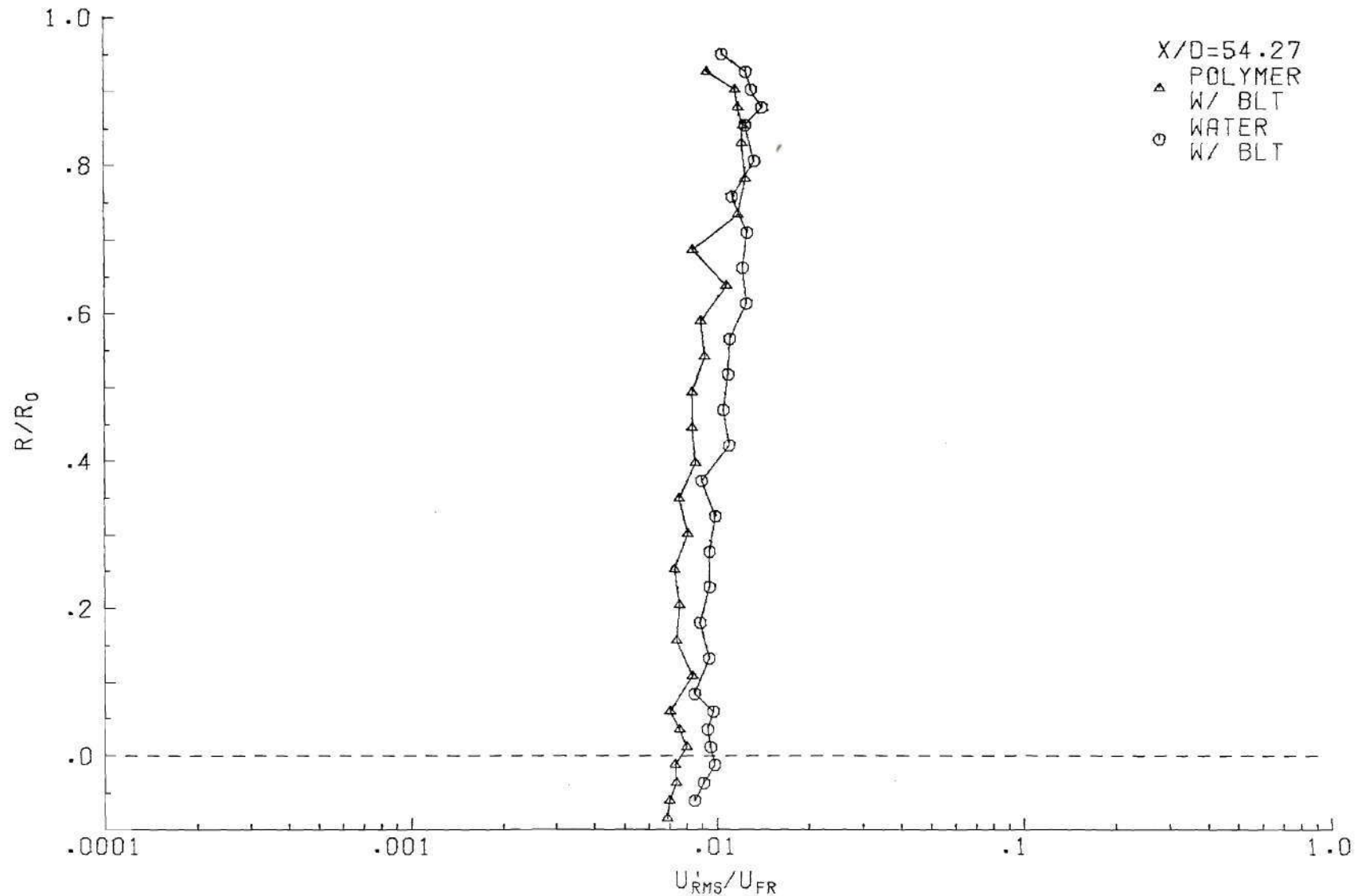


Figure 36. Comparison of Polymer Solution to Water Fluctuation Profile,  $X/D = 54.27$ .

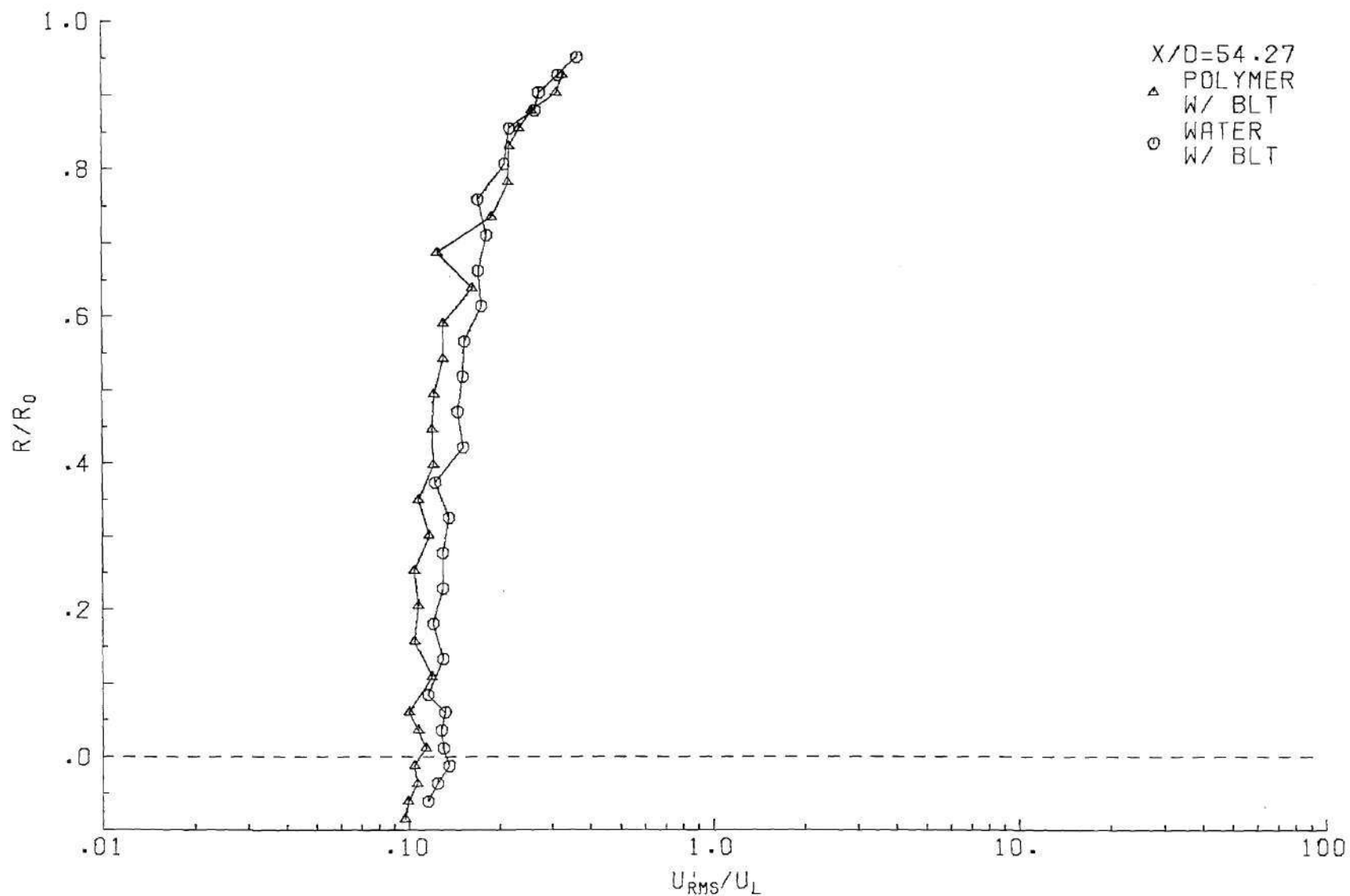


Figure 37. Comparison of Polymer Solution to Water Intensity Profile,  $X/D = 54.27$ .

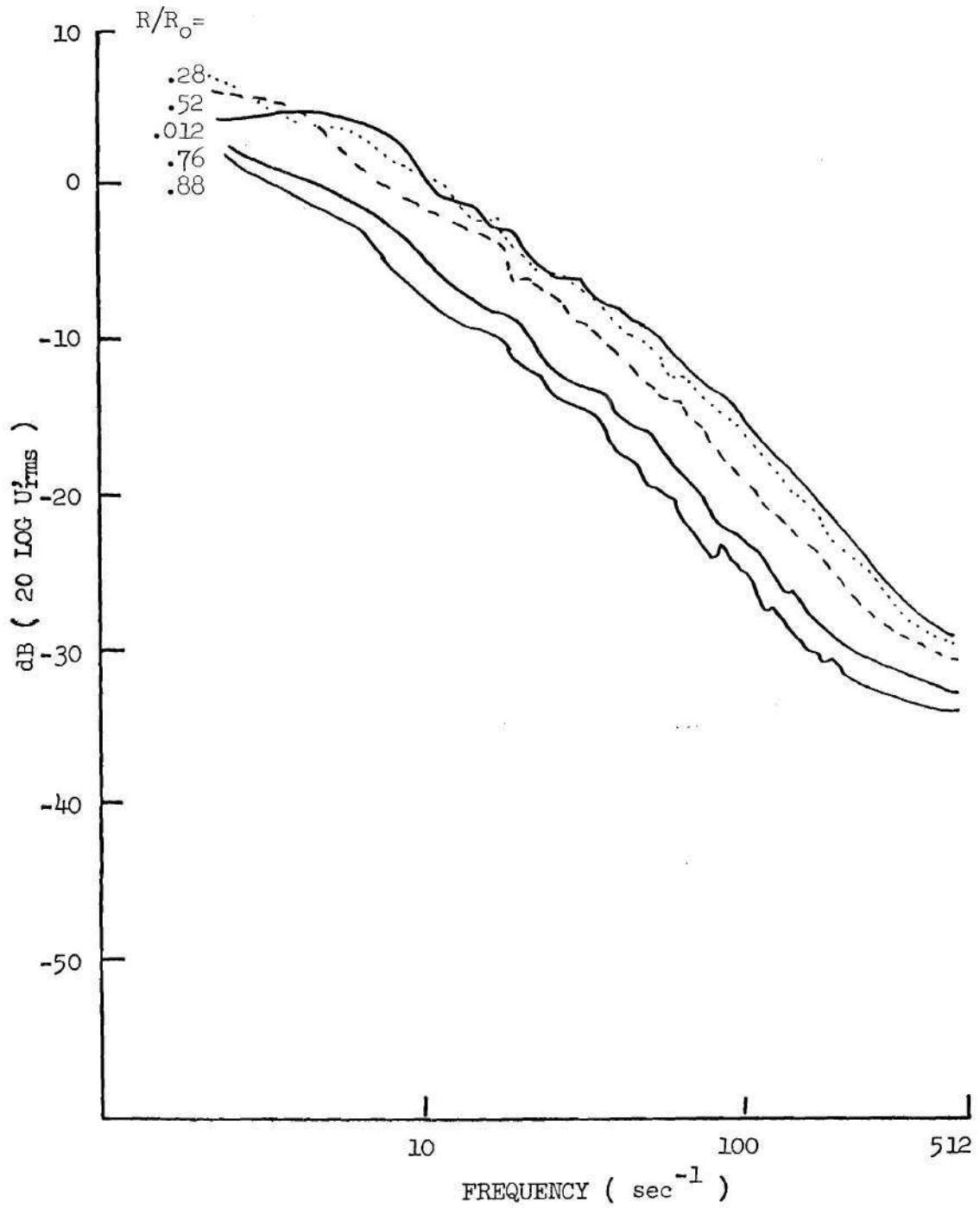


Figure A-38. Radial Variation of Spectra, Water Injection,  $X/D = 21.71$ .

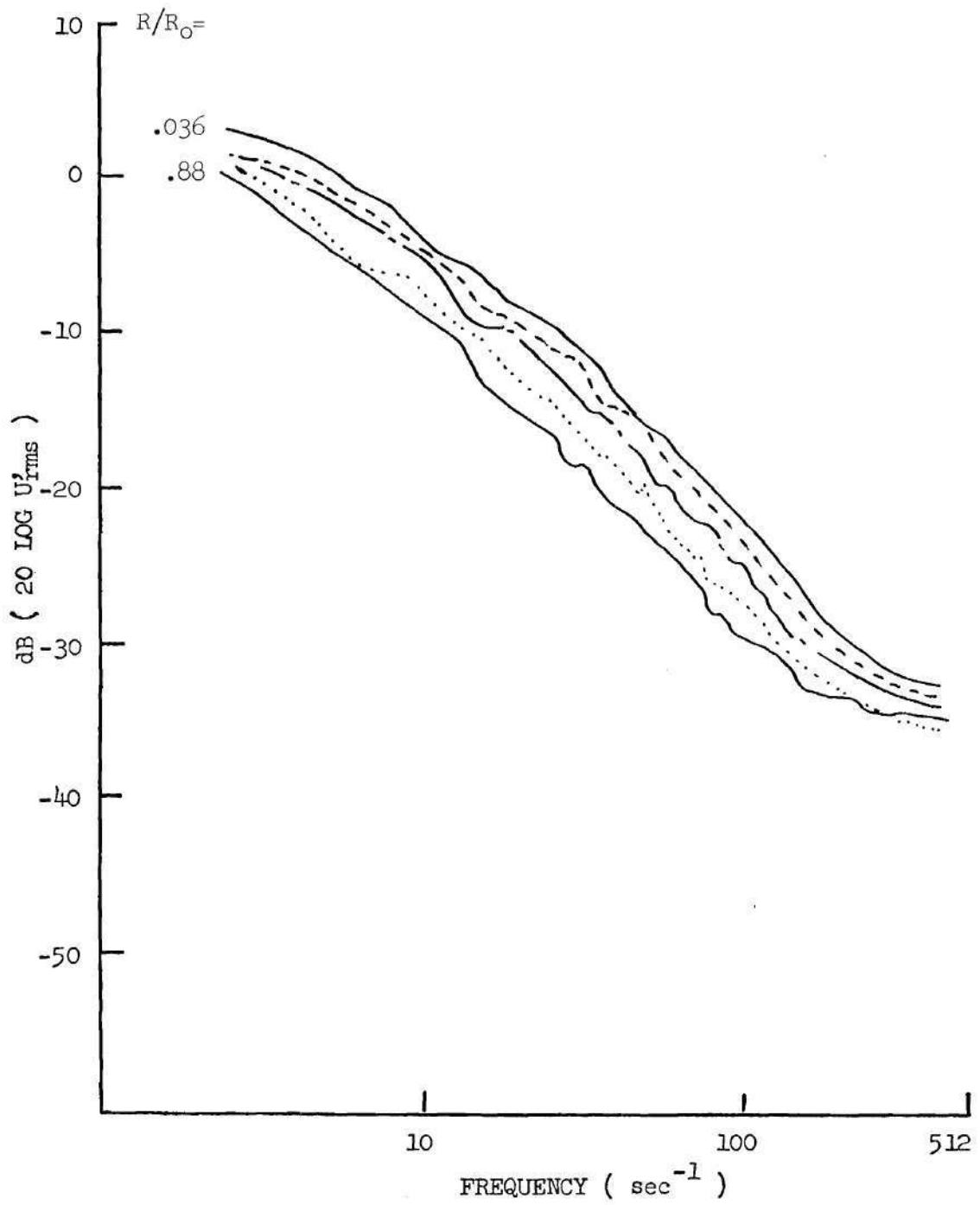


Figure A-39. Radial Variation of Spectra, Water Injection,  $X/D = 27.14$ .

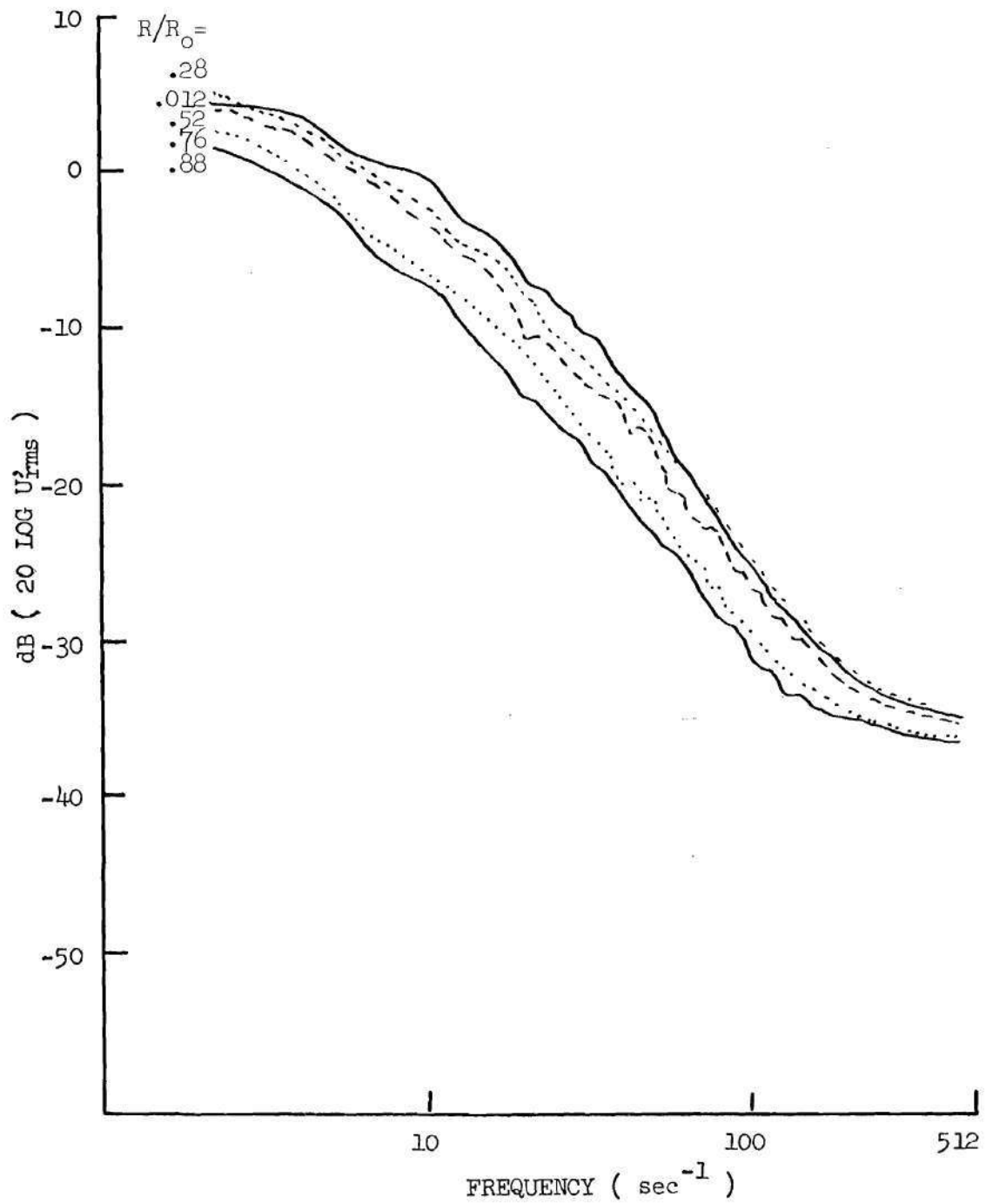


Figure A-40. Radial Variation of Spectra, Polymer Solution,  $X/D = 21.71$ .

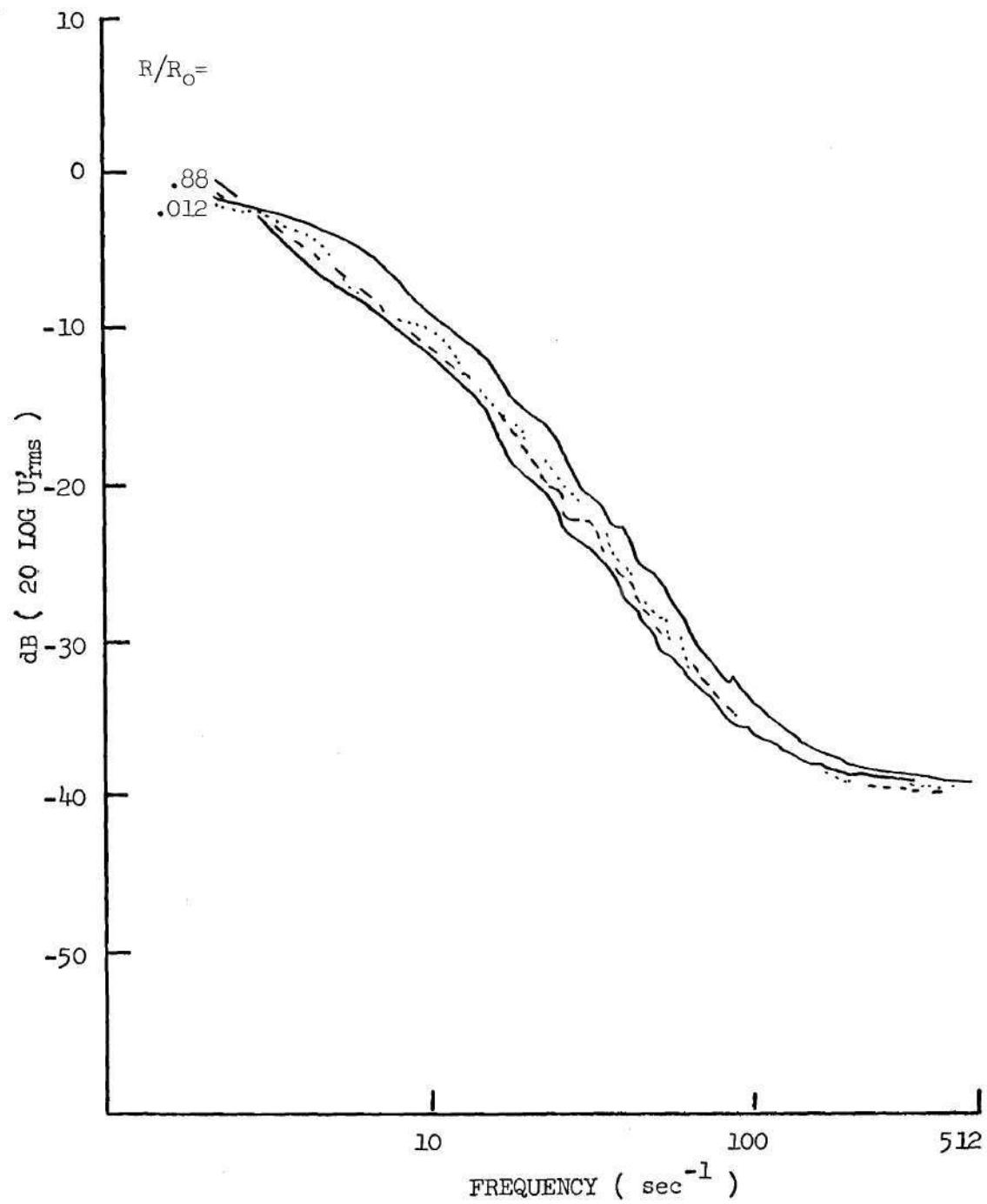


Figure A-41. Radial Variation of Spectra, Polymer Solution, X/D = 27.14.

## BIBLIOGRAPHY

1. Wendth, Jr., Arthur J., "Peripheral Arterography an Overview of its Origin and Present Status," CRC Clinical Radiology and Nuclear Medicine, pp. 369 - 401, July 1975.
2. Seldinger, S. I., "Catheter Replace of Needle in Percutaneous Arteriography: New Techniques," Acta Radiology, Vol. 39, p. 368, 1953.
3. Amundsen, A. K., P. Amundsen and O. Müller, "Blood Pressure and Heart Rate During Angiocradiography, Abdominal Aortography and Angiography of the Lower Extremities," Acta Radiology, Vol. 45, pp. 452-458, June 1956.
4. Austen, W. G., B. R. Wilcox and H. W. Bender, "Experimental Studies of the Cardiovascular Responses Secondary to the Injection of Angiographic Agents," J. Thoracic and Cardiovas. Surgery, Vol. 47, pp. 356-366, March 1964.
5. Fischer, Harry W., "Hemodynamic Reactions to Angiographic Media, A Survey and Commentary," Radiology, Vol. 91, pp. 66-73, July 1968.
6. Haddy, F. J., "Local Effects of Sodium, Calcium and Magnesium upon Small and Large Blood Vessels of Dog Forelimb." Circulation Research, Vol. 8, pp. 57-70, Jan. 1960.
7. Iseri, L. T., M. A. Kaplan, M. J. Evans and E. D. Nickel, "Effect of Concentrated Contrast Media During Angiography on Plasma Volume and Plasma Osmolarity," American Heart Journal, Vol. 69, pp. 154-158., Feb. 1965.
8. Lindgren, P. and G. Tornell, "Peripheral Arteriography: Experimental Study of Effects of Triural (Sodium Acetrizoate) and Hypaque (Sodium Diafrizoate)," Acta Radiology, Vol. 49, pp. 425-440, June 1958.
9. Fry, D. L. "Acute Vascular Endothelial Changes Associated with Increased Blood Velocity Gradients," Circulation Research, Vol. 22, pp. 165-197, 1968.
10. Forestall, W. and A. H. Shapiro, "Momentum and Mass Transfer in Coaxial Gas Jets," Journal of Applied Mechanics, Vol. 17, pp. 399-408, 1950.
11. Becker, H. A., H. C. Hottel and G. C. Williams, "Mixing and Flow in Ducted Turbulent Jets," 9th Symposium on Combustion, pp. 7-20, 1963.

12. Curtet, R. and F. P. Ricou, "on the Tendency to Self-Preservation in Axisymmetric Ducted Jets," *Journal of Basic Engineering*, pp. 765-776, Dec. 1964.
13. Razinsky, E. and J. A. Brighton, "Confined Jet Mixing for Non-Separating Conditions," *Journal of Basic Engineering*, pp. 333-349, Sept. 1971.
14. Hill, Philip G., "Turbulent Jets in Ducted Streams," *Journal of Fluid Mechanics*, Vol. 22, Part 1, pp. 161-186, 1965.
15. Exley, J. T. and J. A. Brighton, "Flow Separation and Reattachment in Confined Jet Mixing," *Journal of Basic Engineering*, pp. 192-198, June 1971.
16. Anderson, A. B. C., "Vortex Ring Structure Transition in a Jet Emitting Discrete Acoustic Frequencies," *The Journal of the Acoustical Society of America*, Vol. 28, #5, pp. 914-921, 1956.
17. Anderson, A. B. C., "Structure and Velocity of the Periodic Vortex-ring Flow Pattern in a Primary Pfeifenton (Pipe tune) Jet." *The Journal of the Acoustical Society of America*, Vol. 27 #6, pp. 1048-1053, Nov. 1955.
18. Becker, H. A. and T. A. Massaro, "Vortex Evaluation in a Round Jet," *Journal of Fluid Mech.*, Vol. 31, Part 3, pp. 435-448, 1968.
19. Crow, S. C. and F. H. Champagne, "Orderly Structure in Jet Turbulence," *Journal of Fluid Mech.*, Vol. 48, Part 3, pp. 547-591, 1971.
20. Chan, Y. Y., "Spatial Waves in Turbulent Jets," *The Physics of Fluids*, Vol. 17 #1, pp. 46-53, Jan. 1974.
21. Gibson, M. M., "Spectra of Turbulence in a Round Jet," *Fluid Mech.*, Vol. 15, pp. 161-173, 1963.
22. Hoyt, J. W., "The Effect of Additives on Fluid Friction," *Freeman Award Review*, Public Affairs Office, Naval Undersea Research and Development Center.
23. Toms, B. A., "Some Observations on the Flow of Linear Polymer Solutions through Straight Tubes at Large Reynolds Numbers," *Proceedings of International Congress on Rheology*, Vol. II, pp. 135-141, 1948, North Holland Publishing Co., Amsterdam.
24. Shaver, R. G., and E. W. Merrill, "Turbulent Flow of Pseudoplastic Polymer Solutions in Straight Cylindrical Tubes," *AIChE Journal*, Vol. 5, p. 181, 1959.

25. Dodge, D. W. and A. B. Metzner, "Turbulent Flow of Non-Newtonian Systems," *AIChE Journal*, Vol. 5, p. 189, 1959.
26. Fabula, A. G., J. W. Hoyt and H. R. Crawford, "Turbulent Flow Characteristics of Dilute Aqueous Solutions of High Polymers," *Bulletin, American Physical Society*, Vol. 8, 1963.
27. Lumley, J. L., "The Toms Phenomenon: Anomalous Effects in Turbulent Flow of Dilute Solutions of High Molecular Weight Linear Polymers," *Applied Mechanics Reviews*, Vol. 20 No. 12 pp. 1139-1149, Dec. 1967.
28. Frummer, M. A., A. Lavy, M. A. Kravs, D. H. Fruman and J. E. Santo, "The Influence of the Chemical Nature of Polymers on Their Drag Reduction Characteristics," *Technical Report*, 1 May 1972-30 Sept. 1973, Hydronautics Inc., Laurel Md., AD-774752; TR 7213-2.
29. Wells Jr., C. S. and J. G. Spangler, "Injection of a Drag-Reducing Fluid into Turbulent Pipe Flow of a Newtonian Fluid," *The Physics of Fluids*, Vol. 10 No. 9, p. 1890-, Sept. 1967.
30. Walters, R. R. and C. S. Wells, "An Experimental Study of Turbulent Diffusion of Drag Reducing Polymer Additives," *Journal of Hydro-nautics*, Vol. 5 No. 2, pp. 65-72, April 1971.
31. Fortuna, Gilead and T. J. Hauratty, "The Influence of Drag Reducing Polymers on Turbulence in the Viscous Sublayer," *Journal of Fluid Mechanics*, Vol. 53, pp. 573-586, June 13, 1972.
32. Virk, P. S. "Turbulent Kinetic Energy Profile During Drag Reducing," *The Physics of Fluids*, Vol. 18, No. 4, pp. 415-419, April 1975.
33. Gadd, G. E. "Turbulence Damping and Drag Reduction Produced by Certain Additives in Water," *Nature*, Vol. 206, pp. 463-467, 1965.
34. White, D. A. "Velocity Measurements in Axisymmetric Jets of Dilute Polymer Solutions," *Journal of Fluid Mechanics*, Vol. 28, p. 195-, 1965.
35. Vlasov, S. A.; V. N. Kalashnikov, B. F. Mul'chenko, B. S. Rinkevichyus and V. I. Smirnov, "The Long Range Nature of Turbulent Submerged Jets of Polymer Solutions," *Fluid Mechanics-Soviet*, Vol. 2 No. 1, pp. 108-111, Jan.-Feb. 1973.
36. Barker, Steven J., "Laser Doppler Measurements on a Round Turbulent Jet in Dilute Polymer Solutions," *Journal of Fluid Mechanics*, Vol. 60, pp. 721-731, 1973.

37. Bove, A. A., Jose L. Gimmenea and Herbert M. Stauffer, "Addition of Polymer to Radiopaque Contrast Material to Decrease Catheter Flow Resistance," *Radiology*, Vol. 93, pp. 381-383, Aug. 1969.
38. Menon, Rajagopala K., "A Study of Ducted Jets Including Effects of Dilute Polymer Solutions," Ph.D. Thesis, School of Aerospace Engineering, Georgia Institute of Technology, Aug. 1976.
39. Becke, H. A. Discussion of "Confined Jet Mixing for Non-Separating Conditions," by Raminsky and Brighton, *Journal of Basic Engineering* p. 347, Sept, 1971.
40. Cook Incorporated, "Diagnostic and Intervention Products for the Radiologist, Cardiologist and Surgeon, 1976-1977, Bloomington Ind. 4740]
41. Squibb Professional Services Department, Communication by letter Lawrenceville-Princeton Rd., Princeton, NJ 08540
42. Feild, J. R., L. Lee and R. F. McBurney, "Complications of 1000 Brachial Arteriograms," *Journal of Nevrosurgery*, Vol. 36 pp.324-331 March 1972
43. Ganong, W. F. "Review of Medical Physiology," 6<sup>th</sup> Ed. 1973, Lange Medical Publications, Los Altos, California.
44. Bryant, M. F. and D. P. Giddens, "Blood Flow Studies Following Carotid Endarterectomy, Cervical Sympathectomy and Ligation of the External Carotid Artery," *J. of the Medical Association of Ga.* pp. 147-150, March 1977.
45. McDonald, D. A., "Blood Flow in Arteries," Edward Arnold (publishers) LTD. Copyright 1960.
46. Tennekes, H. and J. L. Lumley, "A First Course in Turbulence," The MIT Press; Cambridge Mass. and London, England, 1972.
47. DISA Type 55L Laser Doppler Anemometer, Instruction Manual, DISA Information Department
48. Fouries Analyser System 5451B Manual, Hewlett-Packord Company, Santa Clara, California 95050, 1974.
49. Schlichting, Herman; "Boundry Layer Theory," 6<sup>th</sup> Ed., McGraw Hill Book Co., N.Y., St. Louis, San Fransisco, Toronto, London, Sydney, Verlag G. Braun, Karlsruhe, 1968.

50. Cassanova, R. A., "An Experimental Investigation of Steady and Pulsatile Flow Through Partial Occlusions in a Rigid Tube," Ph.D. Thesis, School of Aerospace Engineering, Georgia Institute of Technology, Aug. 1975.
51. Roper, R. G. Direct Communication 1977.
52. DISA Type 55L Laser Doppler Anemometer Mark II, Instruction Manual, DISA Information Department.
53. DISA Information, No. 12, Nov. 1971.
54. Beran, N. S. and J. W. Dunning, "Pipe Flow Measurements of Turbulence and Ambiguity using Laser Doppler Velocimetry, Journal of Fluid Mechanics, Vol. 61 part 2, pp. 289-299, 1973.
55. Goerge, W. K. and J. L. Lumley, "The Laser Doppler Velocimeter and its Application to the Measurement of Turbulence," Journal of Fluid Mechanics, Vol. 60 part 2, pp. 321-362, 1973.
56. Goethest, W. H., "Frequency Broadening in Reference Beam Laser Doppler Velocimeter Data," AEDC TR 71-163, Sept. 1971.
57. Greated, C., "Statistical Ambiguity in Laser Anemometry, DISA Information No. 12, pp. 32-36, Nov. 1971.
58. Casson, N., "A Flow Equation for Pigment-Oil Suspensions of Printing Ink Type," in Rheology of Disperse Suspensions, C. C. Mill editor, Pergamon Press, N.Y., 1959
59. Merrill, E. W. and G. A. Pelleter, "Viscosity of Human Blood; Transition from Newtonian," Journal of Applied Mechanics, Vol. 23, No. 2, Aug. 1967.

## VITA

Walter A. Carpenter was born in Savannah, Georgia on April 14, 1951. He attended schools in Dekalb County and graduated in 1969. He entered Georgia Institute of Technology in September 1969 and received a Bachelor of Aerospace Engineering with high honor in June 1973.

In September 1973 he entered the graduate program and received his masters in A.E. in December 1974. After receiving his masters he continued his studies at Georgia Tech in the area of bio-engineering in the Aerospace Engineering Department. During his graduate studies he was employed as a research assistant.

On April 13, 1977 Mr. Carpenter received his highest honor when he became engaged to Miss Amy Baxter.

In September of 1977 he will enter medical school at Emory University, after which he will become fabulously wealthy.